Fisheries and Oceans Canada | Pêches et Océans Canada
Ecosystems and Oceans Science | Sciences des écosystèmes et des océans

Canadian Science Advisory Secretariat (CSAS)

Research Document 2026/002

National Capital Region

Assessment of Port Ocean Prediction System Developed Under Canada's Oceans Protection Plan: Fraser River

Michael Dunphy[1], Maxim Krassovski[1], Stephanne Taylor[2], Hauke Blanken[1], Rachel Horwitz[2], Simon St-Onge Drouin[3], Adam Drozdowski[2]

[1] Fisheries and Oceans Canada
Institute of Ocean Sciences
9860 West Saanich Road
Sidney, British Columbia V8L 4B2

[2] Fisheries and Oceans Canada
Bedford Institute of Oceanography
1 Challenger Drive
Dartmouth, Nova Scotia B2Y 4A2

[3] Fisheries and Oceans Canada
Maurice Lamontagne Institute
850 route de la Mer
Mont-Joli, Québec G5H 3Z4

February 2026

Canada

Foreword

This series documents the scientific basis for the evaluation of aquatic resources and ecosystems in Canada. As such, it addresses the issues of the day in the time frames required and the documents it contains are not intended as definitive statements on the subjects addressed but rather as progress reports on ongoing investigations.

Published by:

Fisheries and Oceans Canada
Canadian Science Advisory Secretariat
200 Kent Street
Ottawa ON K1A 0E6

http://www.dfo-mpo.gc.ca/csas-sccs/
DFO.CSAS-SCAS.MPO@dfo-mpo.gc.ca

ISSN 1919-5044
ISBN 978-0-660-79954-4 Cat. No. Fs70-5/2026-002E-PDF

Correct citation for this publication:

Dunphy, M., Krassovski, M., Taylor, S., Blanken, H., Horwitz, R., St-Onge Drouin, S., and Drozdowski, A. 2026. Assessment of Port Ocean Prediction System Developed Under Canada's Oceans Protection Plan: Fraser River. DFO Can. Sci. Advis. Sec. Res. Doc. 2026/002. xi + 116 p.

Aussi disponible en français :

Dunphy, M., Krassovski, M., Taylor, S., Blanken, H., Horwitz, R., St-Onge Drouin, S. et Drozdowski, A. 2026. Évaluation des modèles portuaires de prévisions océaniques développés dans le cadre du Plan de Protection des Océans: Le Fleuve Fraser. Secr. can. des avis sci. du MPO. Doc. de rech. 2026/002. xi + 121 p.

TABLE OF CONTENTS

ABSTRACT xi
1. INTRODUCTION 1
2. PORT MODEL DESIGN 1
2.1. MODEL SELECTION 1
2.2. DOWNSCALING STRATEGY 2
2.3. SIMULATION SEQUENCING 2
2.4. SURFACE FORCING 3
2.5. AUTOMATION SUITE 3
2.6. ROBUSTNESS AND LIMITATIONS 4
3. FRASER RIVER 4
3.1. REGIONAL OCEANOGRAPHY 4
3.2. DOMAIN AND CONFIGURATION 5
3.3. INITIALIZATION 6
3.4. OPEN BOUNDARY CONDITIONS 6
3.5. FRESHWATER INPUT 6
3.6. ICE MODEL 6
3.7. MODELLING SYSTEM STABILITY 6
4. EVALUATION METRICS 7
4.1. HINDCAST 7
4.1.1. Water level 8
4.1.2. Water velocity 9
4.1.3. Water properties 10
4.1.4. Drift 11
4.2. FORECAST 12
5. HINDCAST EVALUATION RESULTS 13
5.1. WATER LEVEL 13
5.1.1. Mean sea surface height 13
5.1.2. Tidal water level 13
5.1.3. Non-tidal water level 15
5.1.4. Overall scores 15
5.1.5. Storm surge water level 16
5.2. WATER VELOCITY 16
5.2.1. Horizontal ADCPs 16
5.2.2. Current meters 17
5.2.3. Moored ADCPs 18
5.2.4. ADCP transects 19
5.3. WATER PROPERTIES 20
5.3.1. Sea surface temperature 20

5.3.2. Moored CTDs 20
5.3.3. CTD profiles 21
5.3.4. Ferries 21
5.4. DRIFT 21
6. FORECAST EVALUATION RESULTS 22
6.1. NON-TIDAL WATER LEVEL 22
6.2. HORIZONTAL ADCP 22
6.3. SEA SURFACE TEMPERATURE 22
7. SUMMARY 23
8. KEY FINDINGS 23
9. ACKNOWLEDGEMENTS 24
10. REFERENCES CITED 24
11. TABLES 28
12. FIGURES 45

LIST OF TABLES

Table 1. Key model parameters for the SSS150 and SF30 NEMO configurations. 28

Table 2. Water level station data used for evaluation and offsets used to shift the water level to CGVD28. 29

Table 3. M2 constituent comparison for active tide gauges for year 2018 (upper part) and historical tide gauges (lower part). 30

Table 4. N2 constituent comparison for active tide gauges for year 2018 (upper part) and historical tide gauges (lower part). 30

Table 5. S2 constituent comparison for active tide gauges for year 2018 (upper part) and historical tide gauges (lower part). 31

Table 6. K2 constituent comparison for active tide gauges for year 2018 (upper part) and historical tide gauges (lower part). 31

Table 7. O1 constituent comparison for active tide gauges for year 2018 (upper part) and historical tide gauges (lower part). 32

Table 8. K1 constituent comparison for active tide gauges for year 2018 (upper part) and historical tide gauges (lower part). 32

Table 9. P1 constituent comparison for active tide gauges for year 2018 (upper part) and historical tide gauges (lower part). 33

Table 10. Q1 constituent comparison for active tide gauges for year 2018 (upper part) and historical tide gauges (lower part). 33

Table 11. L2 constituent comparison for active tide gauges for year 2018 (upper part) and historical tide gauges (lower part). 34

Table 12. J1 constituent comparison for active tide gauges for year 2018 (upper part) and historical tide gauges (lower part). 35

Table 13. NO1 constituent comparison for active tide gauges for year 2018 (upper part) and historical tide gauges (lower part). 35

Table 14. OO1 constituent comparison for active tide gauges for year 2018 (upper part) and historical tide gauges (lower part). 36

Table 15. SO1 constituent comparison for active tide gauges for year 2018 (upper part) and historical tide gauges (lower part). 36

Table 16. NU2 constituent comparison for active tide gauges for year 2018 (upper part) and historical tide gauges (lower part). 37

Table 17. 2N2 constituent comparison for active tide gauges for year 2018 (upper part) and historical tide gauges (lower part). 37

Table 18. Tidal water level scores for year 2018. 38

Table 19. Non-tidal water level scores for year 2018. 38

Table 20. Total water level scores for year 2018. 40

Table 21. Average scores for the non-tidal water level during storm surge events. N denotes number of storm events for each station. 41

Table 22. Scores for the along-shore velocity measured by horizontal ADCP at Woodward's Landing. Negative sign corresponds to the downstream flow. 42
Table 23. Error statistics for the model tidal constituents versus observations by horizontal ADCP at Woodward's Landing. 42
Table 24. Total current scores for SSS150 for ADCP records subset to four depths. 42
Table 25. Non-tidal current scores for SSS150 for ADCP records subset to four depths. 43
Table 26. Tidal current scores for SSS150 for ADCP records subset to four depths. 43
Table 27. Scores for sea surface temperature at Fraser River Water Quality Buoy. 44
Table 28. Scores for moored CTD at SEVIP station. 44
Table 29. Number of CTD cast for the period from 2017 to 2021 for the five analysed subregions. 44
Table 30. Drift evaluation statistics for hourly intervals (only one available). 44

LIST OF FIGURES

Figure 1. Schematic of one timestamp's set of pseudo-analysis (PA, in red) and forecast (in blue) runs. Grey dashed lines are spaced six hours apart, and orange arrows indicate where a restart file is generated and used to launch the subsequent step. The PA for today+1 will start with the same restart used to start today's 00Z forecast, and the pattern will repeat. 45

Figure 2. Model domain showing the outer (SSS150) and the inner (SF30) grids; colour scale shows depth. 46

Figure 3. Surface speed (m/s) for CIOPS-W, SS500 and SSS150 (from top to bottom) for the Fraser River. 47

Figure 4. Surface speed (m/s) for SS500, SSS150 and SF30 (from top to bottom) for the lower Fraser River, excluding Pitt Lake. 48

Figure 5. Surface speed (m/s) for SS500, SSS150 and SF30 (from top to bottom) for the Lower Fraser River (zoom of Figure 4). 49

Figure 6. Cyclone locations every six hours from 2010-2021. 50

Figure 7. Locations of instruments used in this evaluation. The double water level markers are Steveston (CHS station) and StevestonEC (WSC station) near the mouth of the Fraser. The green triangle marker represents Woodward's Landing (water level and HADCP) while the blue marker below it represents Deas Island. 51

Figure 8. Mean model water level for 2017-2021. 52

Figure 9. Observed and model amplitude and phase for M2 constituent for the year 2018. 53

Figure 10. Observed and model amplitude and phase for K1 constituent for the year 2018. 54

Figure 11. Non-tidal water level comparison for North Arm for year 2018. 55

Figure 12. Non-tidal water level comparison for Sand Heads for year 2018. 56

Figure 13. Non-tidal water level comparison for Steveston for year 2018. 57

Figure 14. Non-tidal water level comparison for StevestonEC for year 2018. 58

Figure 15. Non-tidal water level comparison for Woodward's Landing for year 2018. 59

Figure 16. Non-tidal water level comparison for Deas Island for year 2018. 60

Figure 17. Non-tidal water level comparison for New Westminster for year 2018. 61

Figure 18. Non-tidal water level comparison for Port Mann for year 2018. 62

Figure 19. Non-tidal water level comparison for Pitt River for year 2018. 63

Figure 20. Power spectra for the total and non-tidal water level at Sand Heads for the year 2018. 64

Figure 21. Power spectra for the total and non-tidal water level at Port Mann for the year 2018. 65

Figure 22. Water level scores variability over years. Markers of same colour denote scores for a single station for individual years. Markers for consecutive years are connected by a line. 66

Figure 23. Observed and model non-tidal sea level during individual storm events for North Arm tide gauge. 67

Figure 24. Observed and model non-tidal sea level during individual storm events for Sand Heads tide gauge. 68

Figure 25. Observed and model non-tidal sea level during individual storm events for Steveston tide gauge. 69

Figure 26. Observed and model non-tidal sea level during individual storm events for StevestonEC tide gauge. 70

Figure 27. Observed and model non-tidal sea level during individual storm events for Woodward's Landing tide gauge. 71

Figure 28. Observed and model non-tidal sea level during individual storm events for Deas Island tide gauge. 72

Figure 29. Observed and model non-tidal sea level during individual storm events for New Westminster tide gauge. 73

Figure 30. Observed and model non-tidal sea level during individual storm events for Port Mann tide gauge. 74

Figure 31. Observed and model non-tidal sea level during individual storm events for Pitt River tide gauge. 75

Figure 32. Model bias for the non-tidal sea level averaged over stations vs minimum atmospheric pressure during the storm for individual storm events. BCFloods storm is omitted due to a lack of pressure data. 76

Figure 33. Same as Figure 32, but for the model CRMSE. 76

Figure 34. Observation location of the horizontal ADCP at Woodward's Landing and current rose diagrams with principal axes of variance for the ADCP data and for the SSS150 and SF30 models. Circular grid lines on rose diagrams indicate velocity in m/s. 77

Figure 35. Observed and model along-shore velocity (a 6-day fragment) from the horizontal ADCP at Woodward's Landing. 78

Figure 36. Non-tidal velocity from the FRDLS ADCP station at 58.5 m depth for eastward (u) and northward (v) components. 79

Figure 37. Non-tidal velocity from the SoG Central ADCP station at 98.06 m depth for eastward (u) and northward (v) components. 80

Figure 38. Non-tidal velocity from the SoG East ADCP station at 58.48 m depth for eastward (u) and northward (v) components. 81

Figure 39. Mean currents (first column) and vector correlations for total (second column), tidal (third column) and non-tidal (fourth column) velocities for FRDLS ADCP deployment. Mean direction is measured clockwise from north. 82

Figure 40. Mean currents (first column) and vector correlations for total (second column), tidal (third column) and non-tidal (fourth column) velocities for SoG Central ADCP deployment. Mean direction is measured clockwise from north. 83

Figure 41. Mean currents (first column) and vector correlations for total (second column), tidal (third column) and non-tidal (fourth column) velocities for SoG East ADCP deployment. Mean direction is measured clockwise from north. 84

Figure 42. Rotary spectra for total velocity from the FRDLS ADCP station at 58.5 m depth. 85

Figure 43. Rotary spectra for total velocity from the SoG Central ADCP station at 98.1 m depth. 86
Figure 44. Rotary spectra for total velocity from the SoG East ADCP station at 15.6 m depth. ..87
Figure 45. Current ellipses for M2 (left) and K1 (right) tidal components from the FRDLS ADCP station. 88
Figure 46. Current ellipses for M2 (left) and K1 (right) tidal components from the SoG Central ADCP station 89
Figure 47. Current ellipses for M2 (left) and K1 (right) tidal components from the SoG East ADCP station. 90
Figure 48. Observed and model current velocity components: Cross-transect (left panels) and along-transect (right panels) at the line FR05a. Positive direction is indicated in true degrees in each panel. Transect location is shown in the upper panels. The black line in the upper right panel shows the transect and the red arrow indicates the direction of the transect.....91
Figure 49. Same as Figure 48, but for the line FR06. 92
Figure 50. Same as Figure 48, but for the line Mungos5. 93
Figure 51. Same as Figure 48, but for the line FR08. 94
Figure 52. Same as Figure 48, but for the line FR10. 95
Figure 53. Same as Figure 48, but for the line Transect8. 96
Figure 54. Scatter plot of mean bias vs mean CRMSE for each transect for along-shore (left) and cross-shore (right) current velocity components. Colour denotes the model and marker shape denotes the transect (marker shapes repeat due to a limited number of shapes). 97
Figure 55. Distribution of the kinetic energy of the model current for SSS150 and SF30 vs kinetic energy of the observed current integrated over each transect for the along-shore (left) and cross-shore (right) components. Colour denotes the model and marker shape denotes the transect (marker shapes repeat due to a limited number of shapes). 97
Figure 56. Observed and model SST at Fraser River Water Quality Buoy. 98
Figure 57. Observed and model temperature and salinity for moored CTD at SEVIP station. Daily series are shown for CIOPS-W and SS500 and hourly for SSS150. 99
Figure 58. CTD profiles (red dots) and subregions (outlined with solid black lines) used for the analysis. 100
Figure 59. CTD comparison for region Strait of Georgia South. 101
Figure 60. CTD comparison for region Lower Fraser. 102
Figure 61. CTD comparison for region Massey to Annacis. 103
Figure 62. CTD comparison for region Port Mann. 104
Figure 63. CTD comparison for region Upper Fraser. 105
Figure 64. Hovmöller diagram for temperature measured along the BC Ferries Tsawwassen-Duke Point route. Top panel shows the observed temperature, and the lower three panels show the model errors for CIOPS-W, SS500 and SSS150, respectively. Units are degrees Celsius, and the Tsawwassen end of the route corresponds to the top of each panel. 106

Figure 65. Hovmöller diagram for salinity measured along the BC Ferries Tsawwassen-Duke Point route. Top panel shows the observed salinity, and the lower three panels show the model errors for CIOPS-W, SS500 and SSS150, respectively. Units are PSU, and the Tsawwassen end of the route corresponds to the top of each panel. 107

Figure 66. Map of the observed drifter tracks for the two drifter types (OSKER and SCT) used in the experiment. 108

Figure 67. Mean Molcard instantaneous score over drifters. The shaded region shows ± one standard deviation....109

Figure 68. Mean separation distance over drifters. The shaded region shows ± one standard deviation....110

Figure 69. Forecast evaluation for non-tidal water level at Sand Heads. 111

Figure 70. Forecast evaluation for non-tidal water level at StevestonEC. 112

Figure 71. Forecast evaluation for non-tidal water level at Woodward's Landing.....113

Figure 72. Forecast evaluation for non-tidal water level at Pitt River.....114

Figure 73. Forecast evaluation for horizontal currents at the Woodward’s Landing HADCP in Fraser River. 115

Figure 74. Forecast evaluation for sea-surface temperature at Fraser River Water Quality Buoy. 116

ABSTRACT

Canada's Oceans Protection Plan (OPP) was launched in 2016 to support initiatives aimed at protecting our marine environment from anthropogenic pressures. To this end, the Improving Drift Prediction and Nearshore Modelling sub-initiative of OPP developed six high-resolution port-scale hydrodynamic models, to improve safe navigation, and provide operational emergency response to events such as marine oil spills. The models were downscaled from the Coastal Ice-Ocean Prediction Systems East and West (CIOPS-E, CIOPS-W). Atmospheric forcing was provided by the High-Resolution Deterministic Prediction System (HRDPS). Model performance is assessed against available observational data and contrasted with the parent model using a multi-year hindcast. Evaluations of 48-hour forecasts are performed during a two-month period.

This document reports on the performance assessment for the Fraser River model (SF30) and the southern part of the South Salish Sea model (SSS150). SF30 domain covers Fraser River South Arm from Steveston to Port Mann with the horizontal resolution of 30 m and adjacent parts of Sturgeon and Roberts Banks, while SSS150 covers the southern part of Salish Sea and the Fraser River to Mission and to Pitt Lake. All model runs were completed without stability issues including periods of extreme weather events and real-time instrument failure.

Results show that the high-resolution models provide either similar or better performance than the lower-resolution models in the areas where they overlap and have adequate performance in the areas not covered by the low-resolution models. The tidal water level error ranges from 5 to 9 cm CRMSE, while the non-tidal water level error is consistently 5-6 cm CRMSE with biases within 6 cm, which brings the total water level error to an order 10 cm.

Both tidal and non-tidal current velocity is captured well with a total error of about 0.25 m/s when compared with the observed horizontal ADCP velocities at Woodward’s Landing. The cross-shore structure of the flow in the Fraser River compares well with the data from ship-mounted ADCPs with a slight underestimation of the outflow velocities.

Surface water temperature in Fraser River has a cold bias of less than 0.5 °C and errors of order 1.1 °C. Vertical distribution of temperature and salinity is represented well and on par with Salish Sea 500 model (SS500).

Drift performance is significantly improved in the high-resolution models relative to SS500.

The forecast evaluation showed that non-tidal water level error increased gradually with forecast lead time as expected.

1. INTRODUCTION

Under the Improving Drift Prediction and Nearshore Modelling (DPNM) sub-initiative of Canada's Oceans Protection Plan (OPP), high-resolution models were developed for six Canadian ports and their approaches to enhance the Government of Canada's ocean modelling capabilities in support of environmental protection and marine safety applications (e.g., drift prediction for oil spills) and safety for navigation via a hydrographic e-navigation application. The six ports (three on the east coast and three on the west coast) were selected as at-risk for environmental incidents owing to their high tanker traffic and complex navigational needs. Models have been developed for the west coast ports of Kitimat, Lower Fraser River and Vancouver Harbour, and for the east coast ports of Saint John, the Strait of Canso, and the St. Lawrence estuary.

The models have been developed with both hindcast and forecast capabilities. For each port, a multi-year hindcast is presented with model validation against observations of water levels, velocities, temperature and salinity, as well as a drift experiment conducted using available drifters. Forecast performance is assessed over a two-month period.

The purpose of this document is to review the performance of the model for the Lower Fraser River. The design is common to all port models and is presented in Section 2, while Section 3 describes the specifics of the Lower Fraser River port model. The evaluation parameters used to evaluate all models are detailed in Section 4, and Sections 5 and 6 respectively analyze the long hindcast evaluation results and the forecast evaluation results. The performance of the Lower Fraser River port model is summarized in Section 7, and the main key findings are listed in Section 8.

2. PORT MODEL DESIGN

The port models ("port ocean prediction systems," or POPS) follow a common structure designed to constrain system complexity. We use the same ocean general circulation model and code version, downscaling strategy, preprocessing tools, surface forcing product, and automation suite for all six POPS. The model grids, configuration/tuning, open boundary forcing, and freshwater input sources differ between POPS configurations.

2.1. MODEL SELECTION

The precursor to much of the OPP port modelling effort was conducted using the Finite Volume Community Ocean Model (FVCOM) (Chen et al. 2003) under the World Class Tanker Safety System (WCTSS) program, yielding prototype models for ports of Canso, Kitimat, and Vancouver Harbour. Even earlier, there have been modelling efforts based on Backhaus (Backhaus 1983; 1985) yielding models for the St. Lawrence estuary (Saucier and Chassé 2000) and the Gulf of St. Lawrence (Saucier 2003). These were then followed by implementation of an equivalent NEMO model by Environment and Climate Change Canada (ECCC), the Regional Marine Prediction System (RMPS) GSL. The RMPS was operational from 2011 to 2021, though none of these earlier models were considered for use in OPP. The WCTSS FVCOM prototypes used unstructured model meshes to resolve the coastal regions to within tens of metres or less, with resolution gradually decreasing to kilometres to match the parent model grid on the open boundary.

FVCOM has no history of operational deployment in Canada, while NEMO 3.6 (Nucleus of European Modelling of the Ocean) is used operationally by the Canadian Operational Network for Coupled Environmental PredicTion Systems (CONCEPTS). In the early part of OPP, a

comparison exercise between FVCOM 4.1 and NEMO 3.6 (Nudds et al. 2020) informed the decision-making process to select which codebase to use for the POPS models. Both codebases were used to construct models of the Bay of Fundy and the Port of Saint John (Paquin et al. 2020), which was chosen due to the large tides and complex circulation. NEMO 3.6's most significant deficiency in this context is the lack of wetting and drying, so if NEMO 3.6 could provide satisfactory results in the Bay of Fundy, then it would likely be suitable for use in the other regions. The two models were evaluated on how well they matched observations, as well as on computational efficiency, stability, and robustness. Both models were found to be skillful at reproducing observed data: neither model was significantly superior, and the choice of model to use going forward rested more heavily on the other factors.

Ultimately the decision was taken to proceed with NEMO 3.6, despite its structured grid, a somewhat coarser nearshore resolution, and higher demand for computational resources, to facilitate operationalization and align with modelling efforts at ECCC. Additional advantages of NEMO include active development that delivers regular code updates and bug fixes, an international NEMO Consortium group where members steer code development, and a well-established international operational modelling community.

Thus the ocean model used for all port ocean prediction systems is the CONCEPTS code: a fork of NEMO 3.6 (Madec 2016) that has been customized to meet the operational needs of CONCEPTS, for example (Dupont et al. 2015).

2.2. DOWNSCALING STRATEGY

The port models are downscaled solutions driven by larger-scale coastal ocean models currently operational at ECCC: the Coastal Ice-Ocean Prediction Systems East and West (CIOPS-E, CIOPS-W; Paquin et al. 2021a; Paquin et al. 2021b) which have 2-2.5 km resolution, and Salish Sea 500 (~500 m resolution; hereafter SS500) which is part of the CIOPS-W system. Output from these models forms the boundary conditions for our higher-resolution, smaller-area models. We use two levels of nesting to achieve a resolution fine enough to reach port scale. The nesting is one-way (coarse to fine), so no information is fed back to the larger scale models, allowing the models to run sequentially but otherwise independently of each other. This one-way nesting strategy also enables systematic errors to be corrected at the open boundaries.

We do not employ a dynamic ice model. Instead, we use a NEMO feature called "ice if", which uses input ice fields and the local freezing point to assess where ice cover exists, and in those locations it restores the sea surface temperature to the local freezing point and sets heat fluxes to -4 Wm^{-2} (Madec 2016).

We do not employ data assimilation or spectral nudging; all model runs are free runs.

River discharge data is used where available to supply the most realistic freshwater input to the model, and climatology is used when this is not available. Gauge data is also used in some cases to construct water level boundary conditions.

2.3. SIMULATION SEQUENCING

The port models operate in three configurations: hindcast, pseudo-analysis and forecast. Hindcasts are the most straightforward, using larger-scale model forcing and quality-controlled gauge data to drive the models. The model begins in the past from a cold-start (temperature and salinity interpolated as initial conditions, water at rest) or a hot-start (temperature, salinity, velocity, and sea-surface height interpolated as initial conditions) and reaches a spun-up state after a period of adjustment to the forcing. The model output is considered usable once spun up, and the model can run nearly up to the present in this configuration, provided that forcing data is

available. Pseudo-analysis runs are daily runs that keep the model state caught up to near-real-time, and do not include a direct data-assimilation component. Rather, the state is indirectly driven by data via boundary and surface forcing terms. These runs are used to initialize the first forecast of each day and may use different input than hindcasts depending on what data is available in real-time.

The pseudo-analysis and forecast schedule is chosen to match the schedule of the parent models that we use for forcing. Shortly after 00Z each day, a 24-hour pseudo-analysis simulation runs to catch up the model state to 00Z. This process uses restart files (so no spin up needed) and, where possible, uses gauge data drawn from a near-real-time data feed which receives limited quality control. Following the pseudo-analysis, the POPS generates four forecasts per day, each 48 hours long, which start from 00Z, 06Z, 12Z and 18Z. The daily 00Z forecast starts using the restart file from the daily pseudo-analysis and runs for 48 hours, saving a restart file six hours into the simulation. The 06Z forecast starts from this restart file, also saving a restart file six hours in, and similarly for the 12Z and 18Z forecasts. A schematic of this setup is shown in Figure 1. We focus only on the 00Z forecasts in this evaluation.

While the 00Z forecast simulation is nominally started at 00Z each day, in practice, the initialization of the simulation is delayed as it can not begin until all inputs are available from the larger scale models and the pseudo-analysis completes. At time of writing, this delay is approximately 5 hours, such that upon completion, each forecast simulation has about 43 hours of output that is in the future.

2.4. SURFACE FORCING

Surface forcing is derived from the High-Resolution Deterministic Prediction System (HRDPS) (Milbrandt et al. 2016) that runs operationally at ECCC and provides atmospheric weather forecasts four times per day at 2.5 km resolution. This is the highest-resolution operational atmospheric product available and is chosen to be consistent with the forcing used in CIOPS-E/W. In hindcast and pseudo-analysis mode, we use a time-blended form of the HRDPS forecasts, where hours 06–17 from successive forecasts are combined using weighted averaging to form temporally continuous fields with the same blending schedule as CIOPS-E/W. Additional details are given in the technical documentation for CIOPS-W version 1.5 (Paquin et al. 2022). Time blending is not used for forecasts.

The surface forcing is applied to the NEMO model using the CORE algorithms (Large and Yeager 2004) with modifications by ECCC to (a) read input data from the in-house RPN file format and (b) use the lowest diagnostic level of the atmospheric model rather than the conventional 2 m and 10 m data. Precipitation and sea-level pressure variations are also applied to the surface of the model.

2.5. AUTOMATION SUITE

The hindcast, pseudo-analysis and forecast simulations are all managed using ECCC's Maestro sequencing software. We have constructed a Maestro suite that is based on ECCC's CIOPS-E/W suites, where we use some of ECCC's functionality for the atmospheric forcing preparation and the mechanics of running the NEMO model, including managing restart files and outputs. We augment this baseline with functionality to prepare boundary forcing, extract data from the real-time data feed, generate the runoff forcing and prepare ice-concentration input files for the "ice-if" feature. Fallback strategies for missing data and persistence strategies for forecasts using gauge data are also implemented here.

2.6. ROBUSTNESS AND LIMITATIONS

For an operational model to be useful, it must be robust and not prone to failure. We have not assessed the models exhaustively in this regard; such testing is an ongoing process. However, some aspects have been explored:

- Where gauge data is needed as a model input, fallback mechanisms are implemented to mitigate missing or bad gauge data. Typically, this means we prepare a climatology for each gauge to stand in when the gauge data is unavailable. With these prepared ahead of time and with appropriate tooling to automate the switchover, the models can run despite missing gauge data and experience a graceful degradation through forcing with lower-quality data rather than a failure. Measuring the severity of the degradation under data-loss scenarios is reserved for future work.
- A long hindcast is conducted for model performance assessment. This long simulation demonstrates that the model is stable subject to a multi-year sample of weather/forcing conditions. In some cases, the hindcast period samples some extreme events, which helps bolster the case for model stability.
- Daily demonstration simulations (pseudo-analysis and four forecasts) have run for order one year on the General Purpose Science Cluster (GPSC) on a best-effort basis, to show that the automation suite can run the models routinely and reveal edge cases that can be fixed to improve robustness further. The purpose of running these pre-operational, best-effort simulations is to demonstrate the functionality/stability of the NEMO-based numerical model and the driving automation suite and identify issues that would impact operational deployment. The dominant source of issues experienced that impede on-schedule daily forecasts are (a) GPSC compute system downtime, both planned and unplanned, and (b) lack of availability of the forcing data from the larger-scale models that are nominally mirrored on schedule from ECCC's systems. These issues are deemed an expected consequence of using a research cluster and would be mitigated using an operational cluster.

The models will have some limitations:

- Intrinsic variability is expected in each model, and this has not been characterized.
- The lack of wetting and drying capability in NEMO 3.6 requires artificial bathymetry deepening in intertidal regions.

3. FRASER RIVER

This section describes the South Fraser 30 m resolution port ocean prediction system.

3.1. REGIONAL OCEANOGRAPHY

The Fraser River is the largest single source of freshwater runoff on the British Columbia coast, with a typical discharge at Hope (150 km from the river mouth) of 900-1100 m^3/s during the December to March period and a freshet from May to July with an average peak discharge of approximately 7000 m^3/s in June. The study area extends to Mission and includes tidal Pitt Lake connected with Fraser River via Pitt River (Figure 2). Due to active tidal exchange with the ocean, a saltwater wedge is formed in the river, which can extend to Annacis Island (Thomson 1981).

Fraser River model development under OPP aims at providing a forecasting tool which would aid navigation and emergency response in addition to the existing prediction systems, (e.g. Avadepth).

3.2. DOMAIN AND CONFIGURATION

The model downscaling setup for the Fraser River model includes an outer and inner grid as shown in Figure 2 which are called South Salish Sea 150 (hereafter SSS150) and South Fraser 30 (hereafter SF30), respectively. The SSS150 grid is a refinement of the tri-polar global grid (Madec and Imbard 1996) and thus shares the same local grid rotation. The outer grid has an approximate resolution of (dx, dy) = (129, 98) m and has three open boundaries: along the west, reaching from the west side of Howe Sound to the north end of Galiano Island; along the south reaching from the same north end of Galiano Island to Point Roberts; and at the east on the Fraser River at Mission.

The inner grid covers approximately 30 km of the Fraser River South Arm downstream from the Port Mann Bridge, where the Port of Vancouver terminals are located and most of the large ship traffic occurs. It also includes parts of Sturgeon and Roberts Banks adjacent to the river mouth. The domain includes the main reach with a typical width of 500 m and typical depths of 12-20 m and several deeper places where the depth reaches 25-30 m. The maximum depth is 32 m, some 200 m downstream of the Alex Fraser Bridge. Except for the river channel extension, the depths on the bank are small and were set to a minimum depth of 4 m for modelling purposes. After the fork at New Westminster the main river channel includes several large islands: Annacis, Tilbury, Deas, Kirkland, and Westham. The grid has open boundaries on each side: An upstream open boundary near the Port Mann bridge, an open boundary along the Fraser's north arm near the east end of Mitchell Island, and a broad open boundary on Roberts Bank that forms the ocean connection to the SSS150 model. The inner grid is not a refinement of the parent grid and thus does not share the same local grid rotation as SSS150.

We employ one-way nesting for downscaling from the SSS150 model, where the setup and forcing of SSS150 is discussed in (Dunphy et al. In press) and as such this document focus primarily on the SF30 domain.

The bathymetry is assembled primarily from the Canadian Hydrographic Service (CHS) data that has been shifted to Canadian Geodetic Vertical Datum of 1928 (CGVD28) (Mitchell O'Flaherty-Sproul, pers. comm.) and patched where available with the most recent bathymetry survey data actual as of May 2020. The high-water coastline (CHS pers. comm.) was used as part of the bathymetry dataset (with local high-water values shifted to CGVD28) and as a polygon for land mask calculation. We impose a minimum depth of 4 m to ensure model stability at low tide as NEMO 3.6 does not have a wetting & drying formulation, which has the impact of artificially deepening inter-tidal areas. The vertical grid uses z-levels with both partial cells and a variable volume formulation (Levier et al. 2007) such that the grid spacing stretches and compresses as the water level rises and falls. The nominal vertical grid spacing in SF30 is inherited from SSS150, which inherits it from SS500, a component of the CIOPS-W v2.0.0 system (Paquin et al. 2021b) and ranges from 1 m near the surface to 11 m at depth in SF30 and to 27 m in SSS150.

Table 1 lists the grid parameters and key NEMO settings used for each grid.

To contrast the resolution of the models, we plot in Figure 3, Figure 4 and Figure 5 the surface layer speed for three levels of zoom. At Figure 3 we see that CIOPS-W does not resolve the Fraser River at all and SS500 coarsely resolves it up to roughly the Pitt River fork with 1-3 grid cells across the river. Meanwhile, SSS150 resolves the river up to Mission and Pitt Lake. Boundary Bay is excluded from the SSS150 model.

Figure 4 shows the same surface speed but dropping CIOPS-W and adding SF30 panels. Here we see that SSS150 does a better job at capturing details and begins to capture cross-river structure with 4-6 grid cells across in the narrow parts. At SF30 we have reached high enough resolution to resolve cross-river structure with 15-20 grid cells. Figure 5 shows a zoom of Figure 4. Note that due to the lack of wetting and drying in NEMO 3.6, tidal flats (intertidal areas) are poorly represented across all four models; we aim to improve upon this in a future revision with wetting & drying included.

Lastly, we note that the resolution of these grids is considerably higher than that of the surface forcing (2.5km). This relatively coarse surface forcing product is unlikely to resolve the differences between over land and over water at the scale of the river, in particular for the wind forcing. We expect the POPS to benefit from higher resolution atmospheric products as they become available.

3.3. INITIALIZATION

The SF30 model initial conditions are interpolated from SSS150 on 2016-12-24 to hot-start the model, where the SSS150 initialization is described in (Dunphy et al. In press). We allow several days for SF30 spinup and consider output from 2017-01-01 onward for evaluation.

3.4. OPEN BOUNDARY CONDITIONS

The SF30 boundary conditions are supplied from snapshot data saved from SSS150 at a 15-minute update frequency. The barotropic mode uses a Flather-type condition (Flather 1976), and the baroclinic velocity and tracers use the flow relaxation scheme (Martinsen and Engedahl 1987). The rationale for a 15 min snapshot frequency is to mitigate tidal peak shaving that otherwise occurs with hourly forcing. No tidal adjustments or offsets are applied at this model connection and there is no discontinuity at this boundary.

3.5. FRESHWATER INPUT

Freshwater is input to the SSS150 model as described in (Dunphy et al. In press). No additional freshwater sources are used in the SF30 model.

3.6. ICE MODEL

The Lower Fraser River is not known for freezing over during the winter, although on rare occasions, it does form river ice for short periods. However, for the lack of data to validate an ice model, we have configured this model to use NEMO’s ice-if feature with an empty ice climatology in lieu of a dynamic ice model.

3.7. MODELLING SYSTEM STABILITY

Model stability for SSS150 is outlined in (Dunphy et al. In press), where the authors note a long 5-year hindcast run and a series of forecasts without any stability issues. Several extreme events during the hindcast period, including a severe flood, periods of freezing temperatures during which an ice cover was formed in the Fraser River, and periods of instrument outage provided natural stress testing opportunity. The modelling system performed as expected during those extreme events, and the runs remained stable. Similar arguments apply to SF30. As in the case of SSS150, systematic stress testing is reserved for future work.

4. EVALUATION METRICS

The model performance is assessed through the analysis of a multi-year hindcast and a shorter set of forecasts, where the dates considered are constrained by available surface and boundary forcing from larger scale models. The hindcast evaluation uses a wide set of observations to analyze the model's representation of ocean conditions, including tidal analysis and model drift that would be difficult to assess on a short model run. Meanwhile, the forecast evaluation focuses on measuring the degradation of model skill as a function of forecast lead time for a smaller set of observations available during the forecast period.

Quality controlled data sources were preferred where possible. We performed additional quality control to some data as needed, including visual inspection, thresholding and automatic de-spiking to eliminate suspect data.

4.1. HINDCAST

Hindcast performance is assessed through comparison with available observational data. For each observation, we extract the corresponding virtual observation from the model. The error is defined as

$$\text{ERROR} = \mathcal{X}_m - \mathcal{X}_o ,$$

where $\mathcal{X}_o$ and $\mathcal{X}_m$ are the observed and modelled values such that a positive/negative value indicates a model over/underestimate. For currents, $\mathcal{X}_o$ and $\mathcal{X}_m$ are taken as complex numbers with the real part representing the eastward and imaginary the northward components of velocity.

We use several scores, the bias, the centered root mean square error (hereafter CRMSE) and the root mean square error (hereafter RMSE),

$$\text{bias} = \frac{1}{N}\sum \text{ERROR} = \frac{1}{N}\sum \mathcal{X}_m - \frac{1}{N}\sum \mathcal{X}_o = \overline{\mathcal{X}_m} - \overline{\mathcal{X}_o} ,$$

$$\text{CRMSE} = \sqrt{\frac{1}{N}\sum (ERROR\text{-}bias)^2},$$

$$\text{RMSE} = \sqrt{\frac{1}{N}\sum ERROR^2} = \sqrt{bias^2 + CRMSE^2},$$

and these measures retain the units of $\mathcal{X}$.

We also use the unitless gamma squared score,

$$\gamma^2 = \frac{CRMSE^2}{\sum(\mathcal{X}_o - \overline{\mathcal{X}_o})^2},$$

which is the ratio of error variance to observed variance, such that zero indicates perfect agreement between model and observation variance, and unity indicates error variance is as large as the signal variance. A value of unity or larger indicates no skill.

For scalar quantities, we use the unitless sample Pearson correlation coefficient score,

$$\text{PEARSONR} = \frac{\sum (\mathcal{X}_m - \overline{\mathcal{X}_m})(\mathcal{X}_o - \overline{\mathcal{X}_o})}{\sqrt{\sum (\mathcal{X}_m - \overline{\mathcal{X}_m})^2 \sum (\mathcal{X}_o - \overline{\mathcal{X}_o})^2}},$$

where zero indicates no correlation and unity indicates perfect correlation. For vector quantities (currents) we have the vector correlation coefficient (Kundu 1976; Röhrs and Christensen 2015)

$$\text{VECTORR}=\frac{\sum(x_m-\overline{x_m})^{*}(x_o-\overline{x_o})}{\sqrt{\sum(x_m-\overline{x_m})^{2}\sum(x_o-\overline{x_o})^{2}}},$$

where the asterisk represents complex conjugation, which is also implied for squaring of complex numbers. This quantity is a complex number, where the magnitude measures the overall correlation and the angle is a measure of the average angle of the modelled current with respect to the observation. Here we compute the angle as positive clockwise to be consistent with the convention of representing the velocity direction as positive clockwise from North. Lastly, the vector correlation angle is only considered meaningful when the correlation magnitude is large (Kundu 1976).

4.1.1. Water level

Water level observations from the Canadian Hydrographic Service (CHS) are transformed from CHS Chart Datum to Canadian Geodetic Vertical Datum of 1928 (CGVD28) by subtracting a station-specific offset. CHS provides these offsets are based on measurements from a GNSS (Global Navigation Satellite System) occupation at each station. Pacific US stations are shifted from the US datum to CGVD28 via NOAA's VDatum and NRCan Vertical Datum Transformations online tools. Atlantic US stations were gathered with a mean low-low water datum and converted to CGVD28 using conversion surfaces provided by CHS. Water level observations from the Water Survey of Canada (WSC) are shifted to CGVD28 using offsets provided by WSC.

Tidal analysis is performed using T_TIDE on one-year segments at an hourly sampling interval. Where data is available at a higher frequency, it is interpolated/subsampled to hourly frequency. Observations missing more than 10% of the data points are not detided. The tidal analysis enables the decomposition of the total water level into tidal and non-tidal parts as

$$H_{total} = H_{tidal} + H_{nontidal}.$$

The annual (SA) and semi-annual (SSA) constituents are excluded from the tidal analysis; these constituents are subsumed into the non-tidal component. For the present purpose this is adequate as the same process is applied to both model and observations, and the extent to which the models do not reproduce SA or SSA is captured in the non-tidal error scores. Constituents with signal-to-noise ratios below 2 are also subsumed into the non-tidal part. Water level bias is included in the non-tidal component. Scores are reported for the total, tidal and non-tidal components. Owing to a negligible cross-correlation between tidal and non-tidal water levels, to a good approximation, we have

$$\mathrm{CRMSE}^2_{total\,wl} \cong \mathrm{CRMSE}^2_{tidal\,wl} + \mathrm{CRMSE}^2_{nontidal\,wl},$$

which shows how these two errors contribute to the total. Amplitude and phase errors are reported for the significant constituents, as is the tidal error,

$$\text{TIDAL ERROR} = \left[\frac{1}{2}({h_o}^2 + {h_m}^2) - h_o h_m \cos(\phi_o - \phi_m)\right]^{\frac{1}{2}},$$

where h_o and ϕ_o are the observed (subscript *o*) amplitude and Greenwich phase lag for a given tidal constituent, while h_m and ϕ_m are the modeled (subscript *m*) amplitude and phase (Cummins and Oey 1997).

4.1.1.1. Storm surge evaluation

To evaluate the port models' performance during storms, a handful of stormy periods are selected for each port. The cyclone database of (Zhang et al. 2019), which provides global

storm tracks from 1958 to 2021 (Figure 6 shows a zoom of North America), guides the selection. The database was queried for storms passing within a few hundred kilometres of each port model domain, and it provides a comprehensive list of storm events during the hindcast period. However, this list is quite extensive for some ports (particularly Canso and Saint John), so longer lists are narrowed down by considering minimum central pressure, examining water level gauges, and local media reports of storm impacts. The evaluation follows the residual water level hindcast evaluation in terms of performance scores and plots but is limited to the storm periods.

Storm surge detiding is done using a 40-day window around the storm's peak, i.e., 20 days before to 20 days after. This differs from the typical water level analysis, which is done in yearly spans and as such can include more constituents. However, using a shorter window does a better job removing the tides during each storm, particularly in areas with non-stationary tides.

We note that storm surges may interact non-linearly with tides to impact water levels, but we do not investigate this phenomenon here.

4.1.2. Water velocity

Velocity data is available from ADCPs and some current metres in one of four configurations: mounted on a mooring, buoy mounted (i.e., floating), in a float towed by a ship, or horizontally mounted on a shore structure (HADCP). Only horizontal (east-west / north-south, u/v) velocities are considered here. The horizontal velocity's u/v and speed/direction decompositions are both considered, and directions are calculated as positive clockwise from north.

Model data is extracted to match the observed data's time span and spatial location. Time series longer than 29 days and with less than 10% of data points missing are detided using T_TIDE; hourly data is used for detiding, and where more frequent data is available, it is first down sampled. As with water level, the SA and SSA constituents are excluded from fitting, a Rayleigh value of 2 is used, and the observations and model data are processed the same way.

Currents are noisier, tend to have more missing data, are less stationary, and are impacted by more non-linear processes than water level observations, and these factors make the detiding process less robust. Owing to nonlinear processes such as bottom friction, some tidal (kinetic) energy will spread into adjacent frequencies, so fitting to tidal harmonics does not capture all variability induced by the tides, and some near-tidal variability remains in the residual velocities. We do not apply low-pass or band-stop filters to the residual to reduce the noise. While doing so would provide a more completely de-tided residual time series, some of the total signal would be unaccounted for by either the tidal or non-tidal evaluation. Given these caveats, the tidal component may be more accurately described as "the component of the currents that T_TIDE is able to fit." Currents are evaluated using similar metrics to water level, using complex formulations. Tidal constituents are evaluated using the ellipse error (Cummins and Thupaki 2018).

$$D_u = \left[\frac{1}{2}(A_o^2 + B_o^2 + A_m^2 + B_m^2) - \cos(g_o - g_m)\cos(\theta_o - \theta_m)(A_o A_m + B_o B_m) - \sin(g_o - g_m)\sin(\theta_o - \theta_m)\,(A_o B_m + A_m B_o)\right]^{1/2},$$

where A and B are semi-major and semi-minor axes, respectively, the subscripts *o* and *m* correspond to observed and modelled, g is phase, and θ is angle of inclination. For the non-tidal and total time series, complex formulations of the metrics listed at the beginning of the section are used, including bias, CRMSE, γ^2, and vector correlation.

We note that for single-location instruments, in particular moored current meters and moored and horizontally mounted ADCPs, we expect the scoring to be sensitive to the details of the model run under evaluation. Small errors in bathymetry can adjust the location of deterministic features (eddies, jets, meanders, etc.) and this can lead to large errors in the scoring. Meanwhile, chaotic internal variability can also affect the location of such features. An ensemble of model runs could help mitigate the latter but is beyond the scope of the current effort.

4.1.2.1. Horizontal ADCPs

HADCP data is decomposed into along- and cross-channel components, and evaluation is done primarily with mid-beam data to avoid edge effects. When a long enough time series is available, a tidal analysis is done as with moored instruments. Time series of the first week of data are plotted, regardless of how long the total time series is, to show the daily variability in the signal and how well the model captures it. Scatter plots are used to show the distribution of speed and direction of the total velocity, and the semi-major axis for the tidal ellipses are compared when feasible.

4.1.2.2. Current meters and moored ADCPs

Current meters report velocity at a single depth, so those velocities are evaluated at instrument-specific depths. For ADCPs on moorings or buoys, a standard set of depths at which to evaluate the velocities is selected on a per-port basis, considering local bathymetry and data availability; for brevity, statistics may be reported only at some depths for each instrument considered. These levels are defined relative to either a nominal surface (i.e., one with no sea-surface height variation) or the time varying sea surface. For regions with ADCPs in relatively deep water without a large tidal range, using the nominal surface is sufficient. For shallow regions and/or those with large tidal ranges, the evaluation is done relative to the time-varying sea surface, using the observed total water depth to process the observations and modelled sea surface to process the modelled currents.

The observations are preprocessed to remove any spurious data points: values larger than 10 m/s are discarded and the data points are resampled if needed to be evenly spaced.

Tidal analysis is done on all timeseries of at least 29 days at depths with less than 10% of the data missing. Tidal ellipses are plotted for the largest tidal constituents, including depth profiles of tidal ellipses for the largest constituents. Time series and histograms are plotted for both the non-tidal and total velocities. Analysis of total velocities only is done for shorter time series or time series with missing data. We note that if data is missing at consistent phases of the tide, then the analyzed results may be aliased, and so time series with substantive regular gaps are not analyzed or presented.

4.1.2.3. ADCP transects

ADCP transects are too short for tidal analysis, so only the total velocities are considered. An along-transect / cross-transect decomposition is used, with a constant angle used for decomposition for the entire transect; this is sufficient as the transects are typically short and straight. Along-transect plots of velocities at depth are used for evaluation. Scatter plots of bias vs CRMSE are also plotted, with the statistics calculated at each physical point and integrated over the transect.

4.1.3. Water properties

Conductivity-Temperature-Depth (CTD) profiles are grouped into manually defined subregions based on the geography of each port domain. This enables an aggregate assessment over areas, including bias and CRMSE as a function of depth for each area. Model results are taken

from the nearest point to the data location and nearest to the observation time. Vertical profiles are interpolated to the model z-levels to bring all data to consistent depths.

Sea surface temperature buoy and moored CTD measurements are evaluated using the bias, CRMSE, γ^2 and Pearson's *r* scores over the evaluation period. Model values are linearly interpolated to observation locations in the horizontal and vertical dimensions. The observed and modelled time series are interpolated to the largest common data interval.

Ferry thermosalinographs are vessel-mounted temperature and conductivity sensors. They provide a measure of near-surface water temperature and salinity by collecting data through one of the vessel's seawater circuits. Model results for comparison with these data are taken from the point nearest to the observed locations both horizontally and vertically and then linearly interpolated to the observation times. Hovmöller plots of observations, model results and differences, plus basic statistics, are used to assess the model performances relating to near-surface water.

4.1.4. Drift

The models' performance in drift trajectory prediction is assessed by comparing the observed tracks of ocean surface drifters with analogous trajectories modelled using the surface currents output by the port models, in combination with wind forcing from the National HRDPS atmospheric forecast. This comparison is done using the drift evaluation tool developed as part of the DPNM sub-initiative, in the OpenDrift configuration (Soontiens and Holden 2024).

Windage on the surface drifters is applied by computing the wind drag coefficient based on the drifters' drag area ratio (Niiler et al. 1995; Daniel et al. 2002; Röhrs et al. 2012; Hourston 2021; Blanken et al. 2021). This coefficient parameterizes the effect of direct wind drag on the parts of the drifter exposed above the water surface and varies with drifter geometry. To account for wave-induced Stokes' drift, an additional 1% of the wind speed is added (Sutherland et al. 2020), and this sum is applied as the windage in the trajectory prediction.

This method of applying windage assumes that currents over the draft of the drifter are known exactly, as are winds directly at the ocean surface. However, in reality, neither of these assumptions is true, since:

1. The representation of surface currents in NEMO is limited by stability restrictions on near-surface vertical resolution and model uncertainty in general; and
2. Wind speed from the HRDPS model is also subject to model uncertainty and given at 10 m where winds are usually ~30% larger than at 1 m but could be as much as five times larger depending on wind speed and atmospheric stability (Smith 1988).

The representation of Stokes' drift as 1% of the wind speed represents a further assumption, as this value was derived by comparing tracks from various types of surface drifters to currents from the Regional Ice-Ocean Prediction System (RIOPS) ocean model and Canadian Arctic Prediction System (CAPS) atmospheric model (Sutherland et al. 2020). As noted in the discussion section of (Sutherland et al. 2020) and references therein, this value can vary widely depending on the combination of ocean and atmospheric forcing, which implies that model uncertainty contributes significantly to the appropriate value here. The authors also note that explicitly including Stokes drift based on a wave prediction system is preferable over parameterization based on wind velocity.

The windage term used here could be optimized by deriving it for each ocean/atmospheric model combination using the procedure in (Sutherland et al. 2020). However, this is beyond the scope of this report: the focus is on improvements to the current forcing for drift simulations

without evaluating the suitability of wind predictions in the port model domains for drift prediction or commenting on the potential utility of a port-scale wave prediction system. The windage parameterization used here is merely intended to provide a consistent, deterministic linkage between modelled currents, winds, and the motion of various drifter types. As considerable uncertainty is associated with this windage term, evaluation of surface currents against observations from ADCPs and current meters is deemed the primary determinant of model suitability for drift prediction, rather than analysis of observed and modelled drifter tracks.

Periods where drifters were active in the model domain are identified, and modelled trajectories are started every hour along the drift tracks. The benefits of starting drift tracks in this manner are to reduce the sensitivity to initial conditions and increase the number of tracks available. However, it means that some drift tracks are not independent and thus the errors may be correlated. Modelled trajectories were computed for a user-specified period of 24 hours or more, where possible. However, in some regions, the majority of the observed drifter tracks were less than 24 hours long, and here a shorter modelled trajectory length was chosen.

Observed drifter tracks were truncated to areas covered by the 'wet' cells of the port model domains to avoid launching virtual drifters in 'dry' parts of the domain where observed drifters are near the shoreline, which may not be precisely resolved. In addition, to facilitate interpolation of starting locations for virtual drifters, observed trajectories were split where time gaps between positional records exceeded two hours. In the remaining portions, positional records were interpolated to a consistent time interval ranging from five minutes to one hour.

For each model – observation pair of trajectories, two statistics are computed to assess the model performance. First is the separation distance, D, which is given by,

$$D(t) = |\dot{x_o}(t) - \dot{x_m}(t)|$$

Here $\dot{x_o}$ and $\dot{x_m}$ are the positions of the observed and modelled drifter, and || denotes the magnitude of the vector difference, i.e., the distance, between them.

Second is the instantaneous skill score, S, following (Molcard et al. 2009), which is given by

$$S(t) \;=\; \max\left(0, 1 - \frac{D(t)}{d_o(t)}\right)$$

Here $d_o(t)$ is the displacement of the observed drifter from the starting point of the pair. The rationale for the normalization by $d_o(t)$ is to increase the skill assigned to a trajectory prediction as the trajectory length increases, even if the separation distance remains constant. A separation distance of, for example, 500 m represents a less grievous error in a trajectory that is 10 km long than in one that is 500 m long. A value of S=1 indicates a perfect prediction.

4.2. FORECAST

The forecast evaluation involves running a set of forecasts (here 48 hours long, each starting at 00Z) and evaluating the performance over the independent forecasts as a function of lead time. Forecast evaluation was performed for a set of about 60 consecutive forecasts by comparing the model values with tide gauge, sea surface temperature and horizontal ADCP records. The set of forecasts were taken from winter 2021/22 for logistical reasons. Forecast performance was evaluated as the discrepancy (bias and CRMSE) with observed values as a function of forecast lead time. The error growth curves represent the discrepancy averaged over the set of evaluated forecasts, and we include 95% confidence intervals computed with a bootstrap method.

To detide the forecast and the corresponding hindcast water level series we subtract the tidal signal precalculated based on the hindcast covering the forecast evaluation period. The tidal

signal is obtained with a T_TIDE fit with a Rayleigh number as low as 0.1 (overfitting) to ensure maximal energy removal at tidal frequencies. Such strong suppression of tidal energy was implemented to clear the error growth curves of any tidal residual, which otherwise would dominate the curve.

5. HINDCAST EVALUATION RESULTS

The focus here is to assess the performance of the SSS150 and SF30 models. Comparisons with results from the larger-scale CIOPS-W and SS500 models are included where possible. However, results from these larger-scale models are available as hourly snapshots for sea level, barotropic currents, surface and bottom currents, and surface and bottom tracers, and available as daily averages for 3D currents and tracers. This lower frequency output of the 3D fields precludes some comparisons (particularly current meter records).

We will also limit the assessment to the southern subset of SSS150 covering an area of the Salish Sea near the Fraser River delta, the Lower Fraser, Pitt River and Pitt Lake. Locations of the instruments used for the present analysis are shown in Figure 7. Locations of instruments used in this evaluation. The double water level markers are Steveston (CHS station) and StevestonEC (WSC station) near the mouth of the Fraser. The green triangle marker represents Woodward's Landing (water level and HADCP) while the blue marker below it represents Deas Island.. The rest of the domain covering Howe Sound and English Bay with the adjacent part of the Salish Sea and Burrard Inlet is assessed in (Dunphy et al. In press).

The hindcast evaluation period spans five years, from 2017-01-01 through 2022-01-01. The SSS150 and SF30 results are saved as snapshots at hourly intervals to enable comparisons that employ tidal analysis.

5.1. WATER LEVEL

We evaluate the water level performance using the water level stations listed in Table 2. We have water level data for our hindcast period for the first nine stations and constituents computed from records of at least 365 days in length for four additional stations. The station list begins from the water level gauge in the North Arm and then is ordered west to east from Roberts Bank and progresses up the Fraser River. An offset of 12 cm was added to the water level output from CIOPS-W and SS500 models to bring them approximately to the CGVD28 datum.

5.1.1. Mean sea surface height

Figure 8 shows a long-term mean water level obtained from the model run for 2017 to 2021. From approximately 0.12 m at the western (oceanic) boundary it rises along the river channel to 0.8 m at the upper (eastern) boundary of the SF30 domain.

5.1.2. Tidal water level

Tidal constituents are evaluated at each station (Table 2) for 15 tidal constituents in Table 3 through Table 17. We compute the observed amplitude and phase via T_TIDE (Pawlowicz et al. 2002) from 2018 water level data for the first nine stations. The last four values are from historical data provided by the Canadian Hydrographic Service (CHS).

The model amplitudes and phases are computed from a one-year long series for the simulation year 2018 and presented as amplitude, phase and total tidal errors with respect to the observed values. Values appearing as 0.000 result from including only three decimal places in our

analysis but should not be considered precisely zero. All tidal constituents that are resolved for a one-year long series with Rayleigh criterion of 1 are included in the tidal analysis.

The CIOPS-W results are included for completeness, although this subsection focuses on the tidal representation of the SSS150 and SF30 models. Here we aim to show that the constituents are well represented and are comparable to or better than SS500 at common stations. To that end, the tidal error is the most revealing score and will receive the most attention.

The first eight constituents presented, M2, N2, S2, K2, O1, K1, P1, and Q1, are included in the forcing of the larger-scale models CIOPS-W & SS500 and the fits to these are coherent. The remaining seven constituents, L2, J1, NO1, OO1, SO1, NU2, and 2N2 are not part of the CIOPS-W & SS500 open boundary forcing. These constituents may be weakly introduced through another mechanism in those models (such as by non-linear generation within the domain where such a pathway exists) or they may be artifacts of the fitting process. We include them in the tables to contrast with the higher-resolution models where these constituents are forced.

M2 tidal error mostly stays within 7 cm for all models and across all stations with amplitude errors within 6 cm and phase errors within 7° (Table 3). Exceptions are SS500 for the upper river stations and SSS150 and SF30 for Deas Island. SF30 performs well and stays within 1 cm of error from the best performing model for each station. SS500 is best at the outside stations, Steveston and the four historical tide gauges and Deas Island, which confirms that the tides were rigorously tuned in this model for the outer stations. SSS150 is best at North Arm, Sand Heads, New Westminster and Port Mann and SF30 at Woodward's Landing. SSS150 has well tuned amplitudes (best or close to best of all models), but the phase is off by 5 to 6° for Steveston, producing a higher total error than for SS500.

All models perform similarly for K1 (Table 8). Tidal error for this constituent does not exceed 7 cm for all models except CIOPS-W. Amplitude errors are within 3 cm, and phase errors are within 4°. The rest of the constituents included in all four models have similar error distributions.

From the constituents included only in SSS150 (and inherited by SF30), L2, J1, NU2 and 2N2 are represented by those models adequately, while OO1 and SO1 have phase errors of 15-30° and NO1 has phase errors of 50-70 °. This suggests that SSS150 could benefit from more tidal tuning in the Fraser River for these constituents.

Figure 9 and Figure 10 summarize progression of amplitude and phase for M2 and K1, respectively, from the outer to inner stations and show correspondence between the observed and the model values. These plots show that the tidal wave in the high-resolution models propagates up the river with the correct speed (good phase correspondence) with a slightly stronger dampening (slight amplitude underestimation at the upper stations).

The non-tidal water level (middle panels in Figure 11 through Figure 19) shows that, at all stations, tides exhibit some degree of non-stationarity, which is reflected in a higher tidal residual during the freshet in the second half of May, 2018. River stage is a primary factor influencing tides in the river, and stage fluctuations during the freshet are observed as low as Steveston. However, tides seem non-stationary even at the outermost station, Sand Heads, where the stage fluctuations during the freshet are negligible.

Power spectra of the water level at an outer station (Sand Heads) and a station further up the river (Port Mann) are shown in Figure 20 and Figure 21, correspondingly. The total water level spectra (the upper left panels) show that both tidal and lower frequency oscillations are captured in all models. The lower panels of those figures show that the high-resolution models have lower errors, particularly in the tidal bands. A higher residual energy level in tidal bands at Port Mann as opposed to Sand Heads (upper right panels in Figure 20 and Figure 21) confirms that the

tides become less stationary as we move upriver. A non-stationary tidal analysis tool, NS_TIDE (Matte et al. 2013), would be better for analyzing tides in the river and will be considered in future.

Despite interannual variations in the stage, major tidal constituents are stable over the years, with K1 amplitudes varying within 2.5 cm and phases varying within 2° and even less for M2 (not shown).

5.1.3. Non-tidal water level

Figure 11 through Figure 19 show the non-tidal water level comparisons for each model. SSS150 and SF30 track each other closely, with CIOPS-W performing similarly for the outermost stations. SF30 has a slightly lower error than SSS150 for two upper stations, New Westminster and Port Mann. SS500 differs from the three. For both Steveston stations, SS500 captures variability during freshet time noticeably better than the rest of the models. However, for all other stations, SS500 does considerably worse and particularly during the freshet. Outside of the freshet time, the errors are mostly within 10 cm except for Sand Heads and Steveston (Figure 12 and Figure 13, correspondingly), whose errors correspond with the offsets found above.

5.1.4. Overall scores

We show three score tables that compare the performance of each model for each station for the year 2018, where missing entries in the table are due to stations not residing in the model domain or missing or unusable data.

Table 18 shows the tidal water level scores for the year 2018 for three scores. Here, scores generally improve with the increase in model resolution. For example, SF30 has CRMSE of 5 to 6 cm consistently over the outer stations, gradually increasing for stations further up the river and reaching 10 cm at Port Mann. Deas Island is an exception (likely due to many missing data) with CRMSE of 14.7 cm for SF30 and SS500 providing better scores here.

Table 19 shows the non-tidal water level scores for the year 2018 for three score types. Here, SS500 has best correspondence with the observed data at both Steveston gauges, while SSS150 and SF30 show better scores for all other stations with SF30 outperforming SSS150 at the stations in the upper part of the river and showing CRMSE of 5-7 cm consistently over most of the stations.

Table 20 summarises the total water level scores for the year 2018 for four score types. Bias for SSS150 and SF30 is 1-3 cm with SSS150 showing slightly lower bias for most of the stations. Woodward's Landing and stations further up the river are not covered by CIOPS-W and are poorly resolved in SS500 producing poor scores. Anomalous bias is observed for Sand Heads and Steveston, which suggests that CD-to-CGVD28 conversion for Sand Heads and Steveston may be offset by approximately -8 and +12 cm, correspondingly. The CRMSE score shows a general improvement as we increase resolution. The CIOPS-W CRMSE is about 15 cm, the SS500 CRMSE is about 12 cm, and SSS150 is about 10 cm and the high-resolution SF30 model is about 8 cm for stations in the lower part of the river and somewhat increases for the stations in the upper part. Similar improvement with model resolution is also reflected in the γ^2 scores that scale quadratically with CRMSE and in the Pearson scores.

To showcase the stability of these scores across years, we include a summarising plot in Figure *22*, where each row depicts a different model, the left panels show total water level bias vs CRMSE, and the right panels show tidal CRMSE vs non-tidal CRMSE. Each colour depicts a different station, and each marker depicts a different year.

Scores are generally consistent between years, with year-to-year bias variations within 10 cm and CRMSE variations within 5 cm. Exceptions include the upper river stations for SS500 which were discussed above, and Deas Island station which has large CRMSE values, and the year-to-year variability for all models the cause of which remains to be determined. Here, we only note the dubious quality of observational data for this station which exhibit random deviations from the “normal” seasonal cycle (not shown).

5.1.5. Storm surge water level

Storm surge evaluation considers non-tidal water level during 4-day intervals corresponding to the passage of low atmospheric pressure systems through the region. Figure 23 through Figure 31 show observed and model water level at 9 stations where each panel represents one storm event for a maximum of 8 events. Water level variability during the events is captured well in all models, with high-resolution models performing better than the lower-resolution ones. Peak values do not show any consistent errors except for the strongest event, BCFloods, in November of 2021. The peak surge for this event is underestimated by 30 cm at the outer stations and 60 cm at the inner stations. No systematic bias is observed in the high-resolution models. SS500 has a positive bias of 20 to 30 cm at the upper river stations, New Westminster and Port Mann, while CIOPS-W has a negative bias of approximately 5 cm at Steveston and StevestonEC and no consistent bias at Sand Heads.

Our analysis in Section 5.1 indicated a possible offset by 12 cm for Steveston datum, and this is consistent with the significant negative bias of all models in Figure 25. Figure 32 and Figure 33 show bias and CRMSE, correspondingly, averaged over stations as a function of the atmospheric pressure during the storm, which can be used as a proxy for storm strength. The bias does not show any dependence on the storm pressure. It stays within -4 to 8 cm, with the high-resolution models having predominantly negative bias and the low-resolution models having predominantly positive bias. The CRMSE tends to be higher for lower pressure in SSS150 and SF30. The bias is lowest on average for SSS150, with SF30 having very close scores. These two figures are intended to explore the dependence of the errors on the storm strength, however, since the averaging in them is performed over a different set of stations for each model, they do not provide a coherent comparison of the models.

Table 21 presents the error scores for the storm surge water level averaged over the storm events. For all stations, the scores improve with an increased horizontal resolution of the model. One exception is Sand Heads, the outermost station, where the SSS150 scores are marginally better than the ones for SF30. The scores are generally better at the outer stations than inner ones.

5.2. WATER VELOCITY

We evaluate water velocity using three instrument types in this subsection.

5.2.1. Horizontal ADCPs

Horizontal acoustic doppler current profiler (HADCP) measurements are available at Woodward’s Landing to capture near-surface currents throughout the tidal cycle. The instrument is fixed to a solid structure with an average depth of 4 m below the surface, which varies from a minimum of 1.5 m to a maximum of 6 m with the tide. The data analyzed here were downloaded from the Integrated Water Level System (IWLS) online service. The period covered by the data is from March 30, 2021, to December 31, 2021. The instrument measures velocity in distance bins of 3 m. The IWLS database records a single series obtained by averaging Bins 66 to 71, corresponding to the distance range of 199 to 217 m from the instrument transducer. Data for

the entire range of bins is recorded internally by the instrument but requires physical access to the instrument for the manual download. This operation is performed by the CHS personnel when the instrument is being serviced (usually a few times per year). Here, we restrict our analysis to a single series, and thus do not analyze the multi-bin data. We only note that the cross-channel structure of the currents (not shown) is highly uniform.

The location of the mid-point of the analyzed range is shown in the upper panels in Figure 34. The lower panels of Figure 34 show rose diagrams of the observed current in the left panel and the current generated by SSS150 and SF30 models at the location and depth of the observations. The diagrams indicate highly rectilinear currents, and the principal component analysis shows that 97 to 99% of the variance is along the semi-major direction corresponding to the along-shore direction. Since the variance along the semi-minor direction is small, we choose to analyze only the along-shore current. The along-shore direction for the observed current is 48.3°N (True North) and, for the sake of consistency, it was taken as the along-shore direction to decompose both the observed and model currents. The semi-major direction for the model currents is 57.0 and 54.7°N (True North) for SSS150 and SF30, respectively. We note this difference here, but do not consider it significant for the component decomposition.

The quality of the analyzed data is generally adequate; however, the multi-bin series (not shown) indicate a possible signal strength loss beyond approximately 200 m distance from the transducer. As a result, the IWLS series (199-217 m average) has multiple missing or possibly unreliable readings. Thus, it would be beneficial if the averaging range of the data reported by the IWLS for this station is shifted closer to the transducer. To evaluate model performance using the Woodward's Landing HADCP, we consider two models, SSS150 and SF30, as they adequately resolve the river channel in the observation area. The error scores for the model velocity series are presented in Table 22 and generally indicate performance improvement with increased resolution. The bias shows that SF30 overestimates the outflow on average (negative bias) by 4.8 cm/s, while SSS150 overestimates it by 13.3 cm/s. Both models' bias is significantly lower than the average observed flow of 79 cm/s. CRMSE for the non-tidal current is very close between both models and is 20 cm/s. Tidal CRMSE is lower for the higher-resolution model. This is consistent with the tidal errors (Table 23), which are lower for SF30 than for SSS150 for all major constituents except for P1 and K2. γ^2 and Pearson's R scores for the non-tidal current are slightly better for SSS150. Tidal flow constitutes 80% of the energy of the total flow. The strongest tidal constituents in the currents are M2 (56 cm/s) and K1 (43 cm/s). The model error for both is 9.3 cm/s for SSS150 and 5.3 cm/s for M2 and 6.8 cm/s for K1 for SF30. The rest of the constituents show similar error ratios between SSS150 and SF30. For both models, the phase errors are mostly within the uncertainty brackets estimated for the observed phases by the bootstrap method. The model amplitude errors for M2 and K1 exceed those uncertainties by 5 to 10 cm/s.

A 6-day fragment of the along-shore velocity at Woodward's Landing in Figure 35 shows a clear improvement in the higher resolution SF30 model relative to SSS150 in both total and residual velocities. Peaks of tidal flow are captured in SF30 to within 0.1 m/s, while SSS150 overestimates the outflow peaks by 0.2-0.3 m/s. Also, a stronger outflow bias (the error stays mostly on the negative side) for SSS150 is evident in the figure.

5.2.2. Current meters

No current meter data available.

5.2.3. Moored ADCPs

Moored ADCP data are available from three locations (two at the slope of Roberts Bank and one in central part of Strait of Georgia (hereafter SoG); see Figure 7) with upward looking instruments mounted near the bottom. None of these sites is covered by SF30, and with a lack of hourly 3D output from CIOPS-W and SS500, we only assess SSS150 against those data. For each of the sites, we selected one deployment which provides more reliable data and covers larger depth range. These are 2016-10-08 to 2017-10-07 deployment at the slope of the Fraser River Delta (FRDLS) with the instrument at 141 m depth, 2017-12-06 to 2018-08-02 deployment at SoG Central with the instrument at 288 m depth, and 2018-10-01 to 2019-08-28 deployment at SoG East with the instrument at 157 m depth.

Our calculations (not shown) indicate that the tidal energy comprises 50 to 70% of the total energy of the observed current at the upper levels. Then it increases to the maximum of 80-85% at mid-depths and reduces again to 75-80% near the bottom. For the model current, the fraction of tidal energy in the total balance is approximately 5% higher than for the observed current.

The non-tidal current velocity time series at mid-depth for the three analyzed deployments are shown in Figure 36, Figure 37 and Figure 38. Reliability of the observed data deteriorates at shallower depths. Main variability is observed at periods of several days. At these frequencies, the observed and model series match during some months, but have discrepancies during other months and these periods of good and poor match vary from station to station. Better model performance for the non-tidal currents is observed near the bottom, as seen in the right-hand panels in Figure 39, Figure 40, and Figure 41.

Figure 42, Figure 43 and Figure 44 show power spectra of the clockwise and the counter-clockwise components (rotary spectra) of the total current at same mid-depth levels. At frequencies lower than diurnal, the model shows best agreement with the observations at the SoG East station. At FRDLS and SoG Central, discrepancies are noticeable, but do not have consistent overestimation or underestimation of energy over these frequencies. For the main tidal frequencies, diurnal tides are slightly overestimated and semi-diurnal tides are slightly underestimated at FRDLS. Slight underestimation of the clockwise component and slight overestimation of the counterclockwise component is seen at SoG Central. At SoG East, the tidal energy levels are close to the observed. At SoG Central and SoG East, the observed background energy level is high at high frequencies, possibly due to instrument noise.

Of the three analysed stations, the inertial currents are observed only at SoG Central. They are one to two orders of magnitude weaker than the major tidal currents. The model is seen to underestimate the inertial energy.

The error spectra (lower panels in Figure 42, Figure 43 and Figure 44) indicate that the errors are concentrated mostly at major tidal frequencies and frequencies corresponding to periods of 12-20 days. At FRDLS and SoG East, tidal currents are stronger than at SoG Central and the associated model tidal errors are higher.

Vertical structure of tidal currents for both M2 and K1 constituents is represented fairly well at all three stations (Figure 45, Figure 46 and Figure 47). Best correspondence is seen at the SoG Central station (Figure 46). Here, the discrepancies for the semi-major and semi-minor ellipse axes for M2 and K1 stay mostly within 0.02 m/s and ellipse direction and phase within 5°. Somewhat larger discrepancies are seen at SoG East (Figure 47) and particularly at FRDLS (Figure 45). The sloping bottom and proximity to the Fraser River mouth are likely the factors challenging the model at those two locations.

Table 24, Table 25 and Table 26 summarise the model error scores for total, non-tidal, and tidal currents, respectively. The scores are shown for four selected depth levels spread between the

topmost depth with reliable data and the bottom. The bias for the eastward and northward components is within 0.09 m/s and tends to be higher at shallower levels. The RMSE for the total current at the three stations is 0.17-0.26 m/s at the upper levels and reduces to 0.11-0.15 m/s near the bottom. The RMSE for the non-tidal current is universally 0.01-0.02 m/s lower than for the total current. Tidal RMSE is comparable to the non-tidal, but higher at deep levels at FRDLS and shallow levels at SoG Central. Vector correlations between the model and observed current for the non-tidal flow are mostly within 0.20-0.40 and directional discrepancy mostly within 10° with lower values and larger directional mismatch for the mid-depths at SoG Central. For the total current, correlation is significantly higher (around 0.80-0.85) due to inclusion of the highly correlated tidal current. Direction of the tidal flow is captured well at SoG Central and SoG East, but has a clockwise bias of 12 to 17° at FRDLS, which is also evident in Figure 39 and Figure 45. The γ^2 scores are good for the tidal component (<0.1), but poor (generally >1) for the non-tidal component, although the values for total velocity indicate modest skill ($0.25 < \gamma^2 < 0.75$). We expect that instrument noise along with any non-stationary component of the tidal velocities may be captured in our estimate of the non-tidal velocity, both of which would contribute to poor γ^2 scores. Further processing to better separate the non-tidal (or sub-tidal) component of the velocity may improve the scoring but is beyond the present scope.

5.2.4. ADCP transects

We restrict analysis for the ship mounted ADCP to two models adequately resolving the Fraser River, SSS150 and SF30. Ship-mounted ADCP transects in the areas covered by both model domains are available from four surveys in February 2019 (two sections), March 2021 (five sections), July 2021 (three sections), and October 2021 (46 sections). The sections in the extensive October 2021 survey are distributed over a few standard lines, many of which are sampled multiple times. The measurements are made with the downward-facing ADCP instrument from a slowly moving vessel. Despite the slow speed of the vessel, the data can still be prone to high noise level depending on the instrument settings. In such cases we smooth the data to suppress variability at periods lower than 10 s since this band is dominated by noise. The 10 s temporal interval corresponds to a 10 to 20 m horizontal distance with the typical vessel speed during sampling. After this smoothing, the noise level is suppressed to roughly 0.1 m/s.

Here we analyze velocity decomposed in the cross-transect and along-transect direction. Since all transect lines go across the river channel, the cross-transect and along-transect directions closely match the along-shore and cross-shore directions, correspondingly. Velocity sign in the plots discussed below depends on the orientation of the transect, but for all transects, the along-shore current is directed down the river.

Figure 48 through Figure 53 show selected transects where the flow exhibits some degree of spatial variability. Typical along-shore velocities are in the range of 0.5 to 2 m/s. The cross-shore velocities are significantly smaller and usually stay within 0.25 m/s but can reach 1 m/s (e.g., Figure 53) where islands or shallows divert the flow. The cross-shore structure of the flow can be uniform but most often is concentrated in a roughly 150 m wide jet. In the vertical, the flow is largely uniform. Within approximately 5 m of the bottom and 100 m from the side wall, boundary friction slows the flow.

In most transects (Figure 49 through Figure 53) the flow structure in SF30 is reflected better than in SSS150, indicating the benefit of the increased horizontal resolution. However, the flow speeds in the jet are often underestimated in SF30. One line where the model flow structure differs from the observed is FR05a (Figure 48). The jet here is shifted to the mid-channel in SF30, while the observational data show the jet closer to the northern bank of the river. FR05a is located off Woodward's Landing horizontal ADCP location and thus indicates that this jet

position mismatch is a likely reason for the outflow overestimation by 4.8 cm/s in SF30. In contrast, outflow overestimation by 13.3 cm/s at Woodward's Landing horizontal ADCP in SSS150 is due to overall higher model velocity. It should also be noted that FR05a has been sampled 18 times throughout the survey, while five other lines were sampled 5 to 8 times, and the remaining eight lines were sampled once each, thus biasing the overall statistics towards FR05a.

Figure 54 shows a distribution diagram of the bias vs CRMSE for SSS150 and SF30 and Figure 55 presents a diagram of the observed vs model kinetic energy of the current. The along-shore component is reflected well in both models, with SSS150 slightly overestimating the current energy and SF30 slightly underestimating it. Although small, the cross-channel velocities are better reflected in SF30 than in SSS150.

5.3. WATER PROPERTIES

5.3.1. Sea surface temperature

Fraser River domain contains one moored buoy measuring sea surface temperature (SST), the Fraser River Water Quality Buoy, deployed approximately 13 km upstream from Steveston near the northern bank of the South Arm (Figure 7). This location is covered by SS500, SSS150, and SF30 domains. The data cover the entire hindcast evaluation period. Since monthly climatology defines the upstream temperature boundary condition in Fraser River in all three models (directly in SS500 and SSS150 and via SSS150 in SF30) they all exhibit very similar variability and their errors are, therefore, similar as well. The amplitude and timing of the seasonal cycle are captured well, however, interannual variations and synoptic variability are missing from the model temperature, which results in errors of 1 to 2 °C. Figure 56 shows cold bias in December-February for all years between 2017 and 2021, and cold bias in July-August for all years except 2020. Based on the above analysis, switching from climatology to real-time Fraser River temperature in the corresponding boundary conditions for SS500 and SSS150 can substantially reduce the temperature error. Meanwhile, in the absence of real-time data, updating the climatology with more weight applied to recent years can potentially reduce temperature errors. Table 27 confirms that temperature error scores for all models are very similar, with bias reducing from -0.60 to -0.37 °C from coarse- to fine-resolution model.

5.3.2. Moored CTDs

Four series at locations near Ocean Networks Canada (ONC) Strait of Georgia East node are available. Here we analyze one of them which has better data coverage (SEVIP in Figure 7). The instrument is located near the bottom on the outer edge of Roberts Bank, off the exit from the Fraser River South Arm, at 165 m depth. The location is outside SF30 coverage but is covered by the other three models. Temperature is captured equally well by all three models with +0.4 °C warm bias (Table 28), which is slightly more pronounced during the first half of the year and has a tendency to diminish towards the last two years of the analysis period (Figure 57). All other scores are similar among the three models. Salinity is captured well by SS500 and SSS150 with an average salty bias of +0.05 PSU which, similarly to the temperature bias, decreases in 2020 and 2021. CIOPS-W, however, shows a considerably higher salty bias of +0.8 PSU. SS500 shows slightly better scores than SSS150. We note, however, that the scores for CIOPS-W and SS500 are based on daily output, while those for SSS150 are from hourly output, which precludes direct comparison.

5.3.3. CTD profiles

We evaluate model performance relative to the temperature and salinity measured by CTD casts over five sub-regions shown in Figure 58. The amount of data for each subregion is listed in Table 29. Fraser River is sampled significantly less (7-27 profiles per sub-region) than the Strait of Georgia (588 profiles). Due to the limited number of profiles in the Fraser River, we analyzed over the entire five-year hindcast period 2017-2021. The per-region summarizing plots (Figure 59 through Figure 63) show mean bias as a function of depth in a solid curve, and the shaded area indicates ± the CRMSE (one standard deviation of the error). Note that the vertical axis on the plots is log-scale in pressure.

In the Southern Strait of Georgia (not covered by SF30), temperature and salinity are reflected better in SS500 and SSS150 than in CIOPS-W (Figure 59). SS500 and SSS150 have +0.5 °C warm bias in the upper 20 m. CIOPS-W is, on average, -0.8 °C colder in the upper 5 m and +1 °C warmer between 10 and 20 m. All models have a +0.5 °C warm bias below 200 m depth. For salinity, SS500 and SSS150 are significantly better in the upper 5 m and below 20 m, where they have almost no bias, and CRMSE is small. Near the surface, SS500 and SSS150 have a fresh bias of -1 to -1.8 PSU, while CIOPS-W is saltier by +3.8 PSU.

The rest of the subregions have significantly more uniform error distribution with depth for all models. Figure 60 shows -0.5 °C bias for SS500, -0.6 °C bias for SF30 and -0.7 °C bias for SSS150. For salinity, SS500 has a low bias varying between +0.3 PSU near the surface and -0.2 PSU near the bottom, while SSS150 has a +1 PSU and SF30 +2 PSU salty bias.

In the Massey to Annacis subregion (Figure 61), all three models show very similar performance with a cold bias of -0.5 to -0.7 °C and nearly no bias in salinity except SF30 very close to the bottom, where it is saltier than the observations by +0.8 PSU indicating an overestimated extent of the salty tongue in the bottom layer.

A similar picture is observed for the Port Mann subregion (Figure 62), which is covered only by SSS150 and SF30. Both models show the same slight cold temperature bias as in the Massey to Annacis subregion and a slight fresh bias of -0.04 PSU. The error distribution repeats in the Upper Fraser River subregion, which is covered by only the SSS150 model (Figure 63).

5.3.4. Ferries

Figure 64 and Figure 65 show Hovmöller plots of the temperature and salinity measured from a thermosalinograph system on BC Ferries' Tsawwassen-Duke Point ferry route. For temperature we see that CIOPS-W is significantly biased cold in the summers and biased slightly warm in the winters. SS500 and SSS150 perform similarly, both showing a smaller cold bias near the Tsawwassen end of the route and a small warm bias as we approach the edge of the SSS150 domain. Meanwhile for salinity, CIOPS-W is strongly biased salty year-round, SS500 improves significantly upon this, and SSS150 manages to improve upon SS500's fresh bias near the Tsawwassen end of the route but performs similarly away from it. This may be due to a better representation of the Fraser Plume. We expect that the SSS150 model will perform like the SS500 near the boundaries as a consequence of using SS500 data as the temperature and salinity data for the west and south open boundaries.

5.4. DRIFT

The drift evaluation experiment used 23 drifter tracks, 18 SCT-type and 5 OSKER-type (for details about drifter types, see Hourston 2021) that were released in the Fraser River during OPP surveys. Drifter tracks are shown in Figure 66. The drifters in the Fraser River have short travel time and allow for a maximum of two-hour simulations. Molcard skill (Figure 67 and Table

30) increases with model resolution, with SSS150 and SF30 having very close scores between 0.3 and 0.4, which degrade slightly with time. The skill for SS500 is half the skill of the high-resolution models. Separation distance (Figure 68 and Table 30) is consistent with the Molcard score and is significantly lower for the SSS150 and SF30, starting at 400 m at 0.5 hours and increasing to 1000 m after 1.5 hours of simulation. The separation distance for SS500 is nearly twice as large.

6. FORECAST EVALUATION RESULTS

The forecast evaluation period is 2021-12-03 through 2022-01-26, where we conduct a 48h forecast from 00Z daily for a total of 55 forecasts. To evaluate forecast performance, we show bias and CRMSE curves with the shaded areas indicating the 95% bootstrap confidence intervals. We note that this period does not cover the late spring freshet period.

6.1. NON-TIDAL WATER LEVEL

Forecast evaluation for four water level stations is shown in Figure 69 through Figure 72. All models perform similarly regarding CRMSE, with the high-resolution models having slightly better scores. The CRMSE ranges between 4 and 6 cm for most of the stations. At Pitt River, where observational data quality is likely an issue, the CRMSE fluctuates around 10 cm. Bias is reasonably small for SS500 and the high-resolution models and ranges from +1 cm at Sand Heads, in the Strait of Georgia, to -2 to -4 cm at the stations in the river. For CIOPS-W, bias fluctuates around zero at Sand Heads and around -8 cm at StevestonEC. There is no significant change in bias as a function of lead hour, while there is an increase in CRMSE as a function of lead hour and it is marginally statistically significant. This increase is order 1 cm CRMSE over the 48 hours of forecast and qualitatively consistent with the expectation that forecasts gradually degrade with lead time. The performance of all four models is similar, and this is expected because (a) the smaller scale models inherit non-tidal water level from the larger-scale models via the open boundary forcing, and (b) we use the same atmospheric pressure forcing at the surface for all four models which imparts the same inverse barometer effect.

6.2. HORIZONTAL ADCP

Figure 73 shows the forecast evaluation for the HADCP instrument at Woodward's Landing, where we consider the alongshore velocity. De-tiding of forecast series for HADCP series is not implemented in the analysis tool as of the time of writing and thus the bias panel shows a strong diurnal signal for both models, which results from discrepancies in tides which dominate the series. Meanwhile, on the CRMSE panel, we also see a diurnal signal in the SF30 curve and no significant trend in error growth.

6.3. SEA SURFACE TEMPERATURE

Sea-surface temperature forecast evaluation is shown in Figure 74 for the Fraser River Water Quality Buoy. CIOPS-W is excluded from this analysis as its' domain does not resolve the Fraser River. From the upper right panel, there is a cold bias of -1.5 to -1.7 °C in all three models, with SS500 showing a slightly larger bias than the high-resolution models. These overall biases are consistent with the cold bias of up to -2 °C in SST in the last 3 months of 2021 (Figure 56) and, if the forecast evaluation was performed over the entire 2017-2021, is expected to be between -0.4 and -0.6 °C as shown in Table 27. However, the focus here is on the forecast performance, and in all three models, we do not see a statistically significant warming or cooling trend as a function of lead hour. Meanwhile, the lower left panel shows a

slight (0.10 - 0.15 °C) decrease in CRMSE as a function of lead hour for the three models. This decrease, however, is within the confidence limits for CRMSE.

7. SUMMARY

The high-resolution models, SSS150 and SF30, were successfully deployed, run, and evaluated against observational data and showed an adequate performance. These models cover the Fraser River from Steveston to Mission (SSS150) and from Steveston to Port Mann (SF30), which is not covered or poorly resolved by the larger-scale models.

The high-resolution models outperform the parent models in tidal representation due to the replacement of tides at the SS500-SSS150 boundary and associated tuning. We reach an error level of 5 cm CRMSE for the tidal component which is comparable to that of the non-tidal component. Efforts to further reduce the tidal error are nearing the point of diminishing returns regarding total water level error: eliminating tidal error completely would only reduce total water level CRMSE to 5 cm.

Meanwhile, deficiencies are inherited from the larger-scale models for some variables. Non-tidal water level variability is similar to that of the parent model.

Increased model resolution shows improvement in velocities representation, which is confirmed by comparing against horizontal and ship mounted ADCPs. In addition, a slight underestimation of the outflow velocity is observed in the models. The higher-resolution models were found to perform better in drift evaluation.

Temperature and salinity biases in the Fraser plume area are similar to the larger-scale models as they cannot accumulate due to the boundary forcing (parent model temperature and salinity amounts to a strong restoring).

Forecast evaluation showed an expected gradual increase in model error and no change in model bias with forecast lead time.

8. KEY FINDINGS

- The high-resolution models resolve areas that any current operational NEMO-based model does not cover: The Lower Fraser River to Port Mann at 30 m resolution and from Port Mann up to Mission and Pitt Lake at 150 m resolution.
- The high-resolution SF30 model provides either better performance than the lower-resolution models or is on par with them in the areas where they overlap and have adequate performance in the areas not covered by the low-resolution models.
- The SF30 model simulated a five-year historical period (2017-2021) without simulation failure, which included a record-setting flooding event in November 2021.
- The automated fallbacks for Mission water level data successfully recovered from a gauge failure in late 2021.
- Tidal water level error ranges from 5 to 9 cm CRMSE.
- Tidal wave in the models propagates up the Fraser River with a correct speed and amplitude.
- Non-tidal water level error is consistently 5-6 cm CRMSE.
- Water level biases are within 6 cm.

- Total water level error is of the order of 10 cm.
- Tidal and non-tidal water level errors are comparable, and both will need improvement to realize improvements in total water level CRMSE.
- Both tidal and non-tidal components of current velocity are captured well with a total error of about 0.25 m/s compared to the observed horizontal ADCP velocities at Woodward's Landing.
- The cross-shore structure of the flow in the Fraser River compares well with the data from ship-mounted ADCPs with a slight underestimation of the outflow velocities.
- Tidal currents are adequately represented at the slope of Roberts Bank and in the central Strait of Georgia. Direction of the tidal flow off the entrance to the Fraser River Main Arm is biased clockwise by 12-17°. Non-tidal flow at those locations shows modest skill with lower skill at the mid-depths in the central Strait of Georgia.
- Surface water temperature in Fraser River has a cold bias of less than 0.5 °C and errors of order 1.1 °C. The model could benefit from using real-time temperature instead of climatology for boundary conditions in the Fraser River.
- Vertical distribution of temperature and salinity are represented well and on par with SS500.
- Ferry track data indicates that SSS150 performs comparably to SS500 in temperature and performs somewhat better near the Tsawwassen ferry terminal in terms of salinity by reducing a fresh bias.
- Drift performance is significantly improved in the high-resolution models relative to SS500.
- The forecast evaluation shows that non-tidal water level error increased gradually with forecast lead time as expected.

9. ACKNOWLEDGEMENTS

We thank ECCC colleagues Jean-Philippe Paquin, Greg Smith, Fred Dupont, and Oleksandr (Sasha) Huziy for advice and ideas in developing and evaluating the models, Pascal Matte for his advice in constructing the NS TIDE model, and Sarah MacDermid and Ji Lei for lending their maestro expertise. We thank Mitchell O'Flaherty-Sproul for help with bathymetric data. We thank Marlene Jeffries, Pete Wills and colleagues at CHS for provisioning tide, bathymetric and survey data. Thanks to Nancy Soontiens and Jennifer Holden for the drift prediction tool and help running it. Thanks also to Roy Hourston for facilitating drift measurements and collecting survey data. We further thank Ocean Networks Canada for providing moored ADCP and CTD data, Ian Darke at Public Services and Procurement Canada for providing ADCP transect data from the Fraser River, Jesse Montgomery at Metro Vancouver for Capilano River discharge data, Patrick Lilley at Kerr Wood Leidal for river discharge data for North Vancouver, and the waterproperties.ca team for their careful data curation. Thanks are also extended to Charles Hannah, Jon Chamberlain, Denis Lefaivre and Youyu Lu for advice and guidance. Lastly, we thank Denis Lefaivre, Joël Chassé, Nancy Soontiens, Yvonnick Le Clainche, Ji Lei, Justine McMillan, Isabelle Gaboury and Phil MacAulay for feedback during writing.

10. REFERENCES CITED

Backhaus, Jan O. 1983. "A Semi-Implicit Scheme for the Shallow Water Equations for Application to Shelf Sea Modelling." *Continental Shelf Research* 2 (4): 243–54. https://doi.org/10.1016/0278-4343(82)90020-6.

———. 1985. “A Three-Dimensional Model for the Simulation of Shelf Sea Dynamics.” *Deutsche Hydrographische Zeitschrift* 38 (4): 165–87. https://doi.org/10.1007/BF02328975.

Blanken, Hauke, Caterina Valeo, Charles Hannah, Usman T. Khan, and Tamás Juhász. 2021. “A Fuzzy-Based Framework for Assessing Uncertainty in Drift Prediction Using Observed Currents and Winds.” *Frontiers in Marine Science* 8 (November):618094. https://doi.org/10.3389/fmars.2021.618094.

Chen, Changsheng, Hedong Liu, and Robert C. Beardsley. 2003. “An Unstructured Grid, Finite-Volume, Three-Dimensional, Primitive Equations Ocean Model: Application to Coastal Ocean and Estuaries.” *Journal of Atmospheric and Oceanic Technology* 20 (1): 159–86. https://doi.org/10.1175/1520-0426(2003)020<0159:AUGFVT>2.0.CO;2.

Cummins, Patrick F., and Lie-Yauw Oey. 1997. “Simulation of Barotropic and Baroclinic Tides off Northern British Columbia.” *Journal of Physical Oceanography* 27 (5): 762–81. https://doi.org/10.1175/1520-0485(1997)027<0762:SOBABT>2.0.CO;2.

Cummins, Patrick F., and Pramod Thupaki. 2018. “A Note on Evaluating Model Tidal Currents against Observations.” *Continental Shelf Research* 152 (January):35–37. https://doi.org/10.1016/j.csr.2017.10.007.

Daniel, Pierre, Gwénaële Jan, Fanch Cabioc’h, Yves Landau, and Erwann Loiseau. 2002. “Drift Modeling of Cargo Containers.” *Spill Science & Technology Bulletin* 7 (5–6): 279–88. https://doi.org/10.1016/S1353-2561(02)00075-0.

Dunphy, M., M. Krassovski, S. Taylor, H. Blanken, R. Horwitz, S. St-Onge Drouin, and A. Drozdowski. In press. Assessment of Port Ocean Prediction System Developed Under Canada’s Oceans Protection Plan: Vancouver Harbour. DFO Can. Sci. Advis. Sec. Res. Doc.

Dupont, F., S. Higginson, R. Bourdallé-Badie, Y. Lu, F. Roy, G. C. Smith, J.-F. Lemieux, G. Garric, and F. Davidson. 2015. “A High-Resolution Ocean and Sea-Ice Modelling System for the Arctic and North Atlantic Oceans.” *Geoscientific Model Development* 8 (5): 1577–94. https://doi.org/10.5194/gmd-8-1577-2015.

Flather, R.A. 1976. “A Tidal Model of the Northwest European Continental Shelf” 6 (10): 141–64.

Hourston, Roy A.S. 2021. *Surface Ocean Circulation Tracking Drifter Data from the Northeastern Pacific and Western Arctic Oceans, 2014-2020*. Sidney, B.C.: Fisheries and Oceans Canada - Pêches et Océans Canada.

Kundu, Pijush K. 1976. “Ekman Veering Observed near the Ocean Bottom.” *Journal of Physical Oceanography* 6 (2): 238–42. https://doi.org/10.1175/1520-0485(1976)006<0238:EVONTO>2.0.CO;2.

Large, WIlliam George, and Stephen G. Yeager. 2004. “Diurnal to Decadal Global Forcing for Ocean and Sea-Ice Models: The Data Sets and Flux Climatologies.” NCAR Technical Note NCAR/TN-460+STR. Boulder, CO: Climate and Global Dynamics Division: National Center for Atmospheric Research.

Levier, B., A.-M. Tréguier, G. Madec, and V. Garnier. 2007. “Free Surface and Variable Volume in the Nemo Code.” MERSEA IP report WP09-CNRS-STR-03-1A.

Madec, Gurvan. 2016. *NEMO Ocean Engine*. Note Du Pole de Modélisation de l’Institut Pierre-Simon Laplace 27. NEMO European Consortium.

Madec, Gurvan, and Maurice Imbard. 1996. “A Global Ocean Mesh to Overcome the North Pole Singularity.” *Climate Dynamics* 12 (6): 381–88. https://doi.org/10.1007/BF00211684.

Martinsen, Eivind A., and Harald Engedahl. 1987. “Implementation and Testing of a Lateral Boundary Scheme as an Open Boundary Condition in a Barotropic Ocean Model.” *Coastal Engineering* 11 (5–6): 603–27. https://doi.org/10.1016/0378-3839(87)90028-7.

Milbrandt, Jason A., Stéphane Bélair, Manon Faucher, Marcel Vallée, Marco L. Carrera, and Anna Glazer. 2016. “The Pan-Canadian High Resolution (2.5 Km) Deterministic Prediction System.” *Weather and Forecasting* 31 (6): 1791–1816. https://doi.org/10.1175/WAF-D-16-0035.1.

Molcard, A., P.M. Poulain, P. Forget, A. Griffa, Y. Barbin, J. Gaggelli, J.C. De Maistre, and M. Rixen. 2009. “Comparison between VHF Radar Observations and Data from Drifter Clusters in the Gulf of La Spezia (Mediterranean Sea).” *Journal of Marine Systems* 78 (November): S79–89. https://doi.org/10.1016/j.jmarsys.2009.01.012.

Niiler, Pearn P., Andrew S. Sybrandy, Kenong Bi, Pierre M. Poulain, and David Bitterman. 1995. “Measurements of the Water-Following Capability of Holey-Sock and TRISTAR Drifters.” *Deep Sea Research Part I: Oceanographic Research Papers* 42 (11–12): 1951–64. https://doi.org/10.1016/0967-0637(95)00076-3.

Nudds, Shannon, Youyu Lu, Simon Higginson, Susan P. Haigh, Jean-Philippe Paquin, Mitchell O’Flaherty-Sproul, Stephanne Taylor, et al. 2020. “Evaluation of Structured and Unstructured Models for Application in Operational Ocean Forecasting in Nearshore Waters.” *Journal of Marine Science and Engineering* 8 (7): 484. https://doi.org/10.3390/jmse8070484.

Paquin, Jean-Philippe, Youyu Lu, Stephanne Taylor, Hauke Blanken, Guillaume Marcotte, Xianmin Hu, Li Zhai, et al. 2020. “High-Resolution Modelling of a Coastal Harbour in the Presence of Strong Tides and Significant River Runoff.” *Ocean Dynamics* 70 (3): 365–85. https://doi.org/10.1007/s10236-019-01334-7.

Paquin, Jean-Philippe, François Roy, Gregory C. Smith, Frédéric Dupont, Yukie Hata, Oleksandr Huizy, Yosvany Martinez, Hauke Blanken, Jennifer Holden, and Nancy Soontiens. 2021a. “Coastal Ice Ocean Prediction System for the East Coast of Canada (CIOPS-E) Update from Version 1.5.0 to 2.0.0.” Canadian Centre for Meteorological and Environmental Prediction Tech. Note. https://collaboration.cmc.ec.gc.ca/cmc/cmoi/product_guide/docs/tech_notes/technote_ciops-east-200_e.pdf.

Paquin, Jean-Philippe, Gregory C. Smith, Frédéric Dupont, Sarah MacDermid, Yukie Hata, Oleksandr Huizy, Ji Lei, et al. 2021b. “Coastal Ice Ocean Prediction System for the West Coast of Canada (CIOPS-W) Update from Version 1.5.0 to 2.0.0.” Canadian Centre for Meteorological and Environmental Prediction Tech. Note. https://collaboration.cmc.ec.gc.ca/cmc/cmoi/product_guide/docs/tech_notes/technote_ciops-west-200_e.pdf.

Paquin, Jean-Phillipe, Gregory C. Smith, Francois Roy, Frederic Dupont, Sarah MacDermid, Ji Lei, Youyu Lu, Stephanne Taylor, Hauke Blanken, and Li Zhai. 2022. “Coastal Ice Ocean Prediction System for the West Coast of Canada (CIOPS-W): System Description for Versions 1.0.0 and 1.5.0.” Canadian Centre for Meteorological and Environmental Prediction Tech. Note. https://collaboration.cmc.ec.gc.ca/cmc/cmoi/product_guide/docs/tech_notes/technote_ciops-west-100_e.pdf.

Pawlowicz, Rich, Bob Beardsley, and Steve Lentz. 2002. “Classical Tidal Harmonic Analysis Including Error Estimates in MATLAB Using T_TIDE.” *Computers & Geosciences* 28 (8): 929–37. https://doi.org/10.1016/S0098-3004(02)00013-4.

Röhrs, Johannes, and Kai H. Christensen. 2015. “Drift in the Uppermost Part of the Ocean.” *Geophysical Research Letters* 42 (23). https://doi.org/10.1002/2015GL066733.

Röhrs, Johannes, Kai Håkon Christensen, Lars Robert Hole, Göran Broström, Magnus Drivdal, and Svein Sundby. 2012. “Observation-Based Evaluation of Surface Wave Effects on Currents and Trajectory Forecasts.” *Ocean Dynamics* 62 (10–12): 1519–33. https://doi.org/10.1007/s10236-012-0576-y.

Saucier, François J. 2003. “Modeling the Formation and Circulation Processes of Water Masses and Sea Ice in the Gulf of St. Lawrence, Canada.” *Journal of Geophysical Research* 108 (C8): 3269. https://doi.org/10.1029/2000JC000686.

Saucier, François J., and Joël Chassé. 2000. “Tidal Circulation and Buoyancy Effects in the St. Lawrence Estuary.” *Atmosphere-Ocean* 38 (4): 505–56. https://doi.org/10.1080/07055900.2000.9649658.

Smith, Stuart D. 1988. “Coefficients for Sea Surface Wind Stress, Heat Flux, and Wind Profiles as a Function of Wind Speed and Temperature.” *Journal of Geophysical Research* 93 (C12): 15467. https://doi.org/10.1029/JC093iC12p15467.

Soontiens, Nancy, and Jennifer Holden J. 2024. "A framework for evaluation and characterization of drift prediction in the marine environment." Can. Tech. Rep. Hydrogr. Ocean Sci. 383: ix + 45 p. https://waves-vagues.dfo-mpo.gc.ca/library-bibliotheque/41252287.pdf.

Sutherland, Graig, Nancy Soontiens, Fraser Davidson, Gregory C. Smith, Natacha Bernier, Hauke Blanken, Douglas Schillinger, et al. 2020. “Evaluating the Leeway Coefficient of Ocean Drifters Using Operational Marine Environmental Prediction Systems.” *Journal of Atmospheric and Oceanic Technology* 37 (11): 1943–54. https://doi.org/10.1175/JTECH-D-20-0013.1.

Zhang, Minghong, William Perrie, and Zhenxia Long. 2019. “Springtime North Pacific Oscillation and Summer Sea Ice in the Beaufort Sea.” *Climate Dynamics* 53 (1–2): 671–86. https://doi.org/10.1007/s00382-019-04627-1.

11. TABLES

Table 1. Key model parameters for the SSS150 and SF30 NEMO configurations.

Parameter	Outer grid (SSS150)	Inner grid (SF30)
Grid dimensions, NX x NY x NZ	710 x 826 x 39	1190 x 419 x 24
Horizontal resolution, ΔX x ΔY	Approx. 129 x 98 m	30 x 30 m
Vertical resolution	1 m surface, 26 m bottom	1 m surface, 11 m bottom
Baroclinic / barotropic time step	20 s / 1 s	4 s / 0.8 s
Open boundary update frequency	1 h (W, S), 30 min (E)	15 min
Open Boundary SSH offset	-12 cm (W, S), 0 cm (E)	0 cm
Tidal constituents forced	M2, S2, N2, K1, O1, Q1, K2, P1, L2, 2N2, NU2, J1, M1, OO1, SO1	Inherited from SSS150
Equation of state	EOS-80	EOS-80
Free surface	Variable volume	Variable volume
Light penetration	Two band	Two band
Lateral boundary condition	Partial slip (shlat=0.5)	Partial slip (shlat=0.5)
Momentum advection	Vector form, 10 sub-steps for vertical advection	Vector form, 8 sub-steps for vertical advection
Momentum lateral diffusion	Horizontal Laplacian and Smagorinsky	Smagorinsky and Horizontal Laplacian and Horizontal Bilaplacian
Tracer advection	Total Variance Dissipation, 10 vertical advection sub-steps	Total Variance Dissipation, 8 vertical advection sub-steps
Tracer lateral diffusion	Iso-neutral Laplacian and Smagorinsky	Iso-neutral Laplacian and Smagorinsky
Vertical diffusion	k-ε (GLS)	k-ε (GLS)
Bottom friction	Quadratic, spatially varying	Log-layer

Table 2. Water level station data used for evaluation and offsets used to shift the water level to CGVD28.

Station name	Station ID	Data available	Offset (m)
North Arm	08MH032	Water level	-2.603
Sand Heads	07594	Water level	2.986
Steveston	07607	Water level	2.098
StevestonEC	08MH028	Water level	-2.700
Woodward's Landing	07610	Water level	1.831
Deas Island	08MH053	Water level	0.000
New Westminster	07654	Water level	1.433
Port Mann	08MH126	Water level	-2.603
Pitt River	08MH035	Water level	-2.603
Dionisio Point	07535	Constituents	—
Canoe Pass	07603	Constituents	—
Roberts Bank	07592	Constituents	—
Tsawwassen	07590	Constituents	—

Table 3. M2 constituent comparison for active tide gauges for year 2018 (upper part) and historical tide gauges (lower part).

	Observed		Amplitude Error (m)				Phase Error (deg)				Tidal Error (m)			
Station name	**Amplitude (m)**	**Phase (deg)**	**CIOPSW**	**SS500**	**SSS150**	**SF30**	**CIOPSW**	**SS500**	**SSS150**	**SF30**	**CIOPSW**	**SS500**	**SSS150**	**SF30**
North Arm	0.850 ± 0.013	46.2 ± 0.7	—	-0.116	+0.017	—	—	+9.6	-3.7	—	—	0.124	0.041	—
Sand Heads	0.887 ± 0.004	30.6 ± 0.2	+0.026	-0.003	+0.003	—	+4.5	+0.5	-0.8	—	0.053	0.006	0.009	—
Steveston	0.865 ± 0.006	37.2 ± 0.4	+0.056	-0.040	+0.011	+0.024	-2.6	+0.3	-5.5	-2.8	0.049	0.028	0.059	0.035
StevestonEC	0.865 ± 0.007	37.0 ± 0.5	+0.043	-0.021	+0.020	+0.023	-3.2	-1.5	-6.3	-2.5	0.046	0.022	0.070	0.032
Woodward's Landing	0.823 ± 0.012	44.1 ± 0.8	—	-0.070	-0.030	-0.013	—	+5.5	-3.8	-3.5	—	0.073	0.044	0.036
Deas Island	0.730 ± 0.011	50.5 ± 0.9	—	+0.023	+0.063	+0.083	—	-0.9	-10.2	-10.2	—	0.018	0.106	0.113
New Westminster	0.636 ± 0.020	60.9 ± 1.6	—	-0.074	-0.054	-0.066	—	+14.0	-1.3	-1.7	—	0.116	0.039	0.049
Port Mann	0.528 ± 0.020	71.6 ± 2.3	—	-0.084	-0.057	-0.099	—	+18.7	-0.2	+0.4	—	0.126	0.040	0.070
Pitt River	0.368 ± 0.018	86.5 ± 2.7	—	—	-0.082	—	—	—	+5.4	—	—	—	0.062	—
Dionisio Point	0.882	32.02	+0.016	-0.016	-0.015	—	+5.1	+0.1	-0.8	—	0.058	0.011	0.014	—
Canoe Pass	0.819	42.16	+0.046	-0.034	+0.036	+0.037	-9.5	-1.4	-8.9	-8.4	0.104	0.028	0.095	0.091
Roberts Bank	0.807	27.71	+0.025	+0.012	+0.011	—	+5.4	+0.5	-1.3	—	0.057	0.010	0.015	—
Tsawwassen	0.809	27.33	+0.010	+0.004	-0.002	—	+5.8	+0.7	-0.9	—	0.058	0.007	0.009	—

Table 4. N2 constituent comparison for active tide gauges for year 2018 (upper part) and historical tide gauges (lower part).

	Observed		Amplitude Error (m)				Phase Error (deg)				Tidal Error (m)			
Station name	**Amplitude (m)**	**Phase (deg)**	**CIOPSW**	**SS500**	**SSS150**	**SF30**	**CIOPSW**	**SS500**	**SSS150**	**SF30**	**CIOPSW**	**SS500**	**SSS150**	**SF30**
North Arm	0.170 ± 0.014	19.8 ± 3.4	—	-0.028	+0.011	—	—	+14.0	-5.2	—	—	0.033	0.014	—
Sand Heads	0.188 ± 0.004	2.3 ± 1.2	0.000	-0.002	+0.004	—	+4.5	+2.5	-1.1	—	0.010	0.006	0.004	—
Steveston	0.180 ± 0.006	9.1 ± 2.1	+0.009	-0.013	+0.009	+0.010	-2.8	+3.3	-5.9	-2.5	0.009	0.012	0.015	0.009
StevestonEC	0.180 ± 0.007	8.8 ± 2.4	+0.006	-0.008	+0.011	+0.010	-3.4	+1.3	-6.5	-2.3	0.009	0.006	0.017	0.009
Woodward's Landing	0.168 ± 0.011	15.9 ± 4.4	—	-0.022	0.000	+0.002	—	+10.4	-4.2	-4.1	—	0.026	0.009	0.009
Deas Island	0.149 ± 0.010	21.9 ± 4.1	—	-0.004	+0.018	+0.021	—	+4.5	-10.1	-10.3	—	0.009	0.023	0.025
New Westminster	0.126 ± 0.017	32.3 ± 9.3	—	-0.018	-0.003	-0.009	—	+21.3	-2.3	-2.2	—	0.033	0.004	0.007
Port Mann	0.103 ± 0.021	42.2 ± 11.0	—	-0.016	-0.004	-0.014	—	+26.9	-1.9	-0.8	—	0.033	0.004	0.010
Pitt River	0.069 ± 0.019	54.1 ± 15.8	—	—	-0.009	—	—	—	+5.7	—	—	—	0.008	—
Dionisio Point	0.184	4.69	0.000	-0.003	+0.003	—	+4.6	+1.8	-1.6	—	0.010	0.005	0.004	—
Canoe Pass	0.164	15.06	+0.013	-0.011	+0.014	+0.013	-10.7	+2.2	-10.2	-9.5	0.024	0.009	0.024	0.022

	Observed		Amplitude Error (m)				Phase Error (deg)				Tidal Error (m)			
Station name	**Amplitude (m)**	**Phase (deg)**	**CIOPSW**	**SS500**	**SSS150**	**SF30**	**CIOPSW**	**SS500**	**SSS150**	**SF30**	**CIOPSW**	**SS500**	**SSS150**	**SF30**
Roberts Bank	0.173	358.11	-0.002	-0.002	+0.003	—	+5.9	+3.2	-1.0	—	0.013	0.007	0.003	—
Tsawwassen	0.173	359.32	-0.004	-0.004	-0.001	—	+4.7	+1.7	-2.1	—	0.010	0.004	0.005	—

Table 5. S2 constituent comparison for active tide gauges for year 2018 (upper part) and historical tide gauges (lower part).

	Observed		Amplitude Error (m)				Phase Error (deg)				Tidal Error (m)			
Station name	**Amplitude (m)**	**Phase (deg)**	**CIOPSW**	**SS500**	**SSS150**	**SF30**	**CIOPSW**	**SS500**	**SSS150**	**SF30**	**CIOPSW**	**SS500**	**SSS150**	**SF30**
North Arm	0.201 ± 0.008	78.7 ± 5.2	—	-0.033	+0.012	—	—	+17.7	-4.1	—	—	0.046	0.013	—
Sand Heads	0.226 ± 0.004	58.8 ± 1.0	+0.010	-0.001	+0.001	—	+6.1	+1.8	-0.1	—	0.019	0.005	0.001	—
Steveston	0.215 ± 0.007	66.6 ± 1.7	+0.022	-0.014	+0.007	+0.008	-2.3	+4.2	-5.6	-1.2	0.017	0.015	0.016	0.007
StevestonEC	0.215 ± 0.007	66.4 ± 1.7	+0.019	-0.008	+0.010	+0.008	-2.9	+1.6	-6.2	-1.0	0.016	0.007	0.018	0.007
Woodward's Landing	0.199 ± 0.013	74.0 ± 3.4	—	-0.026	-0.004	-0.003	—	+13.7	-2.9	-2.0	—	0.037	0.008	0.005
Deas Island	0.176 ± 0.011	80.3 ± 3.5	—	-0.004	+0.019	+0.021	—	+7.5	-9.2	-8.5	—	0.016	0.025	0.025
New Westminster	0.146 ± 0.020	92.8 ± 7.4	—	-0.024	-0.008	-0.015	—	+24.4	-0.3	0.0	—	0.043	0.006	0.011
Port Mann	0.121 ± 0.021	105.1 ± 10.1	—	-0.024	-0.010	-0.022	—	+28.8	+0.8	+1.9	—	0.042	0.007	0.016
Pitt River	0.087 ± 0.020	120.3 ± 14.1	—	—	-0.019	—	—	—	+6.1	—	—	—	0.015	—
Dionisio Point	0.220	60.29	+0.012	0.000	+0.001	—	+6.9	+1.9	+0.7	—	0.021	0.005	0.002	—
Canoe Pass	0.201	73.22	+0.021	-0.011	+0.012	+0.011	-10.5	+3.4	-9.1	-8.0	0.031	0.011	0.025	0.022
Roberts Bank	0.200	55.58	+0.014	+0.005	+0.006	—	+6.9	+1.9	-0.3	—	0.020	0.006	0.004	—
Tsawwassen	0.199	55.24	+0.011	+0.004	+0.003	—	+7.4	+1.8	-0.2	—	0.020	0.005	0.002	—

Table 6. K2 constituent comparison for active tide gauges for year 2018 (upper part) and historical tide gauges (lower part).

	Observed		Amplitude Error (m)				Phase Error (deg)				Tidal Error (m)			
Station name	**Amplitude (m)**	**Phase (deg)**	**CIOPSW**	**SS500**	**SSS150**	**SF30**	**CIOPSW**	**SS500**	**SSS150**	**SF30**	**CIOPSW**	**SS500**	**SSS150**	**SF30**
North Arm	0.077 ± 0.015	57.1 ± 11.8	—	+0.026	-0.010	—	—	-11.0	-4.7	—	—	0.022	0.008	—
Sand Heads	0.062 ± 0.005	62.5 ± 4.6	+0.006	+0.004	+0.002	—	+3.5	-6.2	+0.5	—	0.005	0.005	0.001	—
Steveston	0.066 ± 0.008	61.6 ± 6.7	+0.003	+0.017	-0.008	-0.001	+3.7	-18.8	+1.0	-4.9	0.004	0.021	0.005	0.004
StevestonEC	0.066 ± 0.008	61.5 ± 6.9	+0.003	+0.015	-0.004	-0.001	+4.0	-16.2	+0.1	-4.6	0.004	0.018	0.003	0.004
Woodward's Landing	0.072 ± 0.014	66.3 ± 11.3	—	+0.023	-0.009	-0.002	—	-20.0	-10.8	-10.1	—	0.026	0.011	0.009
Deas Island	0.062 ± 0.014	72.9 ± 11.8	—	+0.033	+0.002	+0.009	—	-26.7	-17.7	-16.7	—	0.034	0.014	0.015
New Westminster	0.071 ± 0.023	71.7 ± 18.4	—	+0.021	-0.009	-0.005	—	-8.4	-8.5	-9.5	—	0.017	0.009	0.009

	Observed		Amplitude Error (m)				Phase Error (deg)				Tidal Error (m)			
Station name	**Amplitude (m)**	**Phase (deg)**	**CIOPSW**	**SS500**	**SSS150**	**SF30**	**CIOPSW**	**SS500**	**SSS150**	**SF30**	**CIOPSW**	**SS500**	**SSS150**	**SF30**
Port Mann	0.065 ± 0.025	76.7 ± 21.7	—	+0.018	-0.007	-0.011	—	+0.5	-12.3	-10.6	—	0.013	0.011	0.011
Pitt River	0.049 ± 0.024	82.4 ± 31.3	—	—	-0.013	—	—	—	-2.3	—	—	—	0.009	—
Dionisio Point	0.060	63.32	+0.008	+0.003	+0.001	—	+3.7	-5.8	+0.2	—	0.007	0.005	0.001	—
Canoe Pass	0.071	55.40	-0.005	+0.020	-0.004	-0.002	+8.7	-13.0	-1.6	-2.9	0.008	0.019	0.003	0.003
Roberts Bank	0.060	57.91	+0.005	+0.002	+0.001	—	+5.6	-5.3	-1.4	—	0.005	0.004	0.001	—
Tsawwassen	0.057	57.68	+0.008	+0.005	+0.002	—	+5.9	-5.5	-1.7	—	0.007	0.005	0.002	—

Table 7. O1 constituent comparison for active tide gauges for year 2018 (upper part) and historical tide gauges (lower part).

	Observed		Amplitude Error (m)				Phase Error (deg)				Tidal Error (m)			
Station name	**Amplitude (m)**	**Phase (deg)**	**CIOPSW**	**SS500**	**SSS150**	**SF30**	**CIOPSW**	**SS500**	**SSS150**	**SF30**	**CIOPSW**	**SS500**	**SSS150**	**SF30**
North Arm	0.407 ± 0.012	271.7 ± 1.6	—	-0.059	+0.007	—	—	+7.6	-1.2	—	—	0.054	0.008	—
Sand Heads	0.481 ± 0.008	264.2 ± 1.0	-0.029	-0.002	-0.002	—	+12.8	+3.0	+0.1	—	0.076	0.018	0.001	—
Steveston	0.456 ± 0.010	267.9 ± 1.3	-0.002	-0.027	+0.013	+0.014	+8.7	+2.2	-1.0	-0.6	0.049	0.022	0.011	0.010
StevestonEC	0.455 ± 0.010	267.9 ± 1.3	-0.001	-0.010	+0.015	+0.014	+8.7	+1.7	-2.1	-0.6	0.048	0.012	0.016	0.011
Woodward's Landing	0.425 ± 0.015	271.3 ± 1.9	—	-0.046	-0.015	-0.010	—	+4.0	-0.6	-1.0	—	0.038	0.011	0.008
Deas Island	0.391 ± 0.015	275.9 ± 2.1	—	-0.013	+0.018	+0.026	—	-0.6	-5.2	-5.7	—	0.009	0.029	0.034
New Westminster	0.326 ± 0.022	277.6 ± 3.4	—	-0.064	-0.024	-0.031	—	+5.3	+0.8	+0.4	—	0.049	0.017	0.022
Port Mann	0.277 ± 0.023	281.6 ± 4.7	—	-0.075	-0.034	-0.042	—	+4.0	-0.5	+1.8	—	0.054	0.024	0.030
Pitt River	0.203 ± 0.021	288.5 ± 6.6	—	—	-0.028	—	—	—	+7.9	—	—	—	0.027	—
Dionisio Point	0.481	264.16	-0.031	-0.002	0.000	—	+13.7	+3.2	+1.0	—	0.081	0.019	0.006	—
Canoe Pass	0.410	269.07	+0.041	-0.001	+0.043	+0.040	+7.2	+2.6	-2.1	-2.5	0.048	0.013	0.033	0.031
Roberts Bank	0.457	262.45	-0.009	+0.019	+0.018	—	+13.6	+3.3	+0.3	—	0.076	0.024	0.013	—
Tsawwassen	0.466	262.02	-0.017	+0.014	+0.014	—	+13.2	+2.7	-0.5	—	0.075	0.018	0.010	—

Table 8. K1 constituent comparison for active tide gauges for year 2018 (upper part) and historical tide gauges (lower part).

	Observed		Amplitude Error (m)				Phase Error (deg)				Tidal Error (m)			
Station name	**Amplitude (m)**	**Phase (deg)**	**CIOPSW**	**SS500**	**SSS150**	**SF30**	**CIOPSW**	**SS500**	**SSS150**	**SF30**	**CIOPSW**	**SS500**	**SSS150**	**SF30**
North Arm	0.774 ± 0.012	295.5 ± 0.9	—	-0.060	+0.014	—	—	+6.5	-1.8	—	—	0.073	0.020	—
Sand Heads	0.862 ± 0.008	286.7 ± 0.5	-0.027	+0.006	+0.002	—	+11.2	+0.2	-0.5	—	0.118	0.005	0.005	—
Steveston	0.824 ± 0.010	290.4 ± 0.7	+0.014	-0.019	+0.015	+0.026	+6.9	+0.6	-2.5	-1.4	0.072	0.015	0.028	0.023

StevestonEC	0.822 ± 0.010	290.3 ± 0.7	+0.010	+0.001	+0.022	+0.028	+6.8	-0.4	-3.2	-1.3	0.070	0.004	0.037	0.024
Woodward's Landing	0.775 ± 0.014	294.2 ± 0.9	—	-0.039	-0.019	-0.009	—	+3.8	-0.9	-1.1	—	0.045	0.016	0.012
Deas Island	0.712 ± 0.013	299.1 ± 1.1	—	+0.024	+0.045	+0.057	—	-1.1	-5.8	-6.1	—	0.019	0.061	0.069
New Westminster	0.620 ± 0.020	305.9 ± 1.9	—	-0.052	-0.033	-0.046	—	+7.5	+1.4	+1.5	—	0.066	0.025	0.034
Port Mann	0.538 ± 0.025	313.8 ± 2.5	—	-0.064	-0.038	-0.065	—	+8.3	+2.0	+4.2	—	0.069	0.030	0.053
Pitt River	0.412 ± 0.019	327.3 ± 3.0	—	—	-0.036	—	—	—	+8.0	—	—	—	0.047	—
Dionisio Point	0.861	287.05	-0.034	+0.001	-0.003	—	+12.0	+0.7	+0.2	—	0.127	0.007	0.003	—
Canoe Pass	0.769	291.79	+0.053	+0.006	+0.054	+0.055	+5.3	+1.5	-2.9	-2.7	0.064	0.015	0.048	0.047
Roberts Bank	0.823	284.77	-0.008	+0.026	+0.020	—	+12.1	+0.9	+0.0	—	0.123	0.021	0.014	—
Tsawwassen	0.830	285.00	-0.021	+0.015	+0.007	—	+11.0	-0.3	-1.1	—	0.112	0.011	0.012	—

Table 9. P1 constituent comparison for active tide gauges for year 2018 (upper part) and historical tide gauges (lower part).

	Observed		Amplitude Error (m)				Phase Error (deg)				Tidal Error (m)			
Station name	**Amplitude (m)**	**Phase (deg)**	**CIOPSW**	**SS500**	**SSS150**	**SF30**	**CIOPSW**	**SS500**	**SSS150**	**SF30**	**CIOPSW**	**SS500**	**SSS150**	**SF30**
North Arm	0.227 ± 0.012	292.5 ± 2.8	—	-0.026	0.000	—	—	+4.7	-1.1	—	—	0.022	0.003	—
Sand Heads	0.272 ± 0.007	285.2 ± 1.6	-0.018	+0.001	-0.011	—	+12.1	-0.6	-0.3	—	0.041	0.002	0.008	—
Steveston	0.253 ± 0.010	287.7 ± 2.2	+0.002	-0.011	+0.001	+0.002	+9.2	-0.3	-0.9	+0.1	0.029	0.008	0.003	0.002
StevestonEC	0.253 ± 0.009	287.7 ± 2.1	+0.001	-0.001	+0.004	+0.003	+8.8	-1.1	-1.8	+0.1	0.028	0.004	0.006	0.002
Woodward's Landing	0.225 ± 0.013	290.6 ± 3.4	—	-0.027	-0.007	-0.009	—	+2.2	+0.5	-1.0	—	0.020	0.005	0.007
Deas Island	0.207 ± 0.012	295.0 ± 3.3	—	-0.009	+0.012	+0.011	—	-2.2	-3.9	-5.6	—	0.008	0.013	0.016
New Westminster	0.160 ± 0.017	299.2 ± 6.5	—	-0.026	-0.006	-0.017	—	+5.7	+1.0	+0.9	—	0.021	0.005	0.012
Port Mann	0.130 ± 0.021	305.5 ± 9.5	—	-0.025	-0.011	-0.020	—	+7.3	+1.3	+3.7	—	0.021	0.008	0.015
Pitt River	0.085 ± 0.017	318.7 ± 11.6	—	—	-0.004	—	—	—	+8.0	—	—	—	0.009	—
Dionisio Point	0.263	284.81	-0.013	+0.005	-0.006	—	+13.0	-0.4	+0.1	—	0.042	0.004	0.004	—
Canoe Pass	0.220	291.12	+0.030	+0.005	+0.023	+0.022	+4.2	-1.9	-4.4	-4.4	0.025	0.006	0.021	0.020
Roberts Bank	0.261	283.03	-0.018	+0.001	-0.012	—	+12.9	-0.0	-0.1	—	0.042	0.001	0.008	—
Tsawwassen	0.258	282.26	-0.010	+0.012	+0.001	—	+13.4	+0.1	+0.1	—	0.042	0.008	0.001	—

Table 10. Q1 constituent comparison for active tide gauges for year 2018 (upper part) and historical tide gauges (lower part).

	Observed		Amplitude Error (m)				Phase Error (deg)				Tidal Error (m)			
Station name	**Amplitude (m)**	**Phase (deg)**	**CIOPSW**	**SS500**	**SSS150**	**SF30**	**CIOPSW**	**SS500**	**SSS150**	**SF30**	**CIOPSW**	**SS500**	**SSS150**	**SF30**
North Arm	0.057 ± 0.013	270.1 ± 12.2	—	-0.004	+0.004	—	—	+20.7	+3.1	—	—	0.014	0.004	—

	Observed		Amplitude Error (m)				Phase Error (deg)				Tidal Error (m)			
Station name	**Amplitude (m)**	**Phase (deg)**	**CIOPSW**	**SS500**	**SSS150**	**SF30**	**CIOPSW**	**SS500**	**SSS150**	**SF30**	**CIOPSW**	**SS500**	**SSS150**	**SF30**
Sand Heads	0.078 ± 0.009	254.6 ± 6.4	-0.004	-0.002	-0.001	—	+20.1	+5.5	+6.6	—	0.019	0.005	0.006	—
Steveston	0.070 ± 0.010	260.2 ± 8.1	+0.004	-0.007	+0.005	+0.004	+14.1	+8.3	+3.4	+5.9	0.013	0.008	0.005	0.006
StevestonEC	0.070 ± 0.011	260.3 ± 8.3	+0.003	-0.003	+0.006	+0.004	+13.6	+6.4	+2.3	+5.7	0.012	0.006	0.004	0.006
Woodward's Landing	0.062 ± 0.014	264.4 ± 13.0	—	-0.009	-0.001	-0.001	—	+16.4	+6.2	+6.0	—	0.013	0.005	0.005
Deas Island	0.059 ± 0.015	269.5 ± 14.7	—	-0.006	+0.002	+0.002	—	+11.5	+1.2	+0.9	—	0.009	0.002	0.002
New Westminster	0.040 ± 0.019	272.6 ± 29.0	—	-0.003	-0.004	-0.006	—	+31.1	+9.0	+10.7	—	0.015	0.005	0.006
Port Mann	0.029 ± 0.022	276.4 ± 47.2	—	0.000	-0.007	-0.007	—	+39.7	+11.9	+14.2	—	0.014	0.006	0.007
Pitt River	0.012 ± 0.019	282.2 ± 104.5	—	—	0.000	—	—	—	+33.1	—	—	—	0.005	—
Dionisio Point	0.077	257.19	-0.001	+0.001	+0.001	—	+18.6	+3.8	+4.6	—	0.017	0.004	0.004	—
Canoe Pass	0.059	266.16	+0.019	+0.004	+0.015	+0.013	+7.3	+5.9	+0.7	+1.1	0.015	0.005	0.010	0.009
Roberts Bank	0.074	256.29	+0.001	+0.003	+0.003	—	+16.8	+3.1	+3.9	—	0.015	0.004	0.004	—
Tsawwassen	0.075	256.36	+0.001	+0.005	+0.007	—	+15.3	+0.0	-0.4	—	0.014	0.004	0.005	—

Table 11. L2 constituent comparison for active tide gauges for year 2018 (upper part) and historical tide gauges (lower part).

	Observed		Amplitude Error (m)				Phase Error (deg)				Tidal Error (m)			
Station name	**Amplitude (m)**	**Phase (deg)**	**CIOPSW**	**SS500**	**SSS150**	**SF30**	**CIOPSW**	**SS500**	**SSS150**	**SF30**	**CIOPSW**	**SS500**	**SSS150**	**SF30**
North Arm	0.037 ± 0.009	62.2 ± 18.9	—	-0.013	0.000	—	—	-6.0	-10.2	—	—	0.010	0.005	—
Sand Heads	0.026 ± 0.003	57.4 ± 7.9	-0.016	-0.019	+0.004	—	+37.9	-41.8	-10.4	—	0.014	0.015	0.005	—
Steveston	0.028 ± 0.006	60.5 ± 11.4	-0.018	-0.015	+0.003	+0.005	+32.4	-37.4	-14.0	-16.4	0.014	0.014	0.005	0.007
StevestonEC	0.028 ± 0.005	60.6 ± 12.3	-0.018	-0.016	+0.003	+0.005	+31.2	-42.2	-14.7	-16.5	0.014	0.015	0.006	0.007
Woodward's Landing	0.029 ± 0.010	68.0 ± 19.5	—	-0.010	+0.003	+0.004	—	-10.8	-14.6	-16.3	—	0.007	0.006	0.007
Deas Island	0.024 ± 0.010	77.5 ± 21.0	—	-0.005	+0.007	+0.009	—	-20.2	-24.1	-26.0	—	0.006	0.010	0.011
New Westminster	0.026 ± 0.014	86.5 ± 36.6	—	-0.008	-0.003	-0.001	—	+5.5	-13.3	-11.5	—	0.006	0.005	0.004
Port Mann	0.022 ± 0.016	98.0 ± 42.8	—	-0.008	-0.004	-0.004	—	+19.1	-11.0	-10.4	—	0.007	0.004	0.004
Pitt River	0.016 ± 0.016	105.9 ± 58.8	—	—	-0.007	—	—	—	+8.9	—	—	—	0.005	—
Dionisio Point	0.026	67.96	-0.016	-0.020	+0.003	—	+35.3	-50.2	-18.6	—	0.013	0.016	0.007	—
Canoe Pass	0.030	61.83	-0.020	-0.011	+0.004	+0.005	+19.0	-35.7	-18.6	-19.8	0.014	0.013	0.008	0.009
Roberts Bank	0.025	58.12	-0.015	-0.017	+0.003	—	+27.6	-35.7	-16.0	—	0.012	0.013	0.006	—
Tsawwassen	0.027	59.71	-0.010	-0.014	+0.011	—	+23.4	-31.4	-17.2	—	0.009	0.012	0.010	—

Table 12. J1 constituent comparison for active tide gauges for year 2018 (upper part) and historical tide gauges (lower part).

	Observed		Amplitude Error (m)				Phase Error (deg)				Tidal Error (m)			
Station name	**Amplitude (m)**	**Phase (deg)**	**CIOPSW**	**SS500**	**SSS150**	**SF30**	**CIOPSW**	**SS500**	**SSS150**	**SF30**	**CIOPSW**	**SS500**	**SSS150**	**SF30**
North Arm	0.033 ± 0.012	329.1 ± 19.6	—	-0.007	+0.003	—	—	+136.9	+6.6	—	—	0.039	0.004	—
Sand Heads	0.048 ± 0.008	314.0 ± 11.3	-0.018	-0.038	-0.002	—	+138.7	+130.5	+8.7	—	0.052	0.039	0.005	—
Steveston	0.043 ± 0.010	319.6 ± 13.8	-0.012	-0.026	+0.002	+0.002	+131.1	+135.8	+5.0	+10.0	0.047	0.039	0.003	0.006
StevestonEC	0.043 ± 0.010	319.6 ± 12.9	-0.013	-0.027	+0.003	+0.002	+130.5	+130.8	+5.2	+10.0	0.047	0.038	0.003	0.006
Woodward's Landing	0.037 ± 0.012	321.3 ± 20.0	—	-0.017	-0.001	-0.001	—	+145.9	+9.0	+9.8	—	0.039	0.004	0.005
Deas Island	0.035 ± 0.013	318.9 ± 21.2	—	-0.014	+0.001	+0.001	—	+148.4	+11.6	+12.2	—	0.038	0.005	0.005
New Westminster	0.026 ± 0.019	334.7 ± 45.6	—	-0.007	-0.001	-0.003	—	+146.7	+6.9	+10.0	—	0.030	0.002	0.004
Port Mann	0.021 ± 0.020	344.4 ± 58.4	—	-0.006	-0.001	-0.003	—	+150.1	+4.3	+8.7	—	0.025	0.001	0.003
Pitt River	0.017 ± 0.017	10.9 ± 70.8	—	—	-0.004	—	—	—	-5.1	—	—	—	0.003	—
Dionisio Point	0.050	323.68	-0.020	-0.041	-0.006	—	+132.5	+130.9	-1.0	—	0.053	0.040	0.004	—
Canoe Pass	0.032	334.00	+0.002	-0.008	+0.012	+0.013	+111.0	+108.7	-1.3	+0.6	0.038	0.032	0.009	0.009
Roberts Bank	0.041	315.42	-0.008	-0.028	+0.003	—	+136.6	+128.3	+8.2	—	0.048	0.035	0.005	—
Tsawwassen	0.046	327.01	-0.014	-0.034	-0.001	—	+129.3	+129.9	-0.2	—	0.050	0.039	0.001	—

Table 13. NO1 constituent comparison for active tide gauges for year 2018 (upper part) and historical tide gauges (lower part).

	Observed		Amplitude Error (m)				Phase Error (deg)				Tidal Error (m)			
Station name	**Amplitude (m)**	**Phase (deg)**	**CIOPSW**	**SS500**	**SSS150**	**SF30**	**CIOPSW**	**SS500**	**SSS150**	**SF30**	**CIOPSW**	**SS500**	**SSS150**	**SF30**
North Arm	0.042 ± 0.023	9.9 ± 37.6	—	+0.076	-0.005	—	—	+78.8	+52.9	—	—	0.083	0.025	—
Sand Heads	0.059 ± 0.018	330.0 ± 16.4	+0.023	+0.018	-0.033	—	+108.1	+112.7	+64.6	—	0.081	0.081	0.038	—
Steveston	0.051 ± 0.020	337.4 ± 22.4	+0.033	+0.043	-0.027	-0.019	+99.6	+109.5	+54.8	+62.9	0.075	0.086	0.030	0.033
StevestonEC	0.051 ± 0.022	337.9 ± 24.5	+0.032	+0.042	-0.023	-0.019	+99.1	+107.8	+53.0	+62.6	0.074	0.084	0.029	0.033
Woodward's Landing	0.040 ± 0.024	349.8 ± 41.4	—	+0.067	-0.013	-0.011	—	+100.4	+71.2	+75.3	—	0.085	0.028	0.030
Deas Island	0.037 ± 0.027	349.1 ± 39.3	—	+0.069	-0.010	-0.009	—	+101.1	+72.2	+76.3	—	0.084	0.027	0.029
New Westminster	0.027 ± 0.036	29.8 ± 86.8	—	+0.075	+0.003	+0.006	—	+66.4	+60.7	+63.0	—	0.067	0.020	0.022
Port Mann	0.024 ± 0.039	54.2 ± 101.5	—	+0.066	+0.006	+0.007	—	+46.0	+48.3	+50.7	—	0.053	0.016	0.017
Pitt River	0.021 ± 0.034	110.8 ± 120.0	—	—	+0.009	—	—	—	+15.5	—	—	—	0.008	—
Dionisio Point	0.019	281.92	+0.053	+0.051	-0.003	—	+160.3	+166.9	+116.2	—	0.064	0.063	0.022	—
Canoe Pass	0.015	350.77	+0.091	+0.103	+0.078	+0.082	+19.4	+26.4	-21.2	-20.0	0.065	0.074	0.056	0.058

	Observed		Amplitude Error (m)				Phase Error (deg)				Tidal Error (m)			
Station name	**Amplitude (m)**	**Phase (deg)**	**CIOPSW**	**SS500**	**SSS150**	**SF30**	**CIOPSW**	**SS500**	**SSS150**	**SF30**	**CIOPSW**	**SS500**	**SSS150**	**SF30**
Roberts Bank	0.052	293.63	+0.057	+0.037	+0.026	—	+93.2	+94.3	+30.1	—	0.087	0.076	0.030	—
Tsawwassen	0.032	305.45	-0.009	-0.017	-0.002	—	+84.3	+116.6	-29.0	—	0.026	0.029	0.011	—

Table 14. OO1 constituent comparison for active tide gauges for year 2018 (upper part) and historical tide gauges (lower part).

	Observed		Amplitude Error (m)				Phase Error (deg)				Tidal Error (m)			
Station name	**Amplitude (m)**	**Phase (deg)**	**CIOPSW**	**SS500**	**SSS150**	**SF30**	**CIOPSW**	**SS500**	**SSS150**	**SF30**	**CIOPSW**	**SS500**	**SSS150**	**SF30**
North Arm	0.043 ± 0.019	344.4 ± 26.6	—	-0.031	+0.009	—	—	+103.7	+21.9	—	—	0.033	0.014	—
Sand Heads	0.042 ± 0.015	336.5 ± 18.3	-0.026	-0.030	+0.014	—	+106.5	+105.1	+26.6	—	0.035	0.033	0.018	—
Steveston	0.043 ± 0.016	340.7 ± 22.4	-0.026	-0.037	+0.013	+0.012	+100.8	+90.0	+24.3	+24.6	0.034	0.031	0.017	0.017
StevestonEC	0.043 ± 0.016	341.0 ± 24.4	-0.026	-0.036	+0.012	+0.012	+99.0	+83.0	+25.4	+24.3	0.034	0.030	0.017	0.017
Woodward's Landing	0.043 ± 0.022	346.3 ± 29.2	—	-0.032	+0.009	+0.011	—	+88.0	+19.5	+18.2	—	0.031	0.013	0.013
Deas Island	0.035 ± 0.022	351.4 ± 38.8	—	-0.024	+0.016	+0.018	—	+82.8	+14.4	+13.1	—	0.025	0.014	0.015
New Westminster	0.034 ± 0.032	3.5 ± 55.9	—	-0.018	+0.005	+0.005	—	+97.7	+17.2	+16.8	—	0.028	0.008	0.008
Port Mann	0.031 ± 0.033	13.6 ± 78.6	—	-0.015	+0.002	+0.001	—	+100.2	+19.3	+19.9	—	0.026	0.008	0.008
Pitt River	0.024 ± 0.029	33.2 ± 78.0	—	—	0.000	—	—	—	+30.2	—	—	—	0.009	—
Dionisio Point	0.043	332.29	-0.028	-0.031	+0.014	—	+109.2	+100.8	+33.2	—	0.035	0.033	0.022	—
Canoe Pass	0.034	343.49	-0.016	-0.022	+0.022	+0.024	+81.6	+55.2	+5.6	+5.4	0.026	0.021	0.016	0.017
Roberts Bank	0.036	335.44	-0.018	-0.022	+0.026	—	+87.9	+79.6	+18.2	—	0.028	0.025	0.021	—
Tsawwassen	0.028	327.70	-0.021	-0.025	+0.011	—	+78.3	+78.0	+19.4	—	0.020	0.020	0.011	—

Table 15. SO1 constituent comparison for active tide gauges for year 2018 (upper part) and historical tide gauges (lower part).

	Observed		Amplitude Error (m)				Phase Error (deg)				Tidal Error (m)			
Station name	**Amplitude (m)**	**Phase (deg)**	**CIOPSW**	**SS500**	**SSS150**	**SF30**	**CIOPSW**	**SS500**	**SSS150**	**SF30**	**CIOPSW**	**SS500**	**SSS150**	**SF30**
North Arm	0.031 ± 0.010	80.7 ± 19.4	—	+0.009	-0.011	—	—	+27.8	-19.5	—	—	0.014	0.010	—
Sand Heads	0.024 ± 0.007	46.6 ± 17.0	+0.016	-0.004	-0.005	—	+55.2	+40.2	-24.2	—	0.023	0.011	0.007	—
Steveston	0.025 ± 0.008	59.2 ± 18.8	+0.015	+0.003	-0.007	-0.004	+41.5	+37.5	-34.9	-26.0	0.019	0.012	0.010	0.008
StevestonEC	0.025 ± 0.009	59.3 ± 19.2	+0.015	+0.002	-0.006	-0.004	+41.1	+34.6	-35.6	-26.1	0.019	0.011	0.010	0.008
Woodward’s Landing	0.025 ± 0.012	73.5 ± 28.1	—	+0.013	-0.009	-0.007	—	+31.5	-21.1	-15.7	—	0.015	0.008	0.006
Deas Island	0.021 ± 0.011	76.3 ± 31.3	—	+0.017	-0.005	-0.003	—	+28.8	-23.5	-18.3	—	0.016	0.007	0.005
New Westminster	0.024 ± 0.016	105.3 ± 39.2	—	+0.013	-0.010	-0.009	—	+20.6	-4.1	-1.3	—	0.012	0.007	0.006

	Observed		Amplitude Error (m)				Phase Error (deg)				Tidal Error (m)			
Station name	**Amplitude (m)**	**Phase (deg)**	**CIOPSW**	**SS500**	**SSS150**	**SF30**	**CIOPSW**	**SS500**	**SSS150**	**SF30**	**CIOPSW**	**SS500**	**SSS150**	**SF30**
Port Mann	0.022 ± 0.019	118.4 ± 51.1	—	+0.009	-0.010	-0.009	—	+20.8	+9.2	+9.4	—	0.009	0.007	0.007
Pitt River	0.018 ± 0.016	146.3 ± 51.8	—	—	-0.006	—	—	—	+17.0	—	—	—	0.005	—
Dionisio Point	0.033	56.98	+0.008	-0.013	-0.016	—	+47.8	+36.7	-25.7	—	0.022	0.015	0.013	—
Canoe Pass	0.032	79.72	+0.006	-0.003	-0.017	-0.017	+24.7	+24.4	-36.4	-32.3	0.011	0.009	0.016	0.015
Roberts Bank	0.026	48.37	+0.011	-0.008	-0.011	—	+54.9	+42.3	-32.6	—	0.022	0.012	0.011	—
Tsawwassen	0.032	48.49	+0.017	-0.003	-0.005	—	+55.5	+45.5	-0.8	—	0.028	0.017	0.004	—

Table 16. NU2 constituent comparison for active tide gauges for year 2018 (upper part) and historical tide gauges (lower part).

	Observed		Amplitude Error (m)				Phase Error (deg)				Tidal Error (m)			
Station name	**Amplitude (m)**	**Phase (deg)**	**CIOPSW**	**SS500**	**SSS150**	**SF30**	**CIOPSW**	**SS500**	**SSS150**	**SF30**	**CIOPSW**	**SS500**	**SSS150**	**SF30**
North Arm	0.035 ± 0.014	28.3 ± 14.4	—	-0.029	+0.002	—	—	-50.3	-2.7	—	—	0.022	0.002	—
Sand Heads	0.036 ± 0.004	11.3 ± 5.7	-0.034	-0.036	+0.002	—	+70.4	+7.6	+0.7	—	0.025	0.025	0.001	—
Steveston	0.035 ± 0.006	18.4 ± 10.6	-0.033	-0.034	+0.002	+0.002	+57.9	+16.4	-5.0	-1.7	0.024	0.024	0.003	0.002
StevestonEC	0.035 ± 0.007	18.3 ± 11.0	-0.033	-0.035	+0.002	+0.002	+57.7	-1.8	-6.4	-1.6	0.024	0.024	0.003	0.002
Woodward's Landing	0.033 ± 0.012	29.1 ± 19.0	—	-0.029	+0.002	+0.001	—	-8.4	-5.3	-3.6	—	0.021	0.002	0.002
Deas Island	0.030 ± 0.009	37.2 ± 19.7	—	-0.026	+0.005	+0.004	—	-17.6	-13.3	-12.0	—	0.019	0.006	0.006
New Westminster	0.025 ± 0.018	50.8 ± 39.6	—	-0.021	0.000	0.000	—	-34.3	-4.3	-5.4	—	0.016	0.001	0.002
Port Mann	0.021 ± 0.019	65.4 ± 60.7	—	-0.018	0.000	-0.002	—	-25.3	-3.3	-4.5	—	0.013	0.001	0.002
Pitt River	0.014 ± 0.017	97.3 ± 77.6	—	—	0.000	—	—	—	-10.4	—	—	—	0.002	—
Dionisio Point	0.037	10.24	-0.034	-0.036	0.000	—	+77.1	+12.0	+3.3	—	0.026	0.026	0.002	—
Canoe Pass	0.034	20.68	-0.032	-0.033	+0.002	+0.002	+59.7	-48.2	-2.9	-3.3	0.023	0.023	0.002	0.002
Roberts Bank	0.031	8.62	-0.029	-0.030	+0.004	—	+62.4	+28.0	+1.2	—	0.021	0.021	0.003	—
Tsawwassen	0.033	7.99	-0.031	-0.032	+0.001	—	+72.4	+57.0	+3.1	—	0.023	0.023	0.002	—

Table 17. 2N2 constituent comparison for active tide gauges for year 2018 (upper part) and historical tide gauges (lower part).

	Observed		Amplitude Error (m)				Phase Error (deg)				Tidal Error (m)			
Station name	**Amplitude (m)**	**Phase (deg)**	**CIOPSW**	**SS500**	**SSS150**	**SF30**	**CIOPSW**	**SS500**	**SSS150**	**SF30**	**CIOPSW**	**SS500**	**SSS150**	**SF30**
North Arm	0.015 ± 0.011	329.3 ± 39.9	—	-0.005	-0.003	—	—	-112.5	-15.8	—	—	0.014	0.004	—
Sand Heads	0.026 ± 0.003	329.3 ± 7.7	-0.020	-0.018	-0.006	—	-53.3	-19.6	-8.0	—	0.016	0.013	0.005	—
Steveston	0.022 ± 0.006	329.8 ± 16.0	-0.016	-0.015	-0.004	-0.008	-62.7	-105.3	-4.0	-5.0	0.014	0.017	0.003	0.006

Observed			Amplitude Error (m)				Phase Error (deg)				Tidal Error (m)			
Station name	**Amplitude (m)**	**Phase (deg)**	**CIOPSW**	**SS500**	**SSS150**	**SF30**	**CIOPSW**	**SS500**	**SSS150**	**SF30**	**CIOPSW**	**SS500**	**SSS150**	**SF30**
StevestonEC	0.022 ± 0.006	329.7 ± 15.8	-0.016	-0.016	-0.005	-0.008	-60.1	-95.7	-4.8	-4.9	0.014	0.016	0.004	0.006
Woodward's Landing	0.019 ± 0.010	330.1 ± 33.5	—	-0.013	-0.005	-0.005	—	-101.8	-12.9	-19.8	—	0.015	0.005	0.005
Deas Island	0.019 ± 0.010	342.9 ± 29.5	—	-0.013	-0.005	-0.005	—	-114.2	-25.8	-33.3	—	0.015	0.006	0.007
New Westminster	0.011 ± 0.015	334.3 ± 95.8	—	-0.009	-0.003	-0.002	—	-119.4	-30.7	-27.9	—	0.008	0.004	0.004
Port Mann	0.007 ± 0.015	342.8 ± 136.0	—	-0.004	-0.003	-0.003	—	+174.7	-30.6	-26.6	—	0.007	0.003	0.003
Pitt River	0.003 ± 0.012	13.3 ± 185.9	—	—	0.000	—	—	—	-34.3	—	—	—	0.001	—
Dionisio Point	0.028	336.73	-0.023	-0.021	-0.009	—	-62.3	-15.1	-10.4	—	0.018	0.015	0.007	—
Canoe Pass	0.016	327.44	-0.009	-0.006	-0.008	-0.009	-106.8	-173.6	-7.3	-2.8	0.013	0.018	0.006	0.006
Roberts Bank	0.022	321.59	-0.017	-0.018	-0.009	—	-87.5	-39.5	-2.7	—	0.016	0.014	0.006	—
Tsawwassen	0.018	321.36	-0.015	-0.014	-0.006	—	+168.0	+109.7	+21.7	—	0.016	0.015	0.006	—

Table 18. Tidal water level scores for year 2018.

Station name	CRMSE (m)				γ^2				Pearson			
	CIOPSW	**SS500**	**SSS150**	**SF30**	**CIOPSW**	**SS500**	**SSS150**	**SF30**	**CIOPSW**	**SS500**	**SSS150**	**SF30**
North Arm	—	0.206	0.070	—	—	0.054	0.006	—	—	0.976	0.997	—
Sand Heads	0.177	0.079	0.040	—	0.034	0.007	0.002	—	0.983	0.997	0.999	—
Steveston	0.135	0.107	0.083	0.061	0.021	0.013	0.008	0.004	0.991	0.994	0.996	0.998
StevestonEC	0.131	0.092	0.095	0.060	0.020	0.010	0.011	0.004	0.991	0.995	0.995	0.998
Woodward's Landing	—	0.156	0.065	0.059	—	0.032	0.005	0.005	—	0.986	0.998	0.998
Deas Island	—	0.118	0.137	0.146	—	0.022	0.030	0.034	—	0.990	0.988	0.988
New Westminster	—	0.181	0.069	0.075	—	0.070	0.010	0.012	—	0.966	0.997	0.998
Port Mann	—	0.183	0.063	0.099	—	0.100	0.012	0.029	—	0.953	0.998	0.997
Pitt River	—	—	0.091	—	—	—	0.046	—	—	—	0.987	—

Table 19. Non-tidal water level scores for year 2018.

Station name	CRMSE (m)				γ^2				Pearson			
	CIOPSW	**SS500**	**SSS150**	**SF30**	**CIOPSW**	**SS500**	**SSS150**	**SF30**	**CIOPSW**	**SS500**	**SSS150**	**SF30**
North Arm	—	0.115	0.066	—	—	0.529	0.171	—	—	0.841	0.912	—
Sand Heads	0.052	0.048	0.049	—	0.148	0.126	0.132	—	0.923	0.935	0.932	—
Steveston	0.075	0.059	0.060	0.062	0.298	0.181	0.193	0.201	0.841	0.910	0.898	0.894

Station name	CRMSE (m)				χ^2				Pearson			
	CIOPSW	SS500	SSS150	SF30	CIOPSW	SS500	SSS150	SF30	CIOPSW	SS500	SSS150	SF30
StevestonEC	0.078	0.055	0.067	0.064	0.320	0.159	0.236	0.219	0.829	0.918	0.874	0.884
Woodward's Landing	—	0.136	0.064	0.056	—	0.652	0.147	0.111	—	0.844	0.927	0.944
Deas Island	—	0.195	0.111	0.110	—	1.173	0.381	0.371	—	0.616	0.787	0.794
New Westminster	—	0.350	0.076	0.057	—	1.254	0.059	0.033	—	0.928	0.978	0.984
Port Mann	—	0.545	0.079	0.072	—	1.668	0.035	0.029	—	0.931	0.987	0.986
Pitt River	—	—	0.105	—	—	—	0.047	—	—	—	0.978	—

Table 20. Total water level scores for year 2018.

Station name	bias (m)				CRMSE (m)			
	CIOPSW	**SS500**	**SSS150**	**SF30**	**CIOPSW**	**SS500**	**SSS150**	**SF30**
North Arm	—	0.025	-0.054	—	—	0.235	0.093	—
Sand Heads	0.061	0.069	0.067	—	0.184	0.092	0.063	—
Steveston	-0.153	-0.061	-0.087	-0.113	0.153	0.120	0.103	0.085
StevestonEC	-0.052	0.014	-0.006	-0.008	0.151	0.106	0.116	0.086
Woodward's Landing	—	0.060	0.006	-0.013	—	0.204	0.090	0.077
Deas Island	—	0.064	0.011	-0.013	—	0.227	0.176	0.183
New Westminster	—	0.318	0.034	0.059	—	0.393	0.093	0.088
Port Mann	—	0.503	-0.002	0.035	—	0.575	0.101	0.122
Pitt River	—	—	0.004	—	—	—	0.138	—
		χ^2				Pearson		
	CIOPSW	**SS500**	**SSS150**	**SF30**	**CIOPSW**	**SS500**	**SSS150**	**SF30**
North Arm	—	0.068	0.011	—	—	0.967	0.995	—
Sand Heads	0.036	0.009	0.004	—	0.982	0.996	0.998	—
Steveston	0.027	0.016	0.012	0.008	0.988	0.992	0.994	0.996
StevestonEC	0.026	0.013	0.015	0.008	0.988	0.994	0.993	0.996
Woodward's Landing	—	0.052	0.010	0.007	—	0.974	0.995	0.996
Deas Island	—	0.079	0.047	0.051	—	0.964	0.980	0.980
New Westminster	—	0.274	0.015	0.014	—	0.894	0.995	0.996
Port Mann	—	0.643	0.020	0.029	—	0.851	0.994	0.991
Pitt River	—	—	0.046	—	—	—	0.982	—

Table 21. Average scores for the non-tidal water level during storm surge events. N denotes number of storm events for each station.

Station	N	score											
		CRMSE (m)				γ^2				Pearson's R			
		CIOPSW	SS500	SSS150	SF30	CIOPSW	SS500	SSS150	SF30	CIOPSW	SS500	SSS150	SF30
North Arm	4	—	0.046	0.033	—	—	0.403	0.213	—	—	0.813	0.895	—
Sand Heads	8	0.033	0.031	0.031	—	0.168	0.152	0.150	—	0.920	0.928	0.930	—
Steveston	8	0.035	0.036	0.033	0.032	0.145	0.198	0.135	0.128	0.931	0.901	0.936	0.940
StevestonEC	7	0.035	0.036	0.033	0.032	0.183	0.227	0.163	0.160	0.913	0.888	0.921	0.923
Woodward's Landing	7	—	0.045	0.039	0.036	—	0.294	0.157	0.137	—	0.861	0.932	0.939
Deas Island	7	—	0.057	0.054	0.051	—	0.530	0.366	0.342	—	0.766	0.836	0.845
New Westminster	8	—	0.064	0.057	0.054	—	0.455	0.287	0.262	—	0.805	0.905	0.916
Port Mann	7	—	0.082	0.081	0.077	—	0.598	0.258	0.245	—	0.763	0.915	0.925
Pitt River	7	—	—	0.099	—	—	—	0.386	—	—	—	0.918	—

Table 22. Scores for the along-shore velocity measured by horizontal ADCP at Woodward's Landing. Negative sign corresponds to the downstream flow.

Water level component	Variance fraction	Mean (m/s) Observed	Bias (m/s)		CRMSE (m/s)		γ^2		Pearson's R	
			SSS150	SF30	SSS150	SF30	SSS150	SF30	SSS150	SF30
Total	1	-0.793	-0.133	-0.048	0.261	0.244	0.149	0.131	0.945	0.941
Non-tidal	0.203	—	-0.150	-0.067	0.203	0.206	0.446	0.459	0.777	0.753
Tidal	0.797	—	0.017	0.019	0.169	0.131	0.078	0.047	0.984	0.984

Table 23. Error statistics for the model tidal constituents versus observations by horizontal ADCP at Woodward's Landing.

Constituent	Observed		Ampl Error (m/s)		Phase Error (deg)		Tidal Error (m/s)	
	Amplitude (m/s)	Phase (deg)	SSS150	SF30	SSS150	SF30	SSS150	SF30
M2	0.559 ± 0.023	18.4 ± 2.7	+0.131	+0.075	+1.44	-0.46	0.093	0.053
N2	0.121 ± 0.023	352.8 ± 11.7	+0.016	+0.010	-1.62	-2.58	0.012	0.008
S2	0.152 ± 0.024	42.5 ± 8.9	+0.015	-0.003	+9.90	+6.97	0.022	0.013
O1	0.217 ± 0.024	207.5 ± 6.4	+0.063	+0.049	+10.29	+2.65	0.055	0.036
K1	0.432 ± 0.028	250.1 ± 3.7	+0.128	+0.097	+3.28	+0.58	0.093	0.068
P1	0.147 ± 0.029	274.0 ± 11.1	-0.014	-0.032	-6.74	-13.73	0.015	0.031
Q1	0.033 ± 0.026	219.3 ± 48.4	+0.006	-0.001	+4.96	-6.12	0.005	0.003
K2	0.078 ± 0.020	10.6 ± 12.7	0	+0.005	+15.80	+16.43	0.015	0.017

Table 24. Total current scores for SSS150 for ADCP records subset to four depths.

Station	Depth (m)	bias u (m/s)	bias v (m/s)	RMSE (m/s)	γ^2	vector correlation magnitude	vector correlation angle (deg)
Fraser River Delta Lower Slope	**40.0**	-0.03	0.07	0.19	0.45	0.80	-11.5
	58.5	-0.02	0.08	0.17	0.41	0.83	-13.6
	98.1	0.00	0.09	0.18	0.45	0.83	-10.4
	141.1	0.02	0.05	0.15	0.42	0.85	-17.6
Strait of Georgia Central	**68.8**	0.03	-0.05	0.17	0.65	0.65	-3.3
	121.9	0.02	-0.02	0.14	0.50	0.74	0.0
	199.6	0.01	-0.01	0.12	0.36	0.83	-4.0
	288.8	0.02	-0.02	0.11	0.27	0.87	-3.4
Strait of Georgia East	**11.6**	0.04	-0.03	0.26	0.75	0.61	-5.6
	44.5	-0.01	0.02	0.16	0.30	0.85	-2.9
	98.1	-0.01	0.03	0.14	0.25	0.89	-3.5
	157.6	0.05	-0.02	0.15	0.29	0.86	-7.7

Table 25. Non-tidal current scores for SSS150 for ADCP records subset to four depths.

Station	Depth (m)	RMSE (m/s)	γ^2	vector correlation magnitude	vector correlation angle (deg)
Fraser River Delta Lower Slope	**40.0**	0.17	1.10	0.33	7.7
	58.5	0.16	1.30	0.28	0.5
	98.1	0.16	1.27	0.27	-5.0
	141.1	0.12	1.17	0.34	-12.3
Strait of Georgia Central	**68.8**	0.15	1.25	0.14	21.2
	121.9	0.12	1.46	0.08	57.2
	199.6	0.10	1.39	0.04	10.7
	288.8	0.09	0.83	0.45	-9.8
Strait of Georgia East	**11.6**	0.25	1.34	0.17	-16.3
	44.5	0.15	1.19	0.30	11.9
	98.1	0.12	1.19	0.32	8.3
	157.6	0.13	0.89	0.44	-6.9

Table 26. Tidal current scores for SSS150 for ADCP records subset to four depths.

Station	Depth (m)	RMSE (m/s)	γ^2
Fraser River Delta Lower Slope	**40.0**	0.17	0.09
	58.5	0.15	0.08
	98.1	0.20	0.09
	141.1	0.21	0.09
Strait of Georgia Central	**68.8**	0.27	0.08
	121.9	0.17	0.07
	199.6	0.10	0.06
	288.8	0.10	0.05
Strait of Georgia East	**11.6**	0.19	0.09
	44.5	0.06	0.06
	98.1	0.10	0.08
	157.6	0.13	0.08

Table 27. Scores for sea surface temperature at Fraser River Water Quality Buoy.

score	SS500	SSS150	SF30
Bias (deg C)	-0.602	-0.446	-0.370
CRMSE (deg C)	1.111	1.107	1.097
χ^2	0.038	0.038	0.037
Pearson's r	0.981	0.981	0.981

Table 28. Scores for moored CTD at SEVIP station.

score	Temperature			Salinity		
	CIOPSW	**SS500**	**SSS150**	**CIOPSW**	**SS500**	**SSS150**
Bias (deg C | PSU)	0.385	0.389	0.388	0.818	0.049	0.051
CRMSE (deg C | PSU)	0.374	0.311	0.363	0.171	0.168	0.204
χ^2	0.348	0.241	0.299	0.335	0.324	0.407
Pearson's r	0.807	0.882	0.859	0.839	0.822	0.781

Table 29. Number of CTD cast for the period from 2017 to 2021 for the five analysed subregions.

Region	Number of casts
Strait of Georgia South	588
Lower Fraser River	7
Massey To Annacis	20
Port Mann	11
Upper Fraser River	27

Table 30. Drift evaluation statistics for hourly intervals (only one available).

Hour	Molcard Skill Score			Separation Distance (km)		
	SS500	SSS150	SF30	SS500	SSS150	SF30
1	0.2	0.35	0.36	1.25	0.65	0.67

12. FIGURES

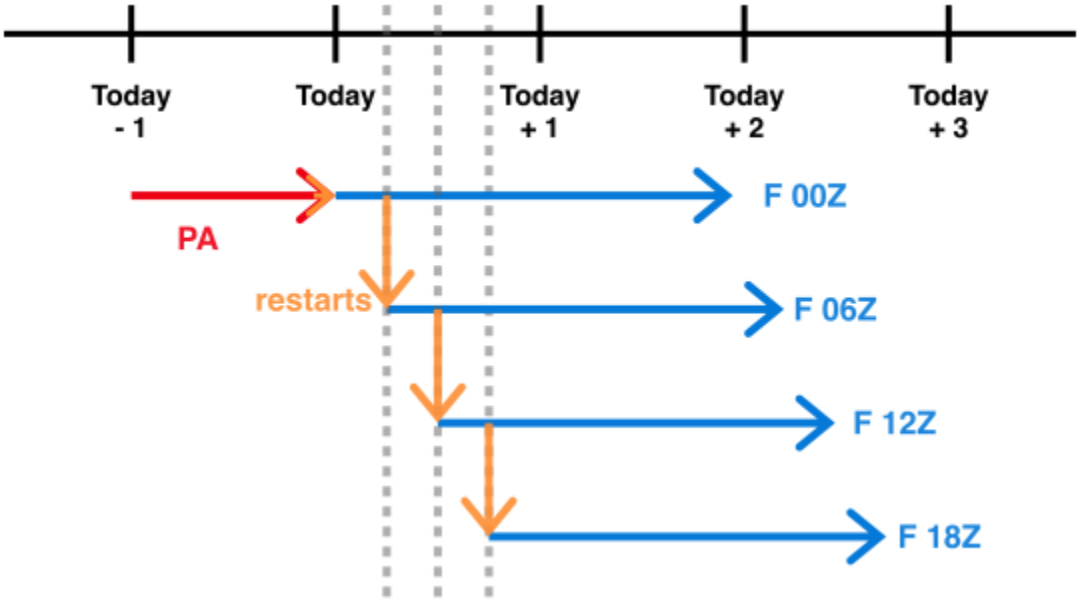

Figure 1. Schematic of one timestamp's set of pseudo-analysis (PA, in red) and forecast (in blue) runs. Grey dashed lines are spaced six hours apart, and orange arrows indicate where a restart file is generated and used to launch the subsequent step. The PA for today+1 will start with the same restart used to start today's 00Z forecast, and the pattern will repeat.

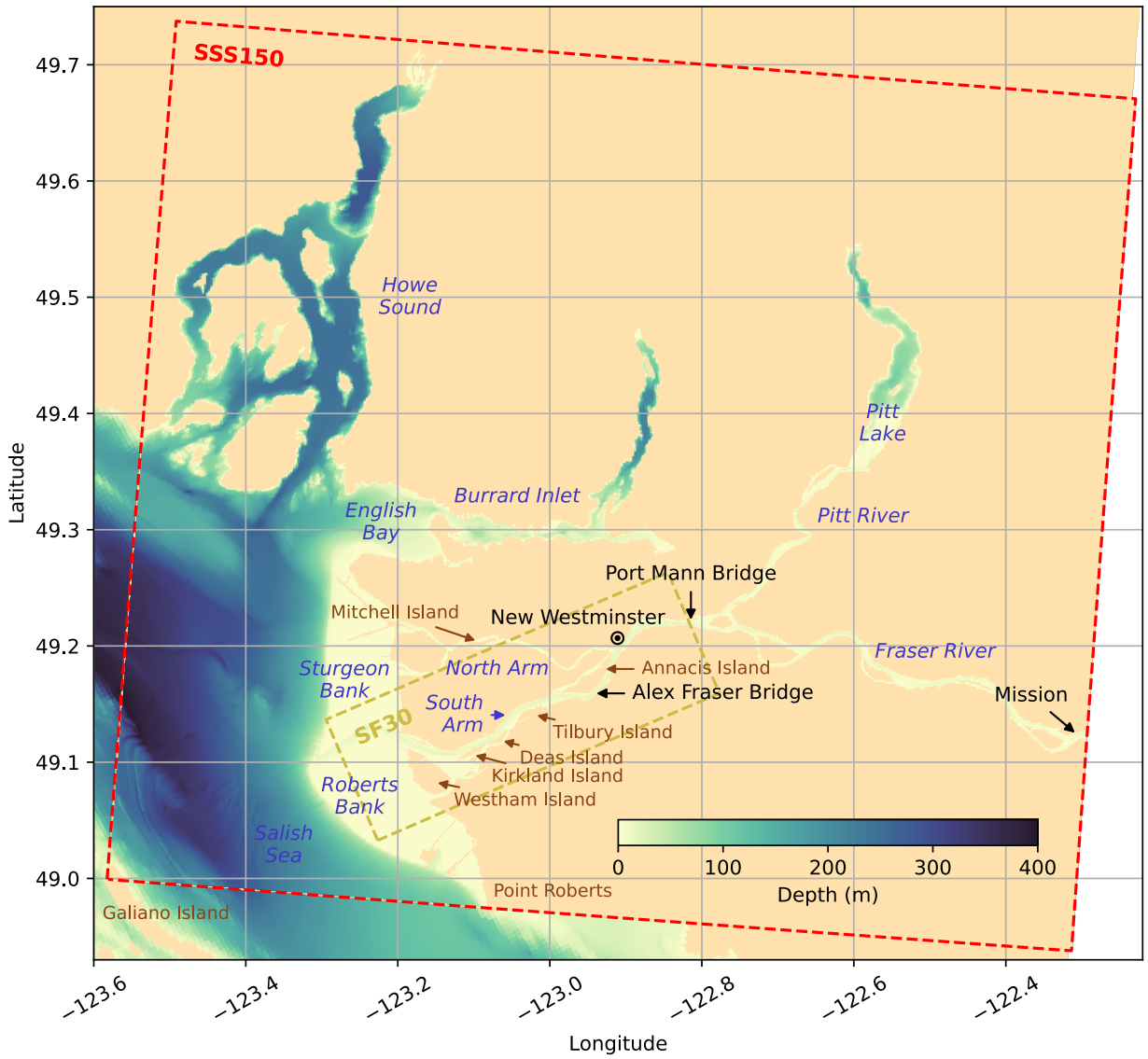

Figure 2. Model domain showing the outer (SSS150) and the inner (SF30) grids; colour scale shows depth.

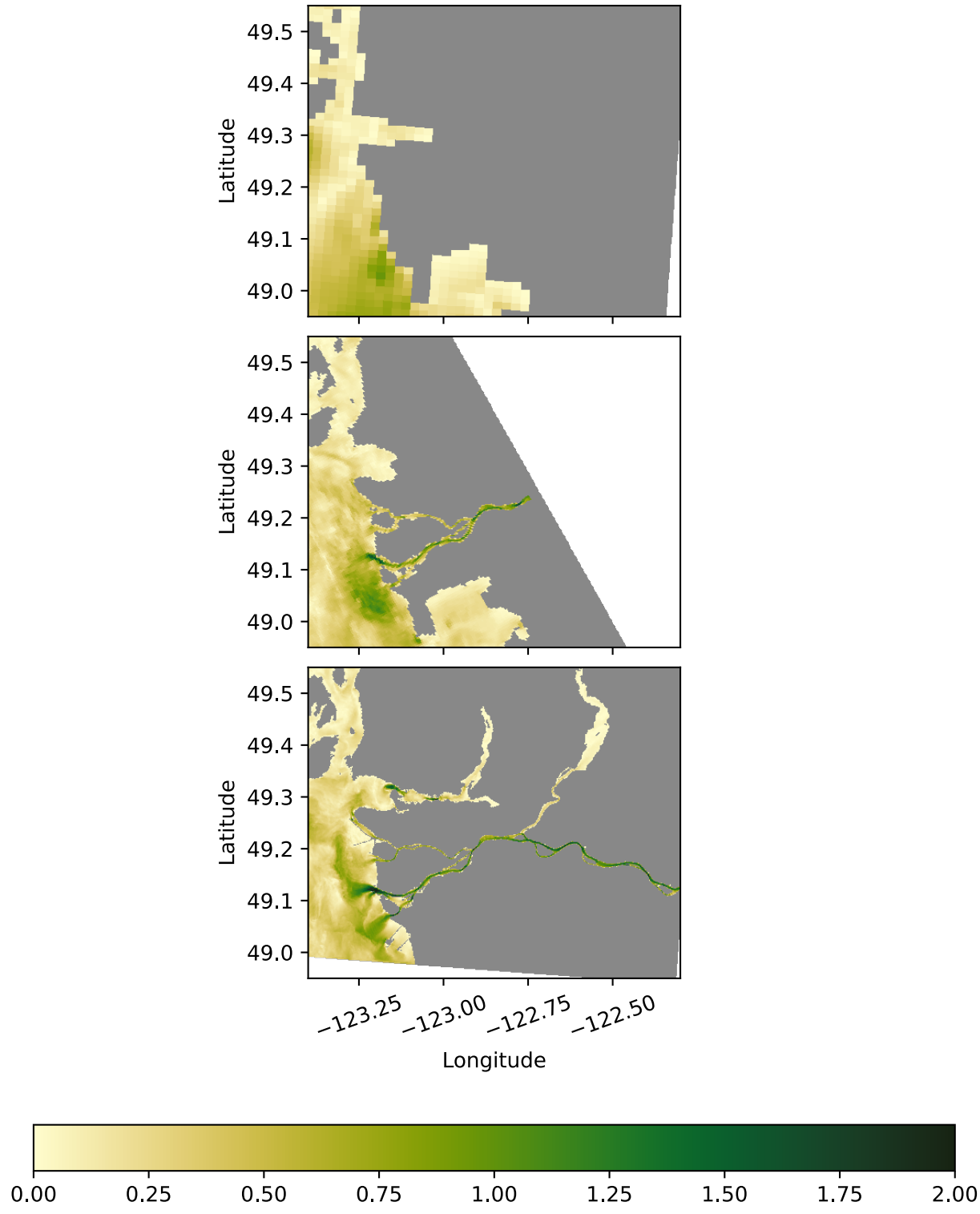

Figure 3. Surface speed (m/s) for CIOPS-W, SS500 and SSS150 (from top to bottom) for the Fraser River.

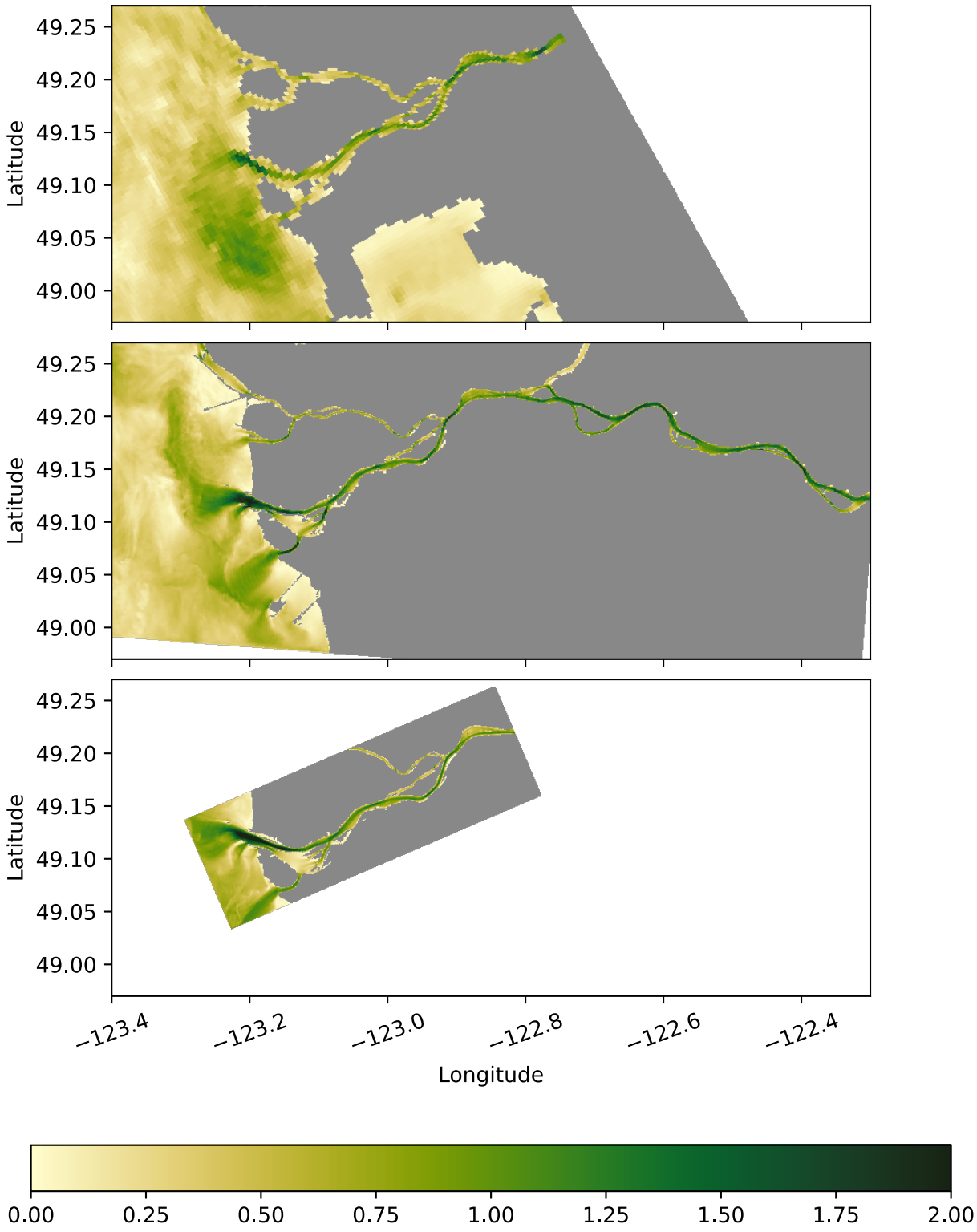

Figure 4. Surface speed (m/s) for SS500, SSS150 and SF30 (from top to bottom) for the lower Fraser River, excluding Pitt Lake.

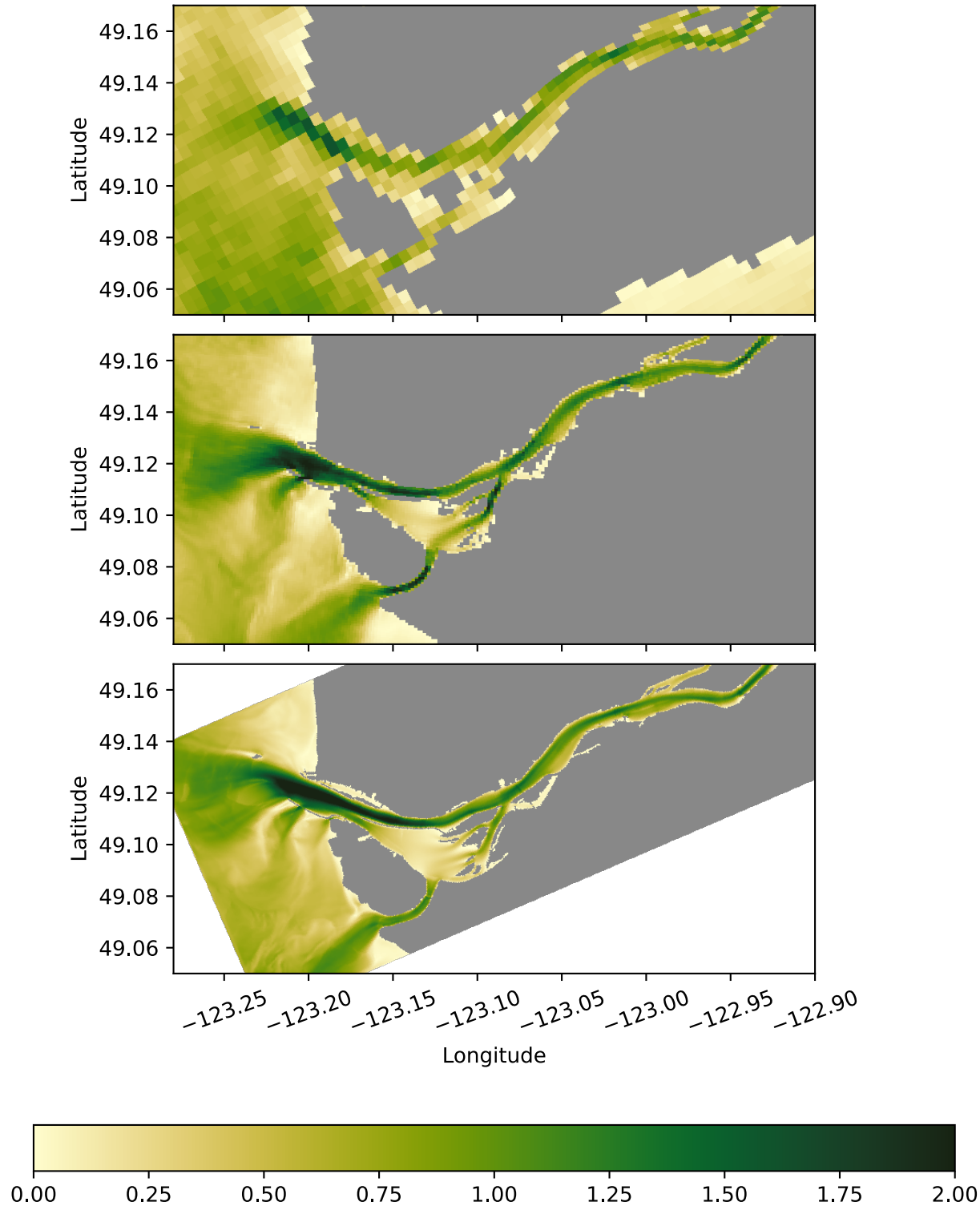

Figure 5. Surface speed (m/s) for SS500, SSS150 and SF30 (from top to bottom) for the Lower Fraser River (zoom of Figure 4).

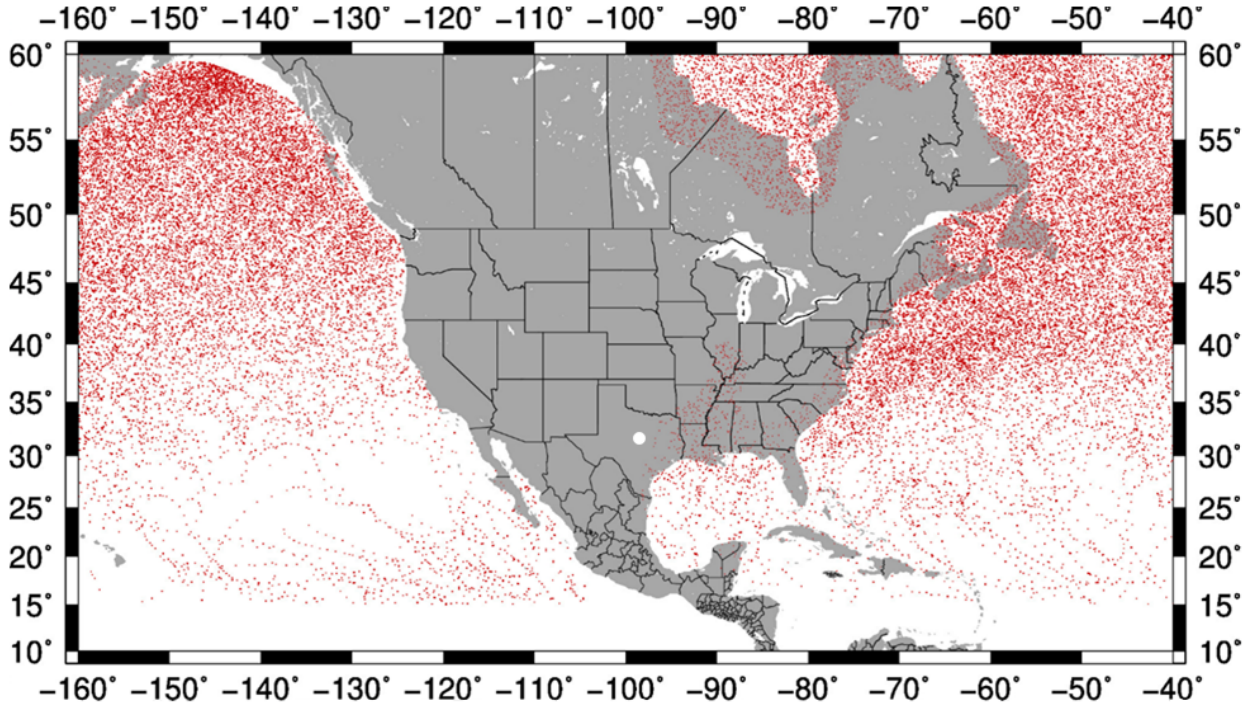

Figure 6. Cyclone locations every six hours from 2010-2021.

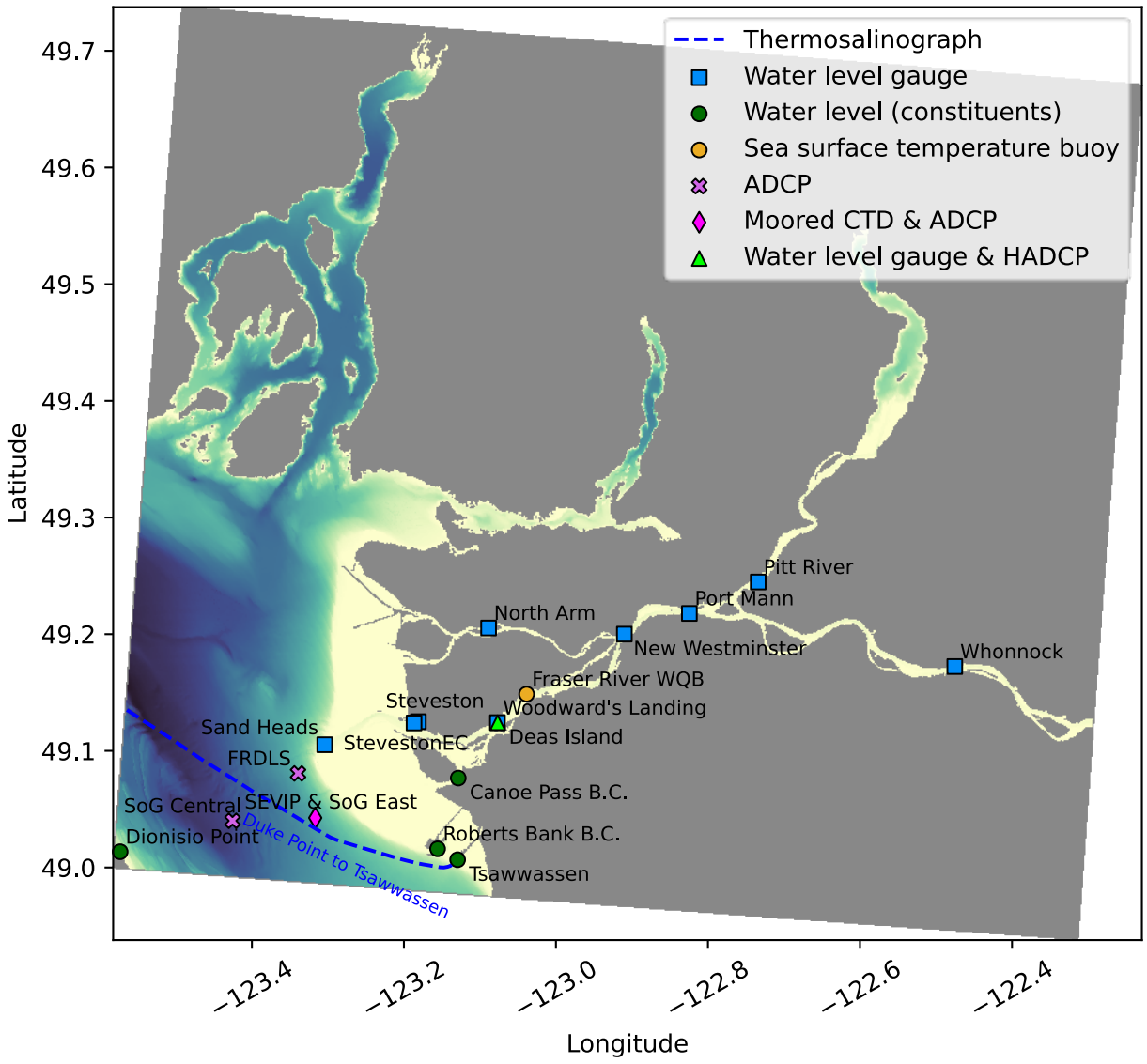

Figure 7. Locations of instruments used in this evaluation. The double water level markers are Steveston (CHS station) and StevestonEC (WSC station) near the mouth of the Fraser. The green triangle marker represents Woodward's Landing (water level and HADCP) while the blue marker below it represents Deas Island.

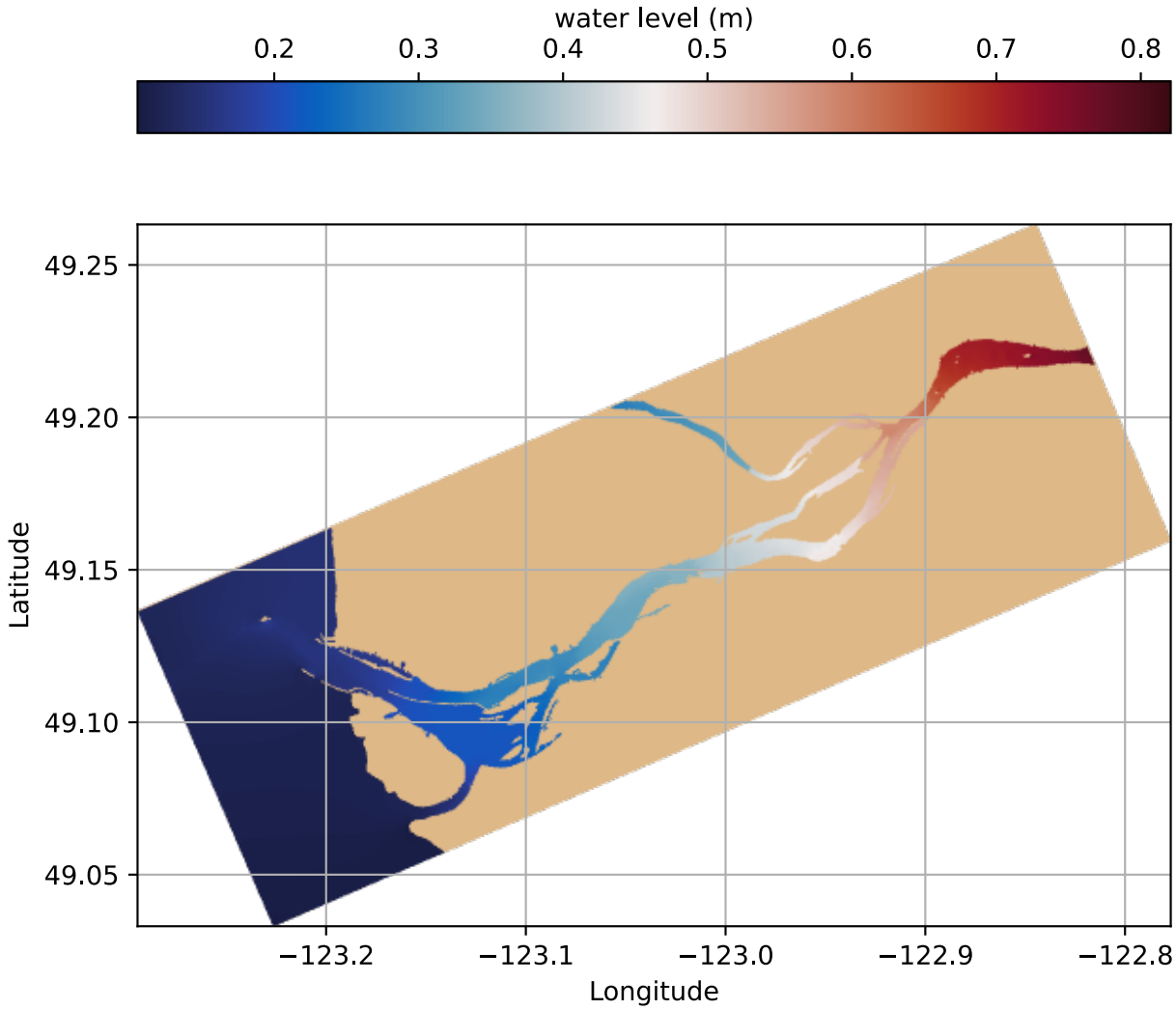

Figure 8. Mean model water level for 2017-2021.

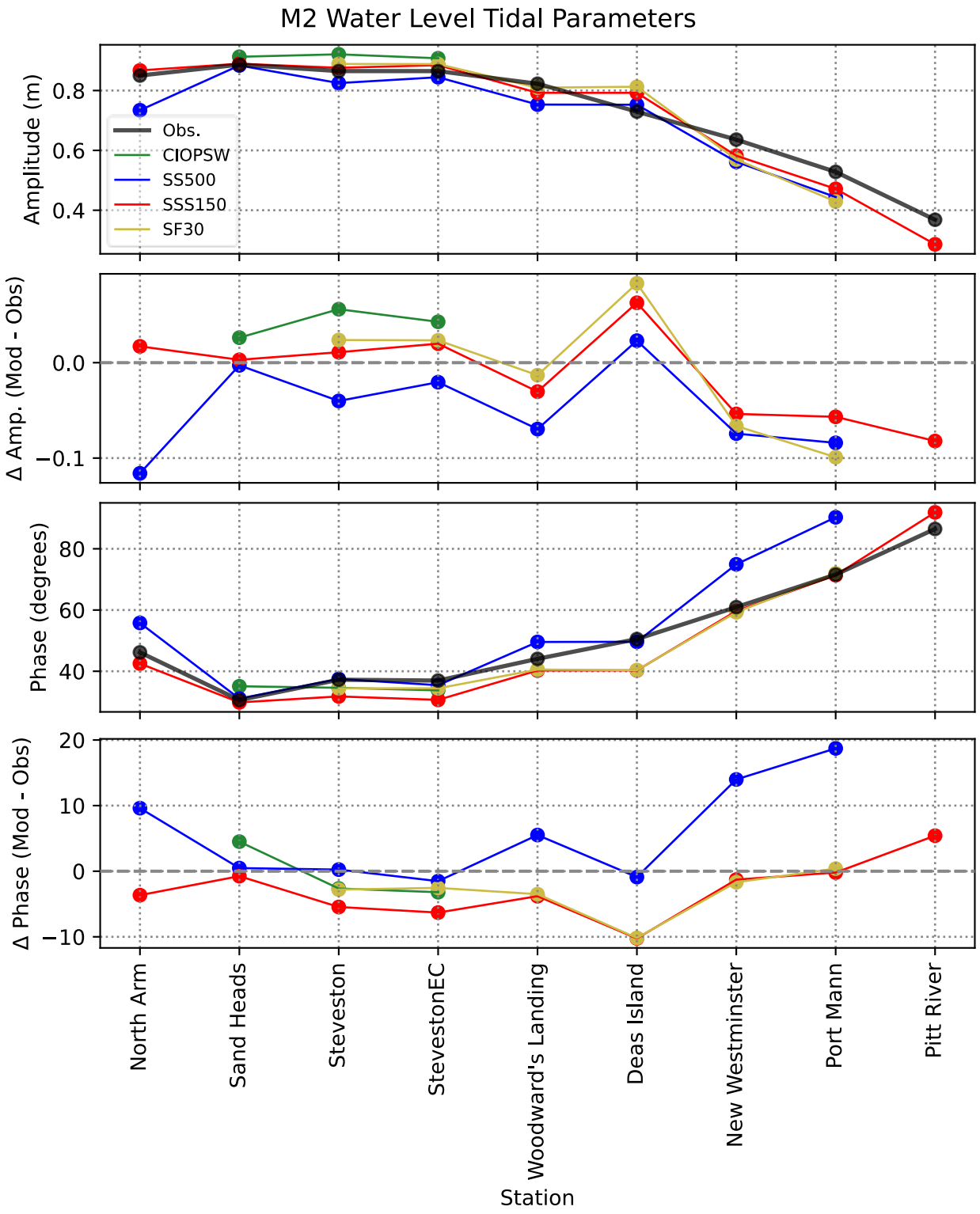

Figure 9. Observed and model amplitude and phase for M2 constituent for the year 2018.

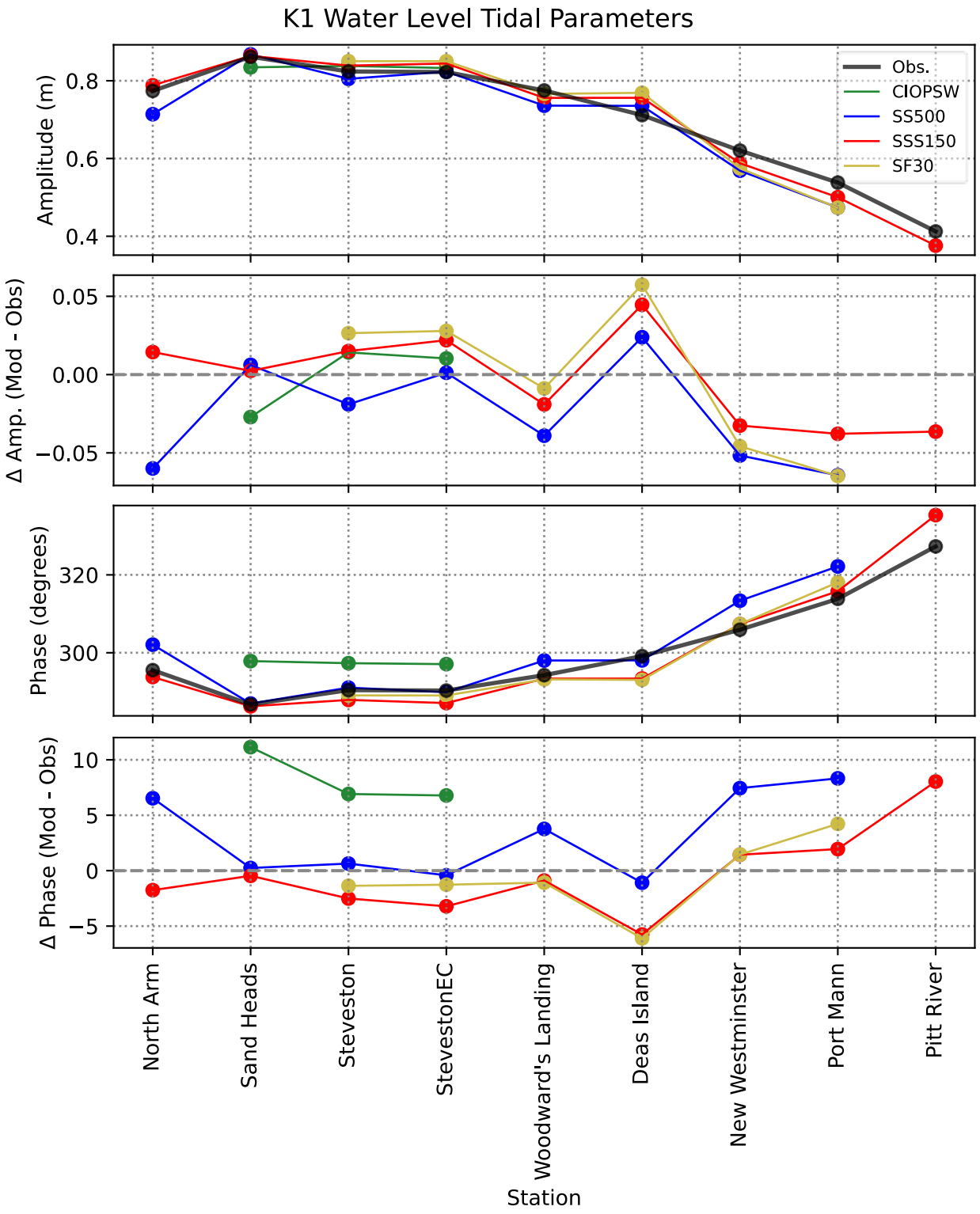

Figure 10. Observed and model amplitude and phase for K1 constituent for the year 2018.

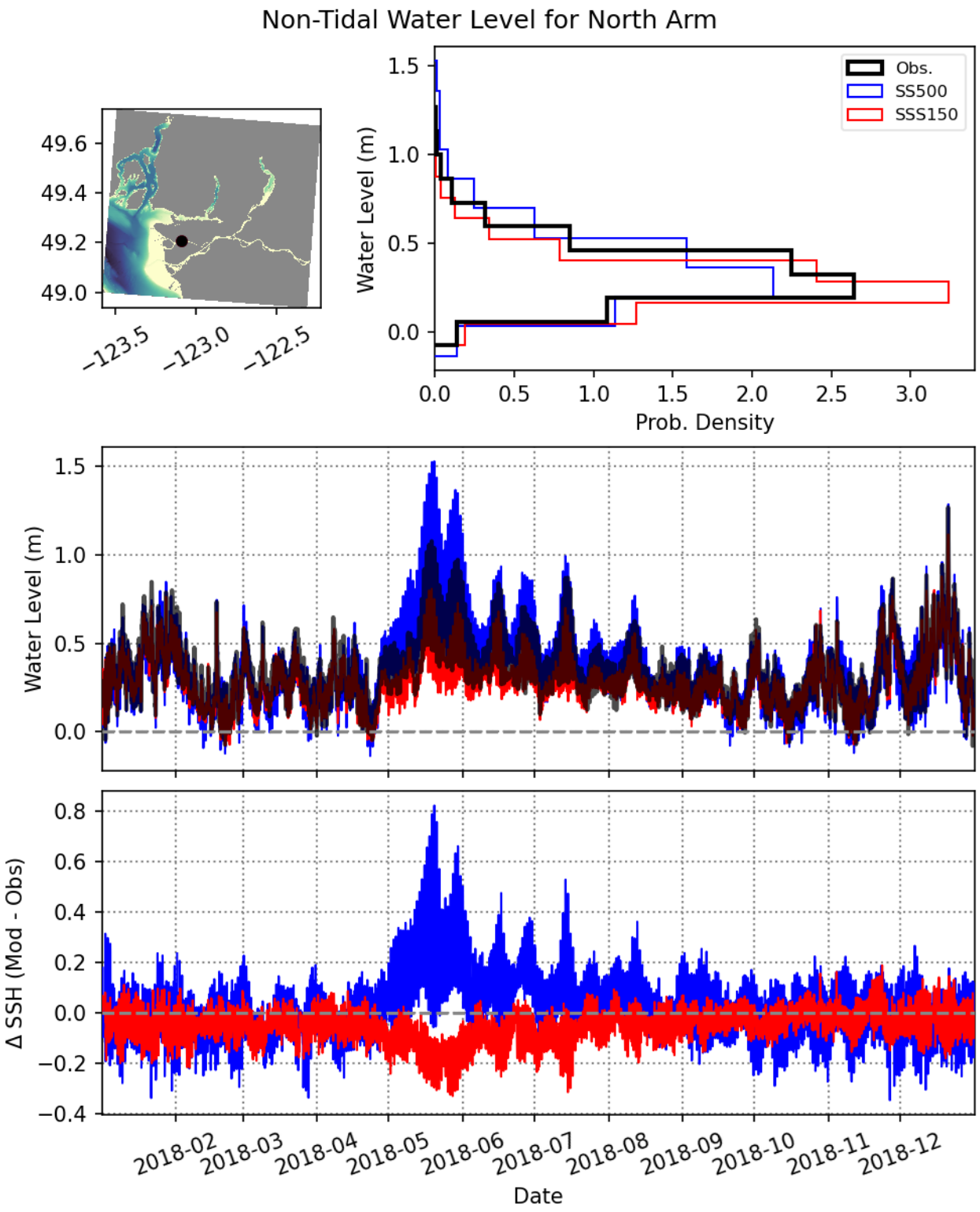

Figure 11. Non-tidal water level comparison for North Arm for year 2018.

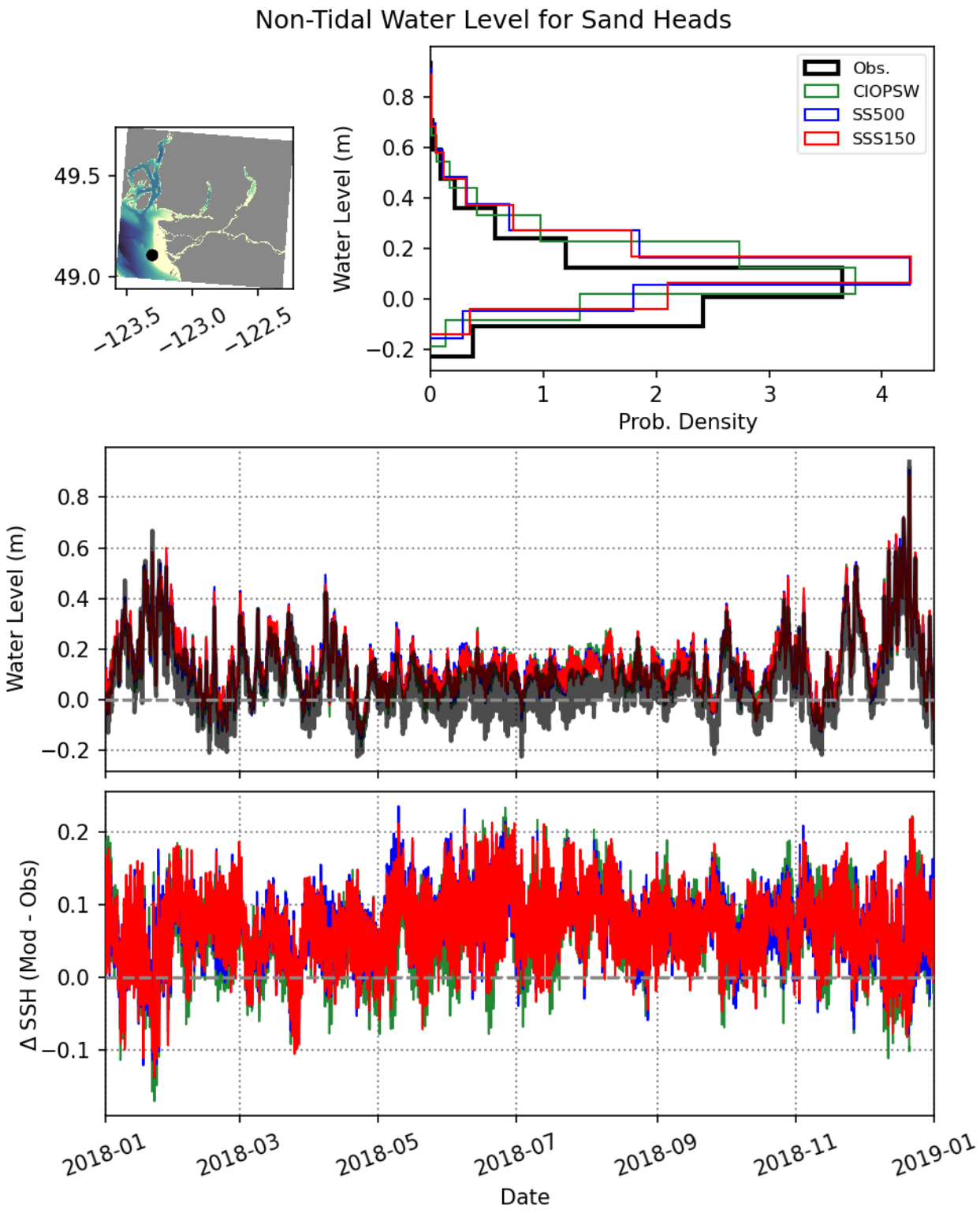

Figure 12. Non-tidal water level comparison for Sand Heads for year 2018.

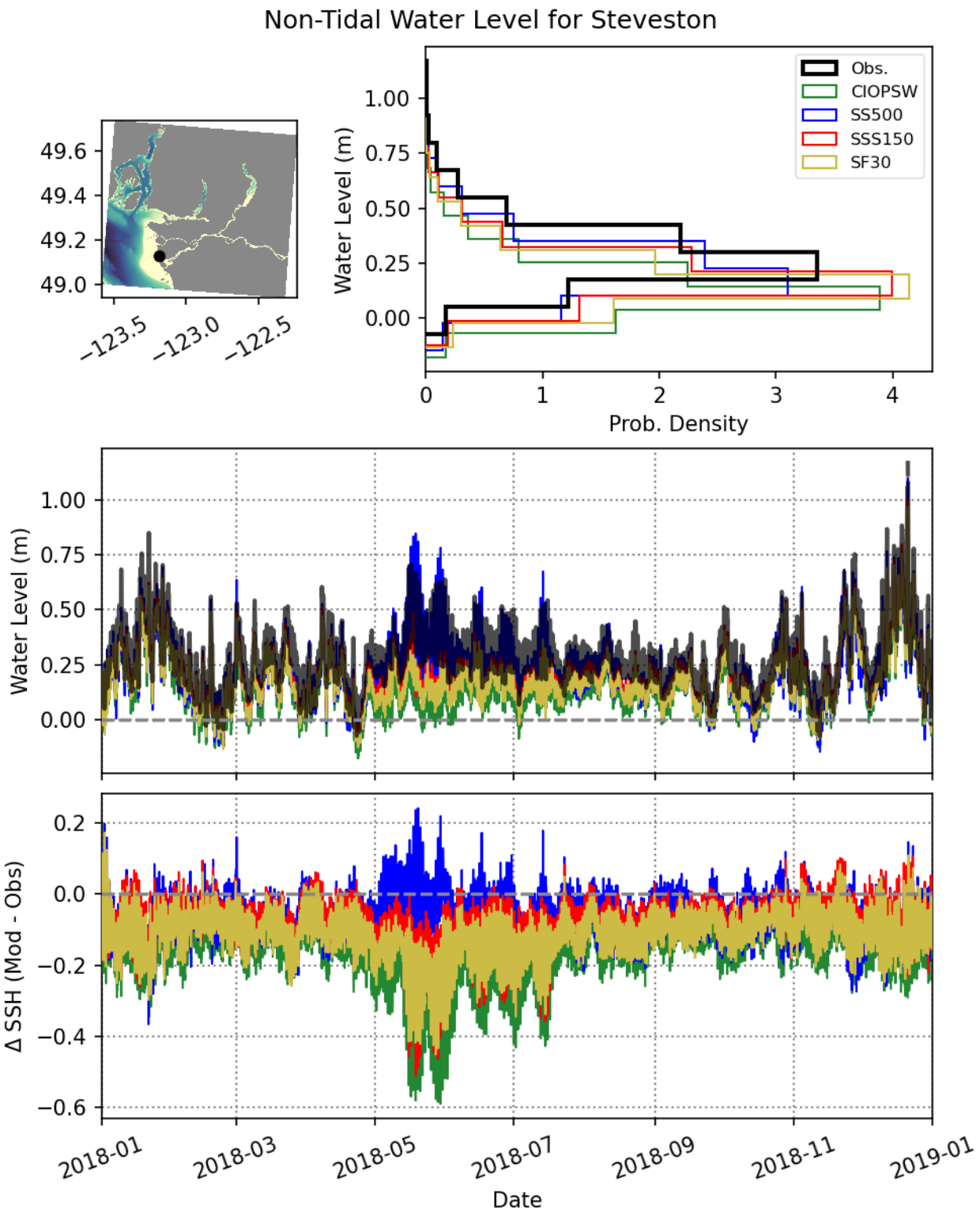

Figure 13. Non-tidal water level comparison for Steveston for year 2018.

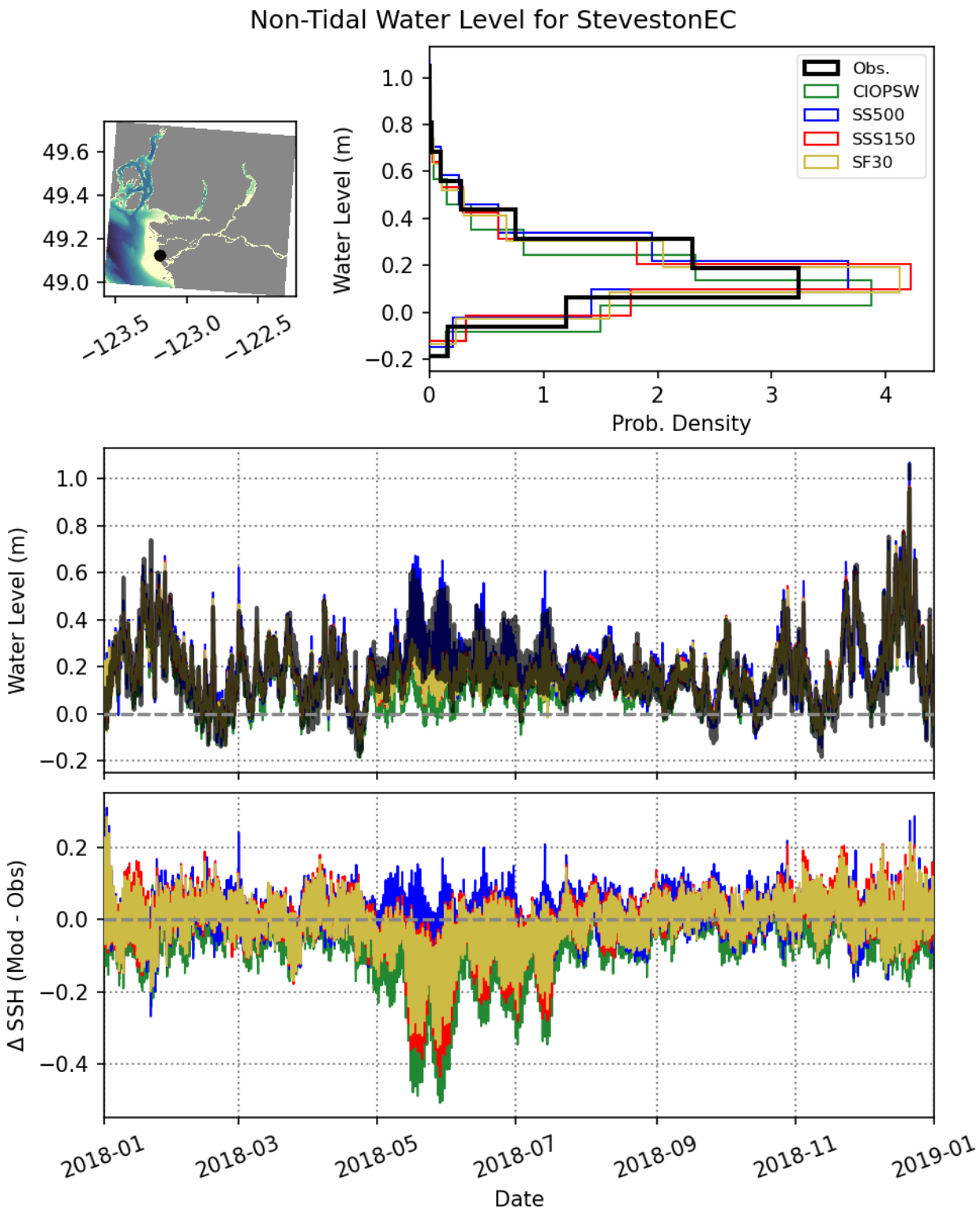

Figure 14. Non-tidal water level comparison for StevestonEC for year 2018.

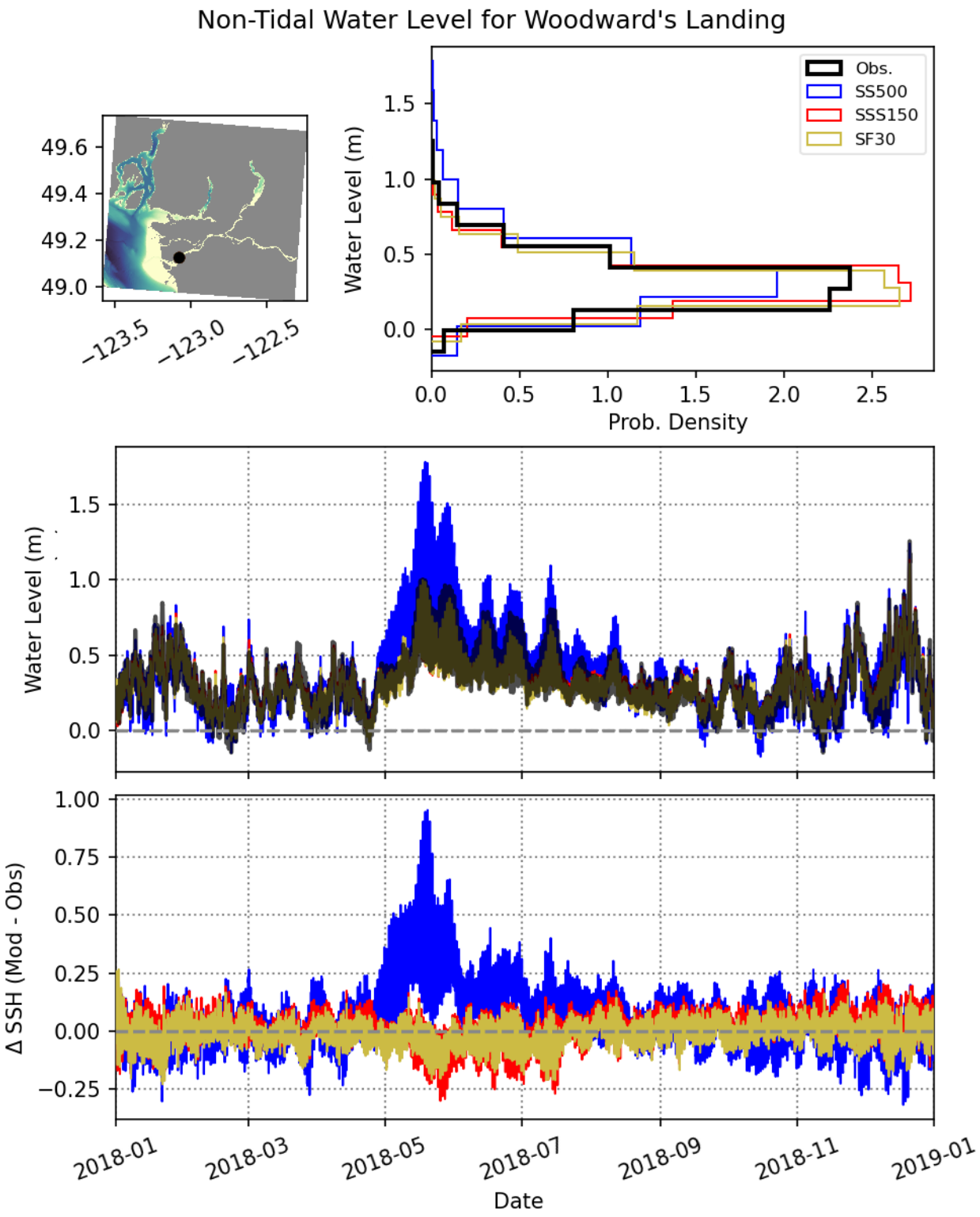

Figure 15. Non-tidal water level comparison for Woodward's Landing for year 2018.

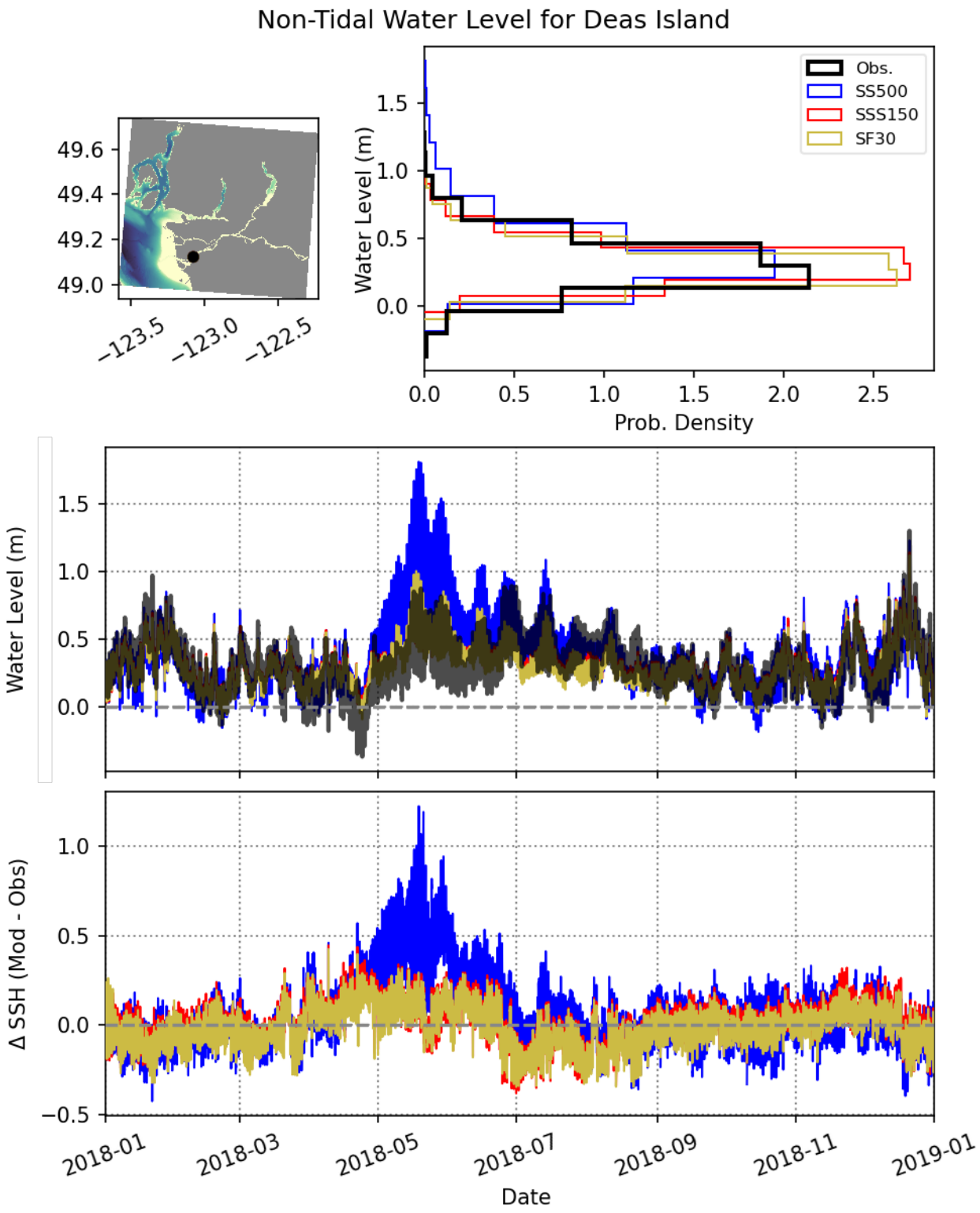

Figure 16. Non-tidal water level comparison for Deas Island for year 2018.

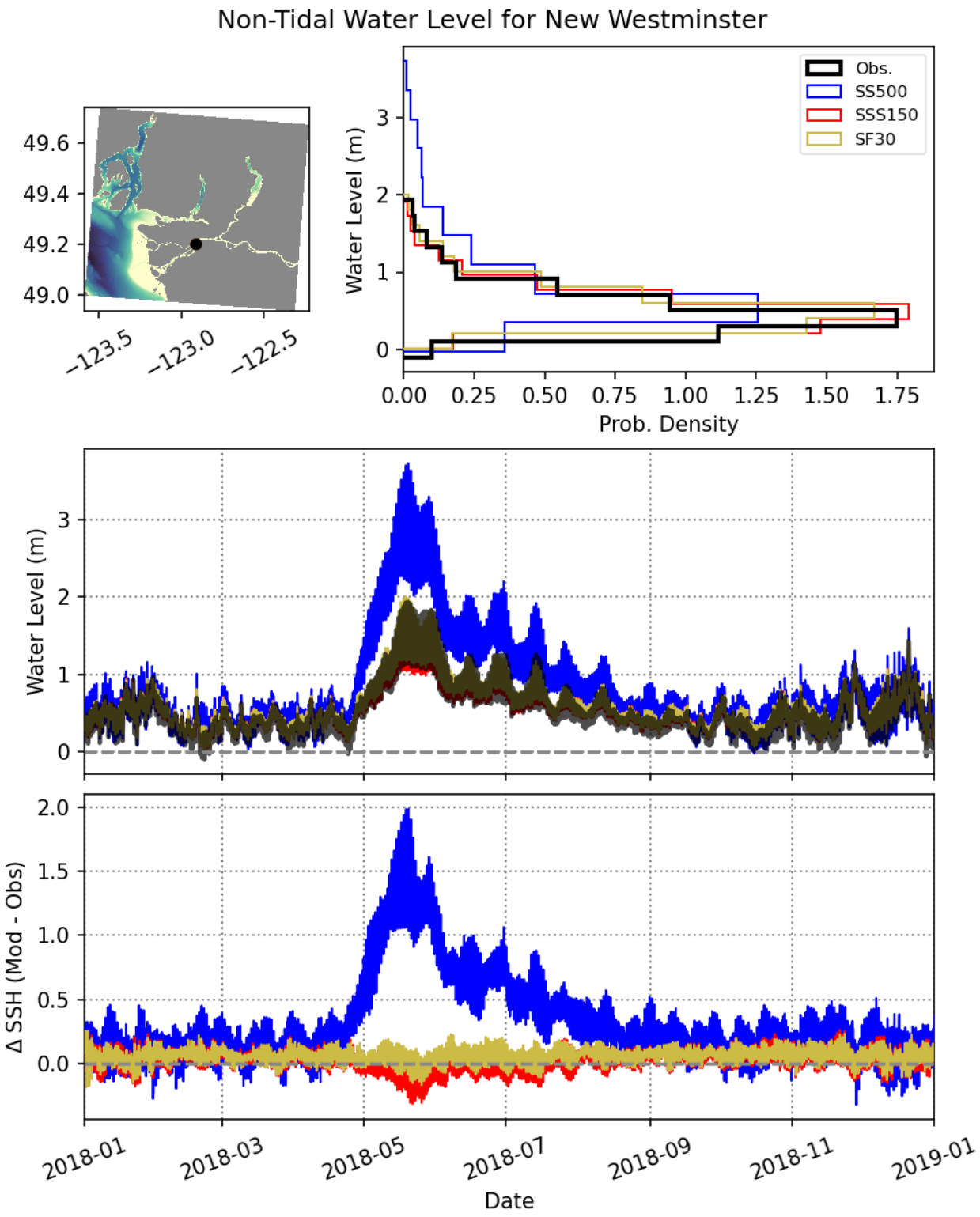

Figure 17. Non-tidal water level comparison for New Westminster for year 2018.

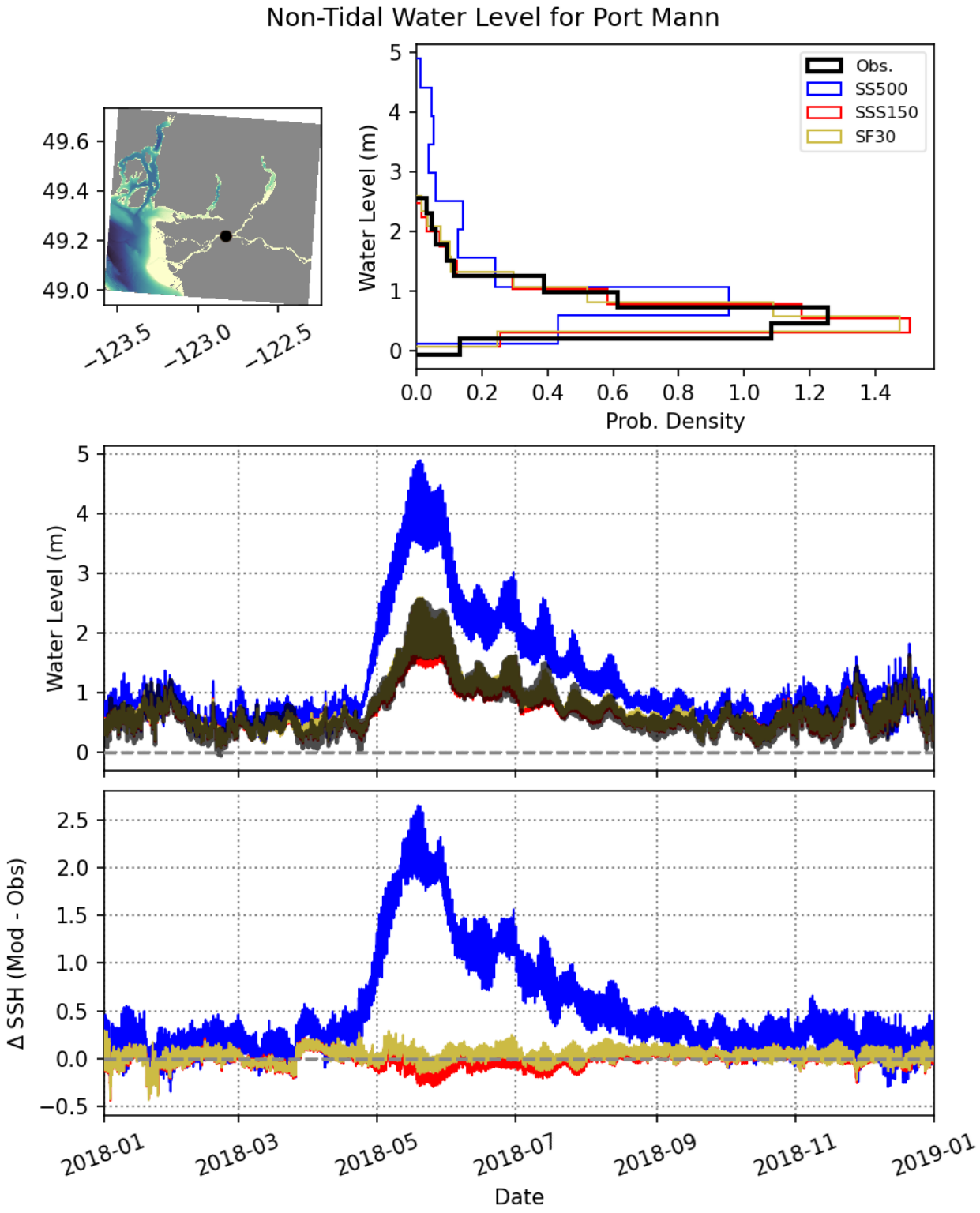

Figure 18. Non-tidal water level comparison for Port Mann for year 2018.

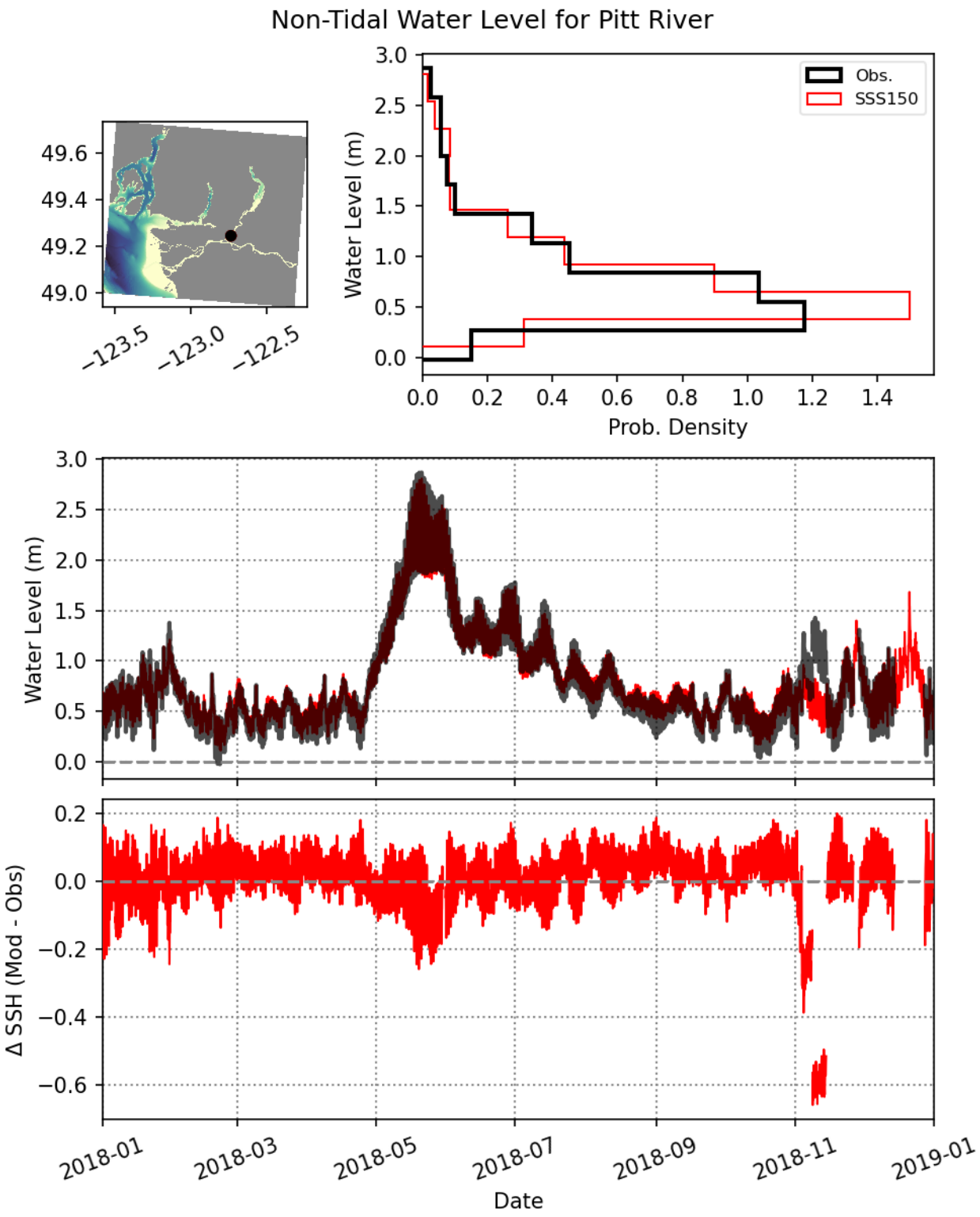

Figure 19. Non-tidal water level comparison for Pitt River for year 2018.

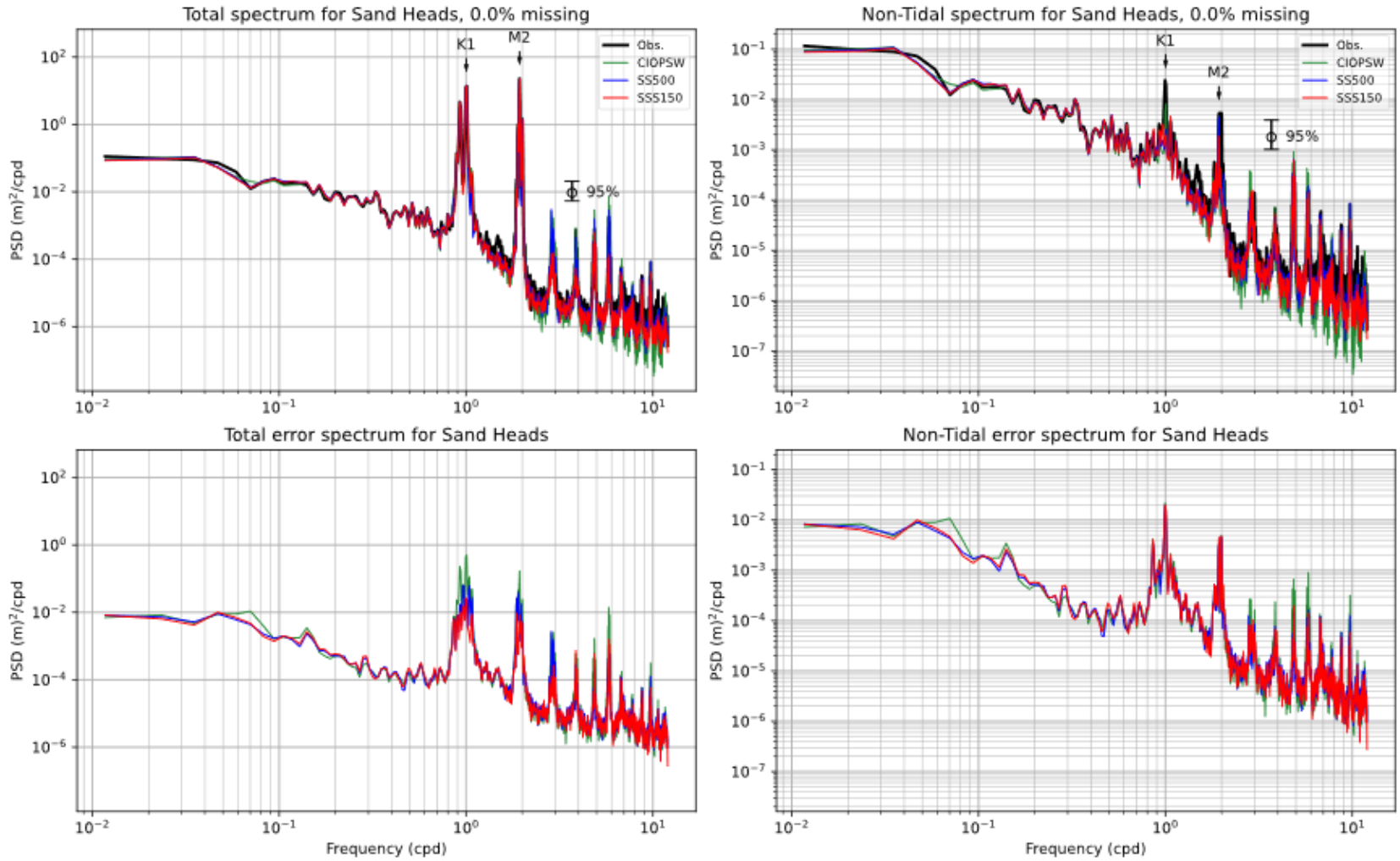

Figure 20. Power spectra for the total and non-tidal water level at Sand Heads for the year 2018.

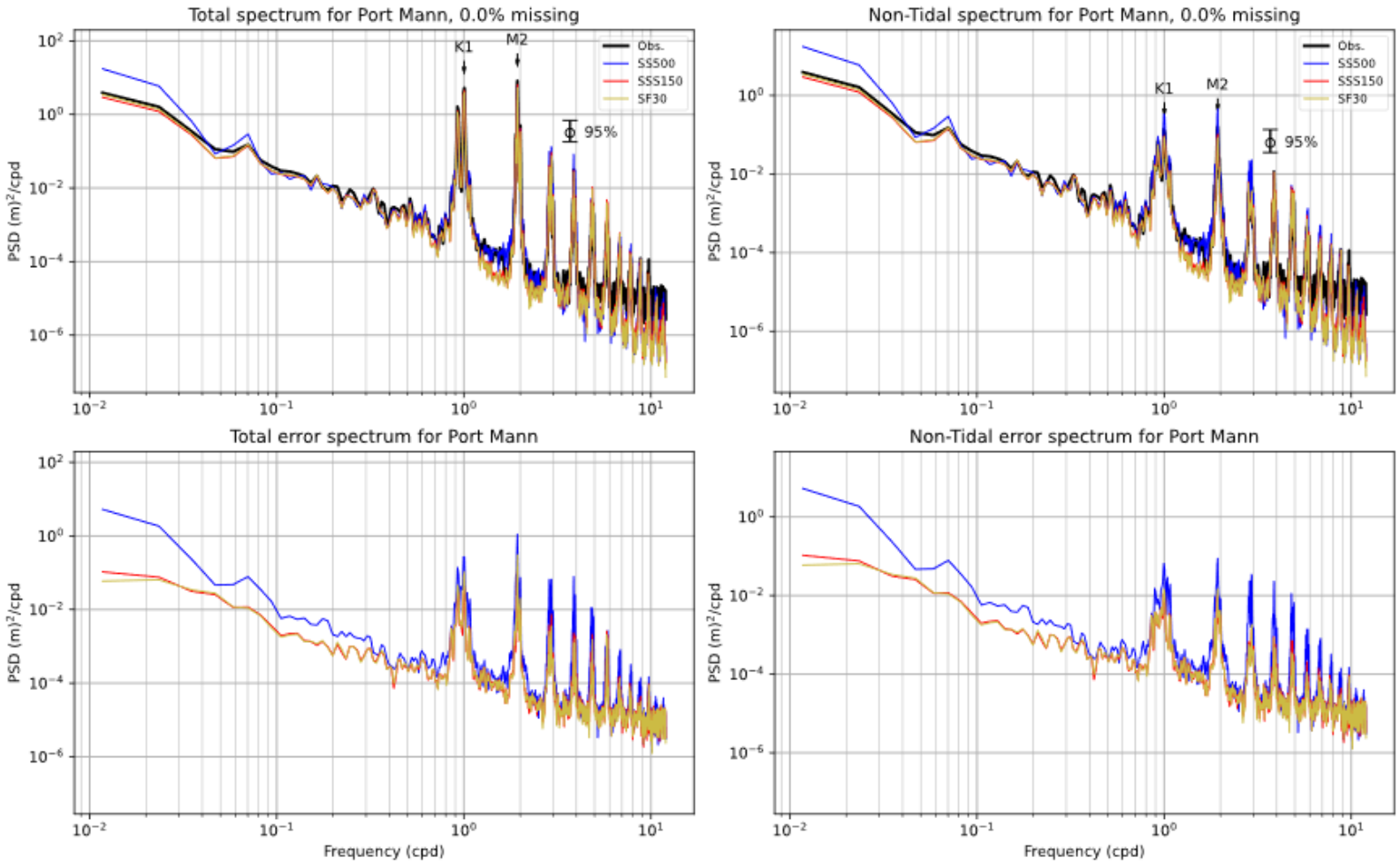

Figure 21. Power spectra for the total and non-tidal water level at Port Mann for the year 2018.

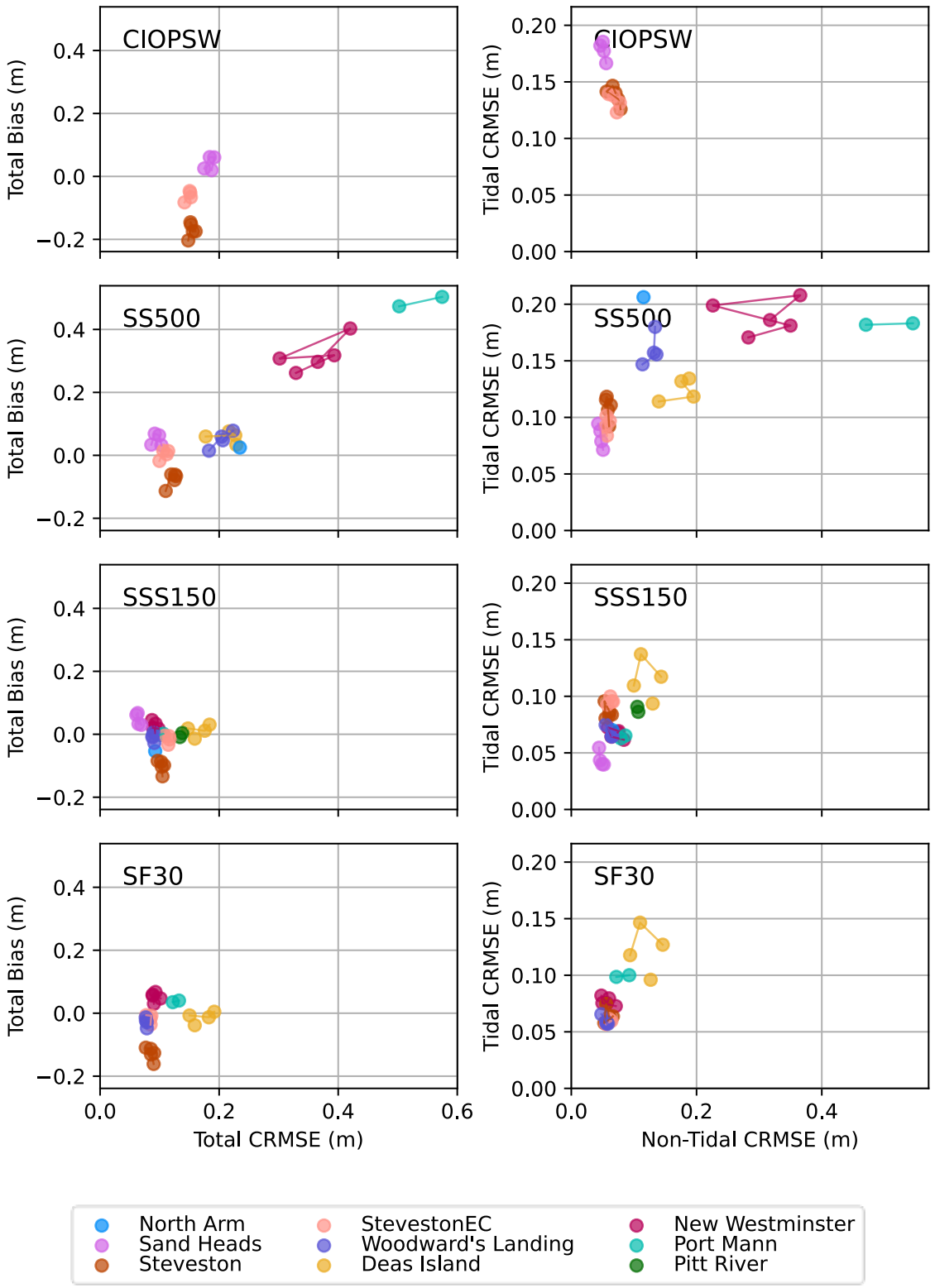

Figure 22. Water level scores variability over years. Markers of same colour denote scores for a single station for individual years. Markers for consecutive years are connected by a line.

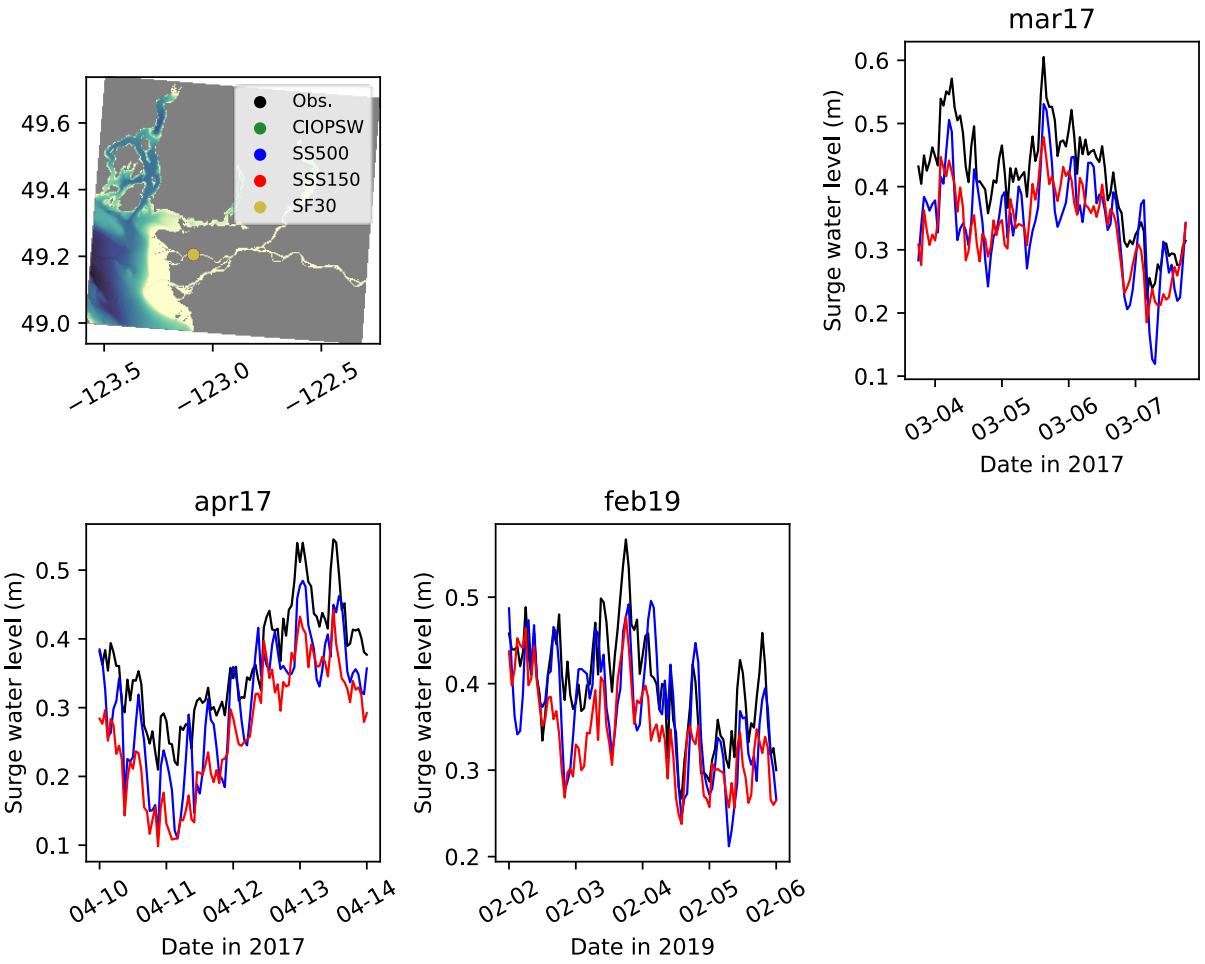

Figure 23. Observed and model non-tidal sea level during individual storm events for North Arm tide gauge.

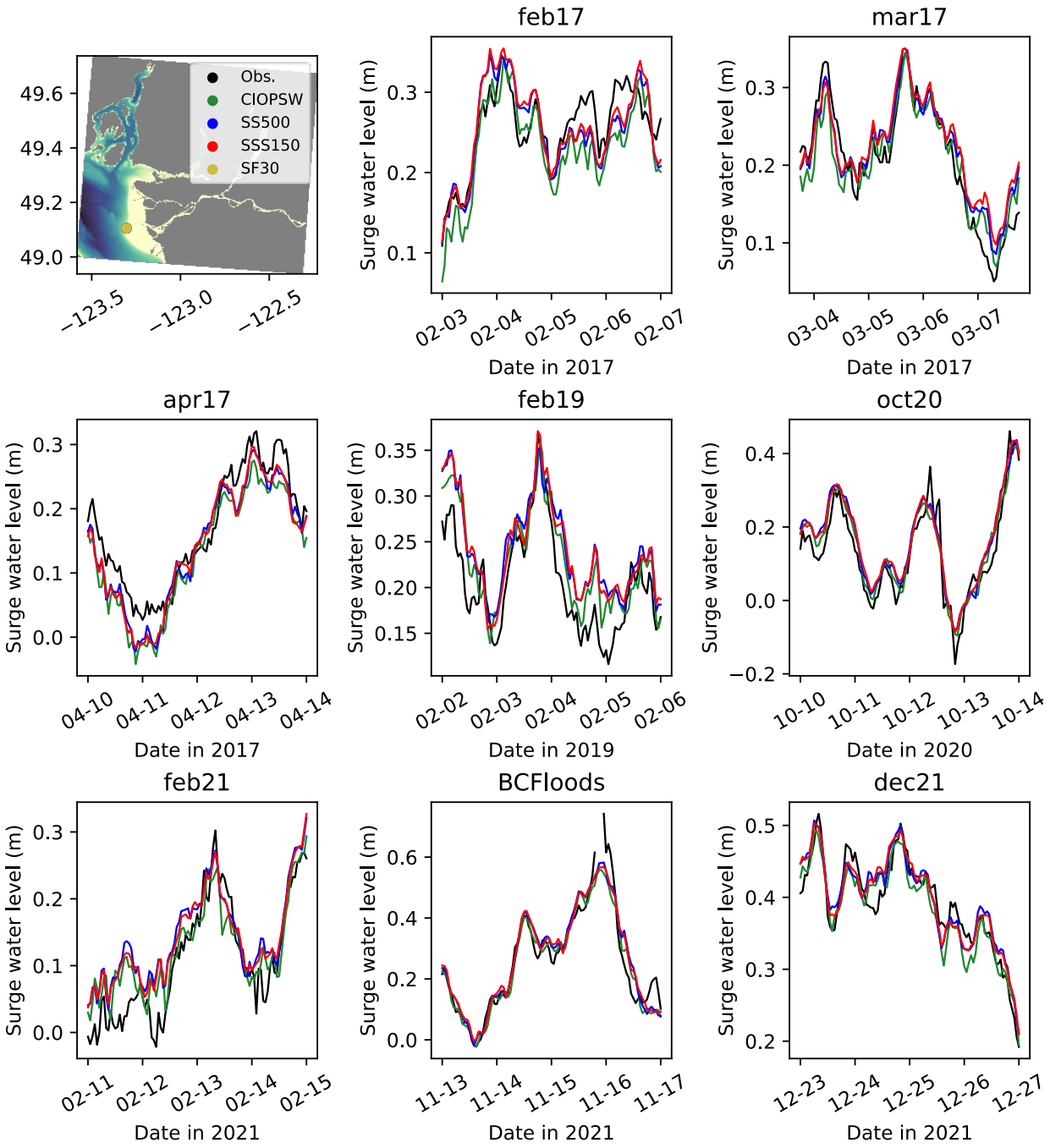

Figure 24. Observed and model non-tidal sea level during individual storm events for Sand Heads tide gauge.

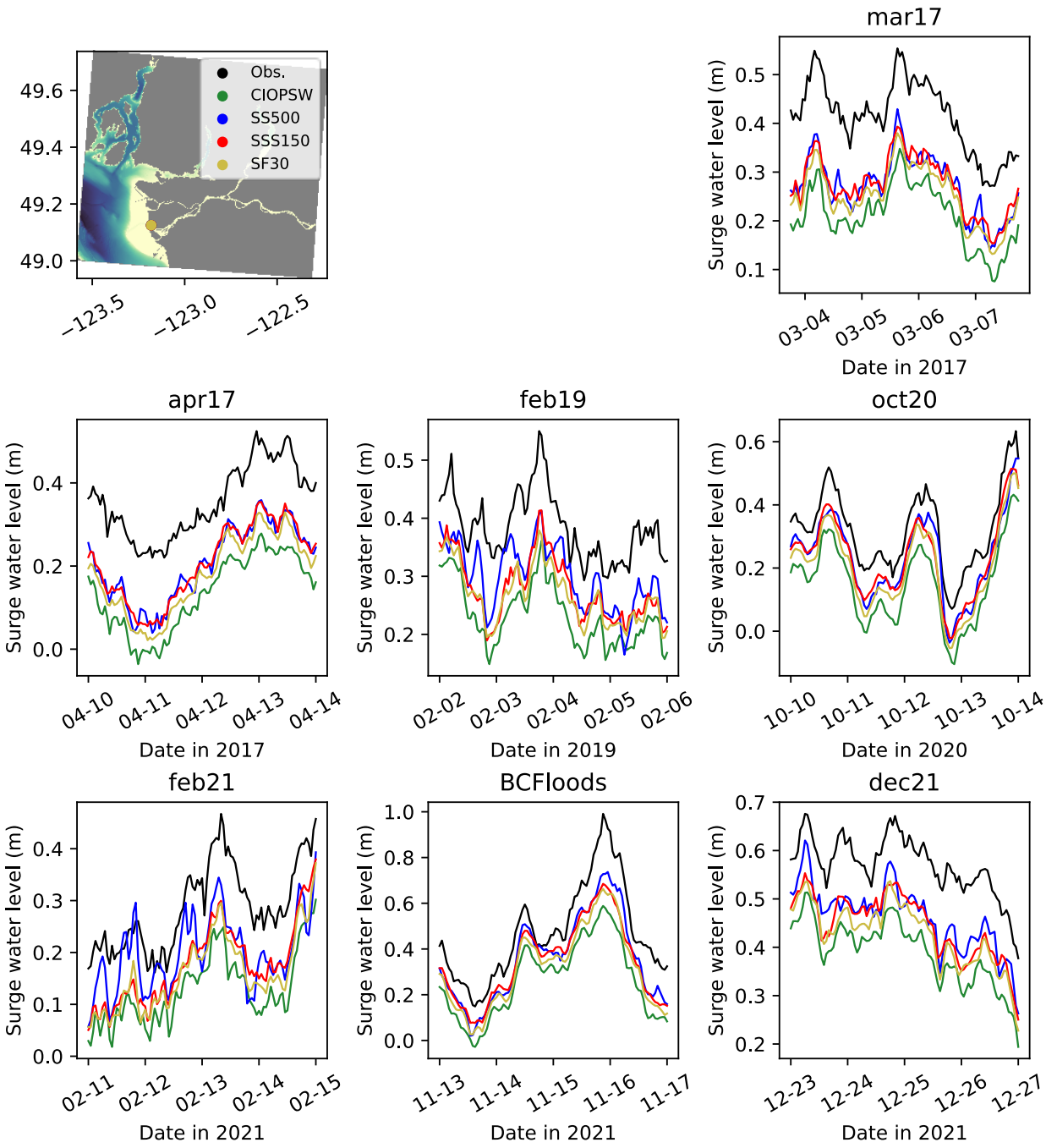

Figure 25. Observed and model non-tidal sea level during individual storm events for Steveston tide gauge.

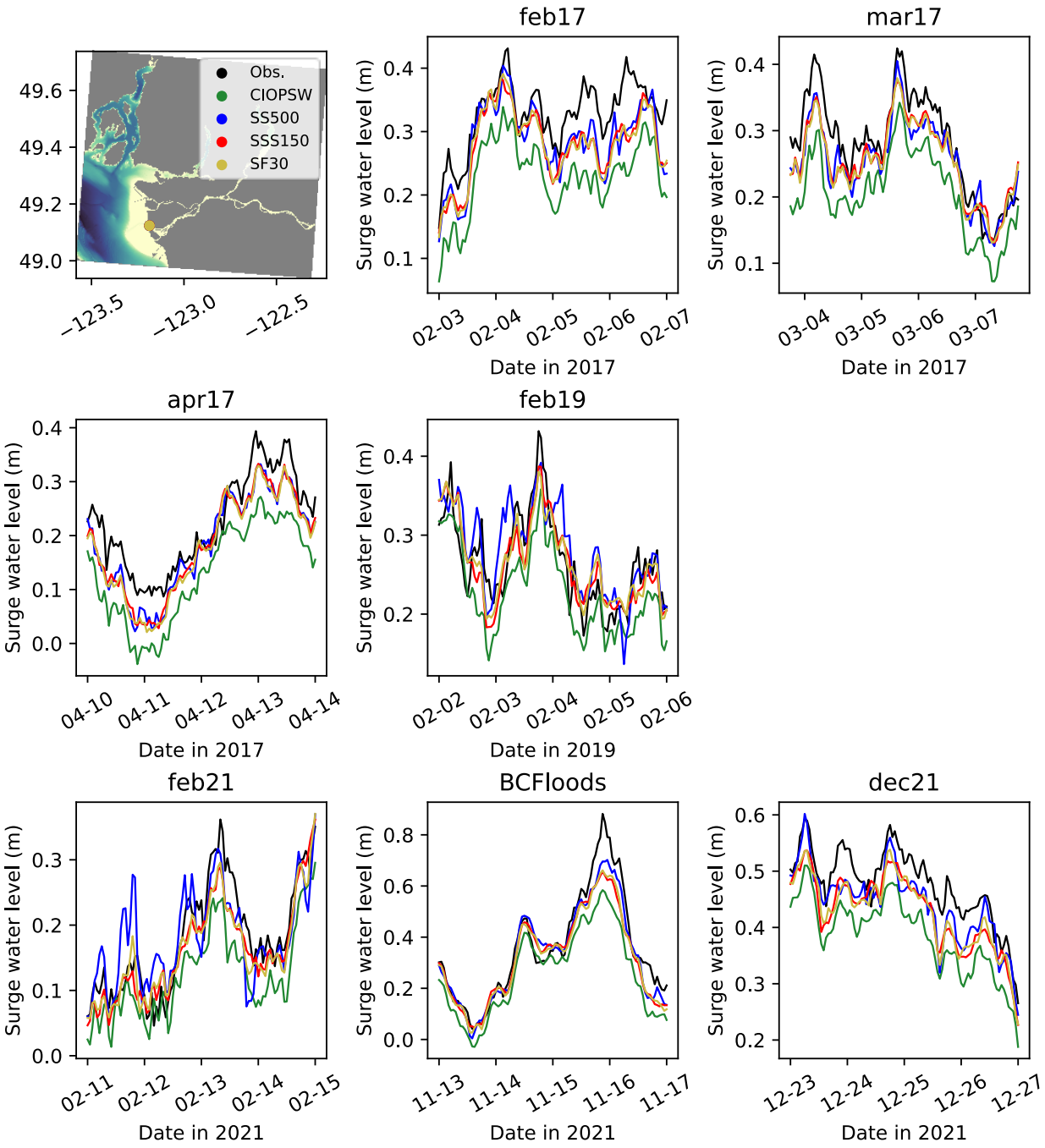

Figure 26. Observed and model non-tidal sea level during individual storm events for StevestonEC tide gauge.

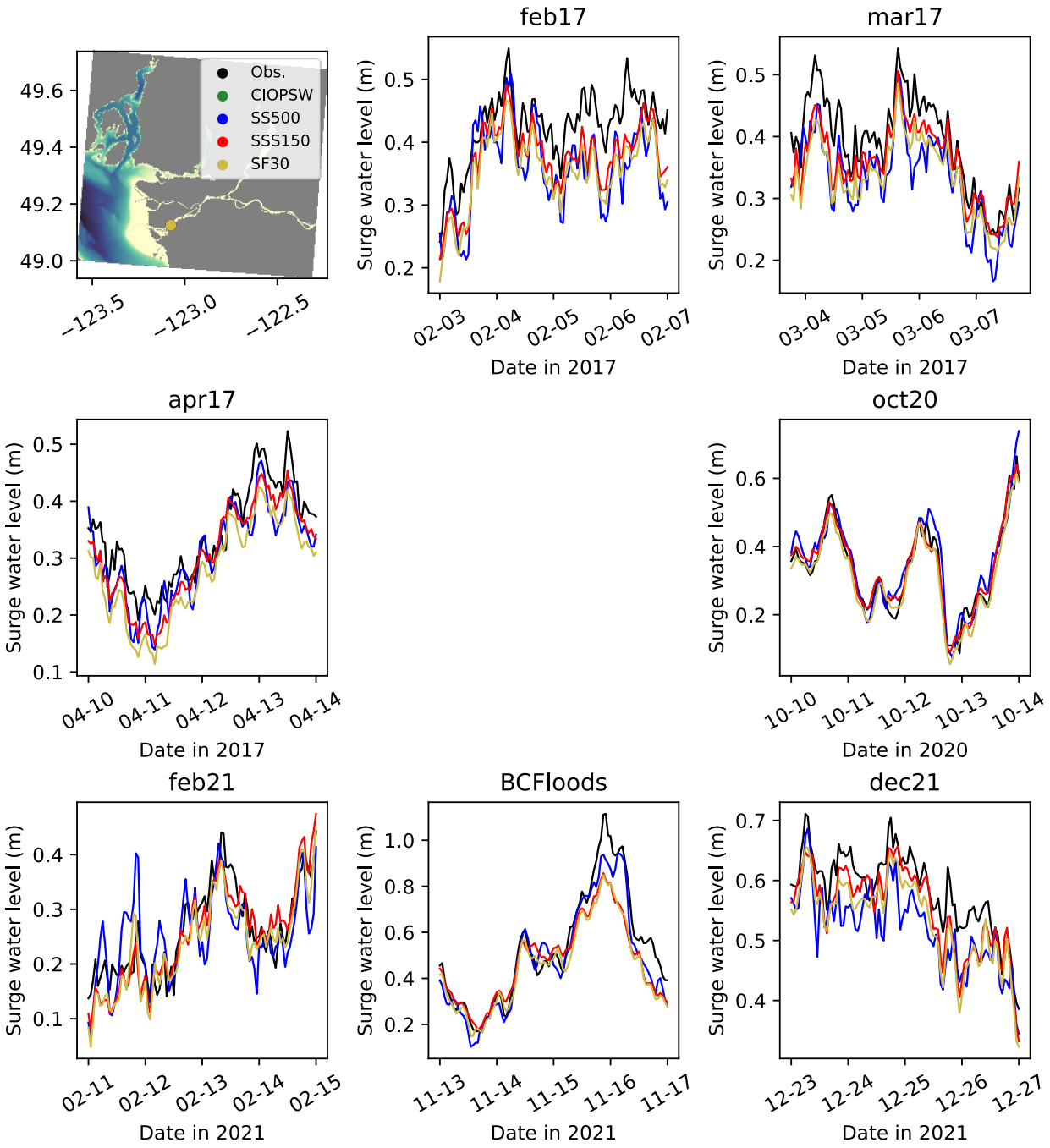

Figure 27. Observed and model non-tidal sea level during individual storm events for Woodward's Landing tide gauge.

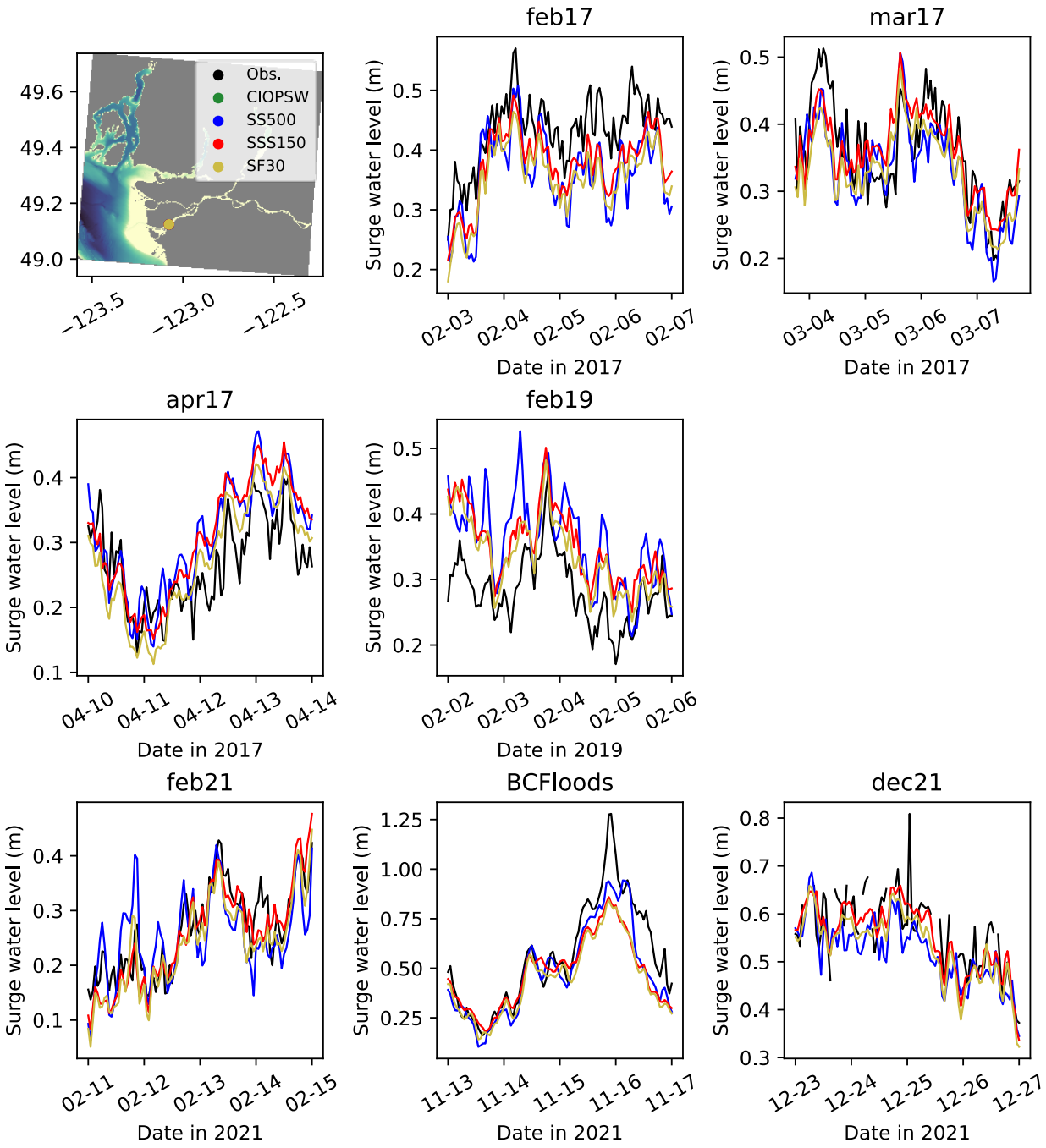

Figure 28. Observed and model non-tidal sea level during individual storm events for Deas Island tide gauge.

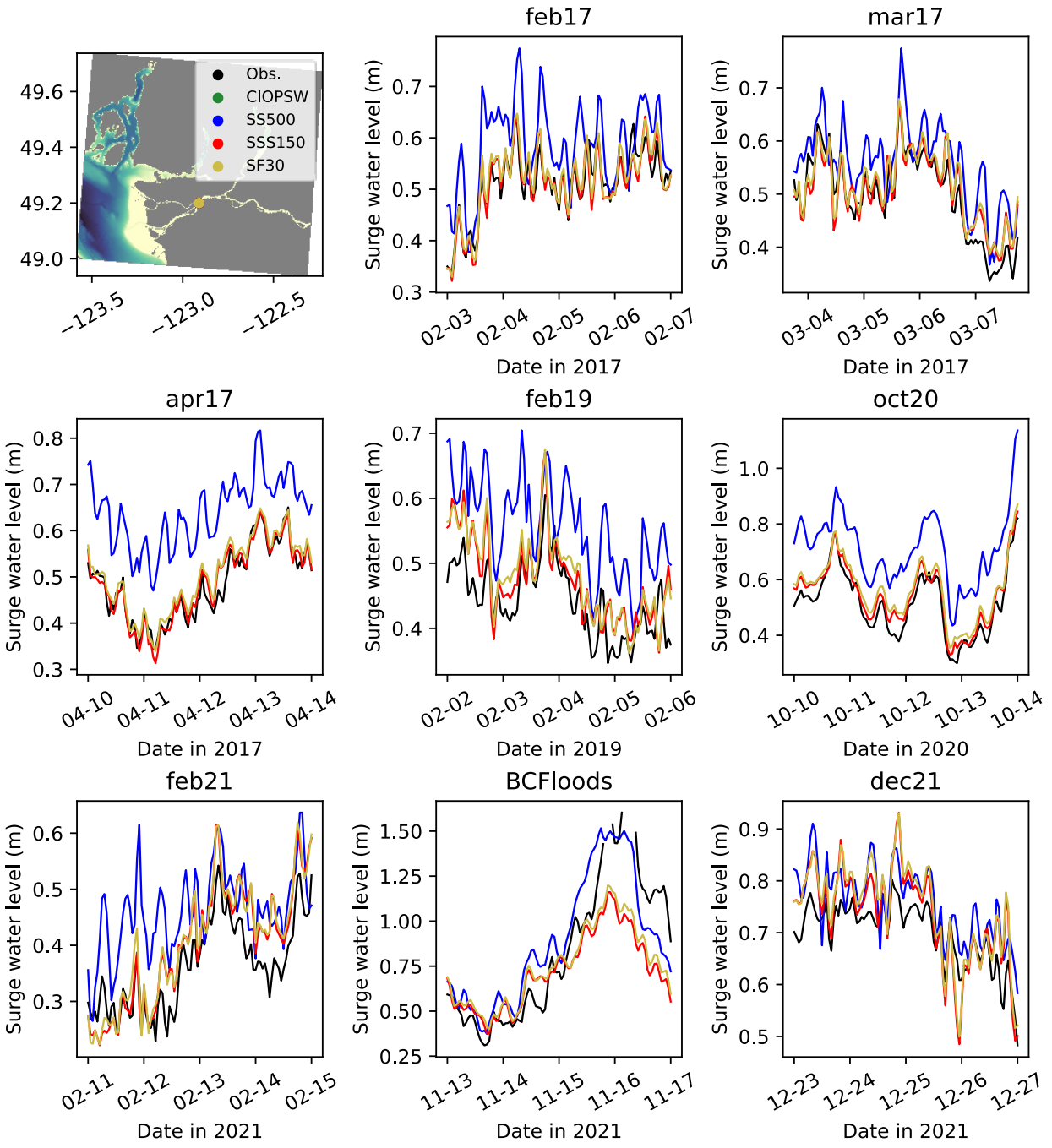

Figure 29. Observed and model non-tidal sea level during individual storm events for New Westminster tide gauge.

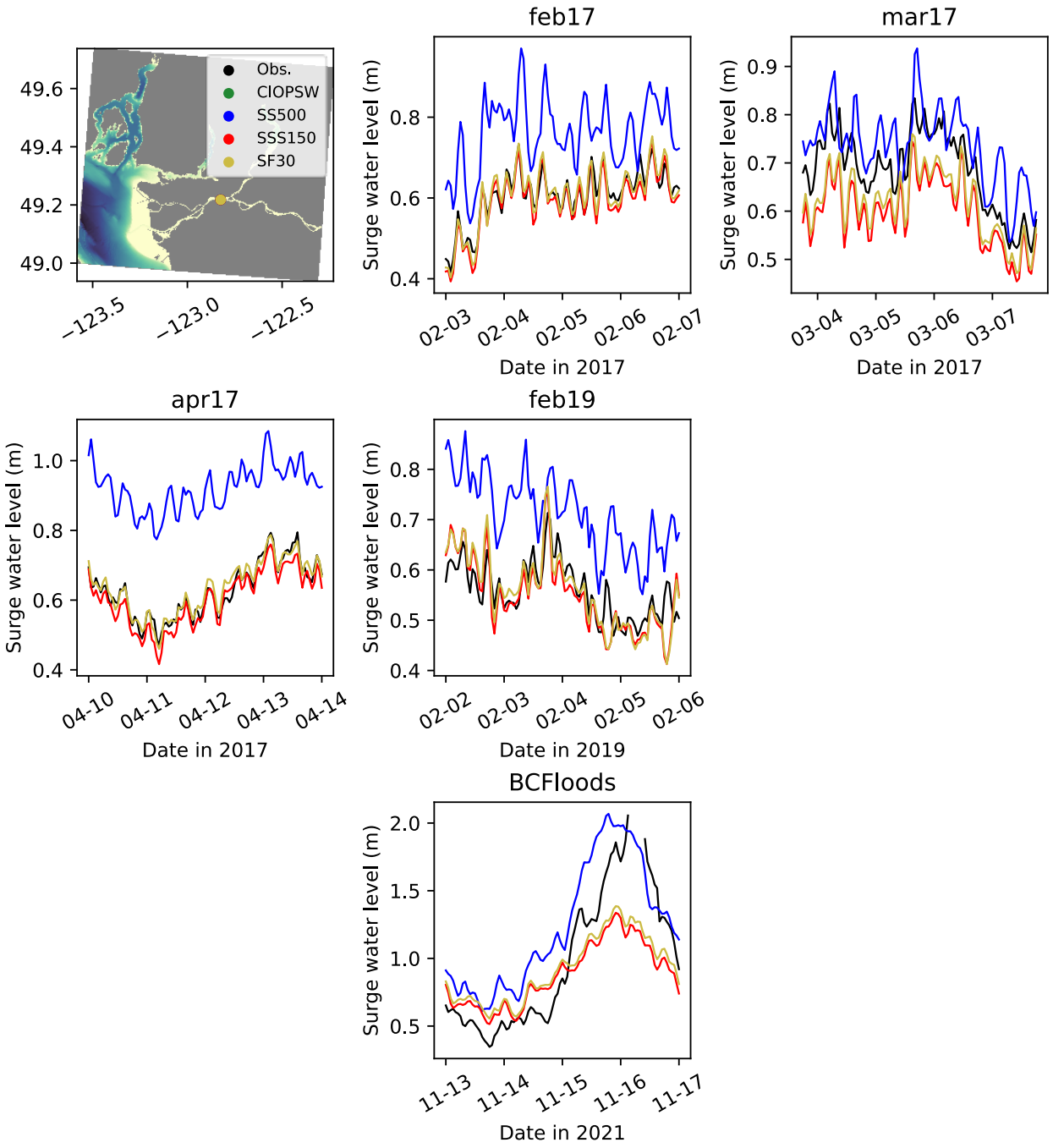

Figure 30. Observed and model non-tidal sea level during individual storm events for Port Mann tide gauge.

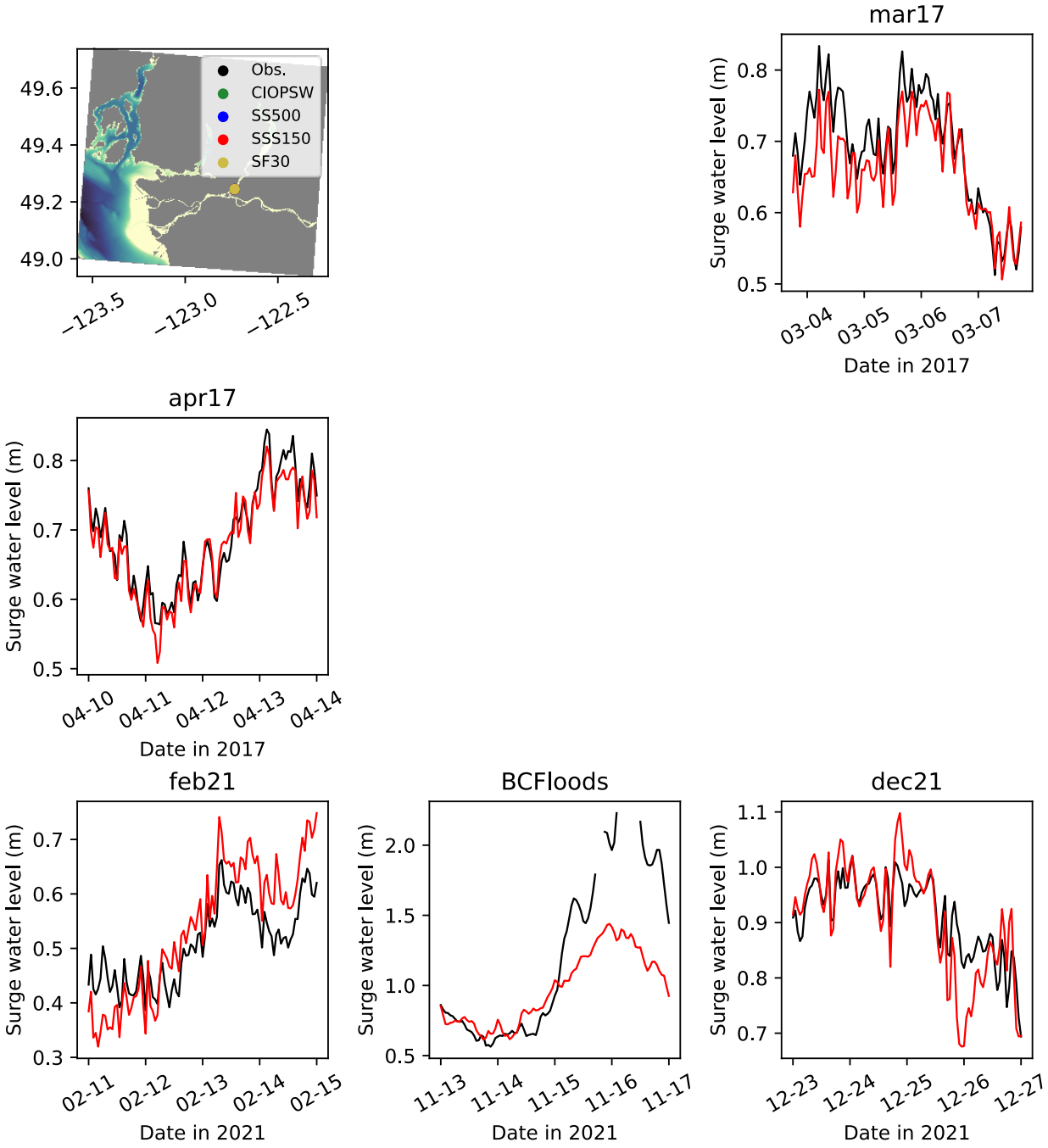

Figure 31. Observed and model non-tidal sea level during individual storm events for Pitt River tide gauge.

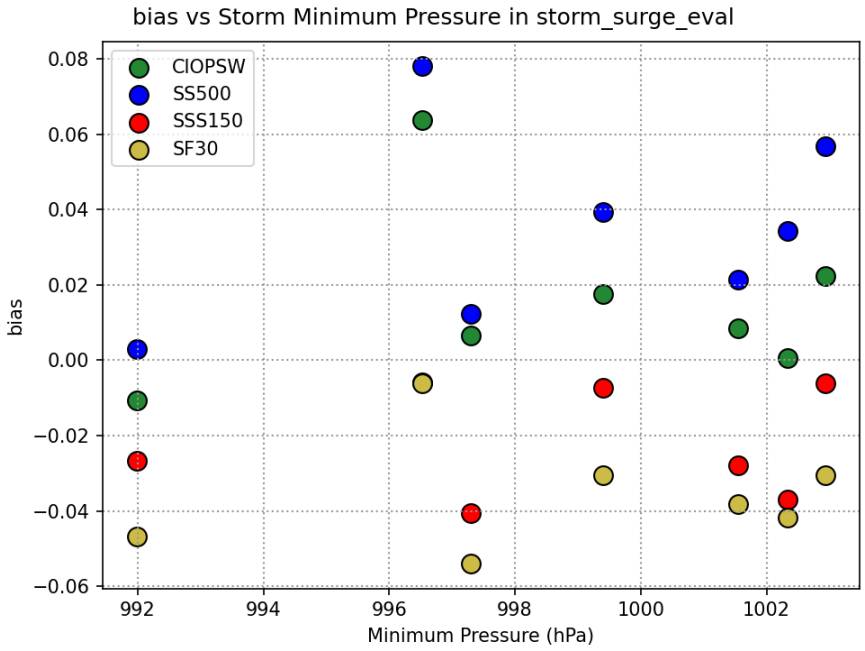

Figure 32. Model bias for the non-tidal sea level averaged over stations vs minimum atmospheric pressure during the storm for individual storm events. BCFloods storm is omitted due to a lack of pressure data.

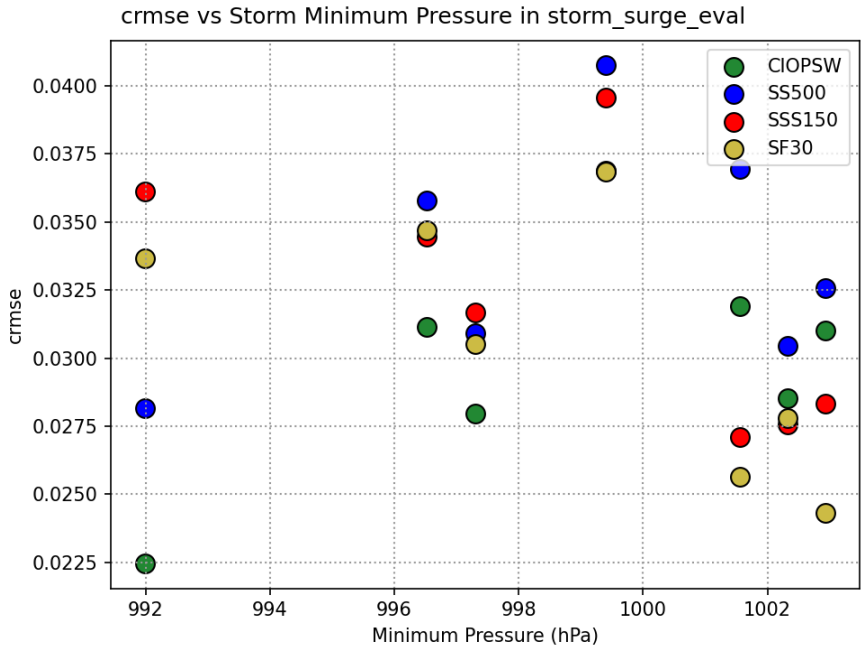

Figure 33. Same as Figure 32, but for the model CRMSE.

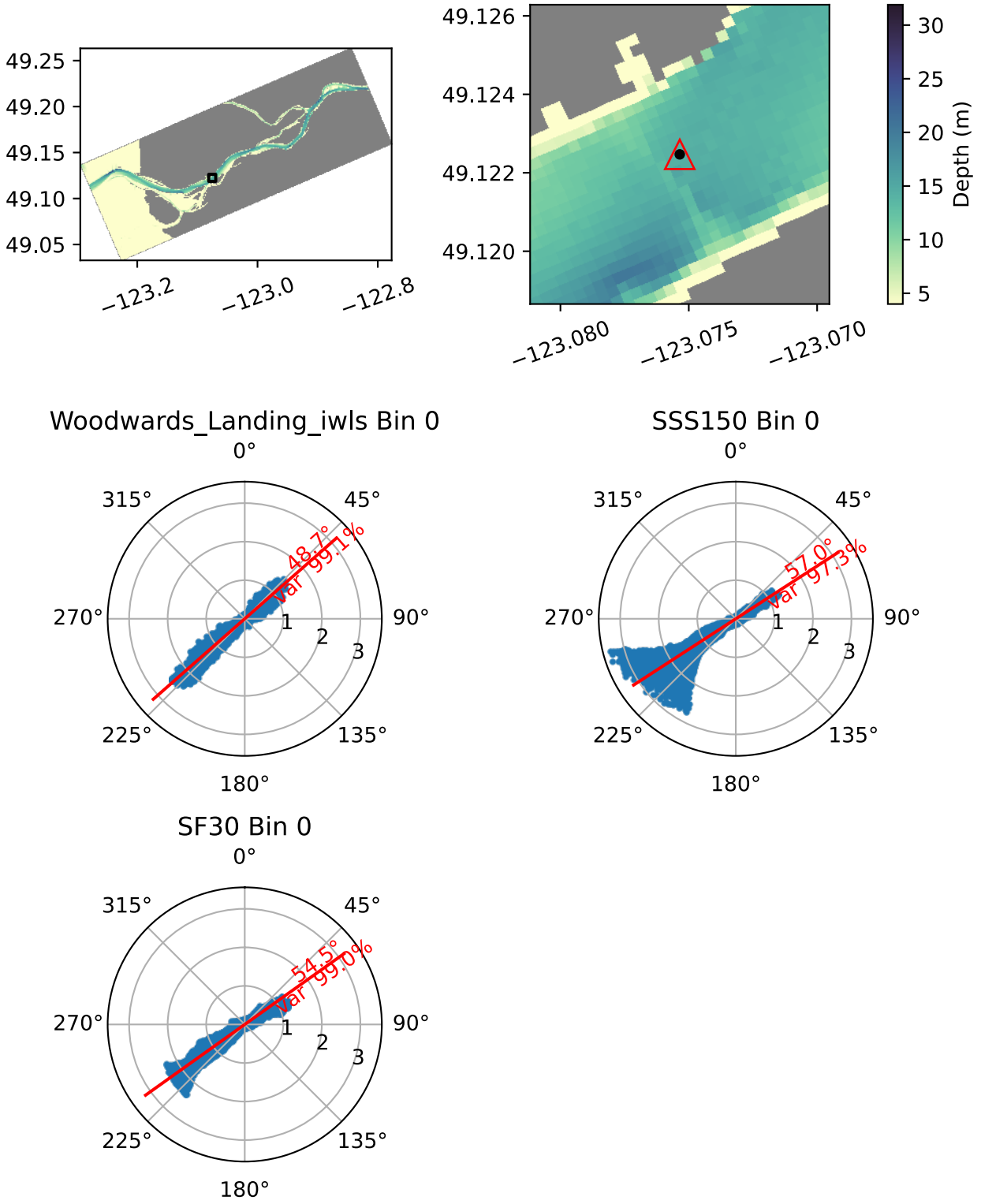

Figure 34. Observation location of the horizontal ADCP at Woodward's Landing and current rose diagrams with principal axes of variance for the ADCP data and for the SSS150 and SF30 models. Circular grid lines on rose diagrams indicate velocity in m/s.

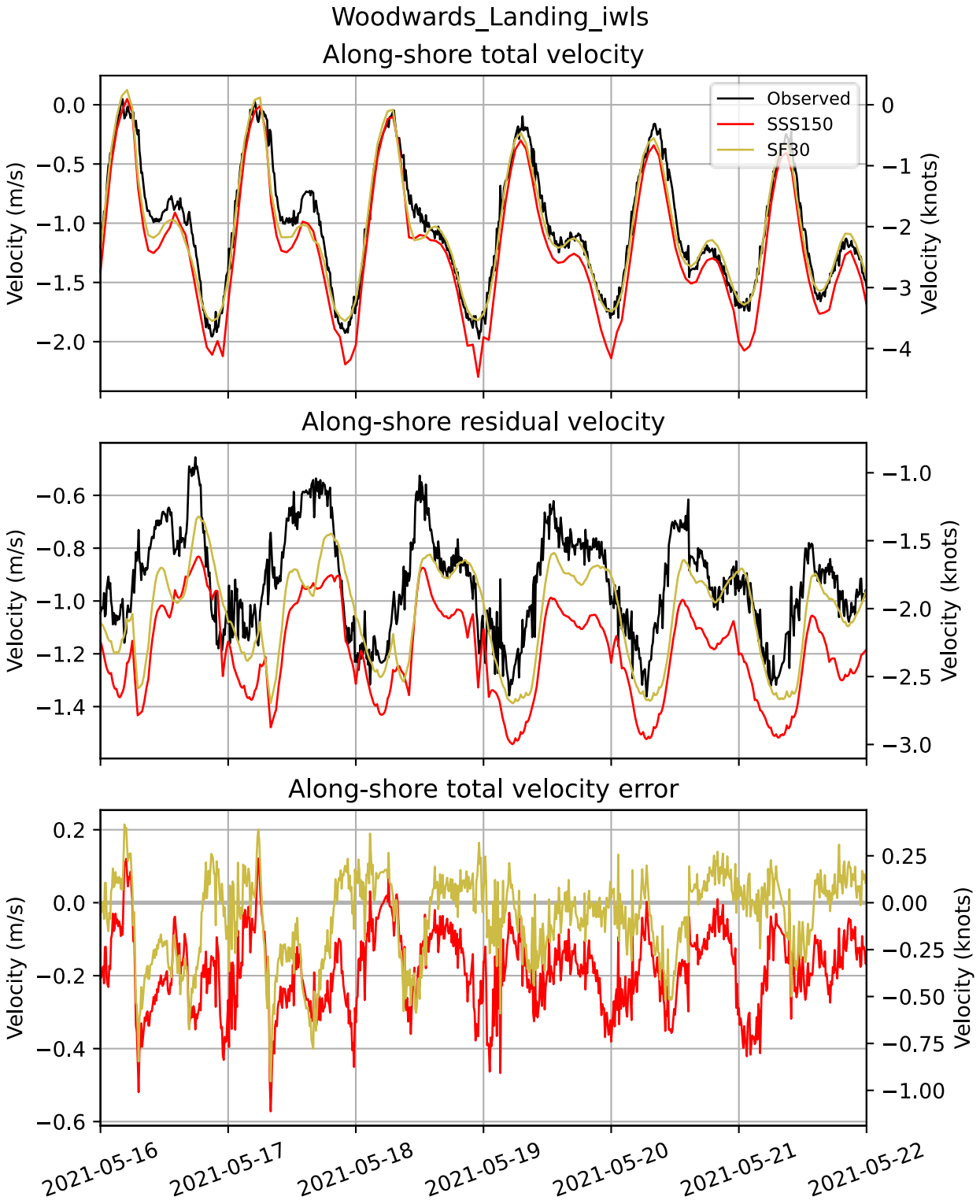

Figure 35. Observed and model along-shore velocity (a 6-day fragment) from the horizontal ADCP at Woodward's Landing.

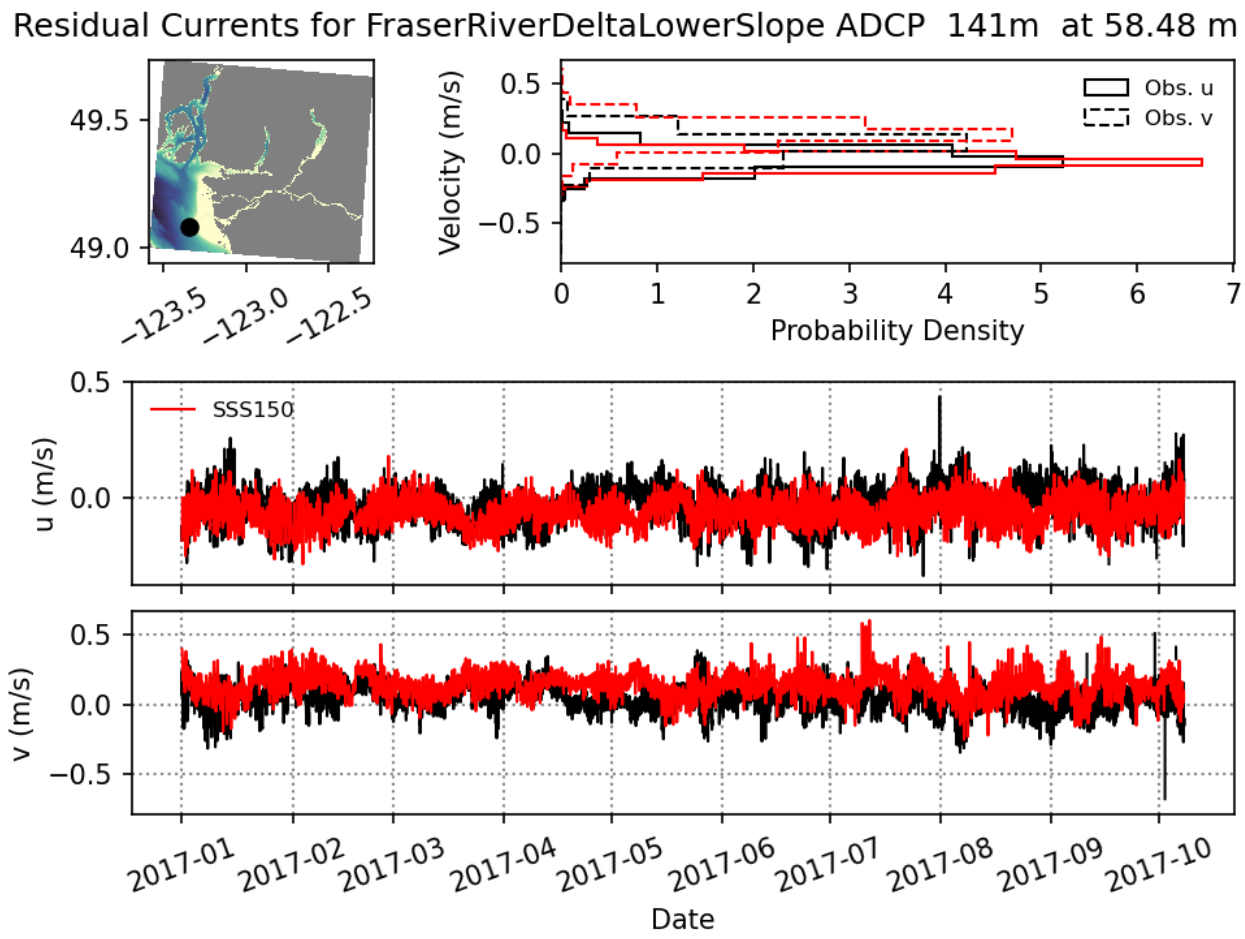

Figure 36. Non-tidal velocity from the FRDLS ADCP station at 58.5 m depth for eastward (u) and northward (v) components.

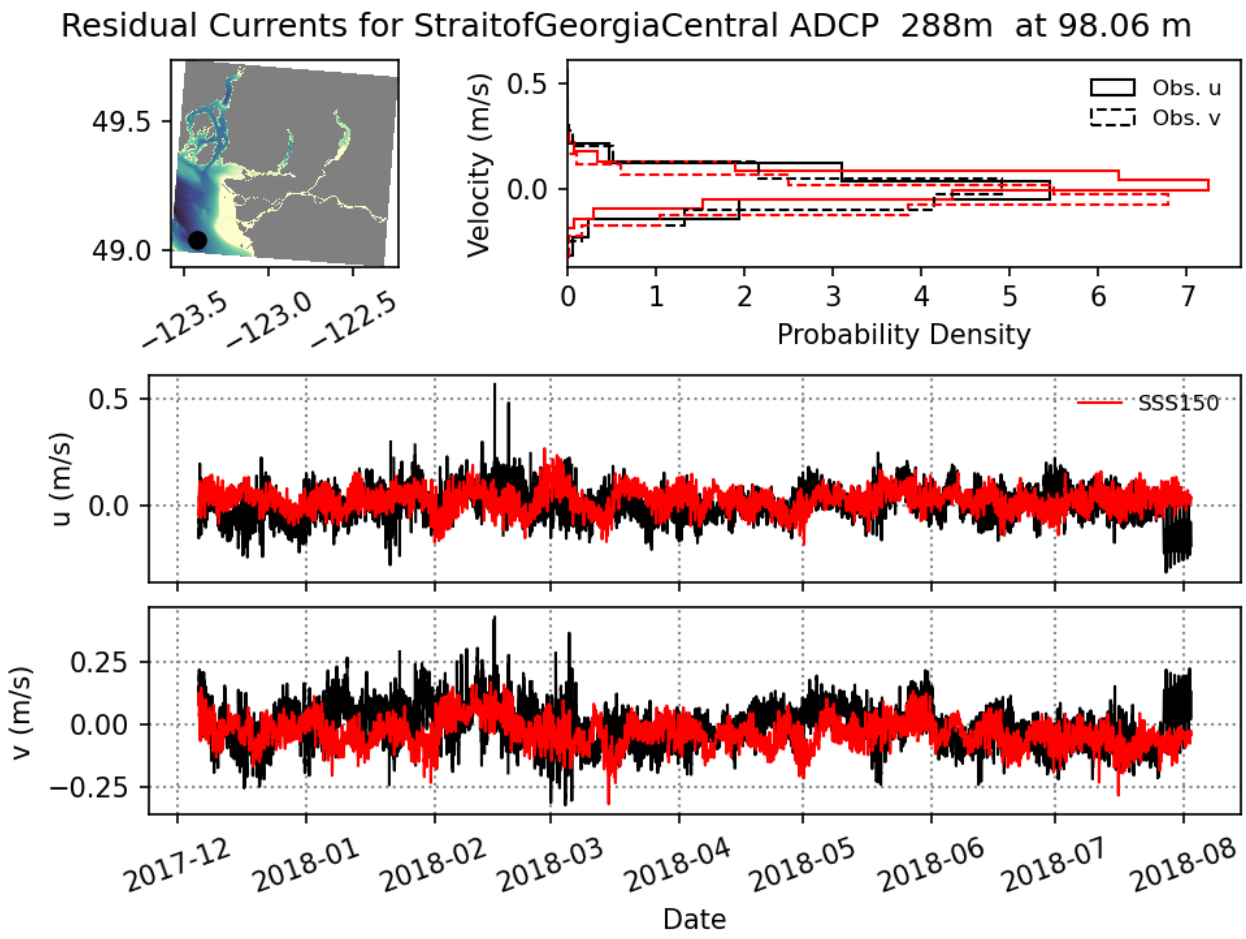

Figure 37. Non-tidal velocity from the SoG Central ADCP station at 98.06 m depth for eastward (u) and northward (v) components.

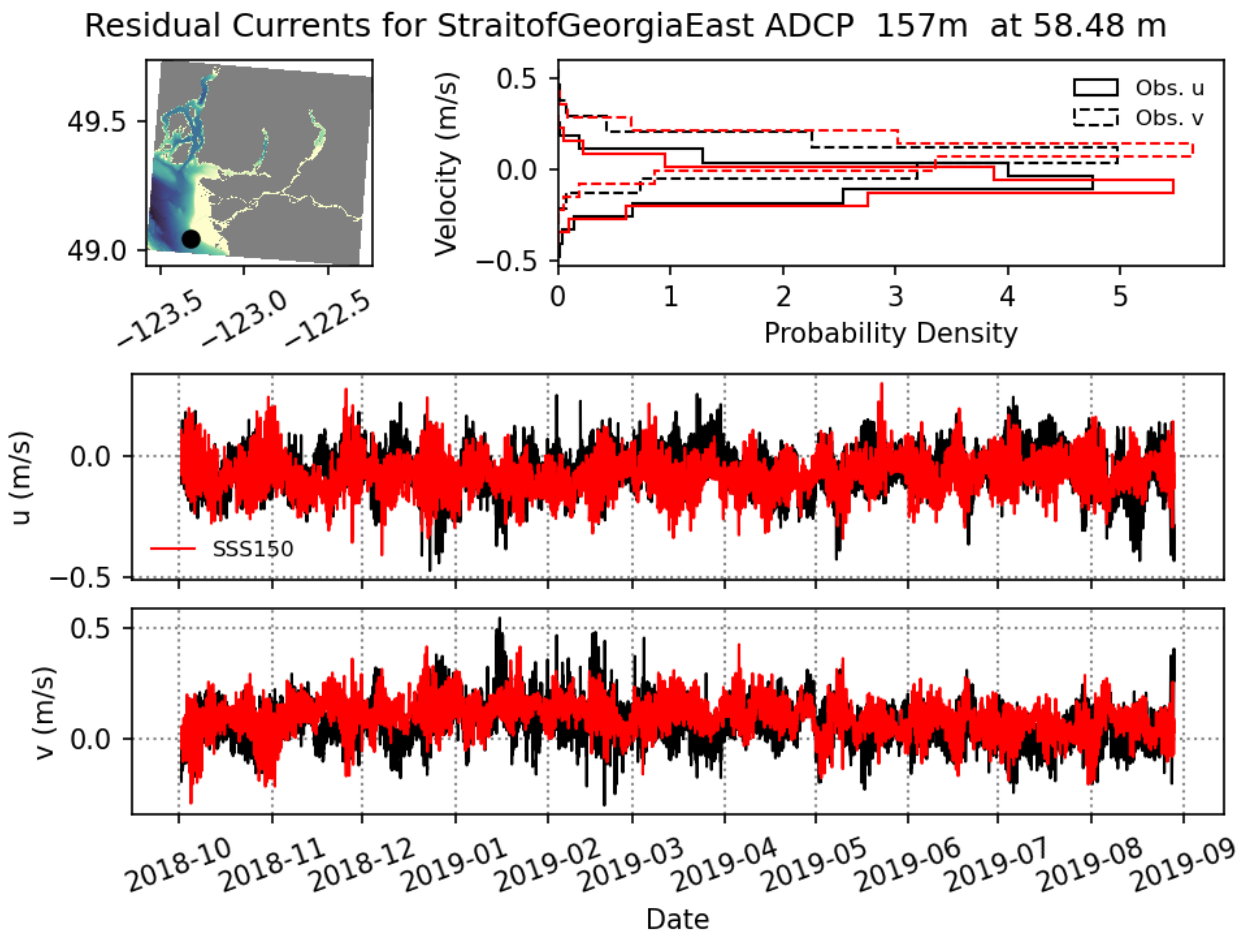

Figure 38. Non-tidal velocity from the SoG East ADCP station at 58.48 m depth for eastward (u) and northward (v) components.

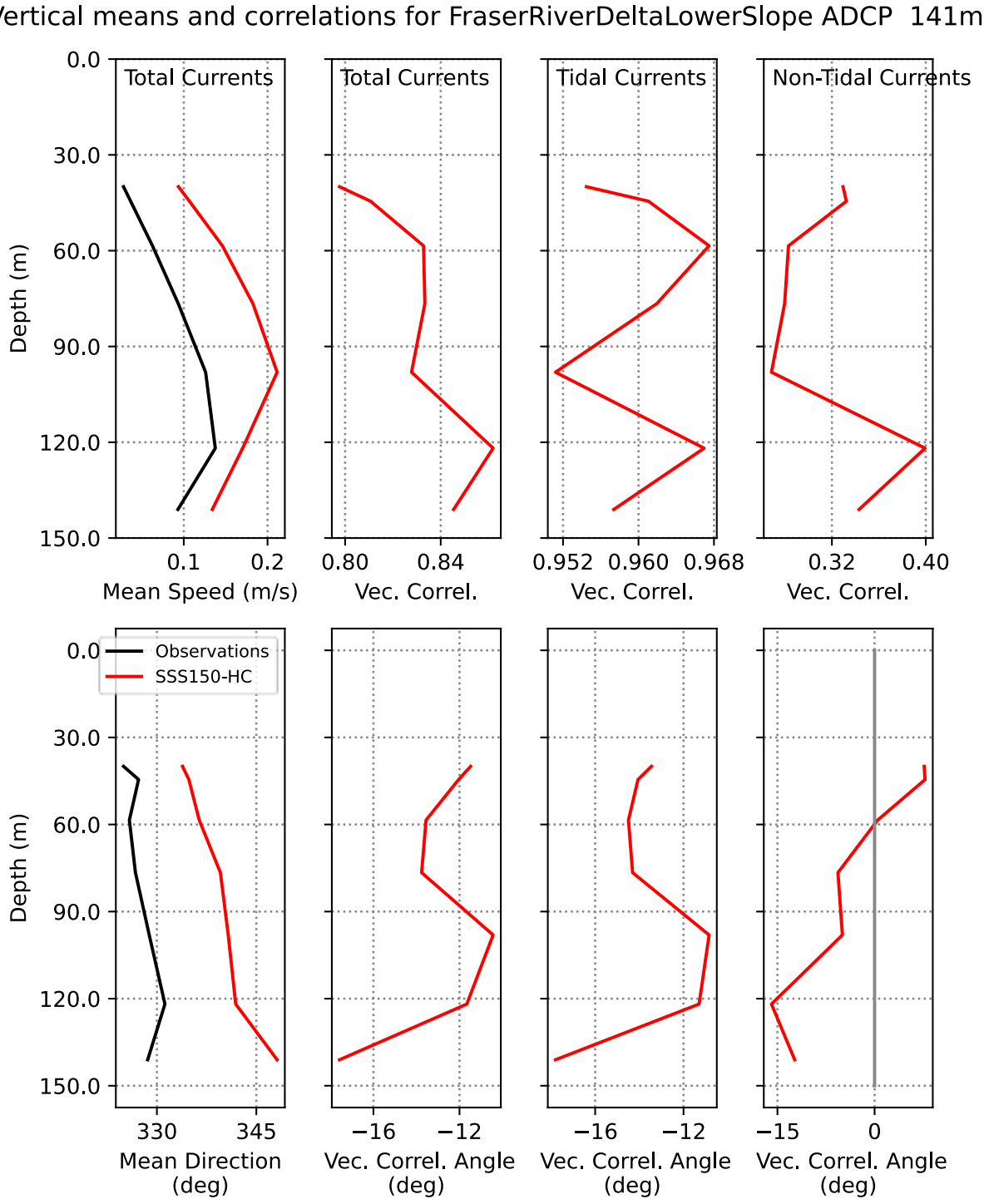

Figure 39. Mean currents (first column) and vector correlations for total (second column), tidal (third column) and non-tidal (fourth column) velocities for FRDLS ADCP deployment. Mean direction is measured clockwise from north.

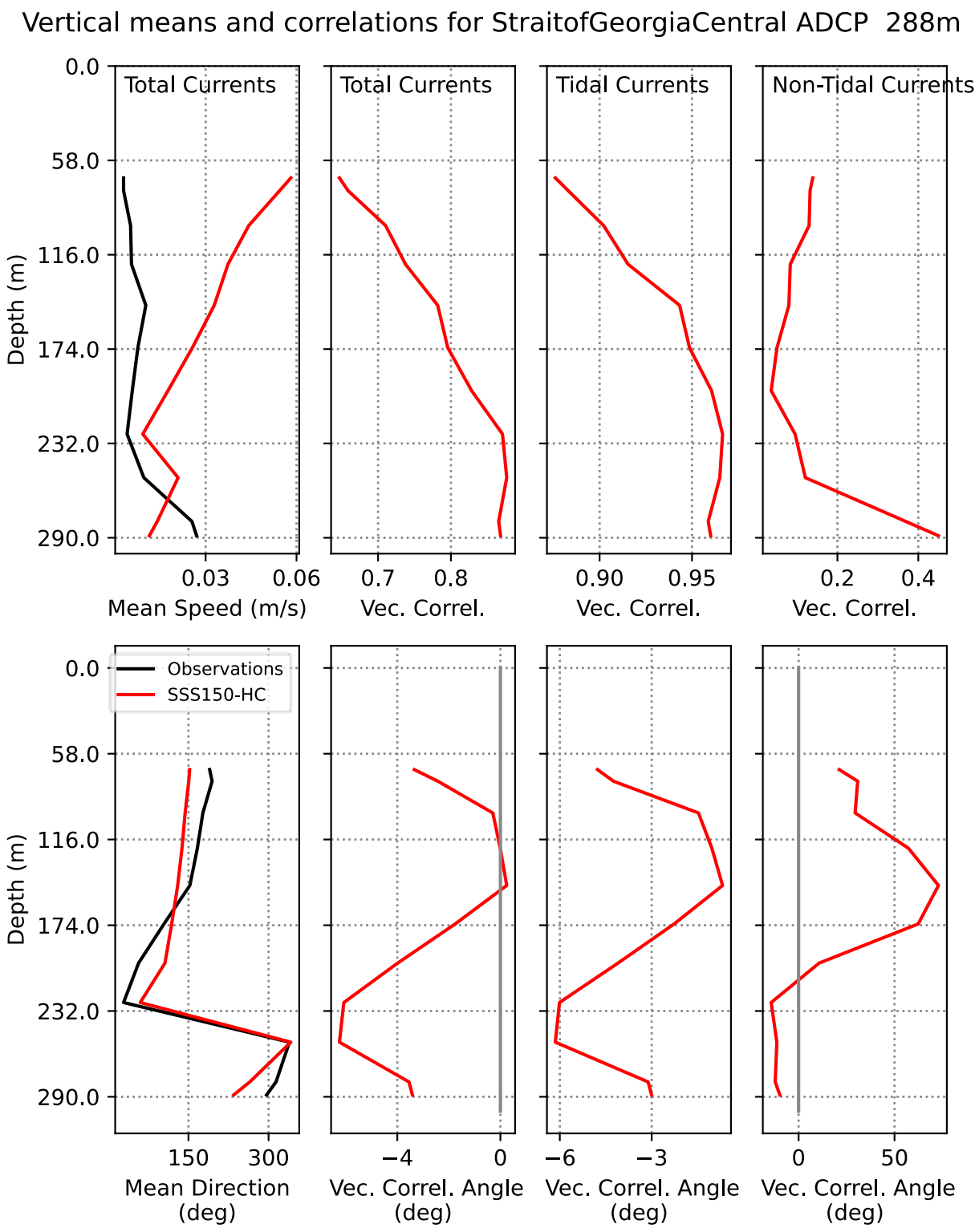

Figure 40. Mean currents (first column) and vector correlations for total (second column), tidal (third column) and non-tidal (fourth column) velocities for SoG Central ADCP deployment. Mean direction is measured clockwise from north.

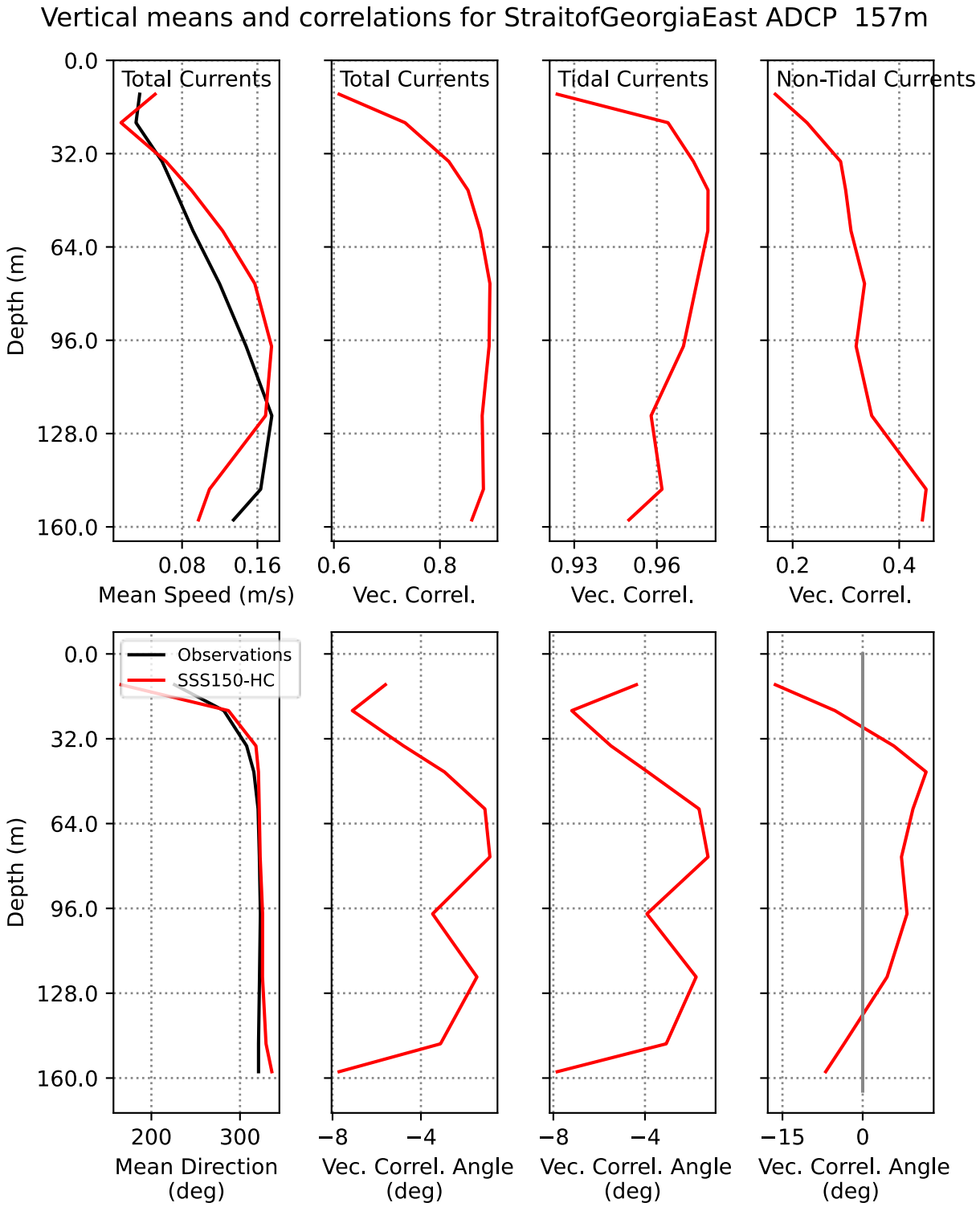

Figure 41. Mean currents (first column) and vector correlations for total (second column), tidal (third column) and non-tidal (fourth column) velocities for SoG East ADCP deployment. Mean direction is measured clockwise from north.

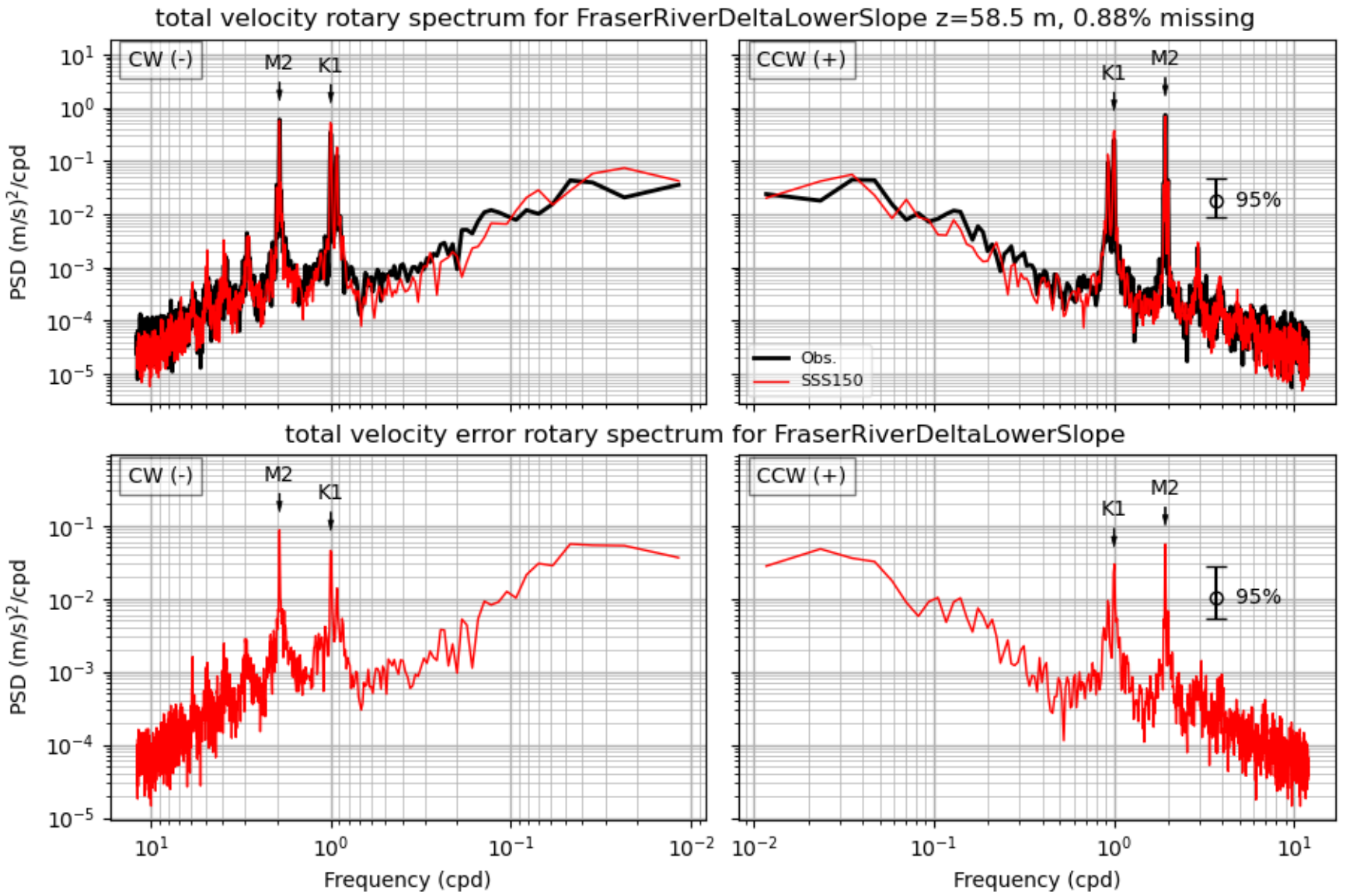

Figure 42. Rotary spectra for total velocity from the FRDLS ADCP station at 58.5 m depth.

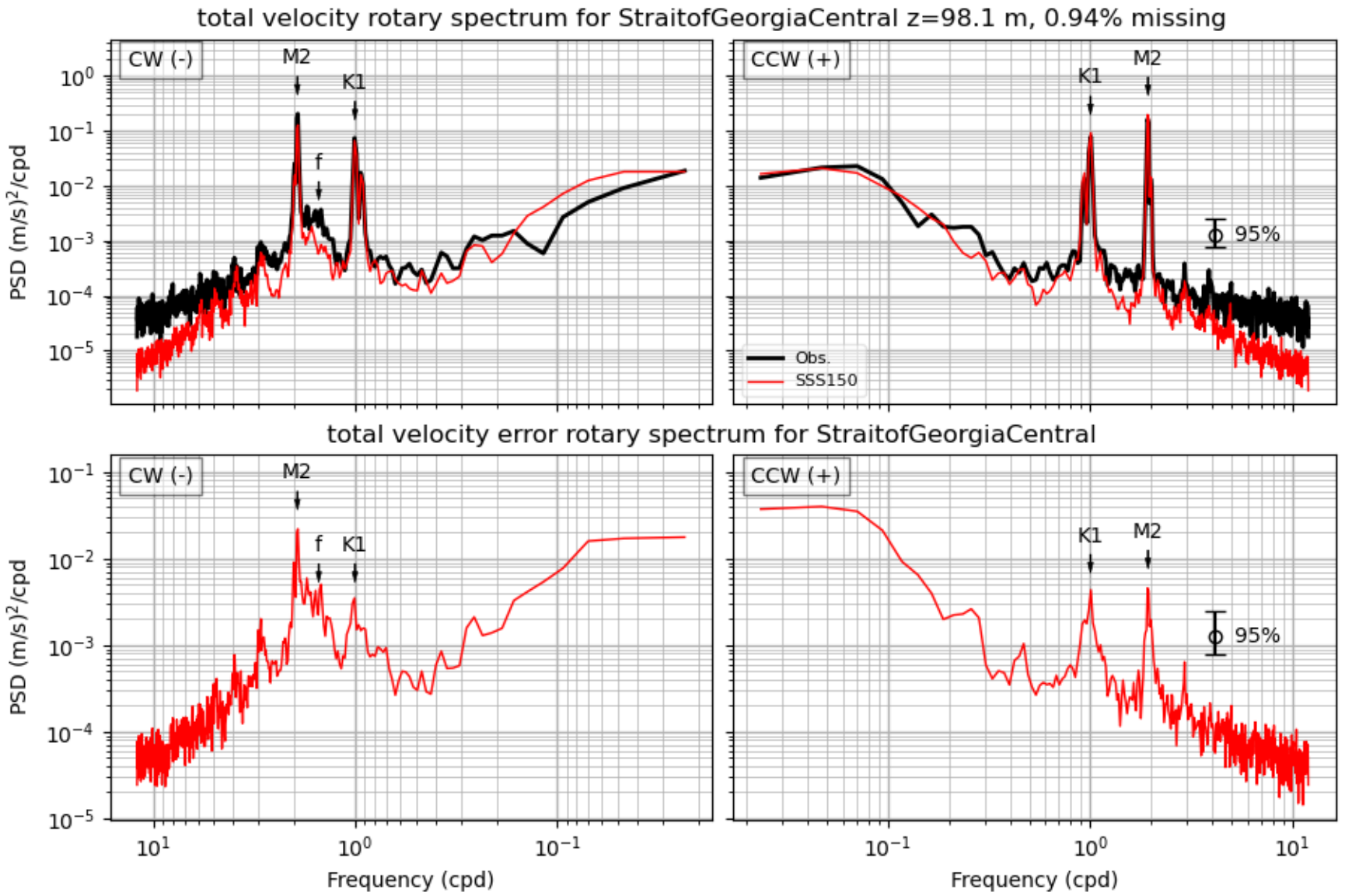

Figure 43. Rotary spectra for total velocity from the SoG Central ADCP station at 98.1 m depth.

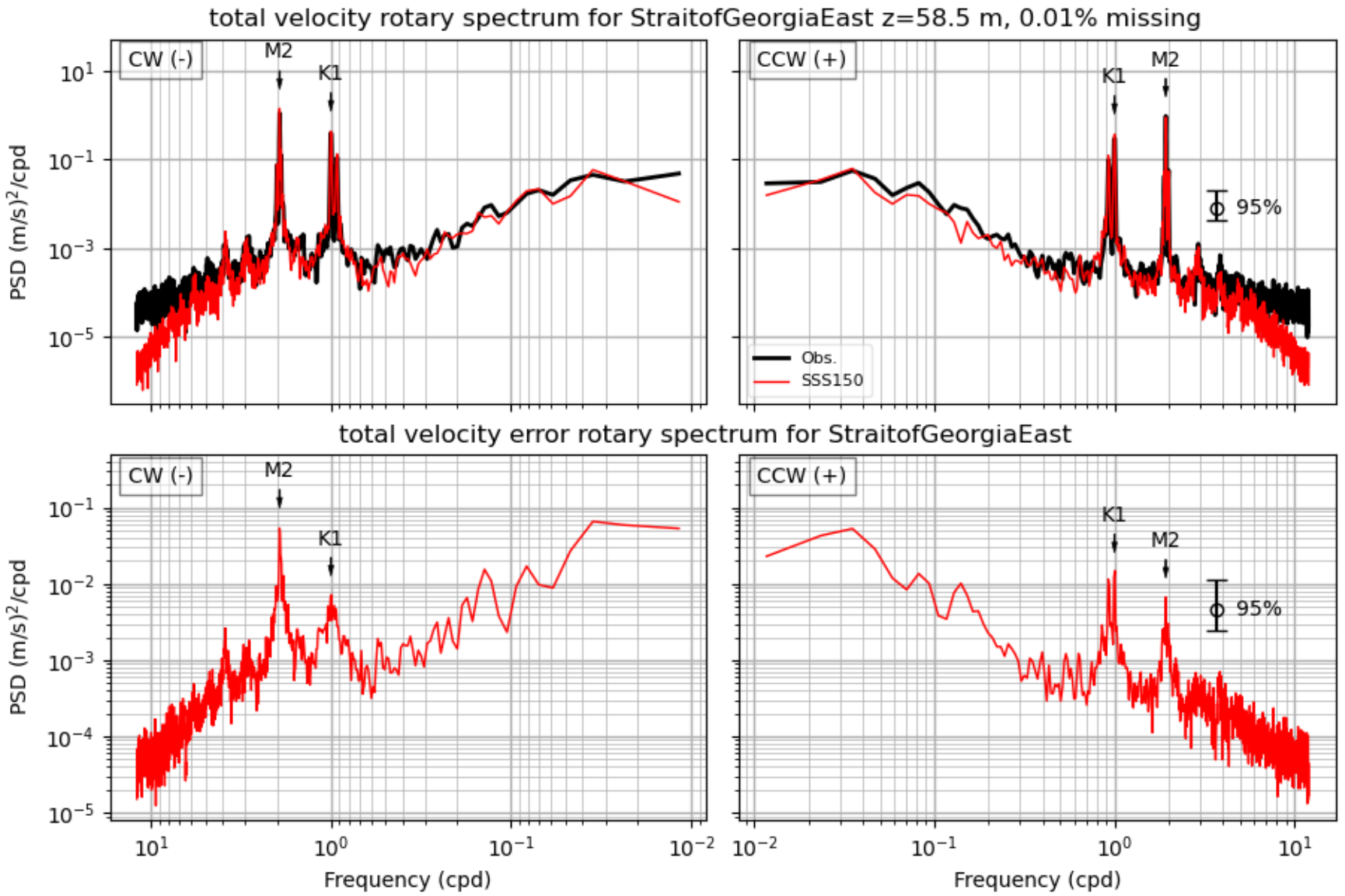

Figure 44. Rotary spectra for total velocity from the SoG East ADCP station at 15.6 m depth.

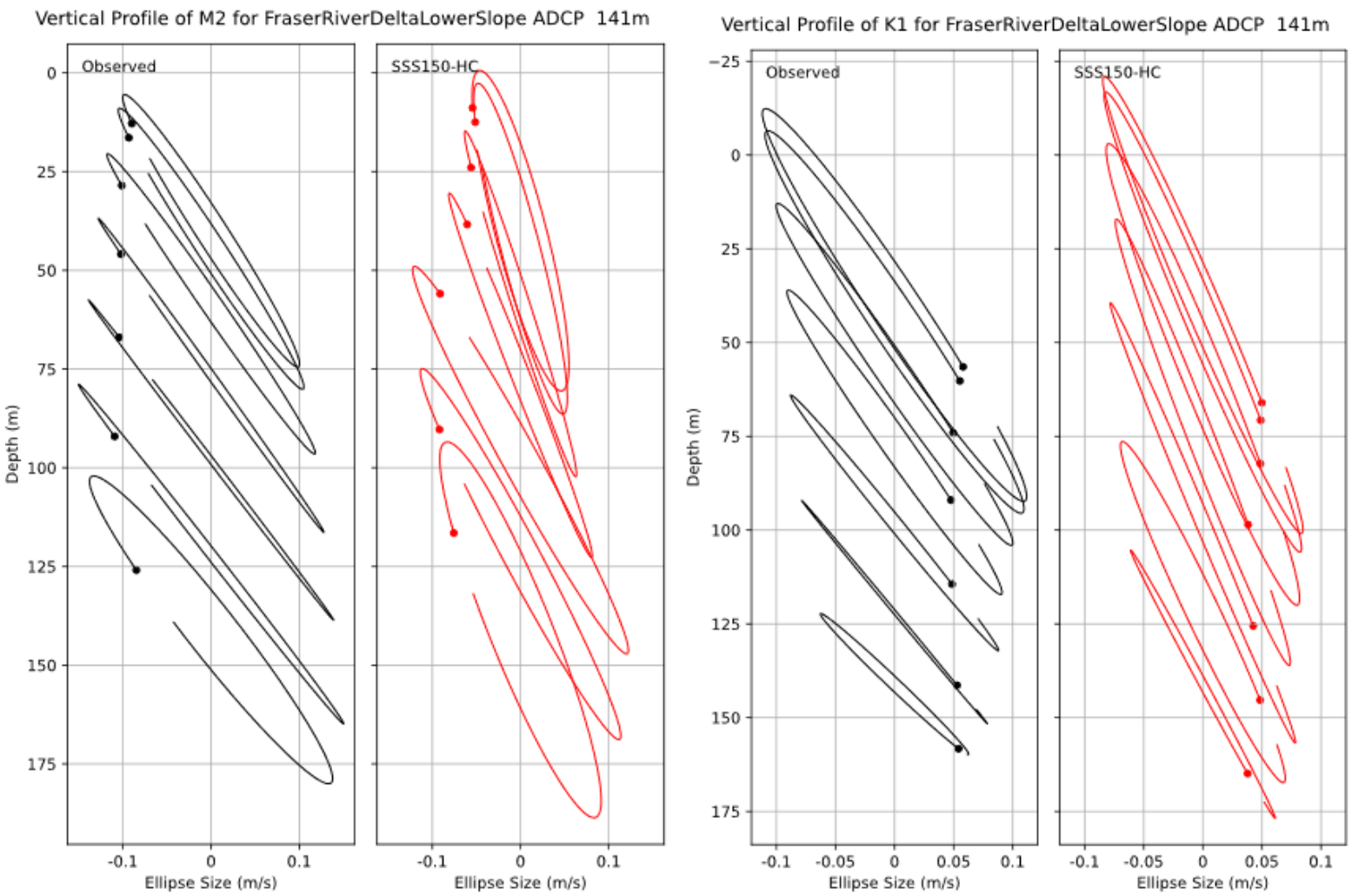

Figure 45. Current ellipses for M2 (left) and K1 (right) tidal components from the FRDLS ADCP station.

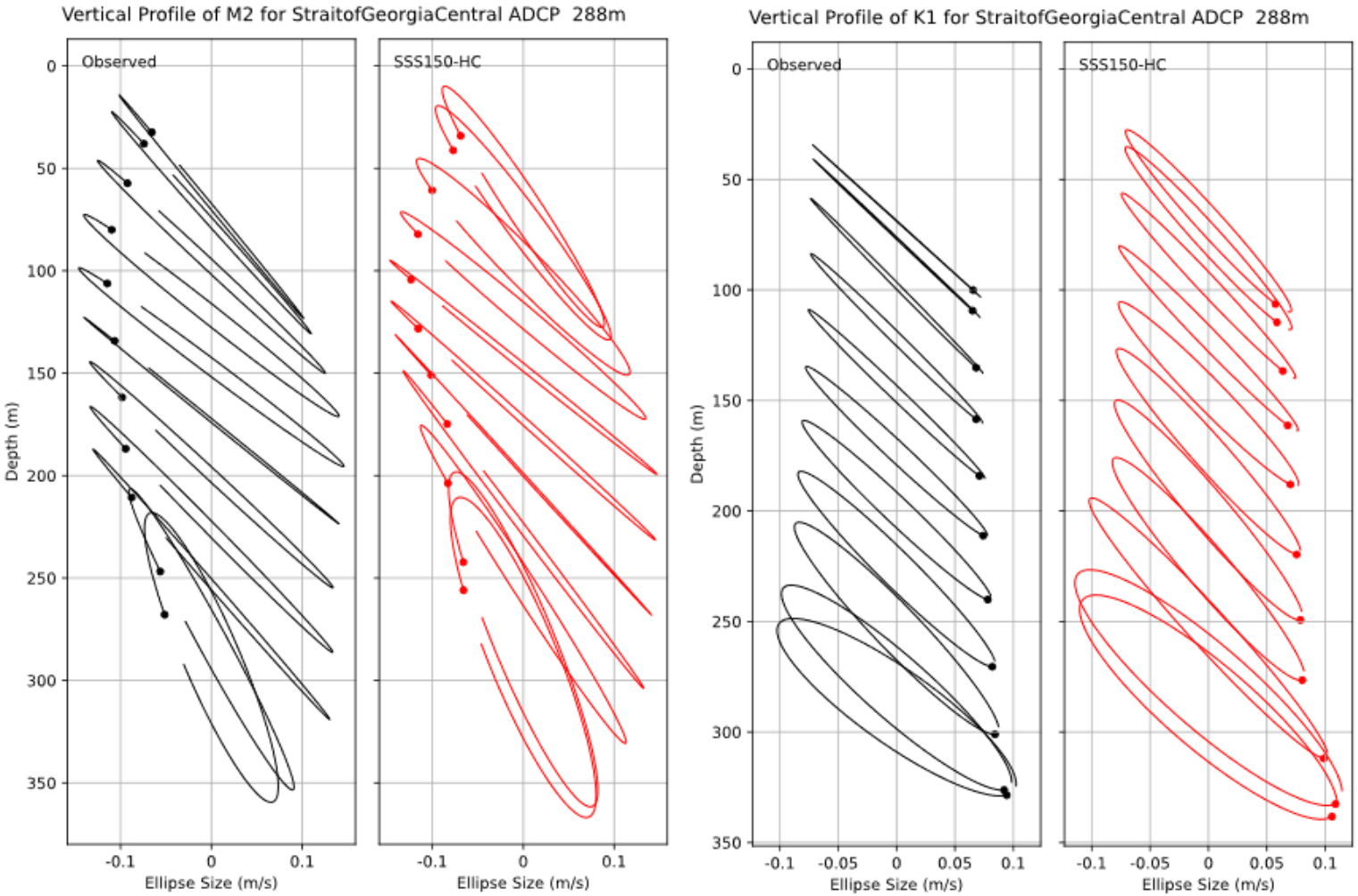

Figure 46. Current ellipses for M2 (left) and K1 (right) tidal components from the SoG Central ADCP station

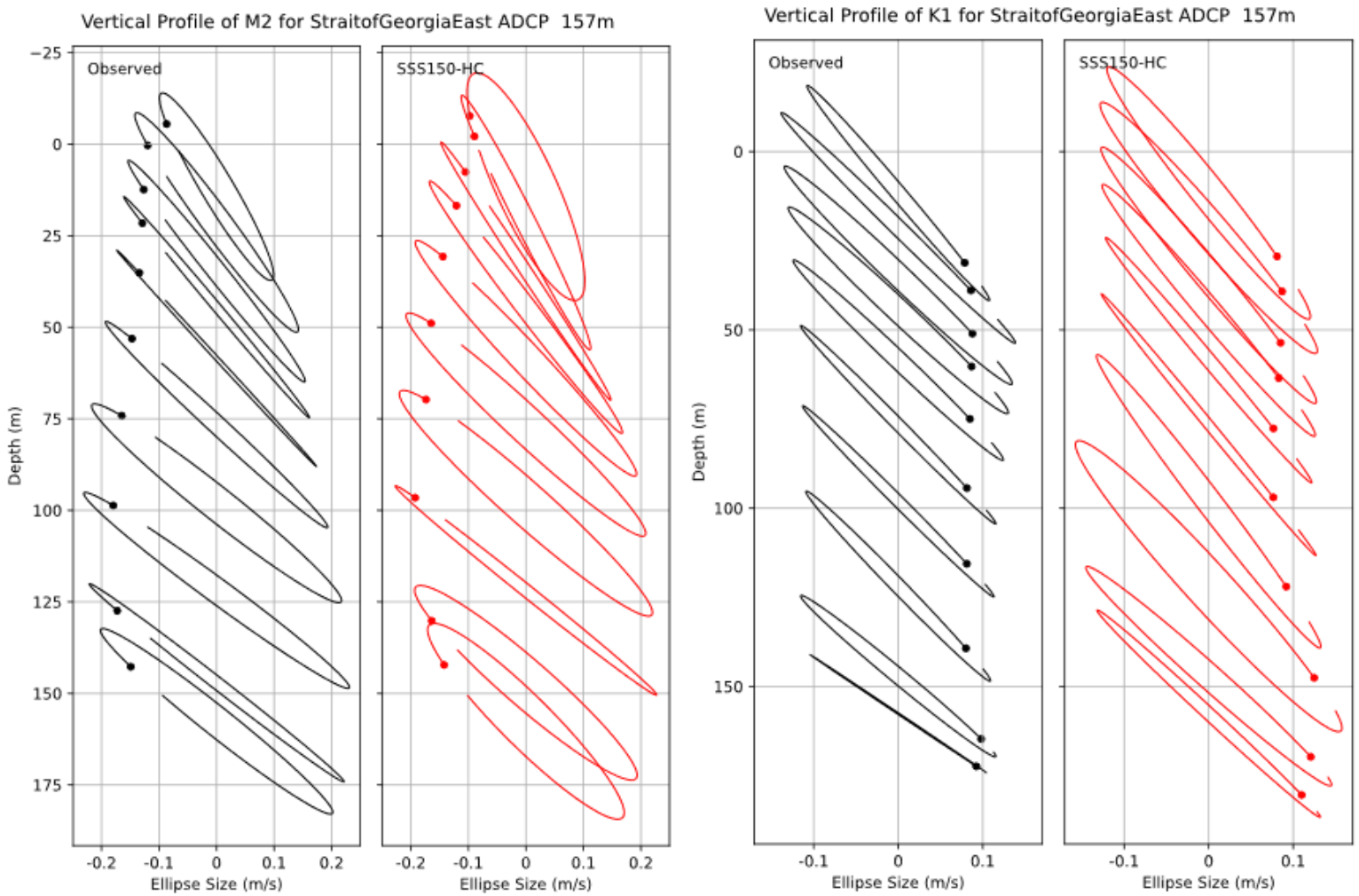

Figure 47. Current ellipses for M2 (left) and K1 (right) tidal components from the SoG East ADCP station.

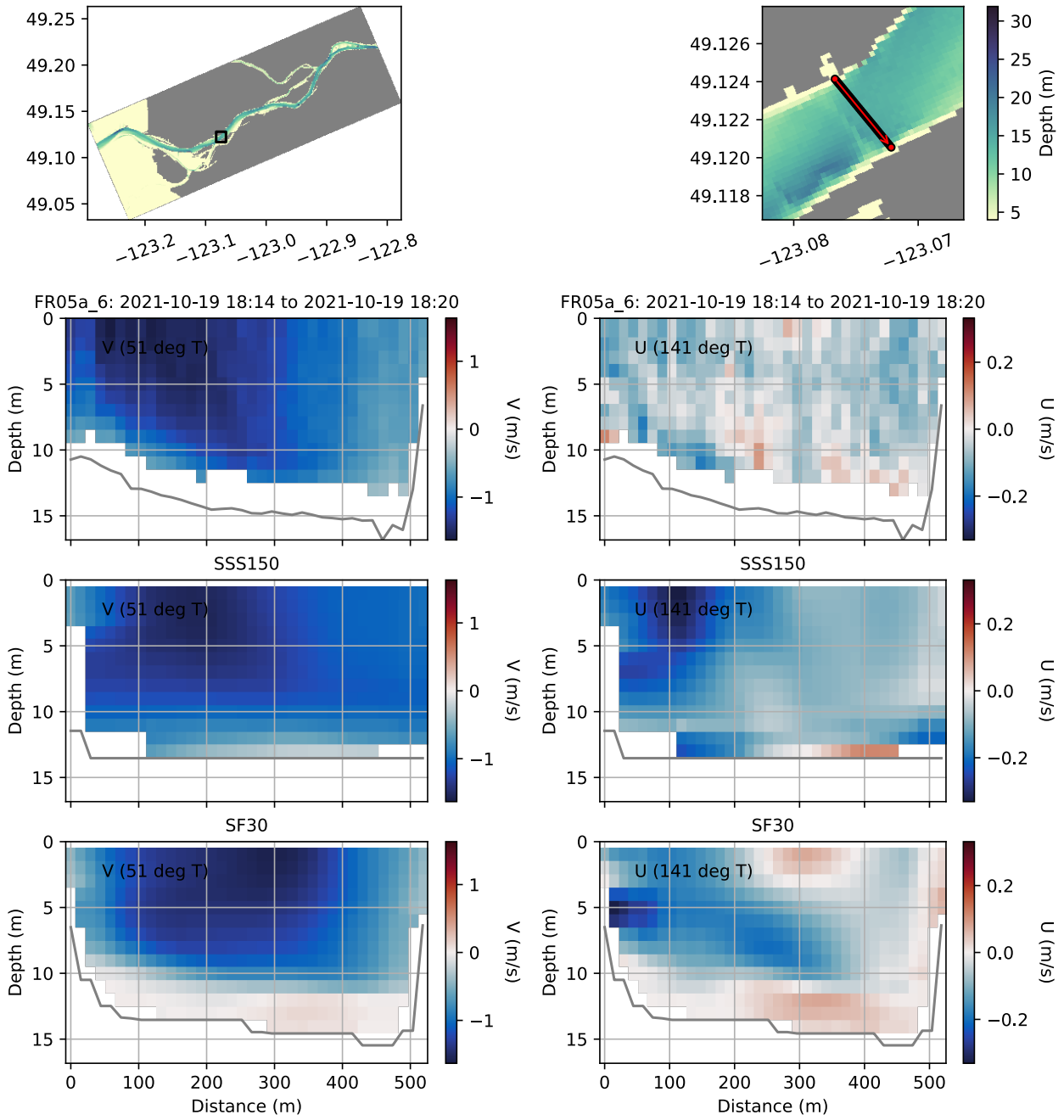

Figure 48. Observed and model current velocity components: Cross-transect (left panels) and along-transect (right panels) at the line FR05a. Positive direction is indicated in true degrees in each panel. Transect location is shown in the upper panels. The black line in the upper right panel shows the transect and the red arrow indicates the direction of the transect.

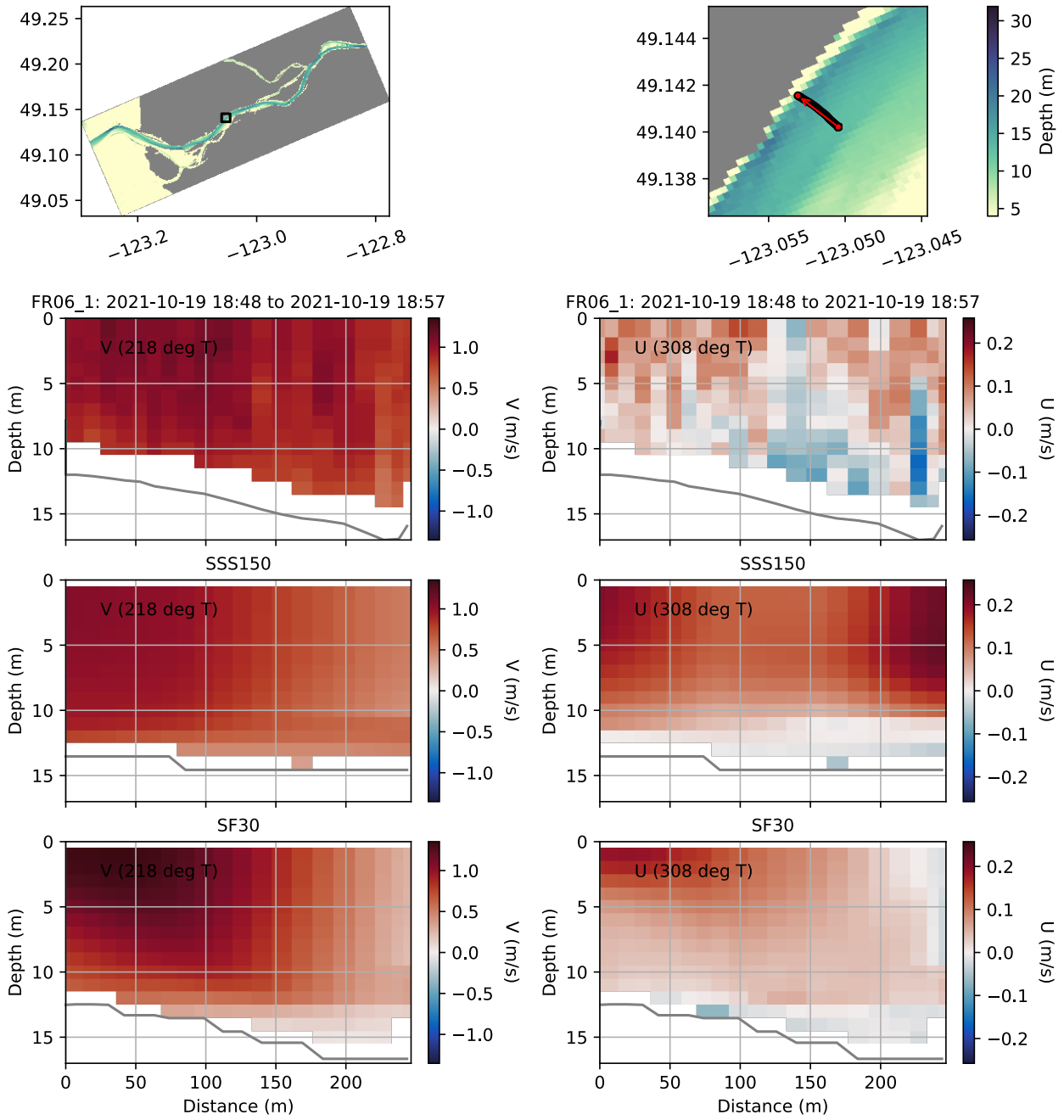

Figure 49. Same as Figure 48, but for the line FR06.

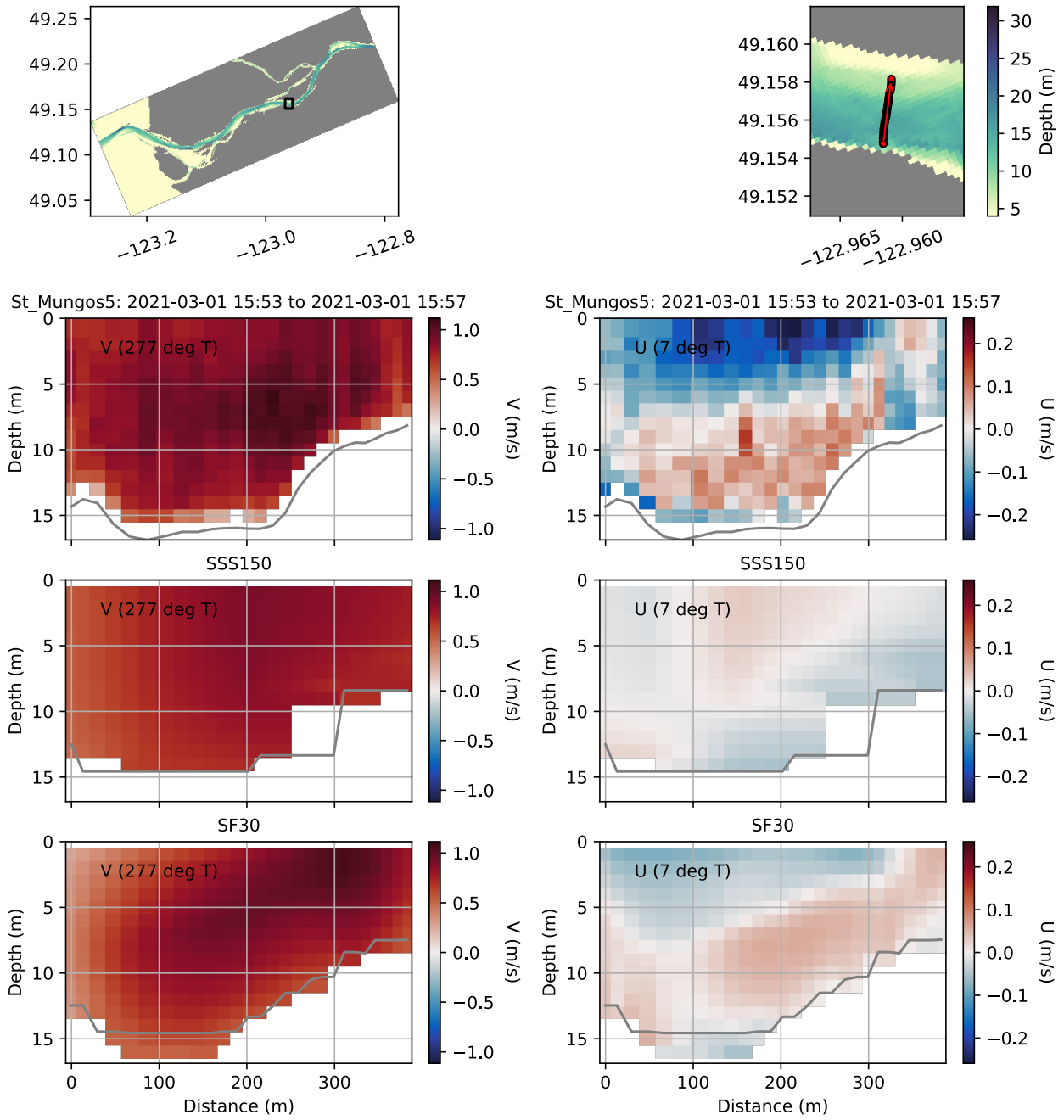

Figure 50. Same as Figure 48, but for the line Mungos5.

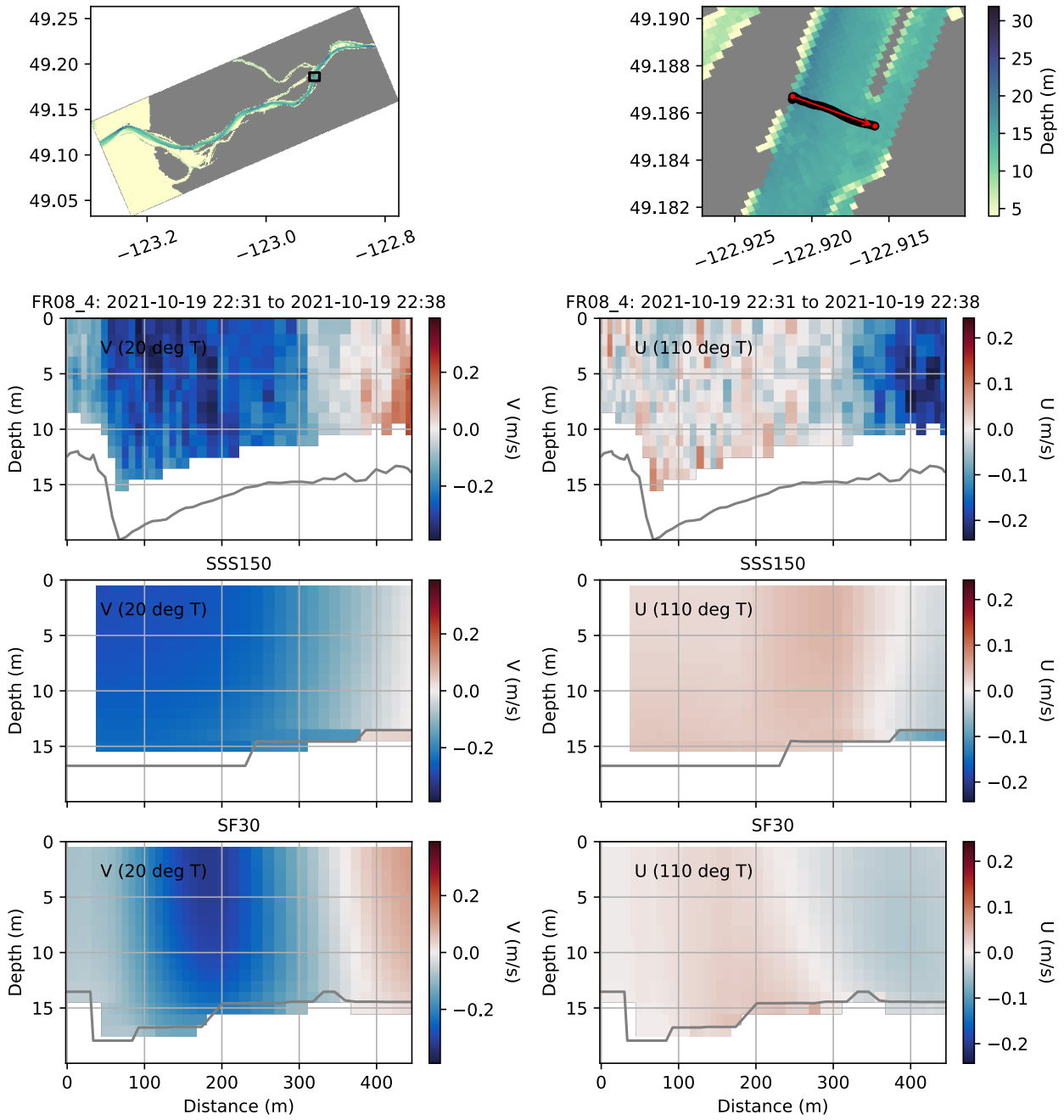

Figure 51. Same as Figure 48, but for the line FR08.

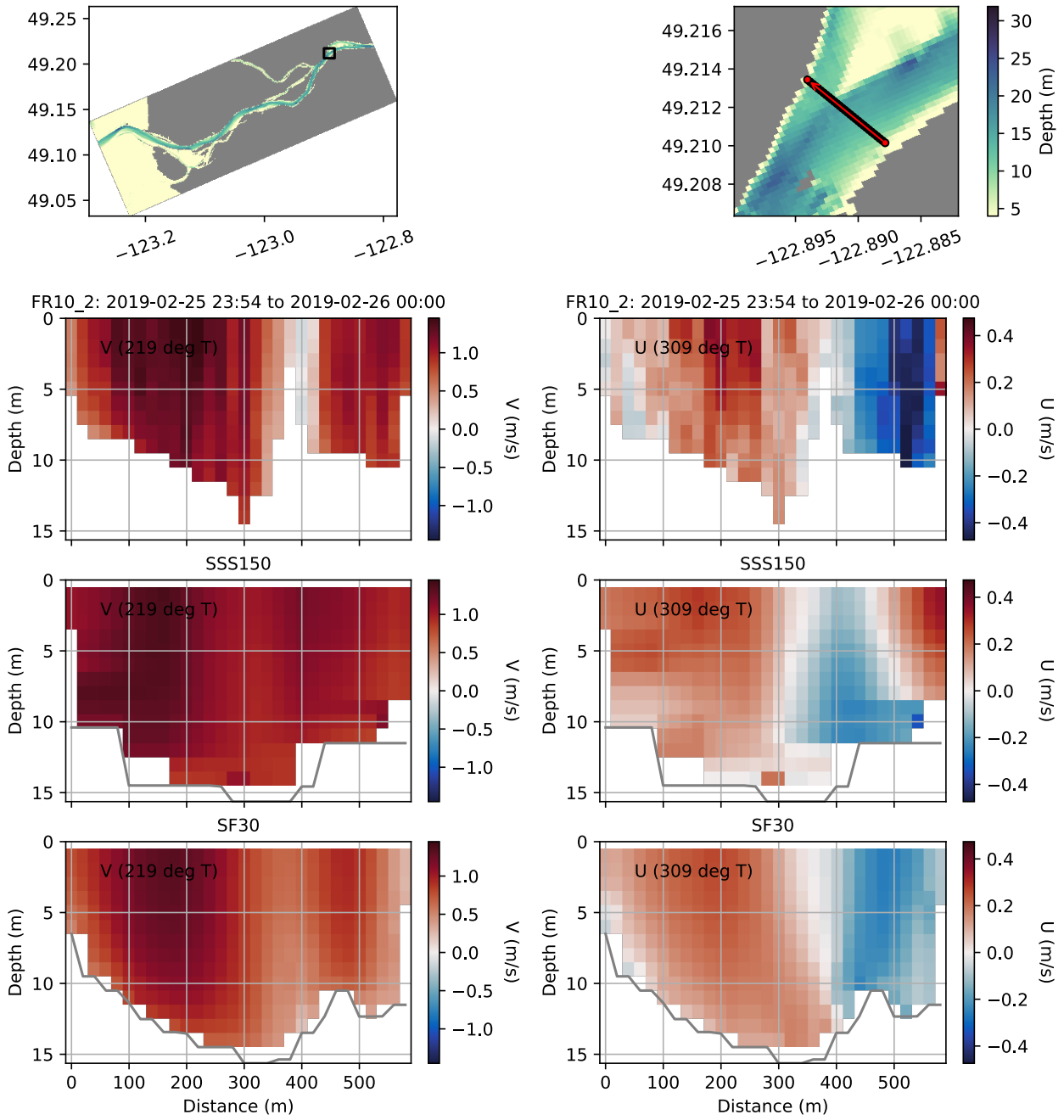

Figure 52. Same as Figure 48, but for the line FR10.

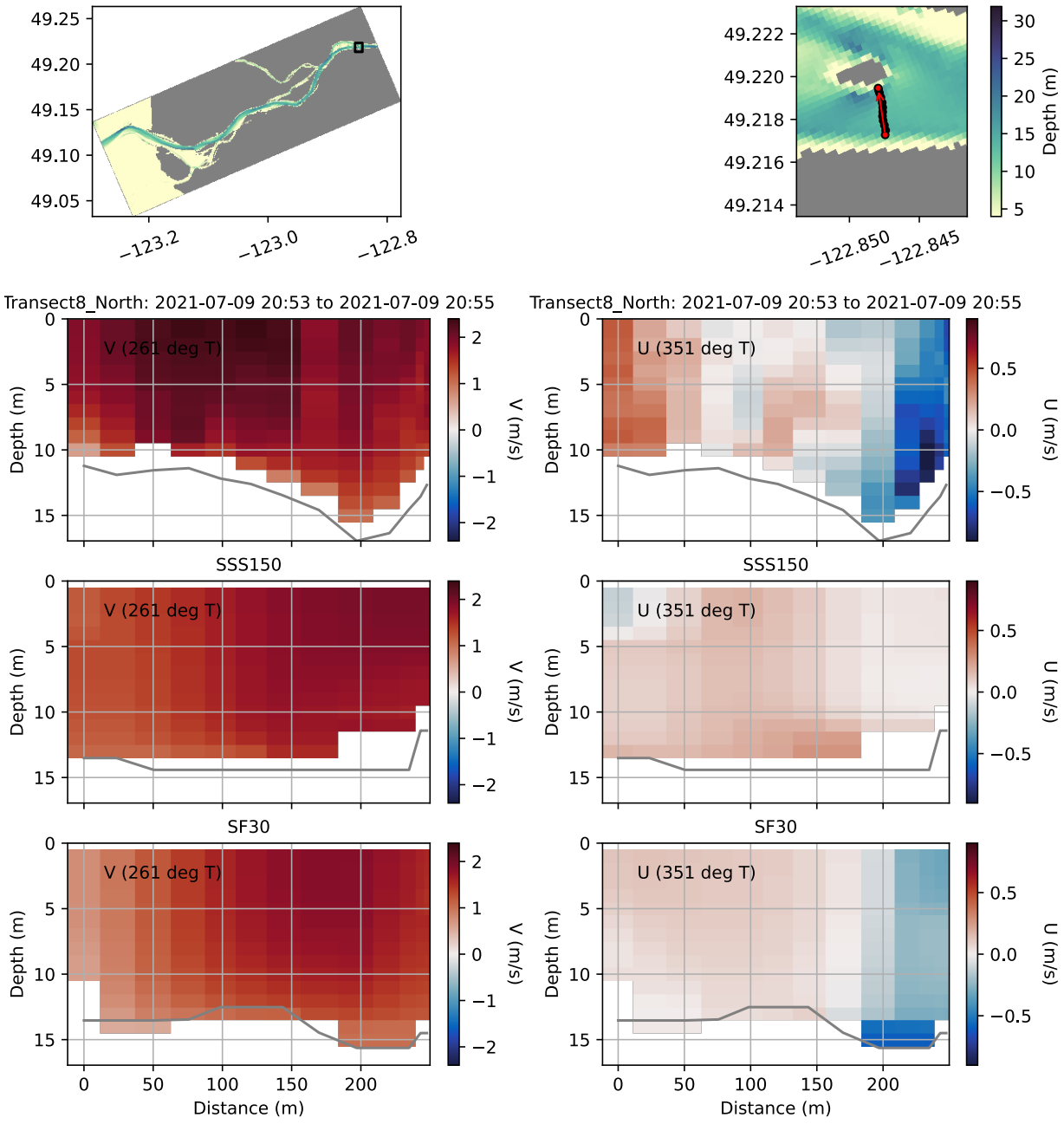

Figure 53. Same as Figure 48, but for the line Transect8.

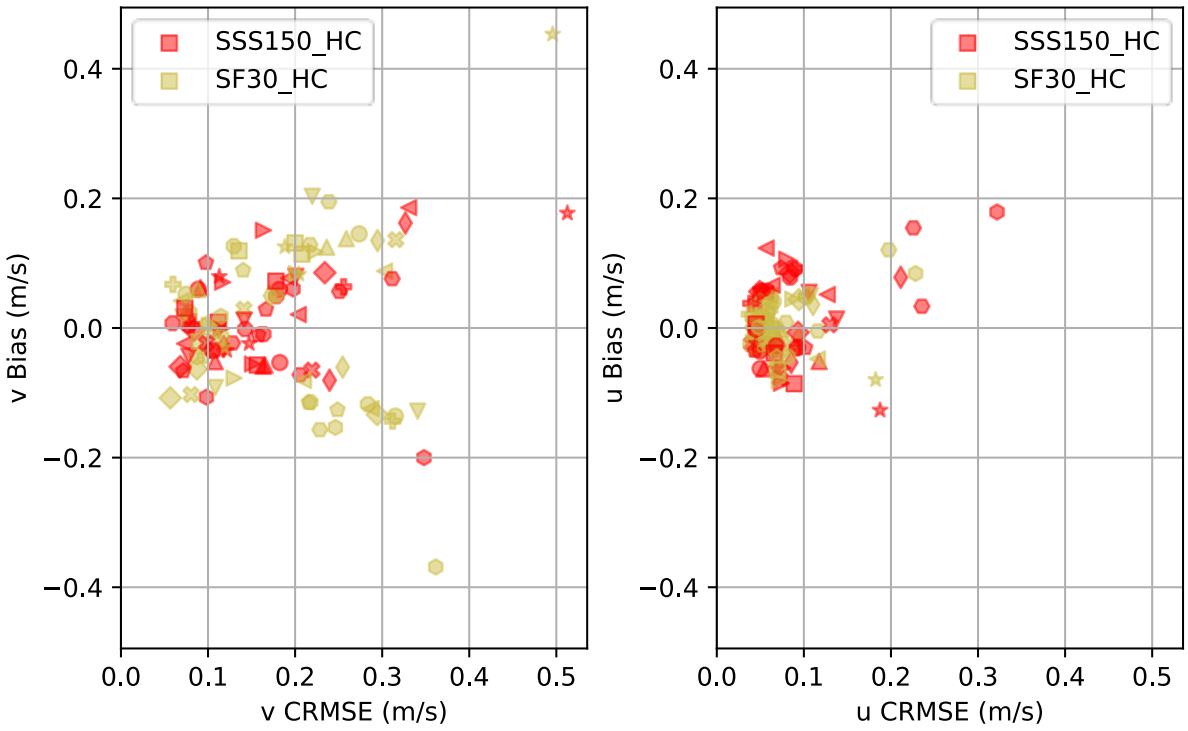

Figure 54. Scatter plot of mean bias vs mean CRMSE for each transect for along-shore (left) and cross-shore (right) current velocity components. Colour denotes the model and marker shape denotes the transect (marker shapes repeat due to a limited number of shapes).

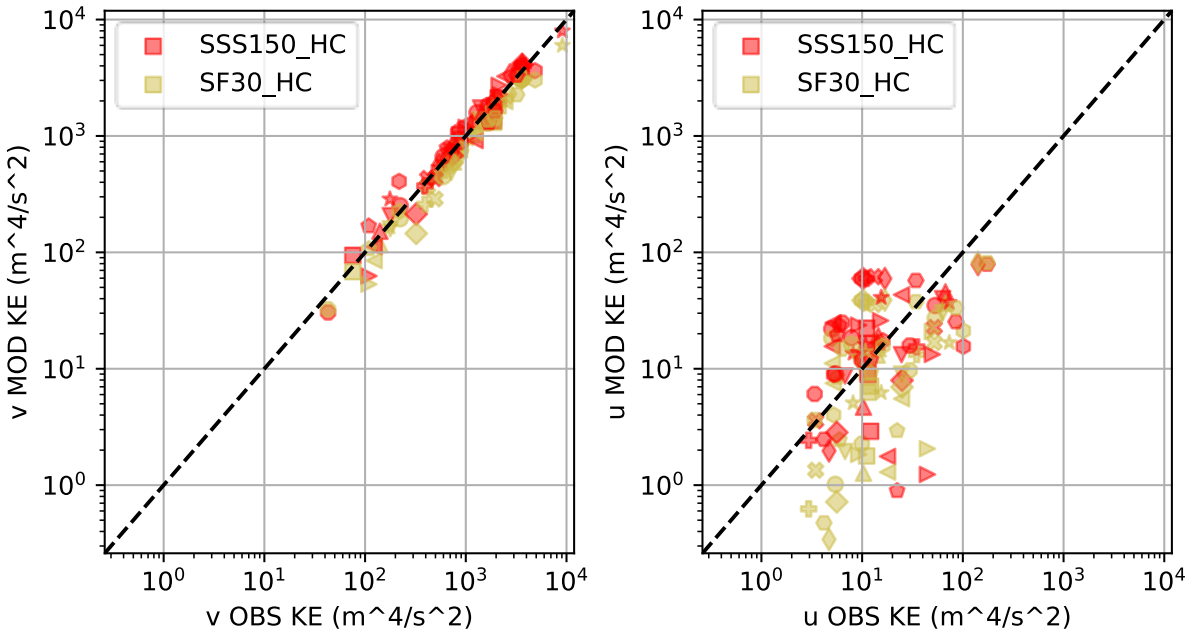

Figure 55. Distribution of the kinetic energy of the model current for SSS150 and SF30 vs kinetic energy of the observed current integrated over each transect for the along-shore (left) and cross-shore (right) components. Colour denotes the model and marker shape denotes the transect (marker shapes repeat due to a limited number of shapes).

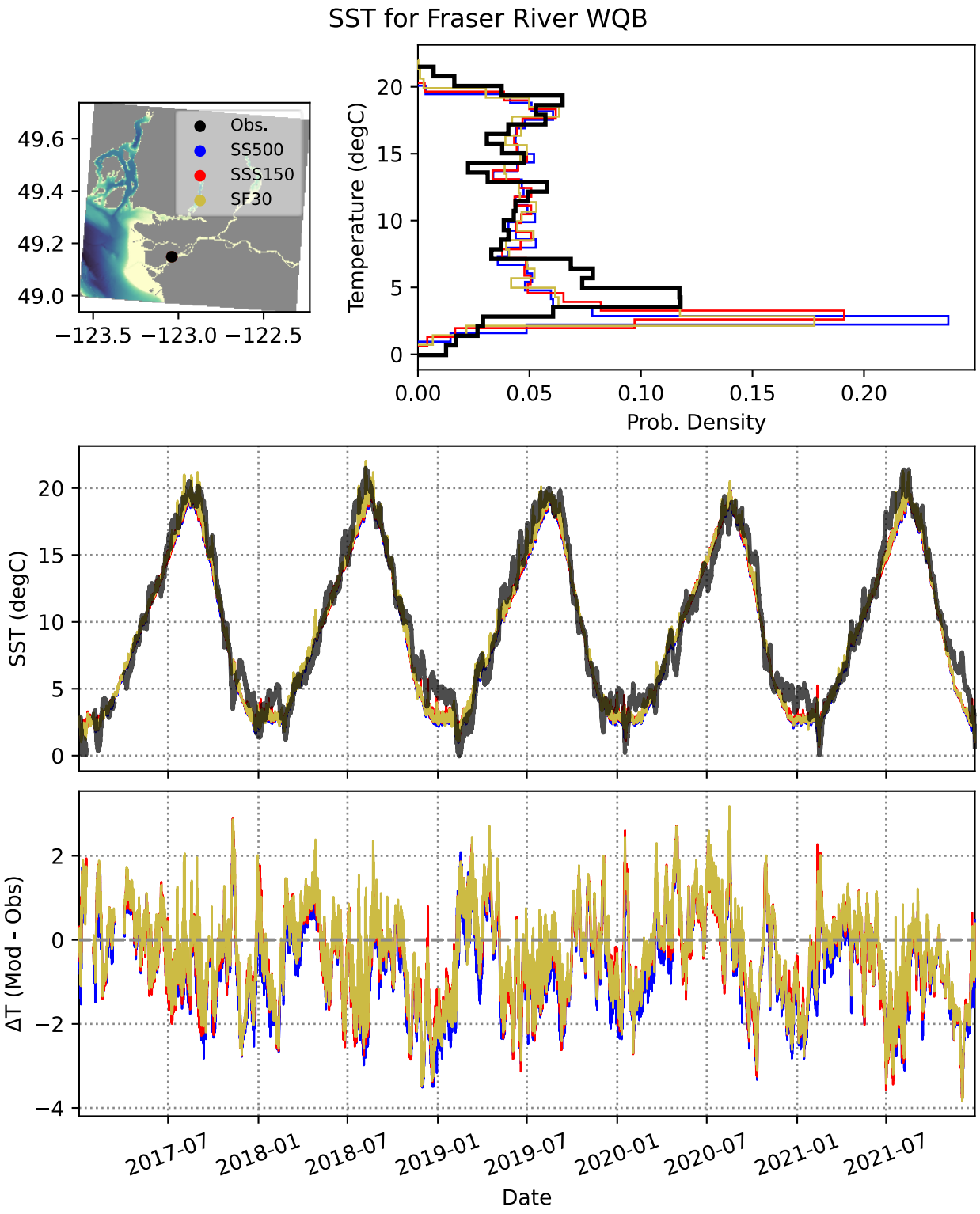

Figure 56. Observed and model SST at Fraser River Water Quality Buoy.

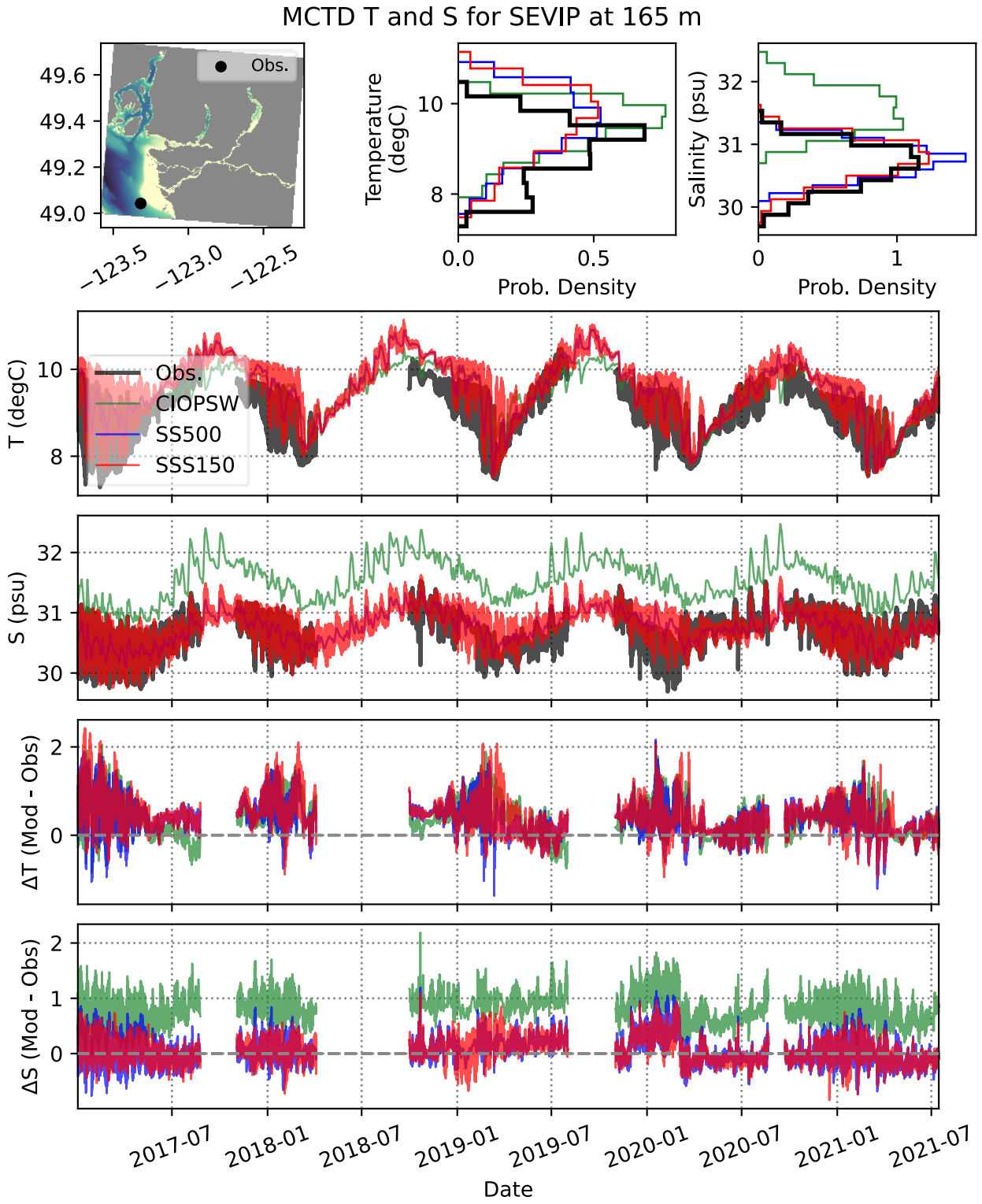

Figure 57. Observed and model temperature and salinity for moored CTD at SEVIP station. Daily series are shown for CIOPS-W and SS500 and hourly for SSS150.

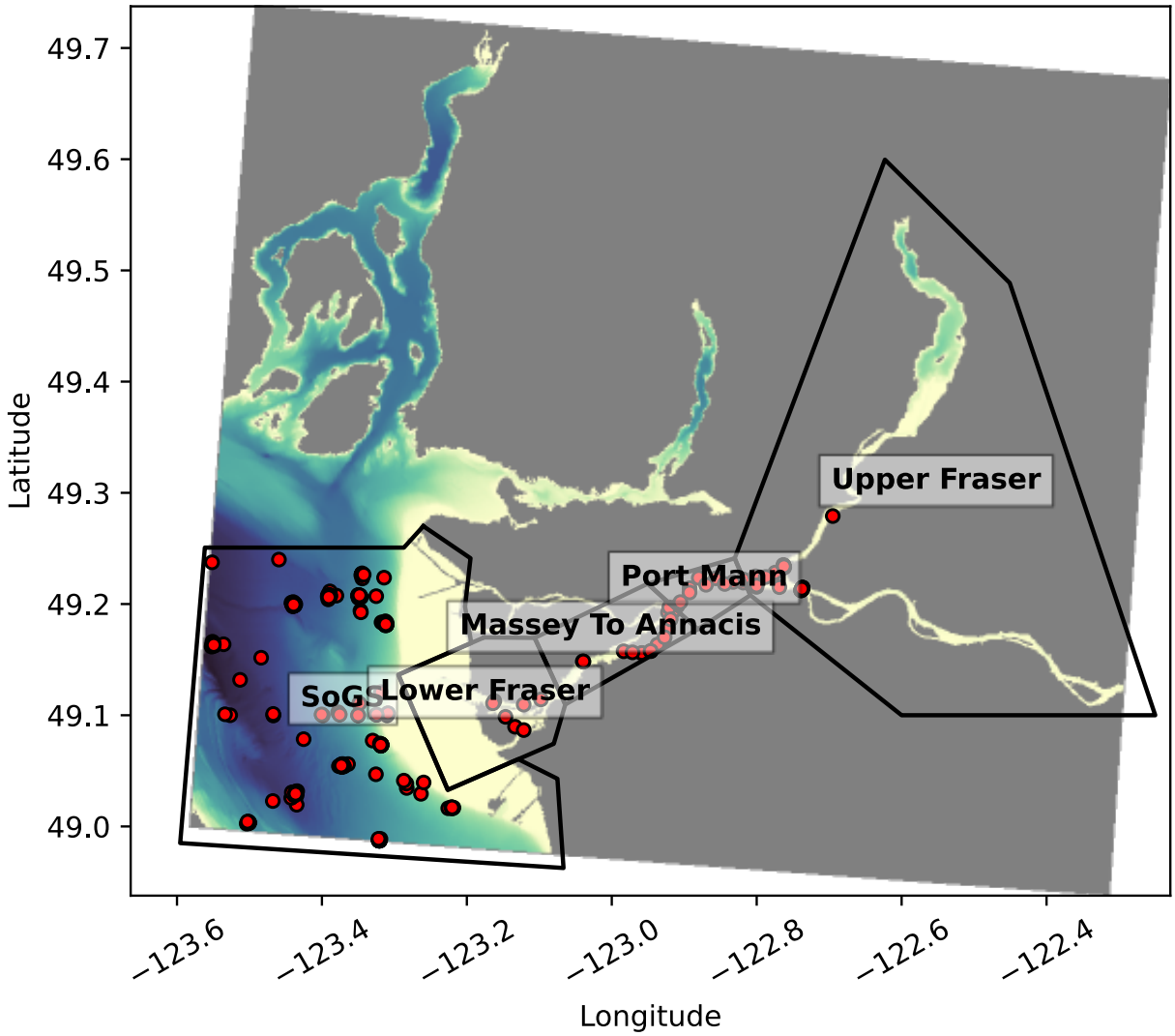

Figure 58. CTD profiles (red dots) and subregions (outlined with solid black lines) used for the analysis.

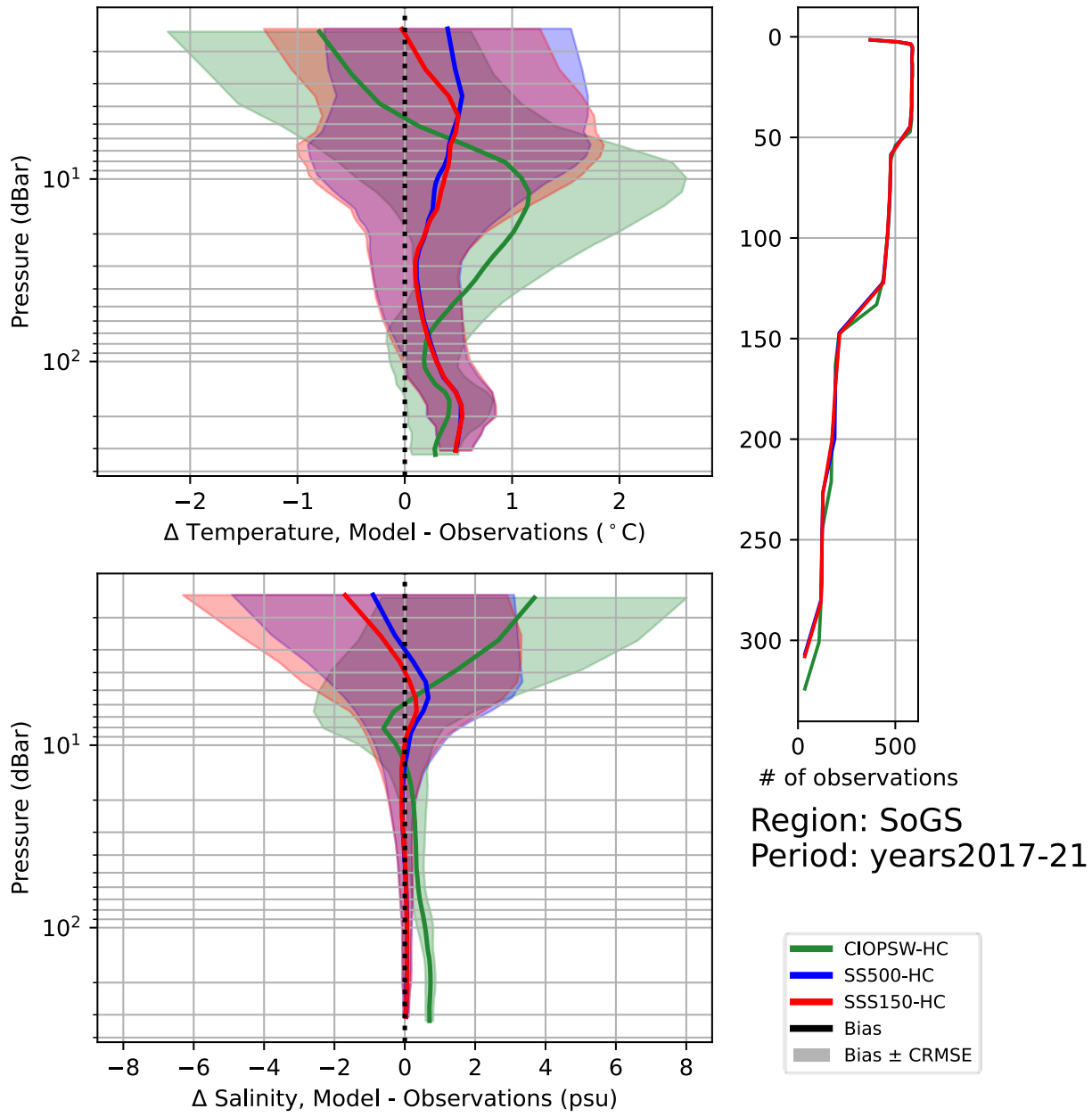

Figure 59. CTD comparison for region Strait of Georgia South.

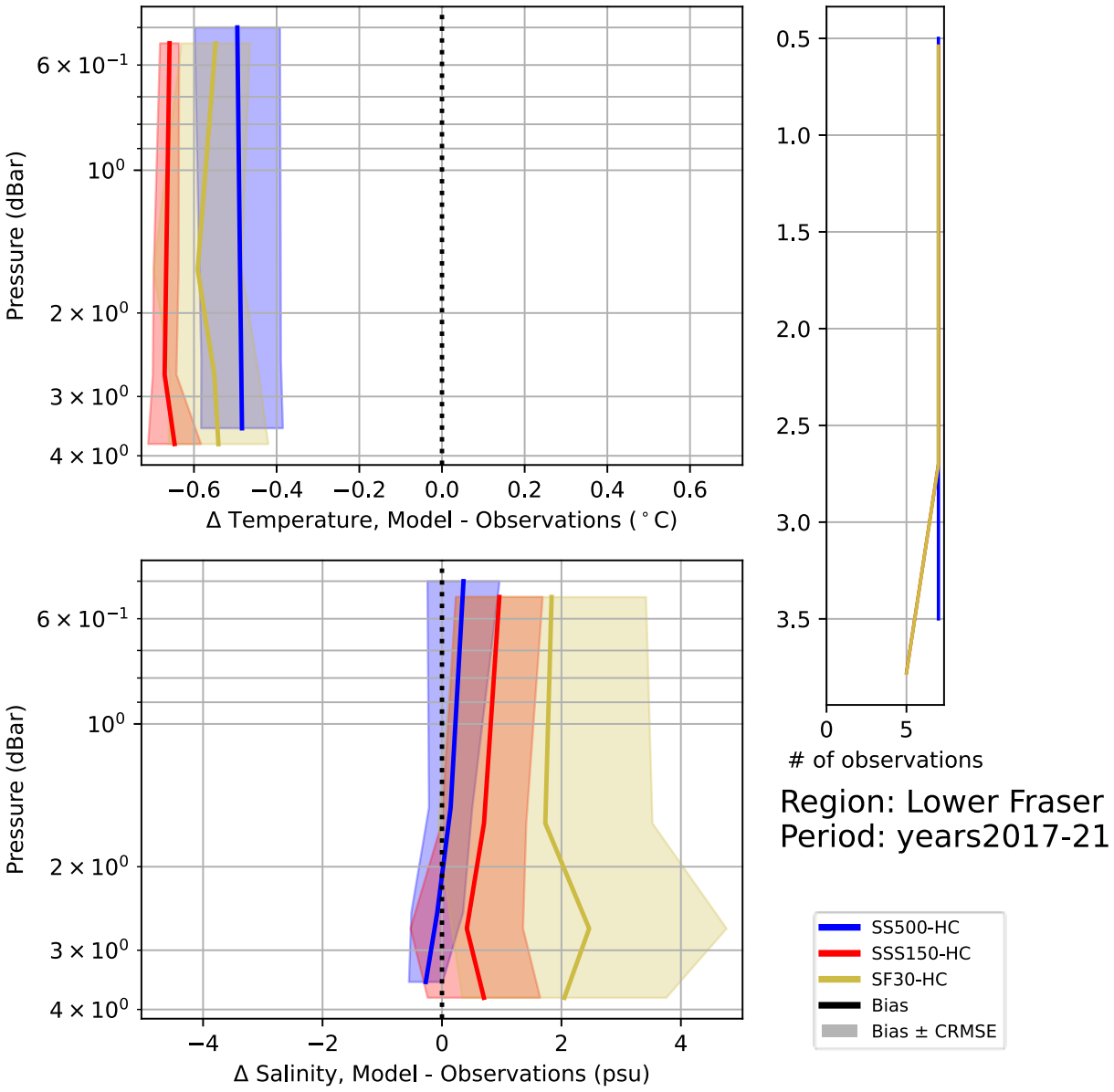

Figure 60. CTD comparison for region Lower Fraser.

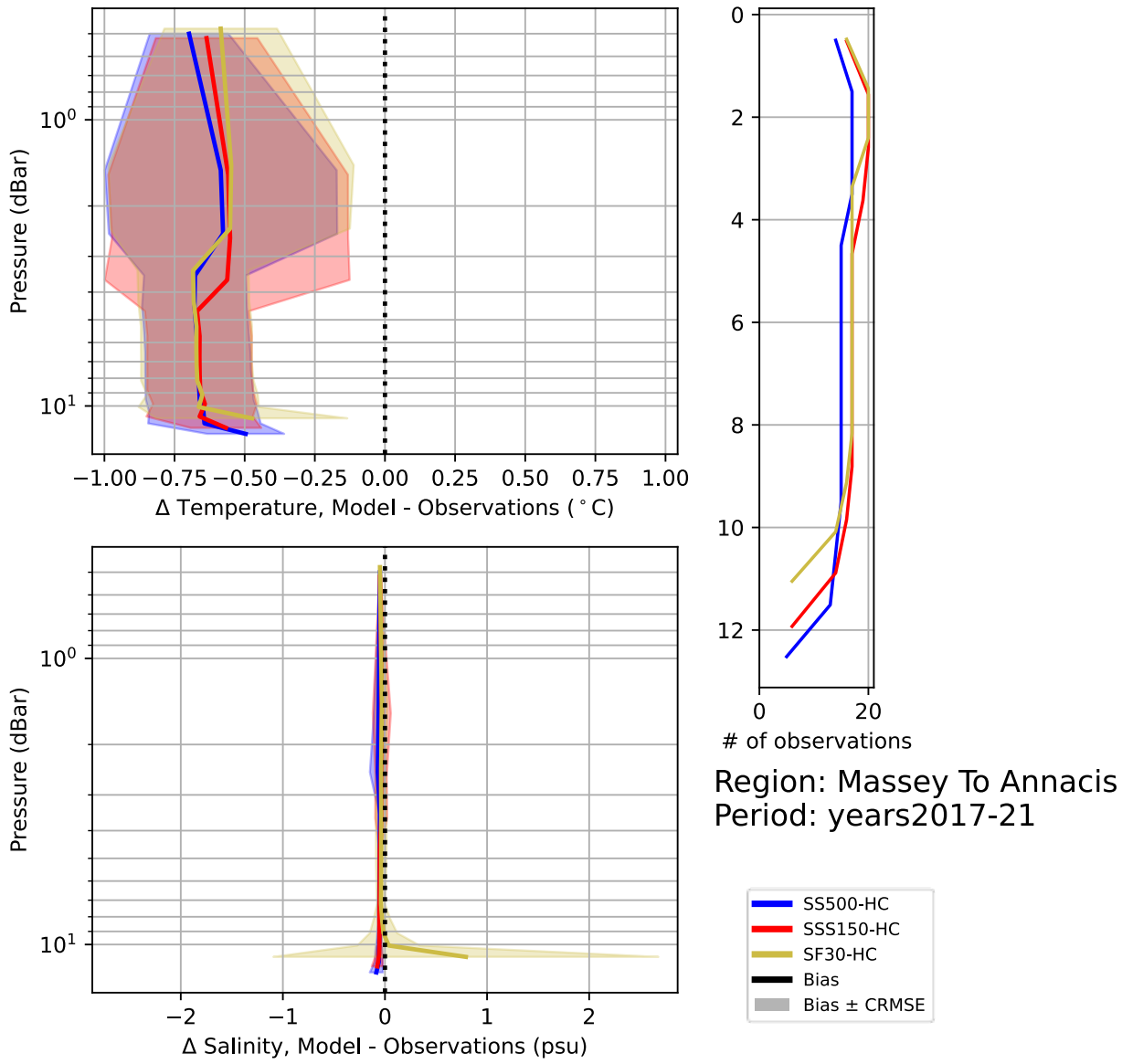

Figure 61. CTD comparison for region Massey to Annacis.

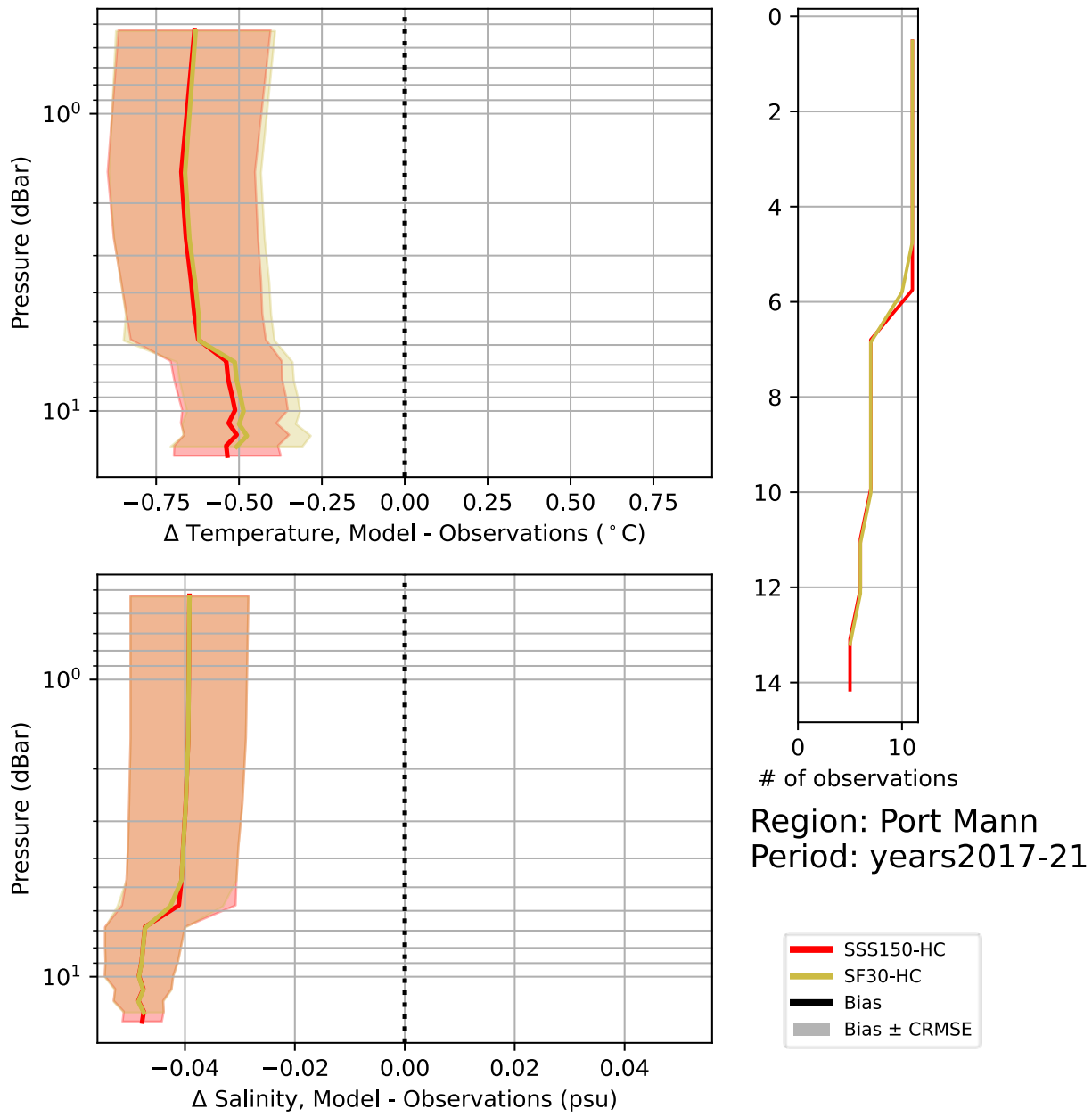

Figure 62. CTD comparison for region Port Mann.

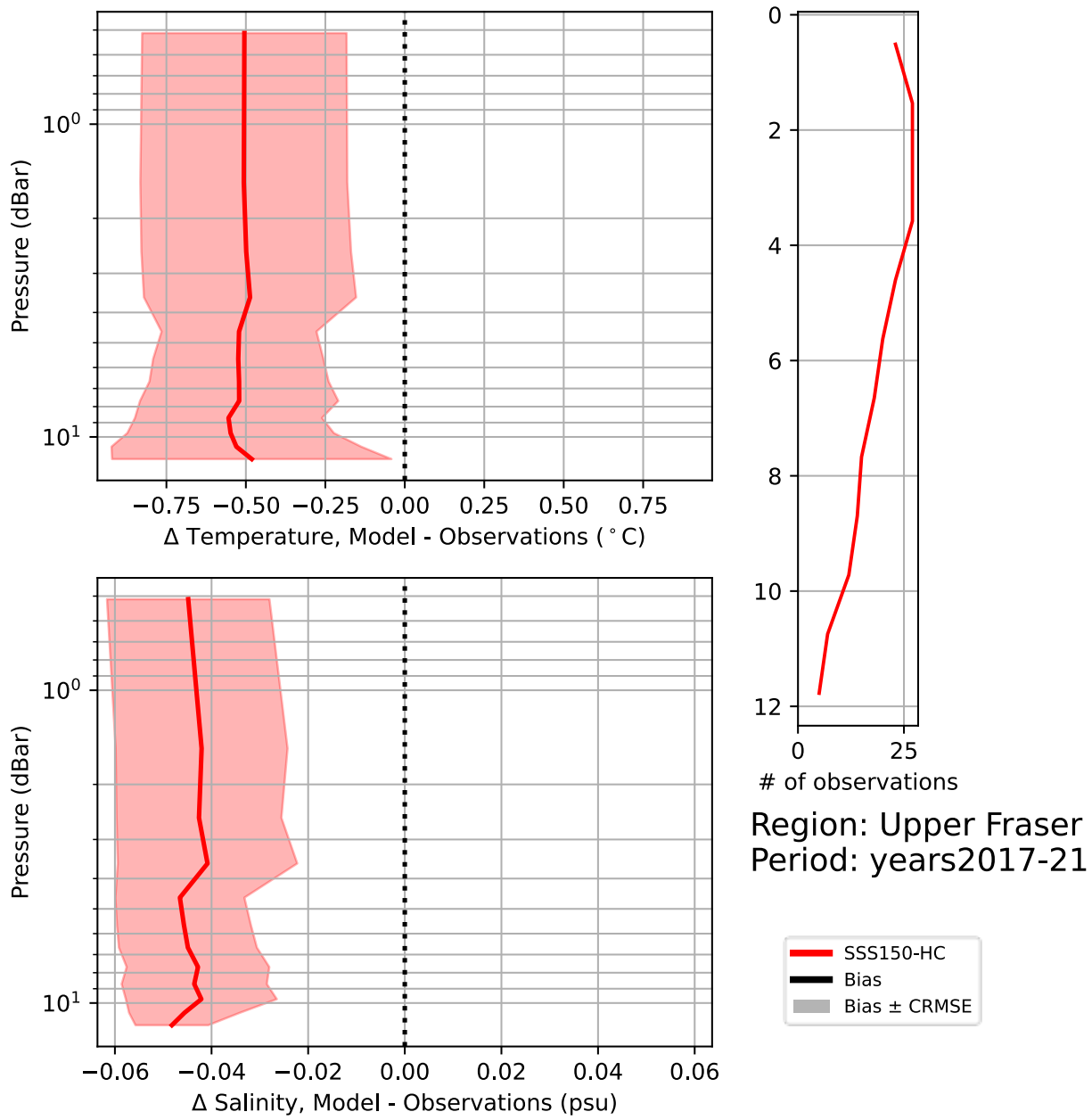

Figure 63. CTD comparison for region Upper Fraser.

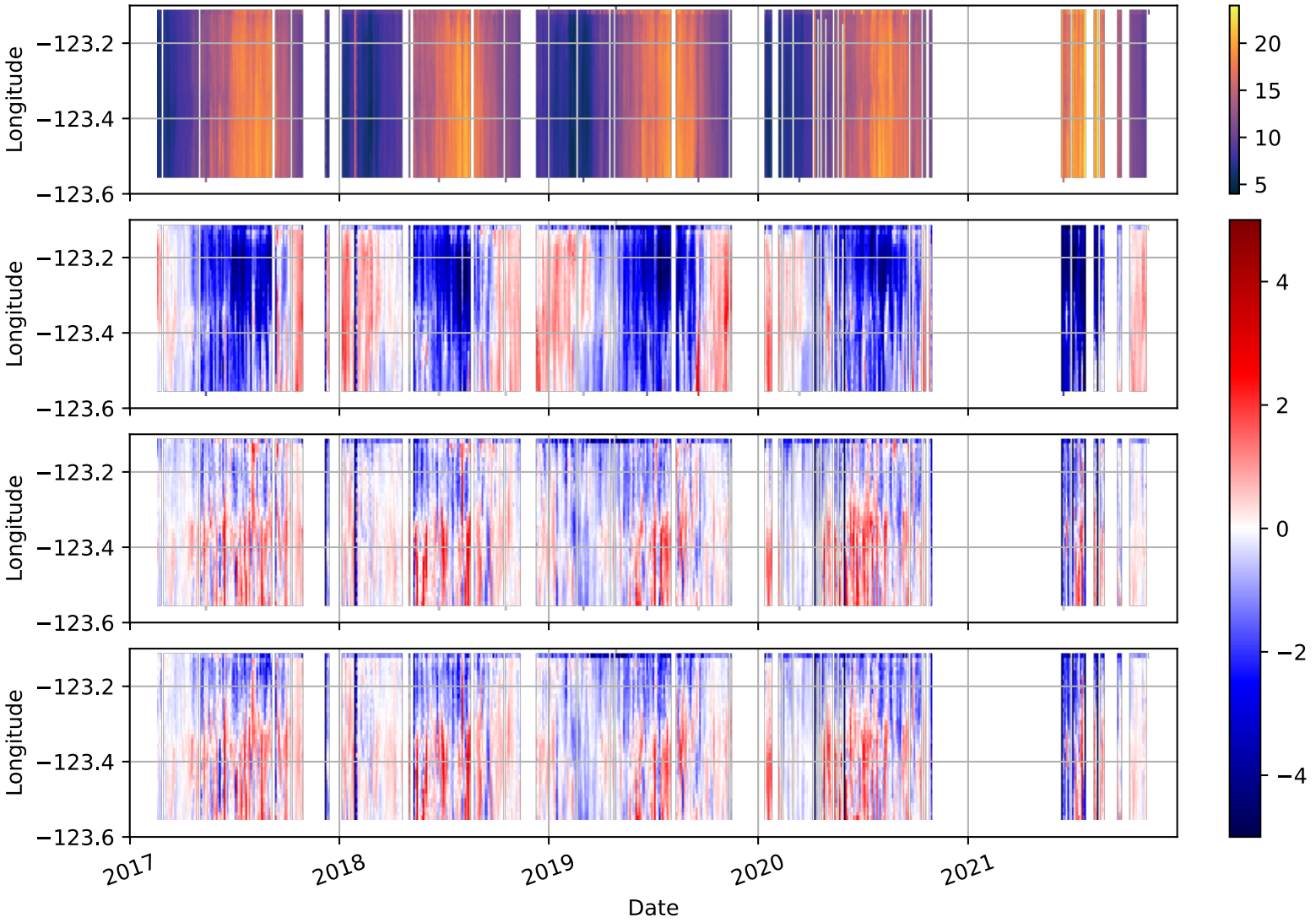

Figure 64. Hovmöller diagram for temperature measured along the BC Ferries Tsawwassen-Duke Point route. Top panel shows the observed temperature, and the lower three panels show the model errors for CIOPS-W, SS500 and SSS150, respectively. Units are degrees Celsius, and the Tsawwassen end of the route corresponds to the top of each panel.

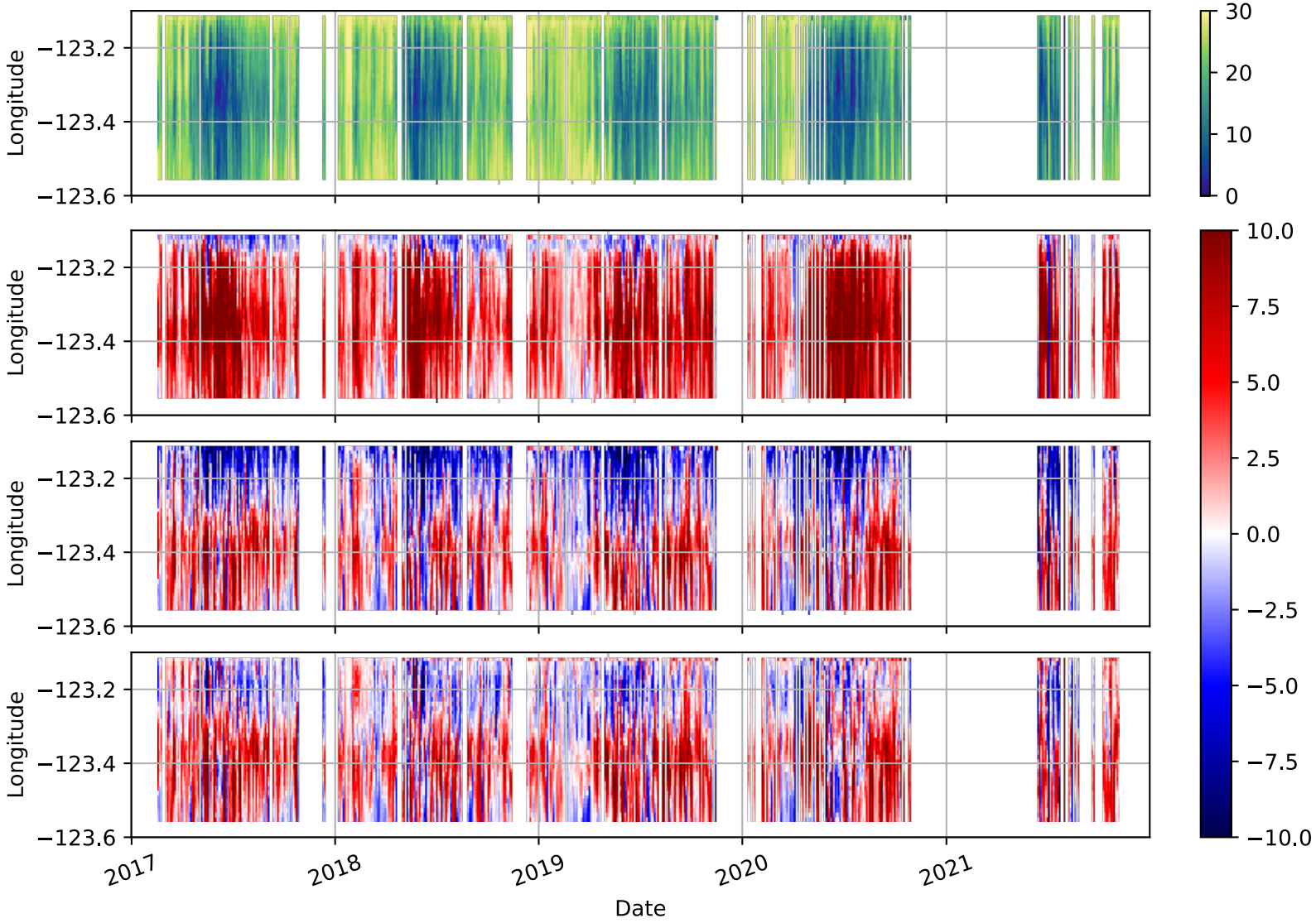

Figure 65. Hovmöller diagram for salinity measured along the BC Ferries Tsawwassen-Duke Point route. Top panel shows the observed salinity, and the lower three panels show the model errors for CIOPS-W, SS500 and SSS150, respectively. Units are PSU, and the Tsawwassen end of the route corresponds to the top of each panel.

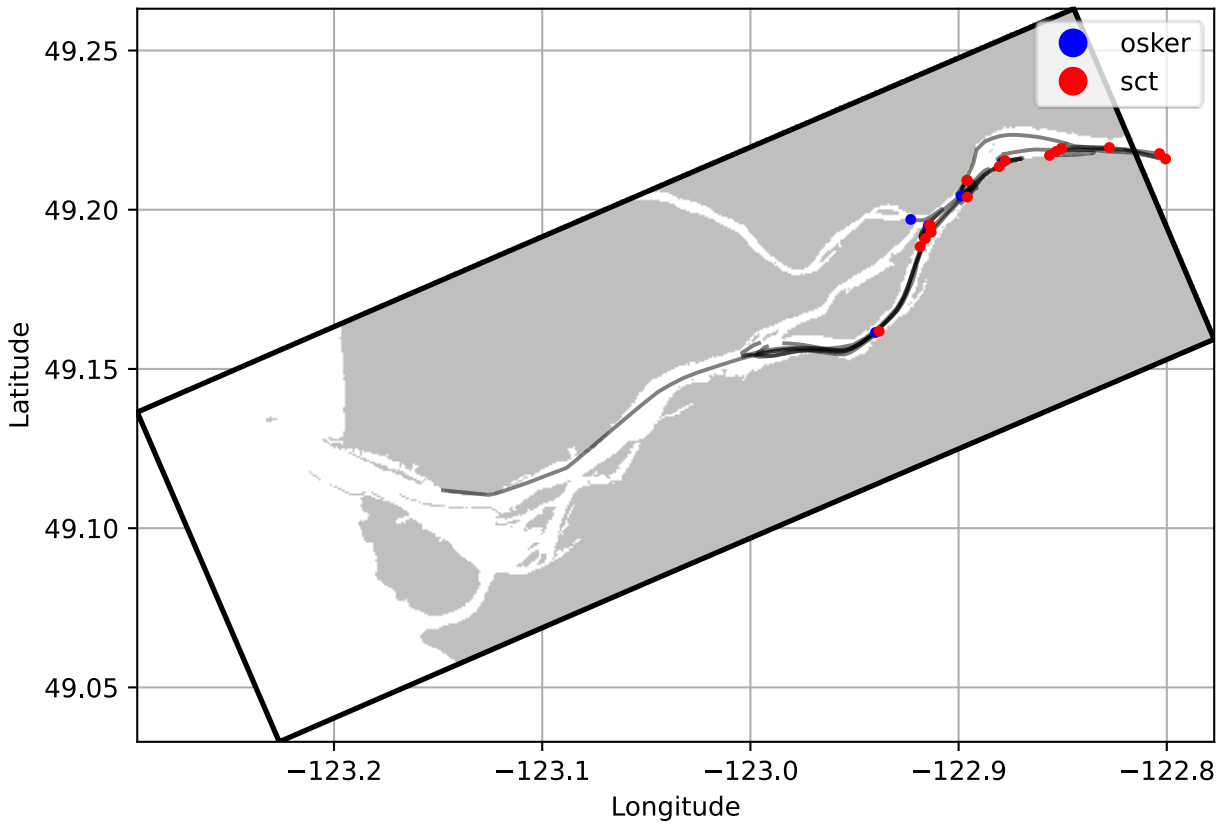

Figure 66. Map of the observed drifter tracks for the two drifter types (OSKER and SCT) used in the experiment.

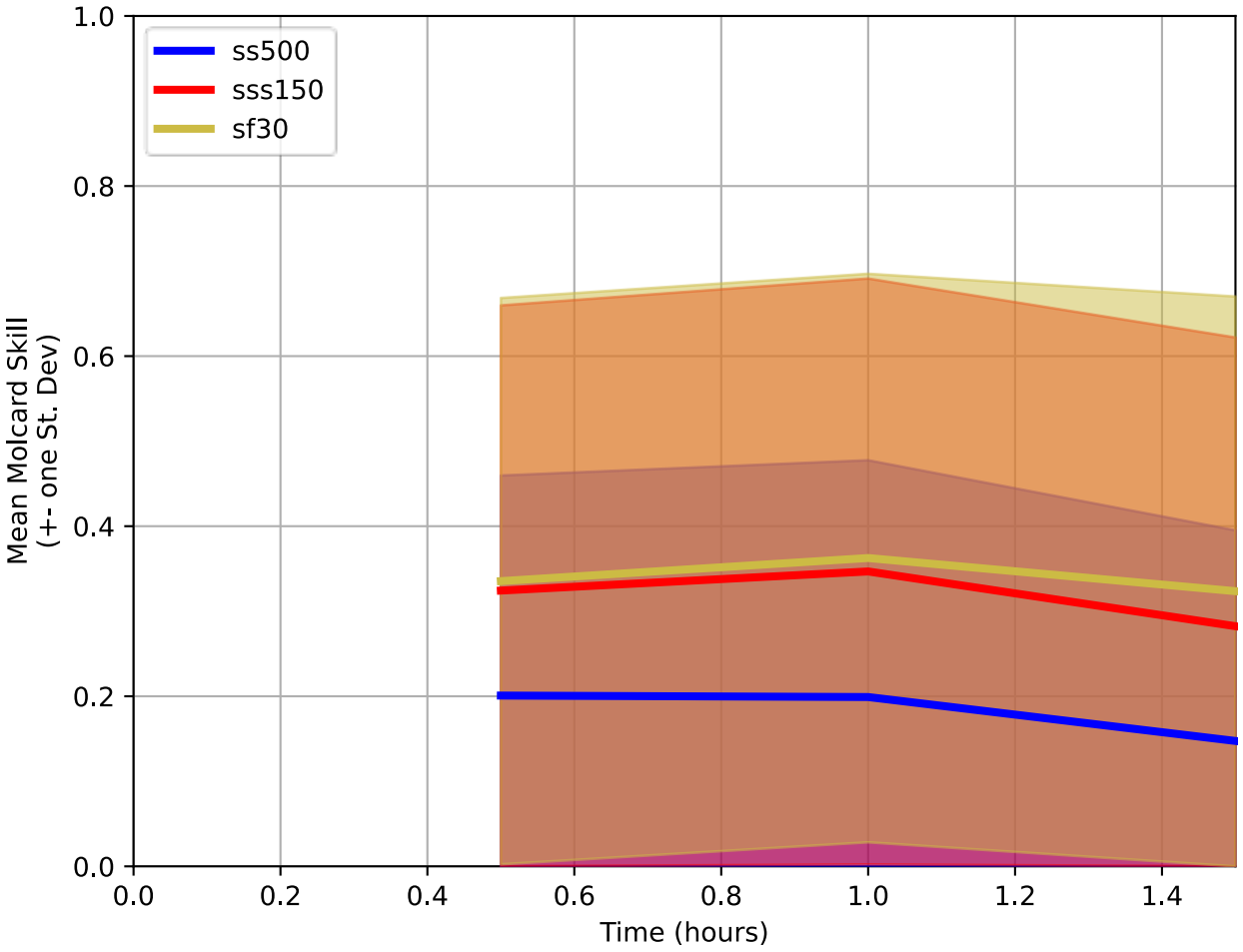

Figure 67. Mean Molcard instantaneous score over drifters. The shaded region shows ± one standard deviation.

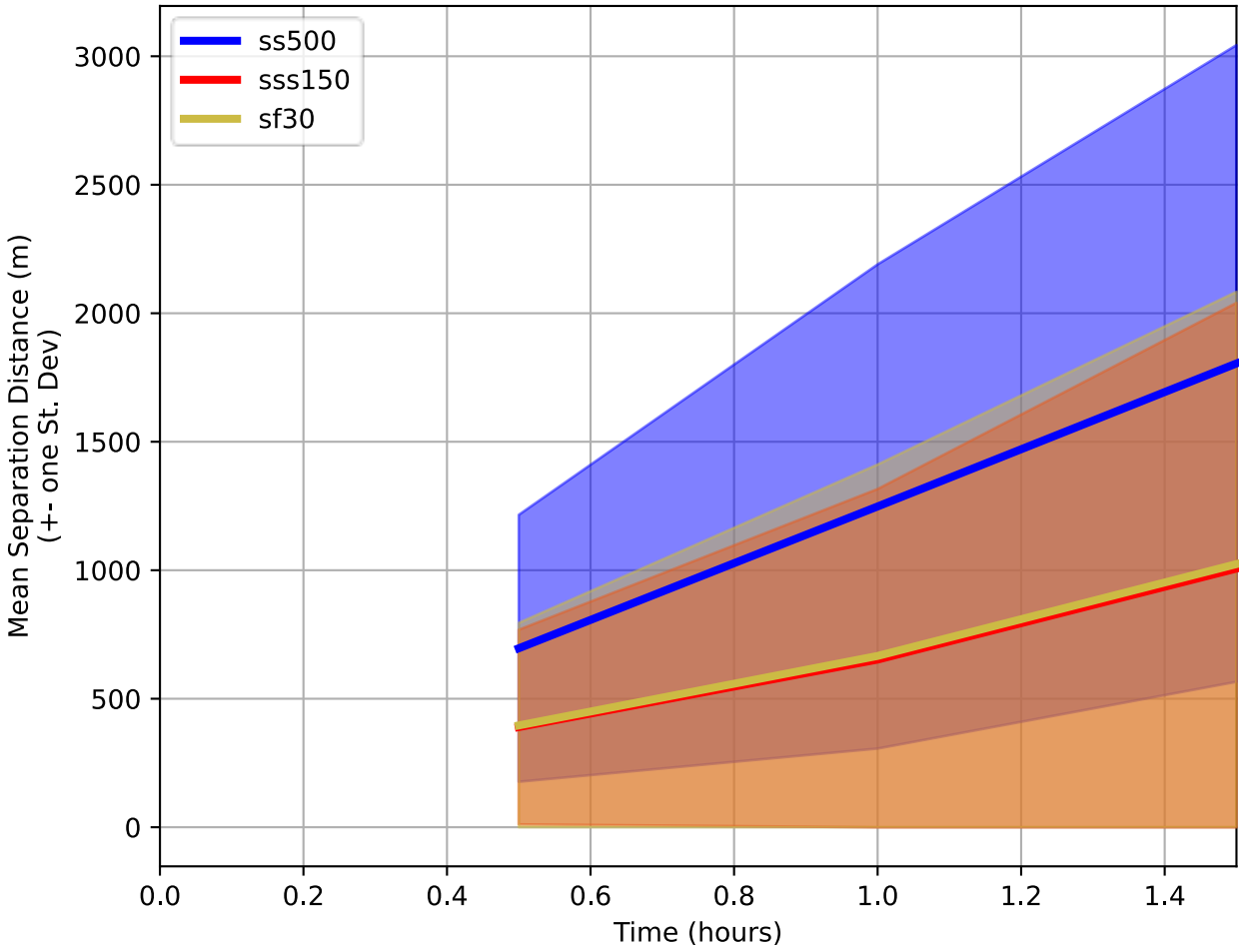

Figure 68. Mean separation distance over drifters. The shaded region shows ± one standard deviation.

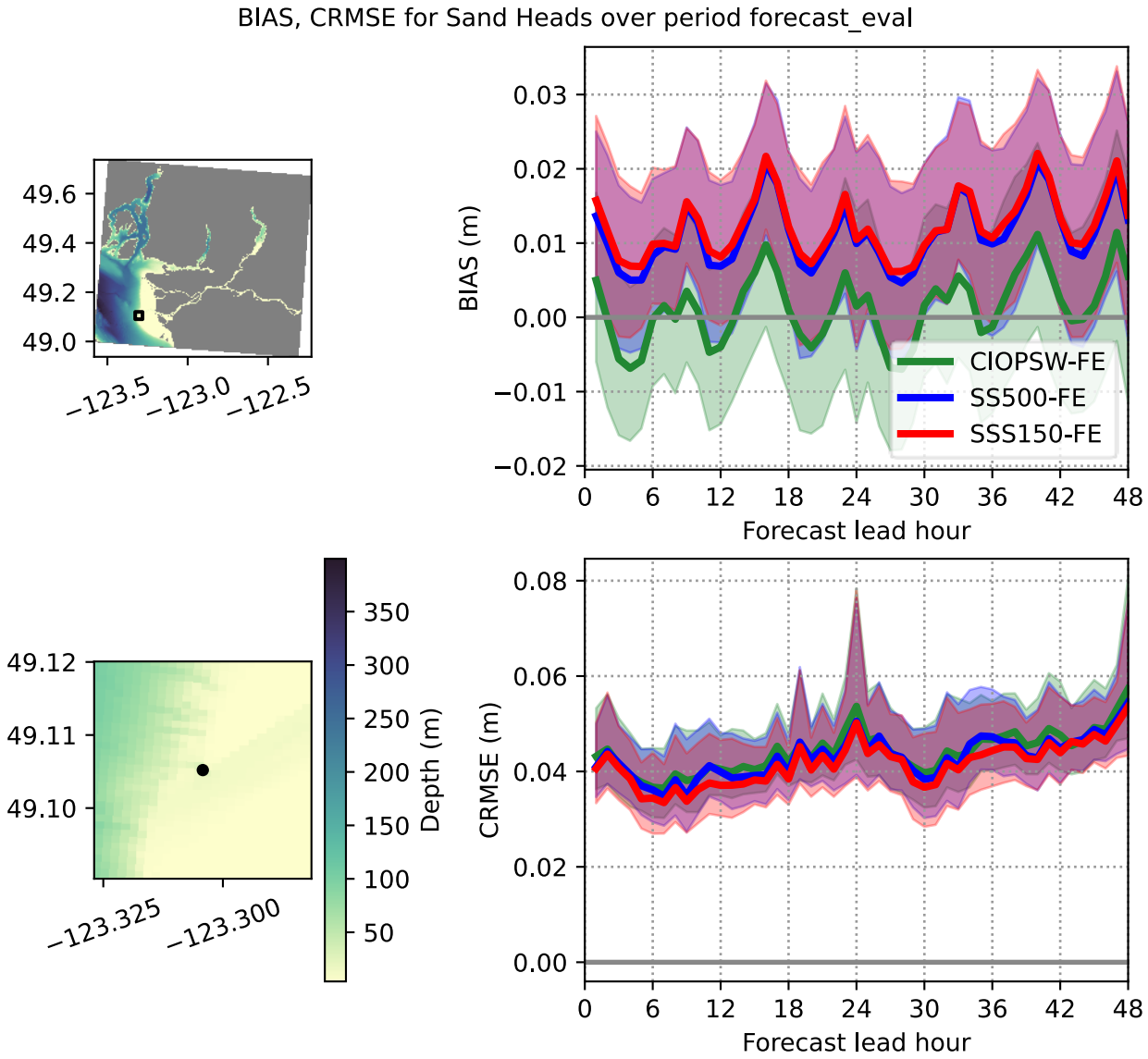

Figure 69. Forecast evaluation for non-tidal water level at Sand Heads.

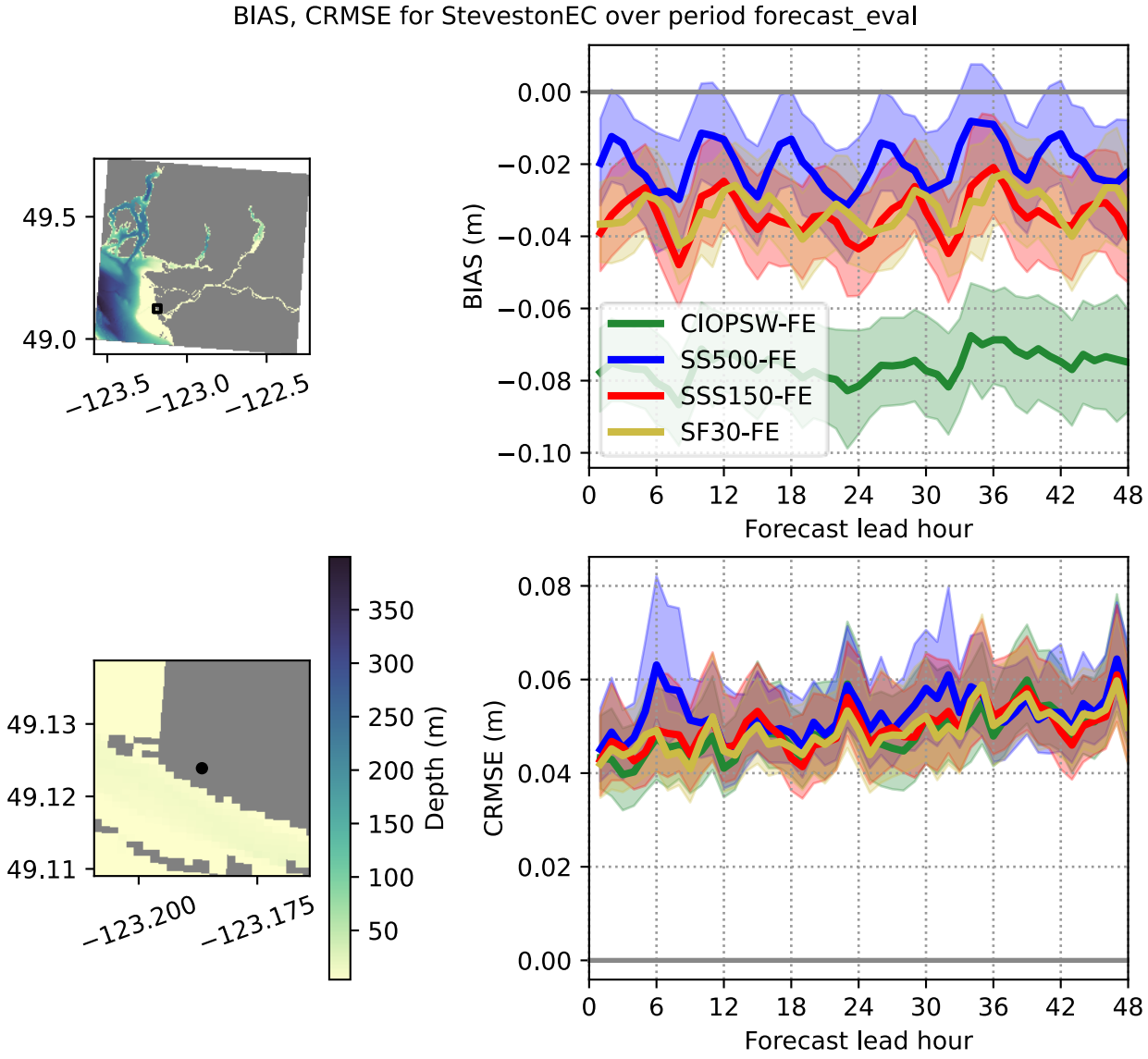

Figure 70. Forecast evaluation for non-tidal water level at StevestonEC.

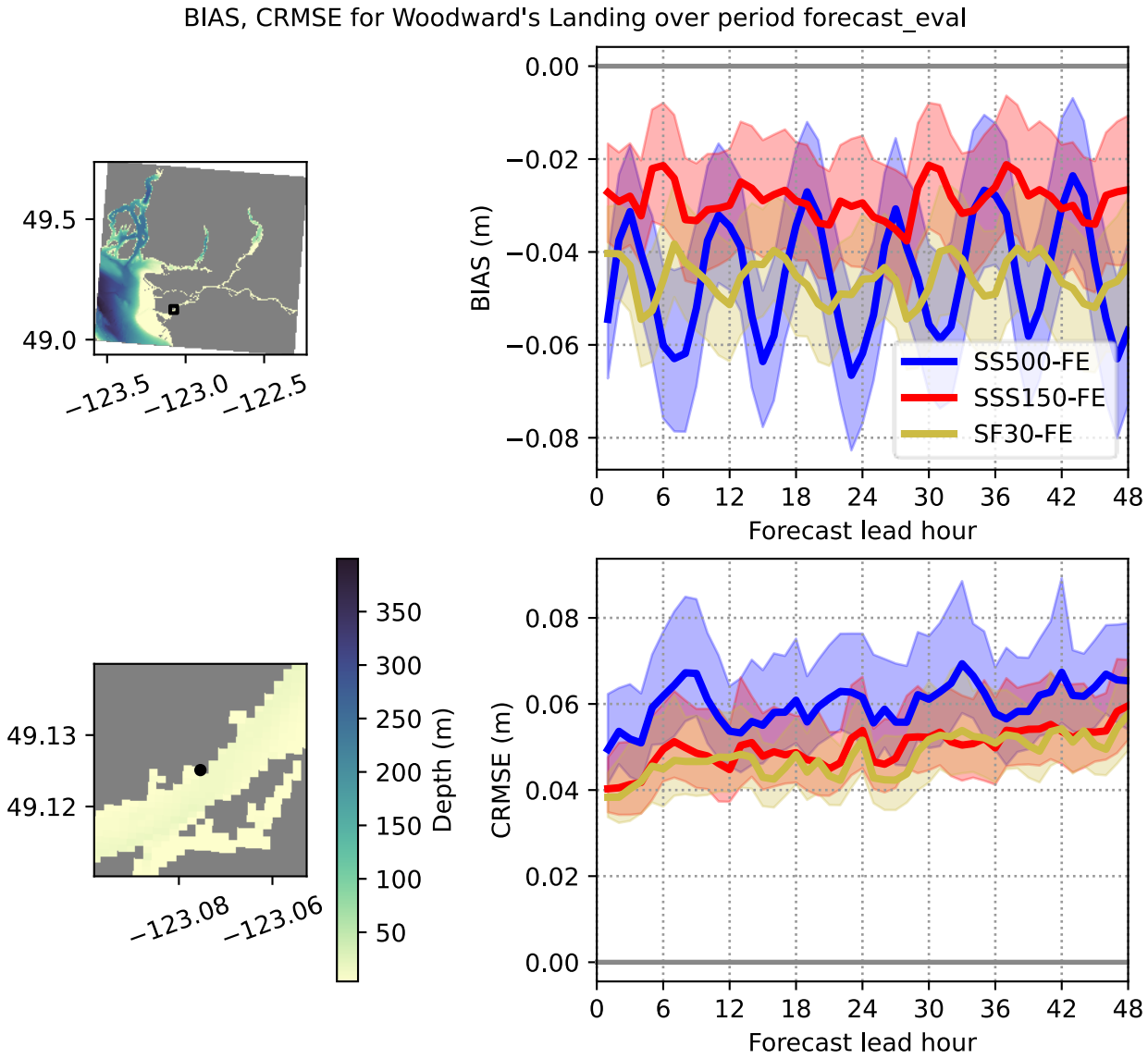

Figure 71. Forecast evaluation for non-tidal water level at Woodward's Landing.

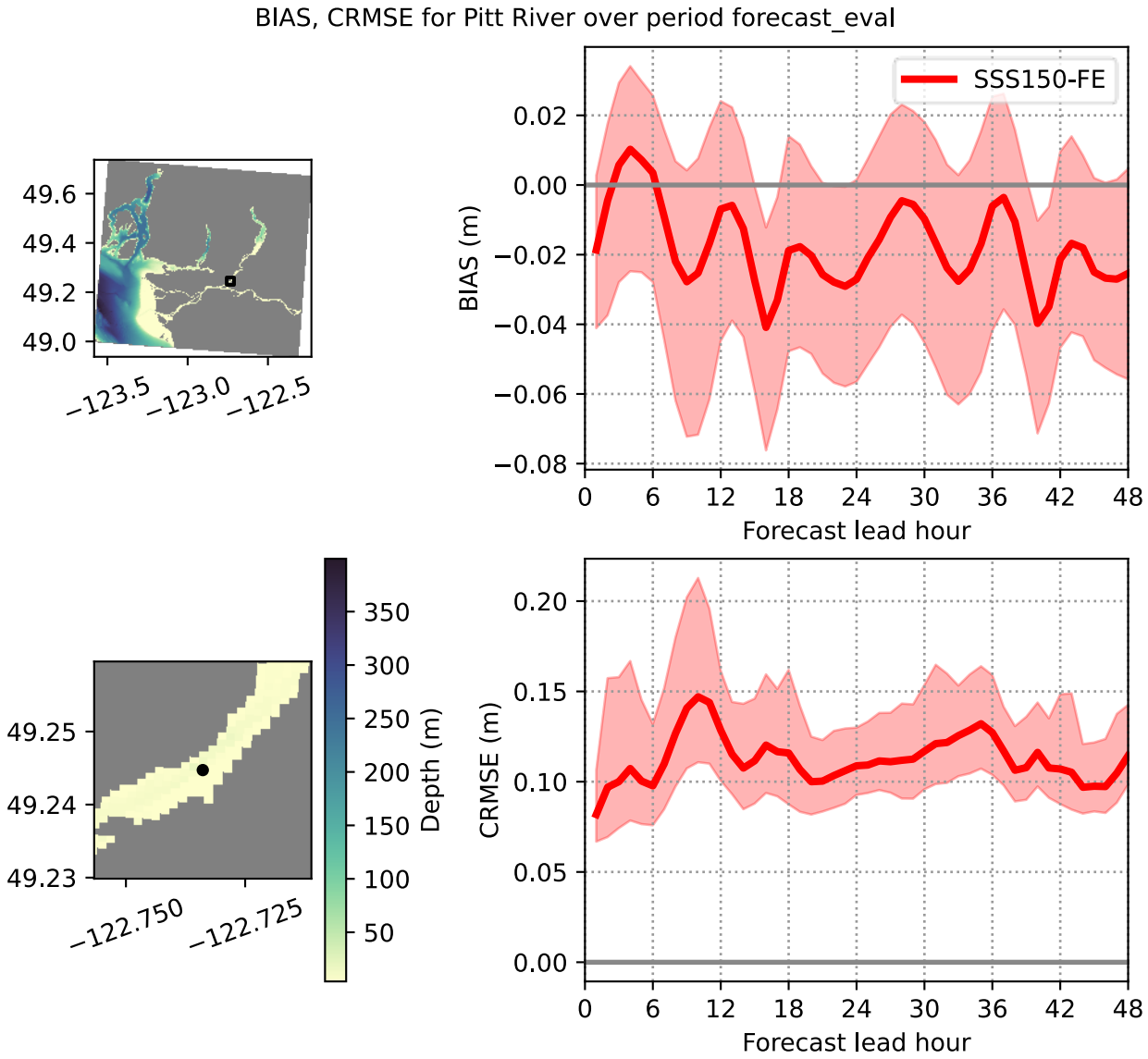

Figure 72. Forecast evaluation for non-tidal water level at Pitt River.

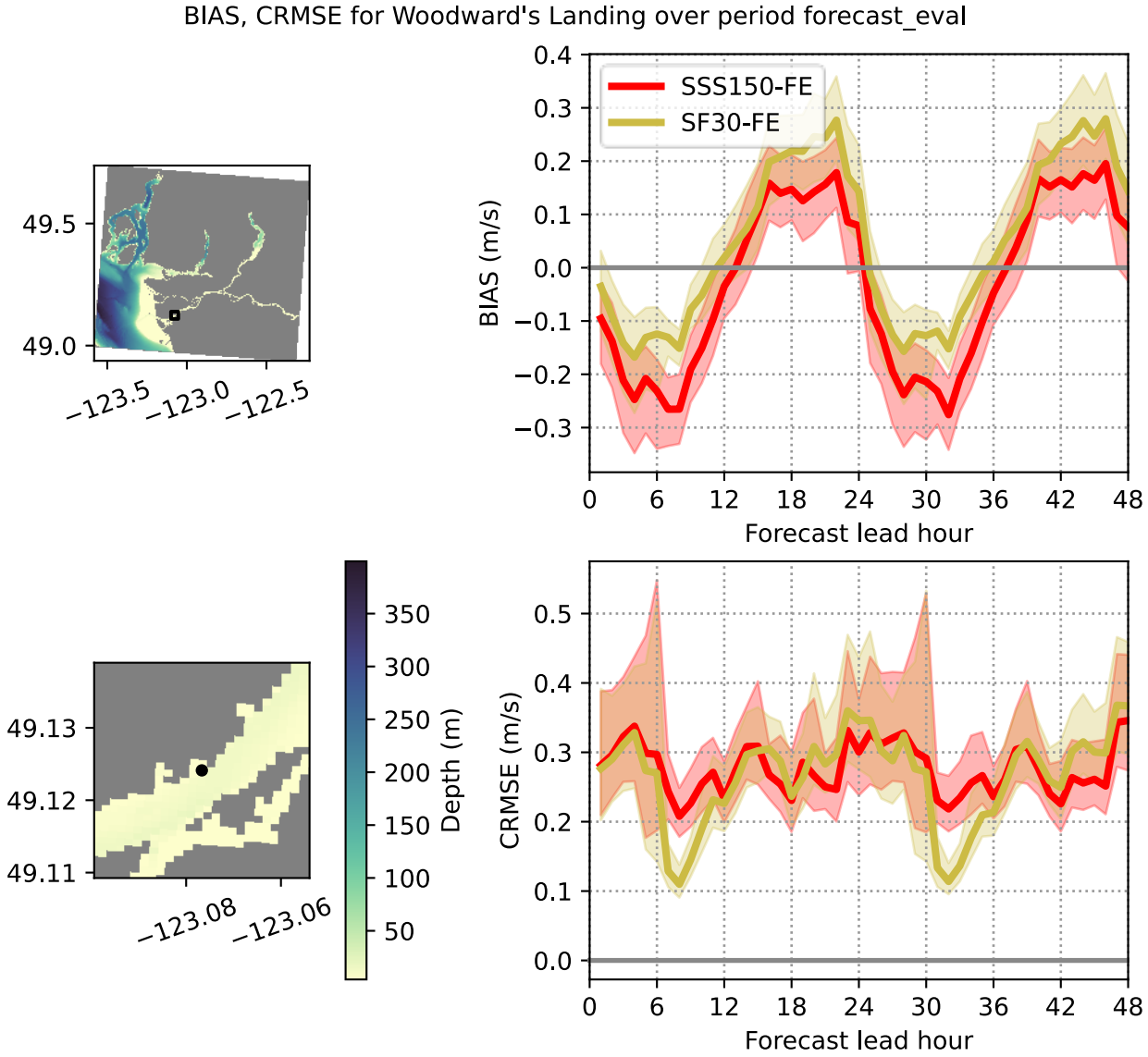

Figure 73. Forecast evaluation for horizontal currents at the Woodward's Landing HADCP in Fraser River.

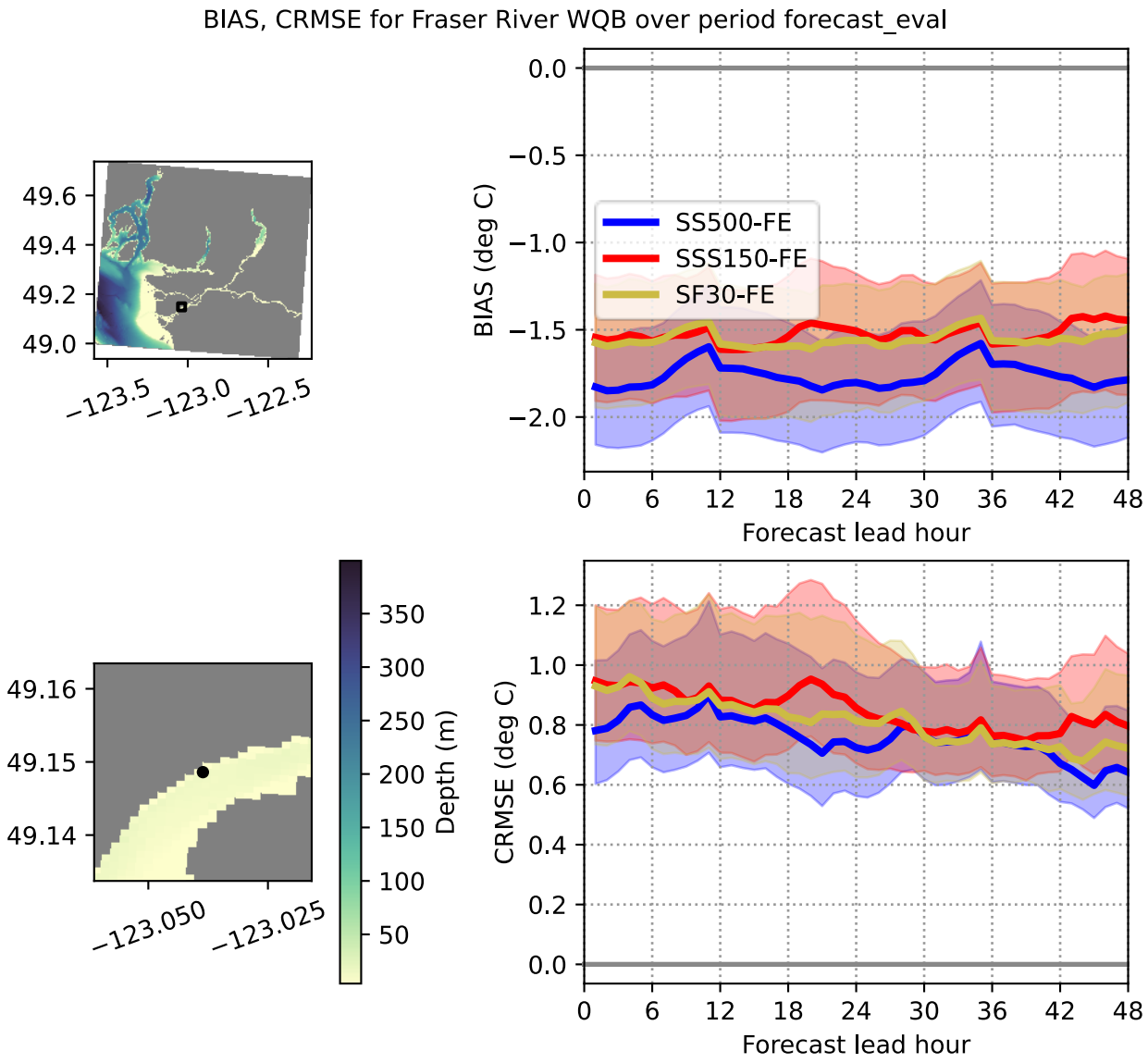

Figure 74. Forecast evaluation for sea-surface temperature at Fraser River Water Quality Buoy.